NASA/TP–2000-209591

V/STOL Dynamics, Control, and Flying Qualities

James A. Franklin

October 2000

The NASA STI Program Office . . . in Profile

Since its founding, NASA has been dedicated to the advancement of aeronautics and space science. The NASA Scientific and Technical Information (STI) Program Office plays a key part in helping NASA maintain this important role.

The NASA STI Program Office is operated by Langley Research Center, the Lead Center for NASA's scientific and technical information. The NASA STI Program Office provides access to the NASA STI Database, the largest collection of aeronautical and space science STI in the world. The Program Office is also NASA's institutional mechanism for disseminating the results of its research and development activities. These results are published by NASA in the NASA STI Report Series, which includes the following report types:

- TECHNICAL PUBLICATION. Reports of completed research or a major significant phase of research that present the results of NASA programs and include extensive data or theoretical analysis. Includes compilations of significant scientific and technical data and information deemed to be of continuing reference value. NASA's counterpart of peer-reviewed formal professional papers but has less stringent limitations on manuscript length and extent of graphic presentations.

- TECHNICAL MEMORANDUM. Scientific and technical findings that are preliminary or of specialized interest, e.g., quick release reports, working papers, and bibliographies that contain minimal annotation. Does not contain extensive analysis.

- CONTRACTOR REPORT. Scientific and technical findings by NASA-sponsored contractors and grantees.

- CONFERENCE PUBLICATION. Collected papers from scientific and technical conferences, symposia, seminars, or other meetings sponsored or cosponsored by NASA.

- SPECIAL PUBLICATION. Scientific, technical, or historical information from NASA programs, projects, and missions, often concerned with subjects having substantial public interest.

- TECHNICAL TRANSLATION. English-language translations of foreign scientific and technical material pertinent to NASA's mission.

Specialized services that complement the STI Program Office's diverse offerings include creating custom thesauri, building customized databases, organizing and publishing research results . . . even providing videos.

For more information about the NASA STI Program Office, see the following:

- Access the NASA STI Program Home Page at *http://www.sti.nasa.gov*

- E-mail your question via the Internet to help@sti.nasa.gov

- Fax your question to the NASA Access Help Desk at (301) 621-0134

- Telephone the NASA Access Help Desk at (301) 621-0390

- Write to:
  NASA Access Help Desk
  NASA Center for AeroSpace Information
  7121 Standard Drive
  Hanover, MD 21076-1320

NASA/TP–2000-209591

V/STOL Dynamics, Control, and Flying Qualities

James A. Franklin
Ames Research Center
Moffett Field, California 94035

National Aeronautics and
Space Administration

Ames Research Center
Moffett Field, California 94035-1000

October 2000

ACKNOWLEDGMENTS

Several individuals, each of whom, in his own way, influenced the author's appreciation of the subject of aircraft stability, control, and flying qualities in general and V/STOL aircraft in particular, deserve recognition in this work. Professors Edwin ("Ted") Parks, Edward Seckel, Courtland Perkins, and Howard ("Pat") Curtiss communicated not only their breadth of knowledge of aircraft aerodynamics, stability, and control but also their enthusiasm for the subject of flight as well. Professor Dunstan Graham provided the same contribution regarding flight control and flying qualities. The overall analytical approach to those subjects pioneered by Duane McRuer and Irving Ashkenas, along with Professor Graham, provided a crucial framework throughout the author's career. That influence should be readily apparent in the analyses performed in the text. An early mentor in industry who helped ground the author in the practical aspects of design was Thomas Paniszczyn. George Cooper, Robert Innis, Michael Stortz, and David Ellis offered crucial insight as experimental test pilots and engineers when it came to understanding the assessment of an aircraft's flying qualities. Curt Holzhauser was a mentor who provided a foundation on the subject of powered lift that has endured, to be augmented in later years by Charles Hynes, Richard Margason, and Richard Kuhn. In the realm of control and display concepts, the original ideas of George Meyer, Richard Bray, Theodor Dukes, and Vernon Merrick are evident in the later chapters. To numerous other colleagues at NASA Ames Research Center, Princeton University, the University of Kansas, and General Dynamics/Fort Worth, who have shared the author's enthusiasm for aeronautics and flight, a hearty thanks to all.

Available from:

NASA Center for AeroSpace Information
7121 Standard Drive
Hanover, MD 21076-1320
(301) 621-0390

National Technical Information Service
5285 Port Royal Road
Springfield, VA 22161
(703) 487-4650

TABLE OF CONTENTS

NOMENCLATURE

A	aspect ratio
a_y	lateral acceleration, g, ft/sec^2
C_D	drag coefficient
C_{Df}	profile drag coefficient
C_L	lift coefficient
c	command
D	drag, lb
D_e	equivalent diameter of jet efflux, ft
d	glideslope position, deg
dB	decibels
$d\gamma/dV$	gradient of flightpath vs airspeed, rad/ft/sec, deg/knot
e	Oswald's efficiency factor
F	force, lb
F_{Total}	total force component
F_X	longitudinal force component, lb
F_Y	lateral force component, lb
F_Z	vertical force component, lb
G	generalized transfer function
g	gravitational acceleration, g; gust component
h	altitude, ft
$\dot{h}$	vertical velocity in Earth reference, ft/sec
IMC	instrument meteorological conditions
I_{xx}	roll moment of inertia, slug-ft^2
I_{xz}	product of inertia, slug-ft^2
I_{yy}	pitch moment of inertia, slug-ft^2
I_{zz}	yaw moment of inertia, slug-ft^2
$j\omega$	imaginary part of a complex number
K_i	gain applied to the ith variable
L	lift, lb; rolling moment, ft-lb
L_w	scale length of gust field, ft
l_x	engine inlet longitudinal moment arm, ft
M	pitching moment, ft-lb
m	mass, slugs
$\dot{m}_e$	engine inlet mass flow, slugs/sec
N	yawing moment, ft-lb; transfer function numerator

N_F	engine rpm, percent
N_j^i	transfer function numerator for the ith state to the jth control
OVC	outside visual cues
P, p	total roll rate, perturbation roll rate, rad/sec
Q, q	total pitch rate, perturbation pitch rate, rad/sec; dynamic pressure, lb/ft^2
$\dot{q}$, $\ddot{\theta}$	pitch angular acceleration, rad/sec^2
R, r	total yaw rate, perturbation yaw rate, rad/sec; generalized response
rpm	revolutions per minute
S	wing area, ft^2
STOL	short takeoff and landing
STOVL	short takeoff and vertical landing
s	Laplace operator
T	thrust, lb; time in trail, sec
T_A	actuator time constant, sec
T_D	Dutch roll mode period, sec
T_e	engine thrust response time constant, sec
T_h	vertical velocity response time constant in hover, sec
T_{h_1}, T_{h_2}, T_{h_3}	numerator root time constants for altitude control with longitudinal stick, sec
T_I	pilot transfer function lag time constant, sec
T_i	integral compensation time constant, sec
T_L	lead compensation time constant, sec
T_p	pilot lag time constant, sec
T_R	roll mode time constant, sec
T_r	low-frequency lateral-directional time constant in hover, sec
T_{rise}	rise time, sec
T_{rp}	yaw rate numerator root time constant for directional control, sec
T_S	spiral mode time constant, sec
T_{s_1}, T_{s_2}	longitudinal characteristic root time constants, sec
T'_{s_1}, T'_{s_2}	closed-loop longitudinal characteristic root time constants, sec
T_{u_1}, T_{u_2}, T_{u_3}	longitudinal velocity numerator time constants in hover, sec
T_{u_δ}	airspeed numerator time constant for thrust control, sec
T_{u_θ}	airspeed numerator time constant for pitch control, sec
T_v	lateral velocity numerator time constant for response to lateral stick, sec
$T_{.5\Delta\gamma max}$	rise time to 50 percent of peak flightpath response, sec
$T_{\beta_{p_1}}$, $T_{\beta_{p_2}}$, $T_{\beta_{p_3}}$	sideslip numerator root time constants for directional control, sec
T_{β_1}, T_{β_2}, T_{β_3}	sideslip numerator time constants for lateral stick, sec
T_{γ_N}	flightpath numerator root time constant for thrust deflection, sec

$T_{\gamma\delta}$, $T_{\gamma T}$	flightpath numerator time constants for thrust control, sec
$T_{\gamma\theta}$	flightpath numerator time constant for pitch control, sec
$T_{\theta_{wg}}$	numerator time constant for pitch response to vertical gust, sec
T_{θ_1}, T_{θ_2}	pitch numerator time constants for longitudinal control, sec
T'_{θ_1}, T'_{θ_2}	time constants of low-frequency longitudinal closed-loop roots, sec
T_{ϕ_1}, T_{ϕ_2}	roll numerator time constants for lateral stick in hover, sec
T_{ψ_1}, T_{ψ_2}	heading numerator time constants for lateral stick, sec
t	time, sec
t_{n_β}	Dutch roll time interval, sec
U, u	total longitudinal velocity, perturbation longitudinal velocity, ft/sec
u_g	longitudinal gust, ft/sec
V	total velocity, ft/sec
VMC	visual meteorological conditions
V/STOL	vertical/short takeoff and landing
V, v	total lateral velocity, perturbation lateral velocity, ft/sec
V_e, V_{ej}	equivalent jet velocity ratio
V_G	ground speed, ft/sec
V_x	longitudinal ground speed, ft/sec
W, w	total vertical velocity, perturbation vertical velocity, ft/sec
w_g	vertical gust velocity, ft/sec
X	longitudinal axis; longitudinal force, lb
X_i	longitudinal distance from engine inlet to center of gravity, ft
x	longitudinal position, ft
Y	lateral axis; lateral force, lb
Y_A	generalized aircraft transfer function
Y_g	generalized gust transfer function
Y_p	generalized pilot transfer function
y	lateral position, ft
Z, z	vertical axis; vertical force, lb
Z_i	vertical distance from engine inlet to center of gravity, ft
α	angle of attack, rad, deg
β	sideslip angle, rad, deg
γ	flightpath angle, rad, deg
ΔL	incremental lift, lb
Δ_{Lat}	lateral-directional characteristic equation
Δ_{Long}	longitudinal characteristic equation
ΔL_β	incremental rolling moment due to sideslip, ft-lb

δ	control deflection, in., deg, percent
δ_{long}	longitudinal control deflection, in.
δ_p	pedal deflection, in.
δ_s	longitudinal or lateral control deflection, in.
δ_T	throttle position, percent
ζ	damping ratio
Θ, θ	pitch attitude, incremental pitch attitude, rad, deg
θ_T, θ_j	thrust deflection angle from horizontal, deg
$\theta(1)$	pitch attitude response in 1 sec, deg
ρ	air density, slugs/ft^3
σ	real component of imaginary number, standard deviation
τ	time constant, sec
τ_p	pilot's equivalent time delay, sec
Φ, ϕ	bank angle, incremental bank angle, rad, deg
Φ_{wg}	vertical gust power spectral density
Φ_θ	pitch attitude power spectral density
ϕ_{osc}/ϕ_{AV}	bank angle excitation parameter $(\phi_1 + \phi_3 - 2\phi_2)/(\phi_1 + \phi_3 + 2\phi_2)$
ϕ_1	peak bank angle response at first oscillation, deg
ψ	heading angle, rad, deg
Ψ_β	sideslip phasing parameter, deg
ω	natural frequency, rad/sec
ω_{BW}	frequency bandwidth, rad/sec
ω_d	Dutch roll natural frequency, rad/sec
ω'_d	closed-loop Dutch roll frequency, rad/sec
ω_p	phugoid natural frequency, rad/sec
ω'_p	closed-loop phugoid frequency, rad/sec
ω'_R	closed-loop roll-spiral mode frequency, rad/sec
ω_{sp}	short period natural frequency, rad/sec
ω'_{sp}	closed-loop short period frequency, rad/sec
$\omega_{\beta p}$	sideslip numerator frequency for directional control, rad/sec
ω_θ	simplified longitudinal characteristic-root natural frequency, rad/sec
ω_ϕ	bank angle numerator frequency for control with lateral stick, rad/sec
ω_ψ	heading numerator frequency for control with lateral stick, rad/sec

Subscripts:

aero	aerodynamic
c, cmd	command
CL, cl	closed loop
d	Dutch roll
max	maximum
OL, ol	open loop
o	initial condition
p	phugoid
prop	propulsion system
sp	short period
ss	steady state

V/STOL DYNAMICS, CONTROL, AND FLYING QUALITIES

James A. Franklin

Ames Research Center

SUMMARY

This publication presents material that constituted the lectures presented by the author as part of course AA 234, Dynamics, Control, and Flying Qualities of V/STOL Aircraft that was taught in the Department of Aeronautics and Astronautics at Stanford University. It covers representative operations of vertical and short takeoff and landing (V/STOL) aircraft, a discussion of the pilot's strategy in controlling these aircraft, the equations of motion pertinent to V/STOL tasks, and their application in the analysis of longitudinal and lateral-directional control in hover and forward flight. Following that development, which applies to the characteristics of the basic airframe and propulsion system, the text concludes with a discussion of the contributions of control augmentation in specific flight tasks and of the integration of modern electronic displays with these controls.

INTRODUCTION

It is pertinent to begin this document with a definition of the term *flying qualities* in order to place the subject in an appropriate context. Flying qualities are determined by the characteristics of an aircraft and its operating environment that influence the pilot's ability to control the aircraft and perform tasks in support of an intended mission. Characteristics of the aircraft concern its stability and control and propulsion system properties that affect its static and dynamic stability and control response to the pilot. In modern V/STOL aircraft, the influence of control augmentation systems and cockpit displays has a significant effect on its flying qualities, as does various aspects of the operating environment, including winds, atmospheric turbulence, and visibility.

A history and background of flying qualities criteria development in the United States is shown in table 1. This history can be traced to the turn of the century when the Army was sufficiently impressed with the Wright brothers' aircraft that a one-page procurement specification was prepared for acquisition of the aircraft. That specification included the need for ease of control of the vehicle by a pilot. That viewpoint reflected the Wright's own interest in and their design of the aircraft for these objectives. In 1911, a book was published in England by G. H. Bryan (ref. 1) that set forth aircraft equations of motion and dealt with linear analysis and estimation of small perturbation linear stability derivatives as approximated by the first term of a Taylor series expansion. Bryan's work formed the theoretical basis for the study and analysis of aircraft stability and control characteristics. The thread of this work was picked up in the United States and extended by Jerome Hunsaker in the first National Advisory Committee of Aeronautics (NACA) technical report, titled "Experimental Analysis of Inherent Longitudinal Stability for a Typical Biplane," as well as in the second NACA report, by Edwin Wilson, "Theory of an Aeroplane Encountering Gusts."

TABLE 1. CHRONOLOGY OF AIRCRAFT FLYING QUALITIES CRITERIA

Year	Fixed wing[a]			Rotary wing
	CTOL	STOL	V/STOL	
1900				
	Wright Flyer Procurement			
1920				
1940				
	NACA Rept. 755			
	MIL-1815 (USAF)			
				MIL-H-8501 (USA)
	BUAER SR-119 (USN)			
	MIL-F-8785 (USAF/USN)			
1960				
				MIL-H-8501A (USA/USN)
			AGARD 408	
		NASA TN D-5594		
	MIL-F-8785B (USAF/USN)		AGARD R-577	
			MIL-F-83300 USN/USAF	
		ASD TR-78-13 (USAF)		
	MIL-F-8785C (USAF/USN)			
1980				
	MIL-STD-1797 (USAF/USN)			
				ADS-33 (USA)
2000				

[a]*CTOL: conventional takeoff and landing; STOL: short takeoff and landing; V/STOL: vertical/short takeoff and landing.*

Considerable time elapsed before procuring authorities became more definitive in the design of an aircraft from a pilot's point of view. The first document that treated the subject of flying qualities in substance and breadth was published by Gilruth of the NACA in 1943 (ref. 2), and was based on experience with aircraft dynamics and flying qualities gained by the NACA up to that time from flight and wind tunnel tests. Following World War II, the first in a series of military specifications appeared, initially in the form of an Air Force document for conventional takeoff and landing aircraft (CTOL), either fighters, transports, or utility aircraft. In the mid-1950s, an Air Force/Navy

specification (ref. 3), following its postwar predecessor, was released and continued in use for over 10 years before it was revised in 1969 into an even more complete specification with an accompanying background and user guide (ref. 4). This latter specification was replaced in recent years by the current Military Standard 1797 (ref. 5).

More time elapsed before definitive requirements for short takeoff and landing (STOL), vertical takeoff, or rotary-wing aircraft were set forth. MIL-H-8501 (ref. 6) was written by the U.S. Army and subsequently updated in 1961 (ref. 7) by both the Army and Navy as a design specification for helicopters. In the late 1960s and going on to the early 1970s, following a good deal of experience with fixed-wing V/STOL in the 1950s, formal documents were written on this class of aircraft (refs. 8-10), as well as on their short takeoff and landing fixed-wing counterparts (ref. 11). The evolution of these requirements for flying qualities, particularly in the V/STOL category, is toward aircraft that perform more complex missions and that move into areas of the flight envelope that have not been explored to date. Thus, continued developments in these design specifications can be anticipated, particularly as they focus on applications of electronic controls.

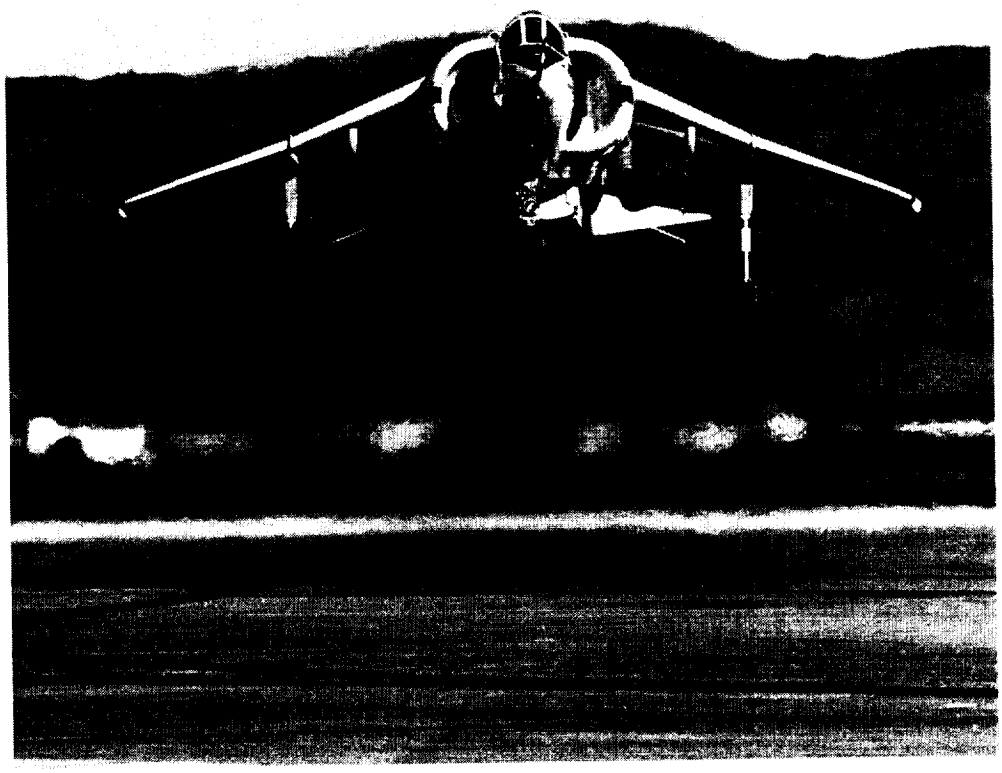

REPRESENTATIVE OPERATIONS OF V/STOL AIRCRAFT

There are several aspects of V/STOL aircraft operations that encompass the tasks the pilot is required to perform to accomplish the intended mission. For military use, these aircraft may be required to operate from airfields, from austere forward sites, or from amphibious assault ships. Airfields and large ships provide ample room for takeoff and landing and precision approach guidance for operations conducted under low-visibility conditions. These tasks do not pose a significant challenge to the experienced pilot. The capability for hover and slow-speed flight and for rapidly accelerating between jet-borne and wing-borne flight that characterizes V/STOL aircraft, permits operation into the more confined spaces that are associated with austere shore-based sites and from the decks of small aviation-capable ships. However, these operations enforce a greater precision of control and the capability for rapid deceleration to hover than are associated with more generously proportioned facilities. For shore-based sites, these aircraft may operate from temporary pads with dimensions of 96 by 96 ft and near buildings and trees (fig. 1). Consequently, the ability to position the aircraft, to control height precisely, to stop quickly, and to do so under conditions of winds, turbulence, and low visibility is essential to ensure routine operational capability.

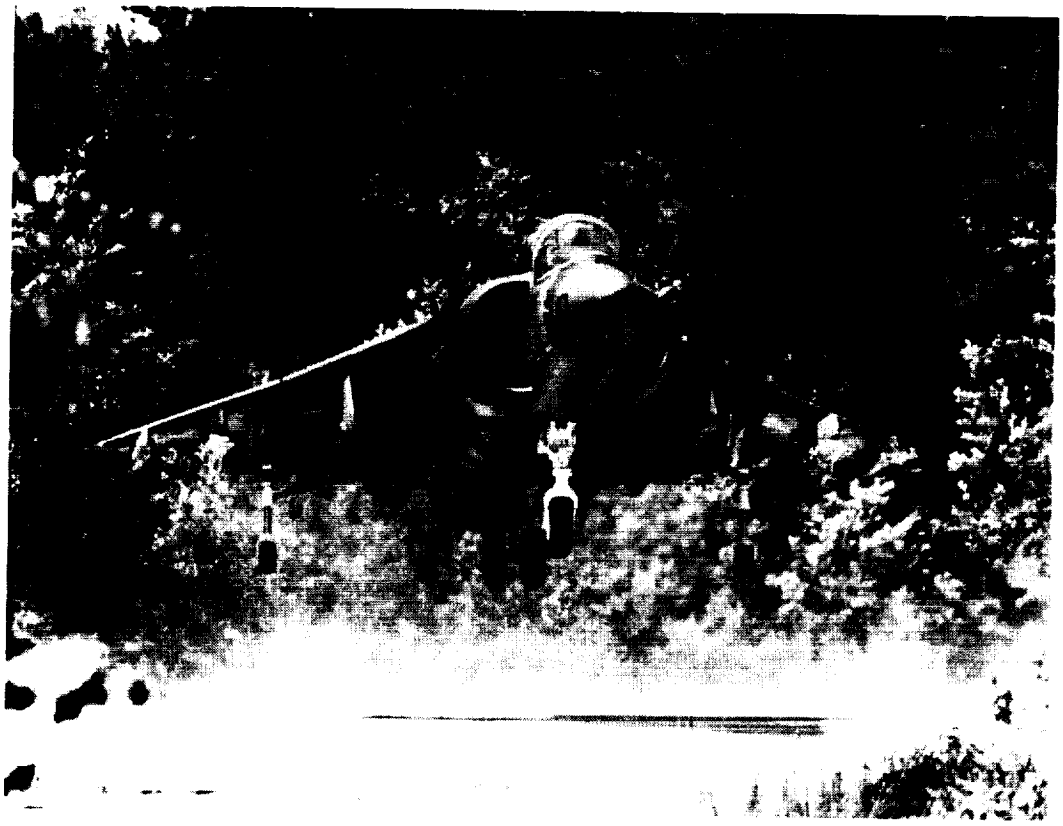

Figure 1. Harrier performing a vertical landing at an austere site.
(Photo courtesy of McDonnell Douglas)

Operations at sea may entail vertical takeoff, short takeoff, and ski-jump launch and vertical landing, and routinely take place from the decks of amphibious assault ships. Ski-jump takeoffs (fig. 2) are generally described by pilots as uneventful maneuvers, unless the pilot neglects to deflect the thrust vector upon leaving the ramp. With the aircraft properly trimmed in pitch for the departure from the ski-jump ramp, there are no demands for immediate control action as the aircraft leaves the ramp. The semiballistic trajectory ensures adequate performance as the aircraft accelerates to wing-borne flight. The pilot must establish the desired climb attitude and gradually rotate the thrust vector aft to continue the acceleration. For flat-deck operations (fig. 3), short takeoffs are most challenging with a pitching deck, since downward excursions of the deck reduce clearance margins above the sea and require greater maneuver capability when leaving the deck. Short takeoffs can be more demanding at shore-based sites in the winds and turbulence that flow over lines of trees and structures and that can disturb the vehicle enough to make the pilot's control task difficult. For vertical takeoffs, the primary concern is to avoid the ship's superstructure and to transition away from the ship.

Figure 2. Ski jump takeoff. (Photo courtesy of McDonnell Douglas)

Approach to landing proceeds through transition from conventional flight speeds of around 200 knots to an initial approach speed of about 120 knots at a range of 3/4 mile from the ship or shore-based site. From that point, the pilot executes a deceleration to hover over the landing pad. At sea, that operation is carried out by bringing the aircraft to a stabilized hover alongside the ship, translating in level flight to a stable hover over the deck, and then descending to touchdown.

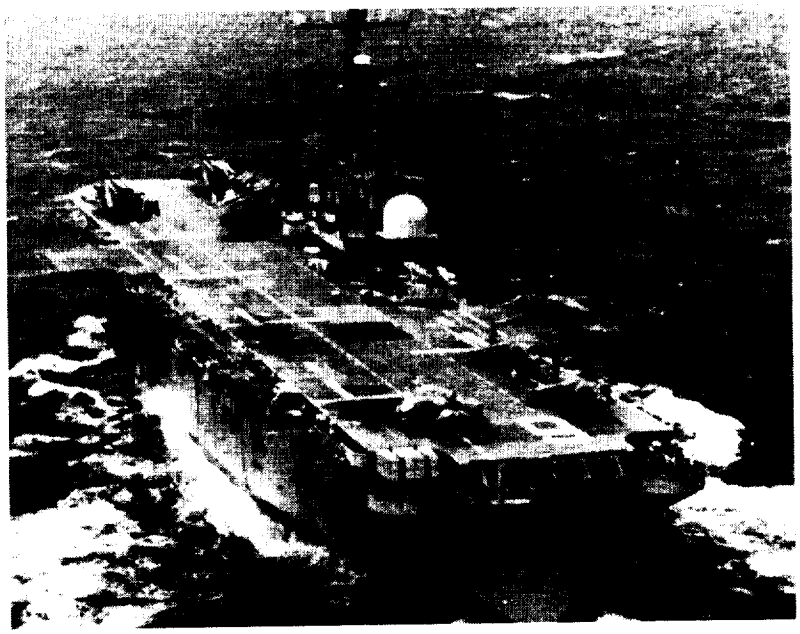

Figure 3. Representative assault carrier. (Photo courtesy of U. S. Marine Corps)

During recovery to the ship (fig. 4), the vertical, lateral, and rolling motion of the landing pad may present a significant control challenge; therefore, restrictions are placed on operations under high sea conditions. For the hover and landing, the aircraft must have height and speed control capability for the translation and hover in order to successfully accomplish the landing in the presence of ground effect or to abort the landing and accelerate to wing-borne flight. The precision of control for attitude, heading, and horizontal and vertical velocities is greatest in this phase of flight, and it is important to be able to initiate, arrest, and stabilize all these motions rapidly if acceptable hover-position control is to be achieved. Control authority must also be sufficient to counter disturbances from air wakes, hot gas ingestion, and ground effect.

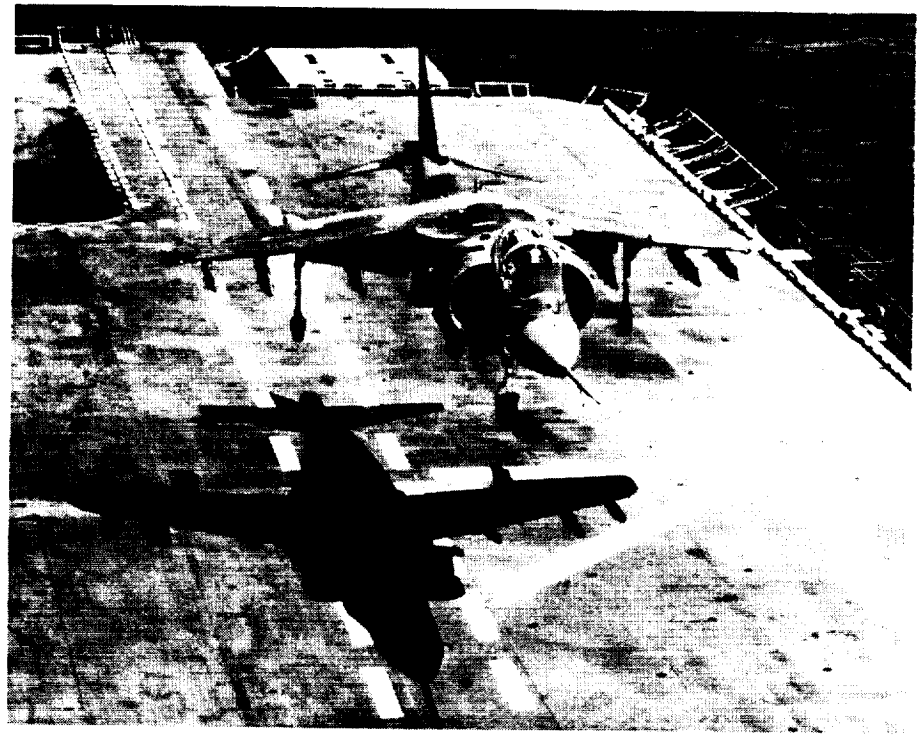

Figure 4. Harrier performing a vertical landing aboard assault carrier.
(Photo courtesy of McDonnell Douglas)

Visibility in adverse weather is another factor that will influence the manner in which the aircraft is maneuvered and controlled. In visual flight, cues for attitude and translational control are easily extracted from the external scene and no constraints are imposed on operations. As visual information degrades, however, cues for attitude control diminish and translational rate information becomes marginal. At the extreme, full instrument meteorological conditions (IMC) require that all guidance and control cues be presented to the pilot through artificial means. Such conditions normally require a higher level of aircraft stability than is necessary under visual flight conditions.

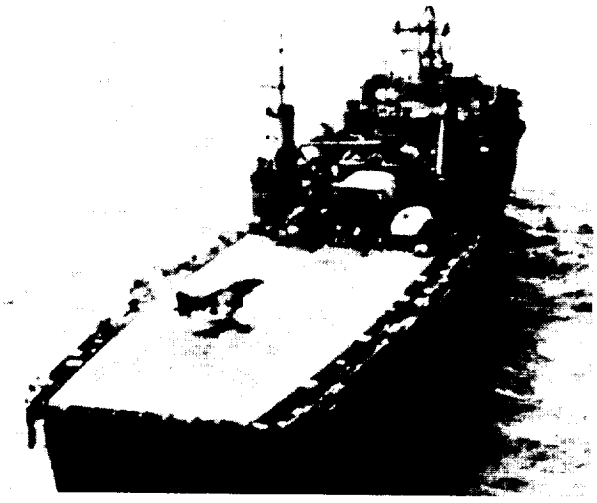

Figure 5. Harrier landing aboard a destroyer.
(Photo courtesy of U. S. Marine Corps)

A final example (fig. 5) shows a Harrier landing on the stern of a destroyer. Landing an aircraft in the wake of a ship like this when the deck is rolling and heaving is an extremely

difficult task. In fact, in high sea states helicopters have to be winched down to the deck rather than landing under their own control. Operations like these are the most challenging tasks confronting the V/STOL pilot and place a high demand on precise control of the aircraft.

The following series of figures provides examples of time histories of the V/STOL aircraft's behavior during these maneuvers. A representative time history of a vertical takeoff for the Harrier is shown in figure 6 to illustrate the pilot's actions that are necessary to execute this maneuver. The thrust vector is deflected to the hover setting of 82 deg with respect to the water line of the aircraft. The pilot applies maximum thrust, the aircraft lifts off, and the pilot then initiates the acceleration to wing-borne flight. The acceleration is accomplished by rotating the thrust vector aft in discrete increments, but not so rapidly as to cause the aircraft to settle. No precise closed-loop control is required except perhaps to maintain the aircraft pitch attitude, and even that is not a tight closed-loop task. The short takeoff (fig. 7) is initiated with maximum thrust and the thrust vector full aft. The aircraft accelerates to the desired takeoff speed at which time the pilot deflects the thrust vector to the appropriate takeoff setting. The aircraft lifts off and the acceleration hesitates momentarily. Climb pitch attitude is established, and the aircraft continues to accelerate as the thrust vector is gradually brought to the full aft position. Discrete step inputs in control of thrust, thrust-vector angle, and pitch attitude are evident. Some

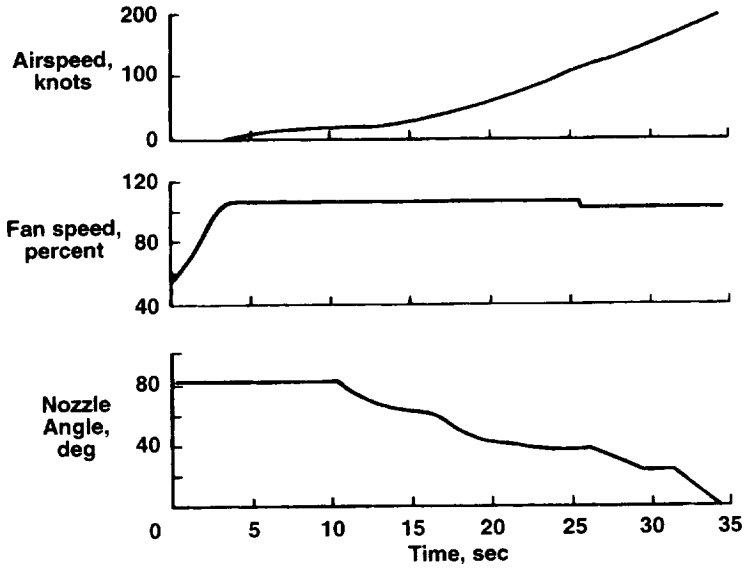

Figure 6. Time history of a vertical takeoff.

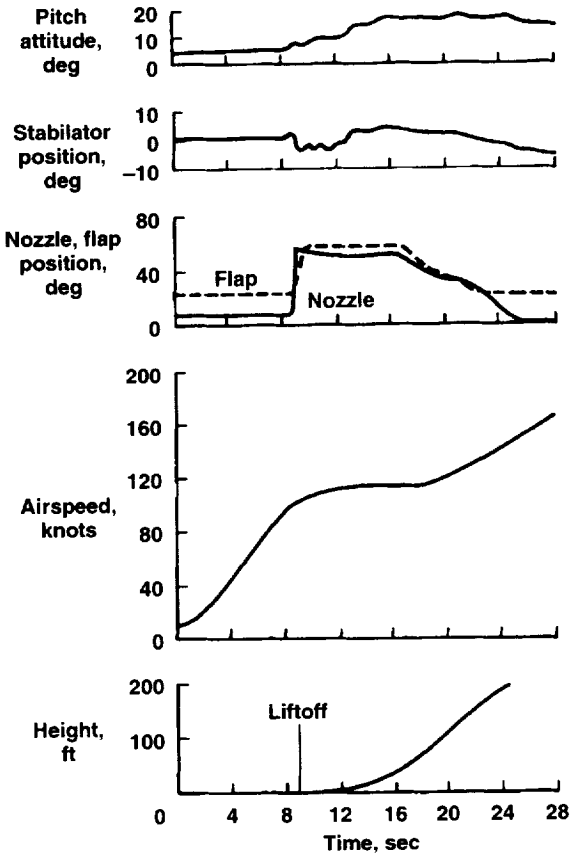

Figure 7. Time history of a short takeoff.

modulation of pitch might be necessary to precisely hold that reference attitude for climb; however, this is generally not a maneuver that demands very precise control.

The next example, shown in figure 8, is the time history for a decelerating transition to hover. The transition is initiated in level flight at an airspeed of about 180 knots. The pilot first deflects the thrust vector to 40 deg and, as the aircraft decelerates, adds thrust to provide jet lift. Again, pitch attitude is a relatively constant value. The aircraft decelerates to 140-150 knots, and the pilot selects another intermediate thrust vector setting at around 60 deg. As the aircraft decelerates further, the hover setting of 82 deg is selected and held constant for the remainder of the approach. As wing lift is lost, it is necessary to add engine thrust to sustain flight, which is done in discrete steps. Further, pitch attitude is adjusted to the reference attitude for vertical landing, again in discrete steps. None of this involves extremely high workload or pilot-in-the-loop operation. As long as this operation is carried out in clear weather, the requirement to control thrust-vector angle, thrust magnitude, and pitch attitude is not overburdening to the pilot. However, if the operation were conducted under instrument conditions, then the use of an additional control, that is, thrust-vector angle, would complicate the pilot's task significantly, particularly if required to perform a continuous deceleration to the hover. Otherwise, if this additional control manipulation were not required, the approach would be a very conventional control process, one that is performed routinely on conventional aircraft. It should be noted that control of the V/STOL aircraft is a different process than that performed on a helicopter for which the deceleration is carried out using the pitch control. Thus there are different workload implications for fixed-wing and rotary-wing aircraft for decelerating transitions.

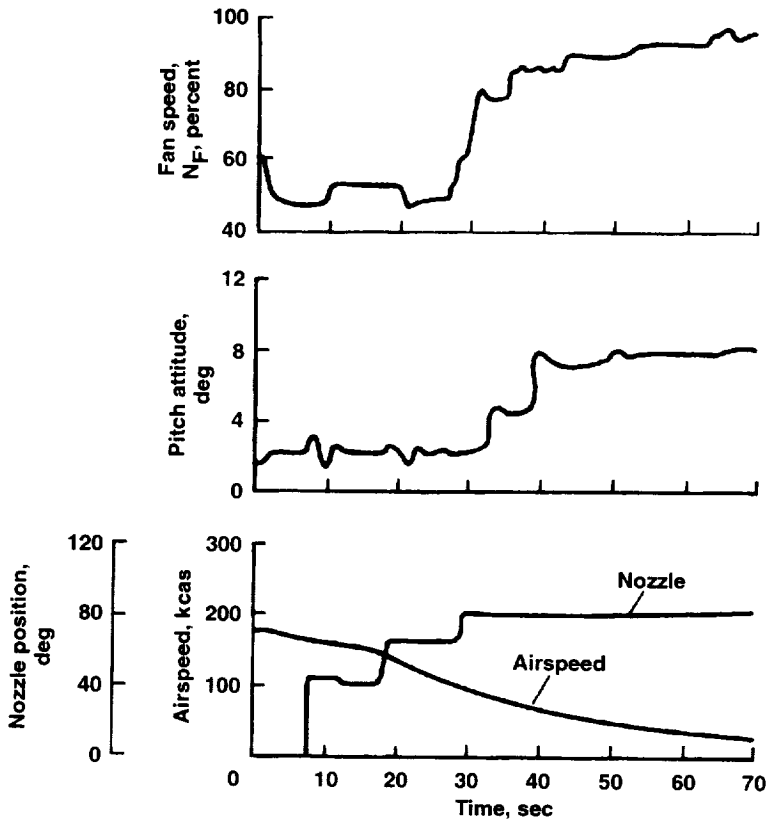

Figure 8. Time history of a decelerating transition.

Representative time histories of the vertical landing are shown in figure 9; they are typified by wandering height control, with frequent throttle corrections made in an attempt to establish a steady hover altitude and to control sink rate within limits until touchdown. A number of pitch adjustments about the nominal landing attitude were necessary to position the aircraft during the translation to the hover point and during the descent to landing. Thrust-vector angle is fixed during this maneuver. Although not shown, roll and yaw controls are typically very active for control of the lateral translation and position and for maintaining a steady heading. Thus, the

pilot is constantly in the loop controlling the hover position of the aircraft. Another variable that is important to consider for V/STOL aircraft is the temperature at the engine inlet. Temperature rise at the engine inlet from re-circulation of hot exhaust gases as the aircraft nears the ground is adverse for any V/STOL aircraft, because elevated temperatures reduce engine thrust and thus reduce hover performance. Once the aircraft enters this region of flight, the pilot finds it necessary to increase thrust to maintain an acceptable sink rate to touchdown.

The previous examples give a qualitative feel for the kinds of maneuvers that will be described analytically in the material that follows and that are illustrated with pertinent examples. The objective will be to show how pilots interact with these characteristics and how they try to control the aircraft in order to successfully perform a given task.

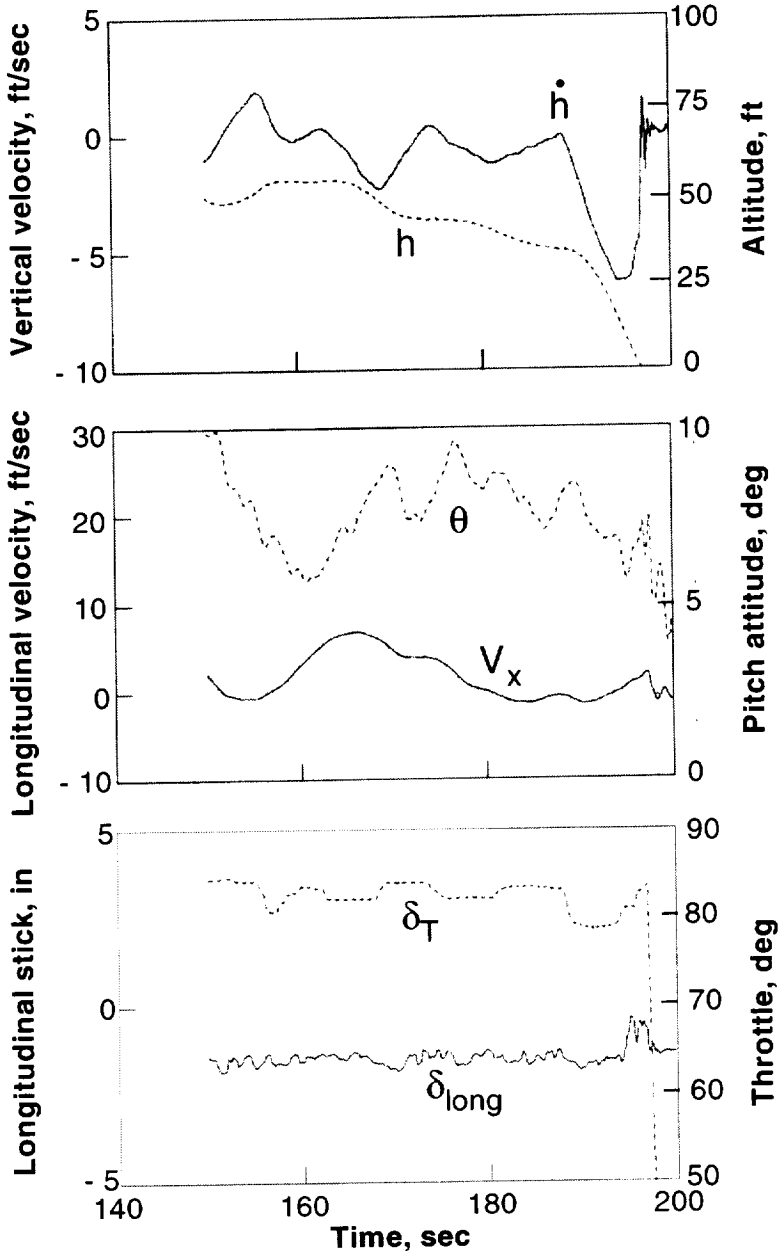

Figure 9. Time history of a vertical landing.

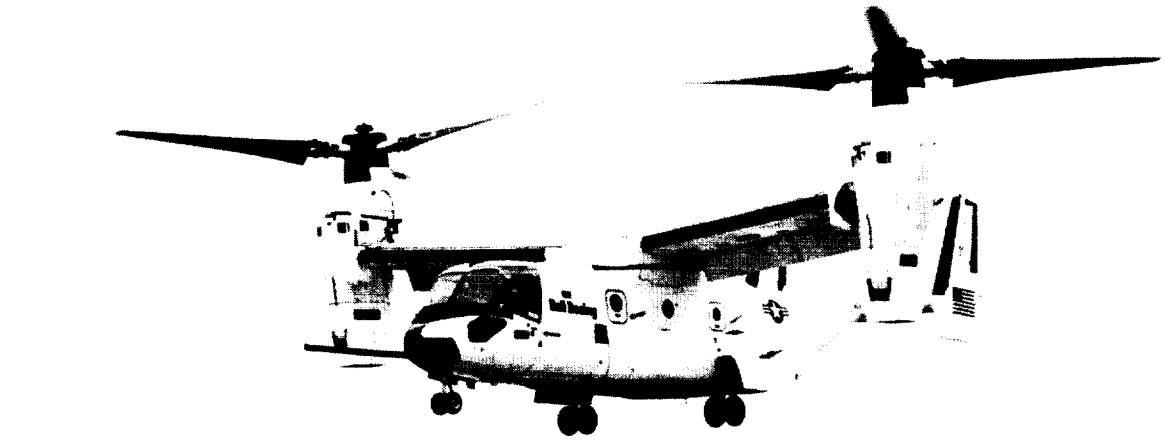

CONTROL STRATEGY AND DESIRED CONTROL CHARACTERISTICS

Control Strategy

In order to determine the pilot's control strategy, it is first necessary to define the tasks the pilot must perform to accomplish the elements of the mission. As a tool for use in describing the task and conducting the analysis, control loops such as the one shown in figure 10 are useful. The first concern is with appropriate command inputs that are associated with the control task the pilot is trying to perform. Then the response of the aircraft to those command inputs and to the individual aerodynamic or propulsion control effectors must be considered. The influence of the surrounding environment, associated with winds and atmospheric turbulence or jet-induced aerodynamic disturbances in ground proximity and hot-gas ingestion all must be taken into account.

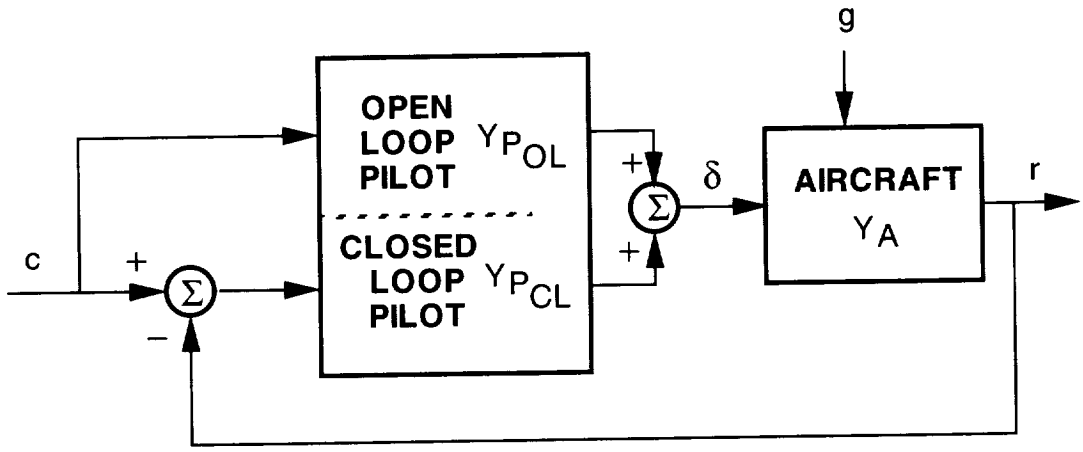

Figure 10. Pilot-in-the-loop structure.

Two control paths that the pilot employs for compensatory and precognitive control should be considered. For compensatory control, the pilot observes errors between the desired and actual response of the aircraft and applies the control to reduce or eliminate the error, as exemplified by the block labeled closed-loop pilot. If the pilot has the ability to directly observe the task command, the aircraft can be controlled to immediately follow that command without waiting for the error to develop. With a priori knowledge of the aircraft's behavior, the pilot can shape these control commands to achieve the desired response. That control action is precognitive and is exercised by the block labeled open-loop pilot. With a view of the task command, the task becomes one of pursuit tracking.

The response of the aircraft to either control inputs or disturbances may be represented by the transfer function of the aircraft with respect to the controls or by the transfer function of the aircraft with respect to the disturbances. The control input is defined both by the pilot's open-loop inputs to the command and the pilot's closed-loop inputs in reaction to the error between the

command and the aircraft's actual response. From the block diagram of figure 10, the equation describing the aircraft's response to the command inputs is

$$r = Y_A\delta + Y_g g$$

where the control input is

$$\delta = Y_{Pol}\, c + Y_{Pcl}\,(c - r)$$

Combining these equations produces the response-to-command relationship:

$$\frac{r}{c} = \frac{Y_A(Y_{Pol}+Y_{Pcl})}{1 + Y_A Y_{Pcl}}$$

It should be noted that if Y_{Pol} is nearly equivalent to $1/Y_A$, then $r/c \approx 1$ and the response follows the command almost exactly. Thus, if the pilot understands the aircraft's behavior and can tailor the control inputs such that they are effectively the inverse of the aircraft's open-loop transfer function, the aircraft's actual response can track the commanded response precisely. This presumes that the aircraft's characteristics are simple enough for the pilot to approximate in the inverse. Further, the pilot's closed-loop control can be relaxed substantially without degrading the correspondence between the aircraft's commanded and actual response. This precognitive control can make the pilot's task easier to perform, even in the face of control deficiencies in the basic aircraft. An example to consider is the coordination of the rudder with aileron during the entry into a turn. If the pilot applies the appropriate coordinating rudder along with the lateral control, the maneuver will be executed with minimal sideslip. Absent that input, if the open-loop element Y_{Pol} is zero, the only way to get reasonable correspondence between the response to the command is to drive the combined transfer function of the pilot's compensatory loop closure with the aircraft to much larger than 1. If $Y_A Y_{Pcl}$ is much larger than 1, then the response-to-command relationship is nearly 1:1. However, that places the burden on the pilot for closed-loop control, to observe the error between desired and commanded response and to manipulate the controls accordingly.

It should also be noted that for control against external disturbances where the pilot must suppress the effects of winds, turbulence, and ground effect, the pilot is unable to anticipate their effect on the aircraft. The pilot simply must react to these disturbances in compensatory fashion, and the closed-loop equation that governs this response is

$$\frac{r}{g} = \frac{Y_g}{1 + Y_A Y_{Pcl}}$$

Thus to suppress the aircraft's response to turbulence, the transfer function numerator must be small relative to the denominator. The pilot has no recourse but to increase gain until $Y_A\, Y_{Pcl}$ is large with respect to Y_g, at least over the range of frequency of the particular external disturbance and that required for the control task.

Principles concerning the structure of the pilot's closed-loop control should be stated before proceeding to specific analysis of the aircraft. Figure 11 presents control-loop structures for longitudinal and lateral-directional control based on the assumption that longitudinal control of the aircraft in the vertical plane, which involves the aircraft's pitch attitude, flightpath angle, and airspeed, can be decoupled from control in the horizontal plane, which involves bank angle, heading, and sideslip. In figure 11, the control loops that must be considered first are those that are concerned with aircraft attitudes. Pitch or roll attitudes, with respect to the horizon, are of primary importance for longitudinal or lateral control. Control of the aircraft attitude, that is, the orientation of the wing, controls the orientation of the primary force vector, which is the aircraft's lift vector, and allows the pilot to maneuver the aircraft longitudinally or laterally. Attitude changes are typically the quickest response that the pilot can generate since the controls produce very powerful moments for rotation of the aircraft. These rapid responses of the aircraft will demand the most attention of the pilot. It will be made apparent later in the text that proper control of attitude is important for improving the dynamic behavior of more slowly responding variables such as flightpath, altitude, airspeed, and heading. Thus it is essential to first understand the characteristics of the inner loops associated with attitude response.

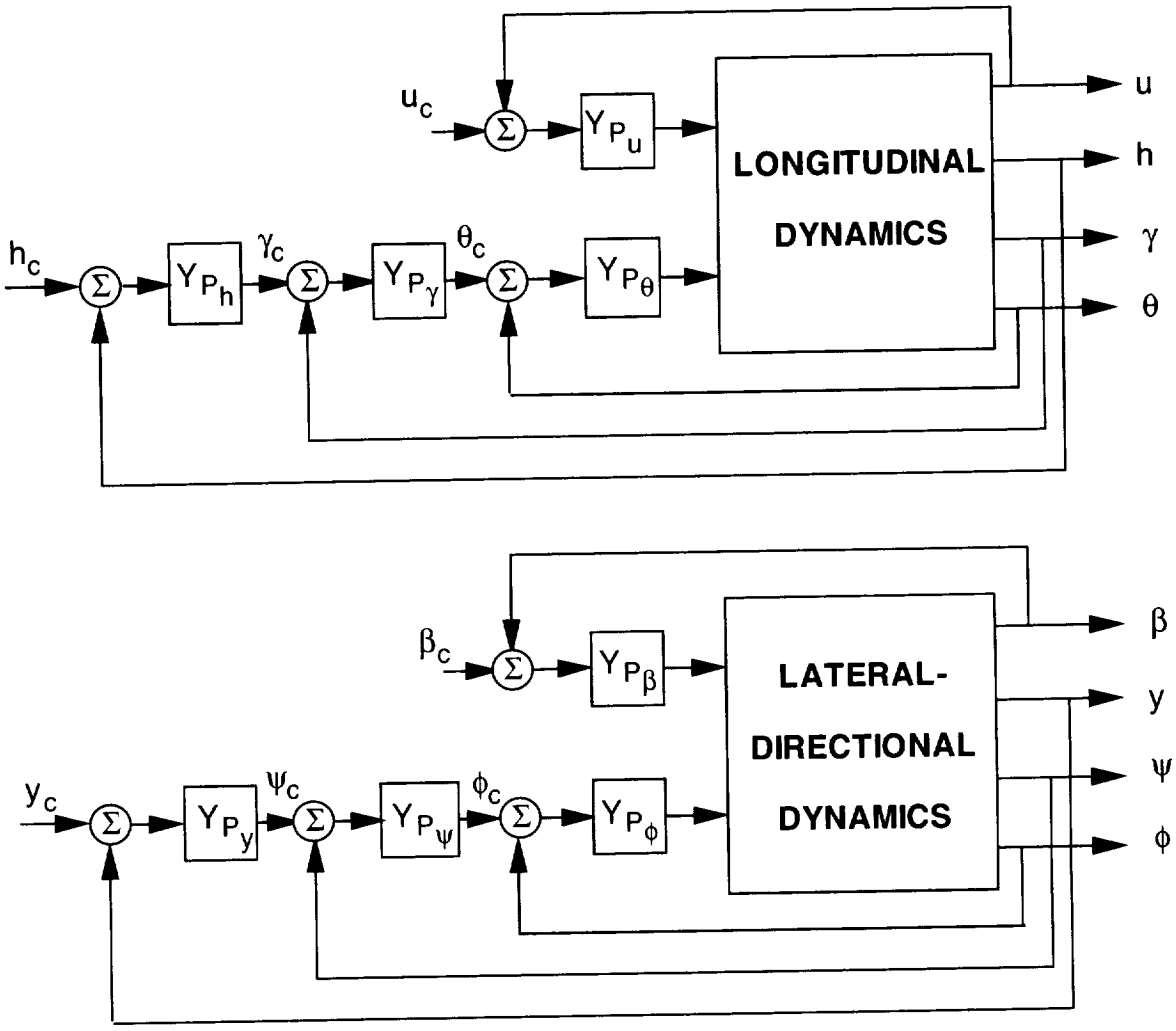

Figure 11. Loop structure for longitudinal and lateral-directional control.

Moving to the outer loops, the next concern is with the aircraft's velocity vector magnitude and orientation. Thus velocity along the flightpath, flightpath angle, heading, and course are all-important in controlling the aircraft's path through space. These are typically governed by the forces generated by the aircraft and are typically slower to respond than are the aircraft attitudes. Proper control of attitude can improve the dynamic response of the velocity vector and can help separate the time response of variations in magnitude and orientation of the vector. Finally the loops that are ultimately of concern for the aircraft's mission are the position loops, that is, altitude, lateral position with respect to track, or, in a hover control task, horizontal and vertical position with respect to the intended hover spot. These are the outermost control loops that must be considered. The discussion that follows concerning control of the aircraft will follow this loop structure, first with attitude response, followed by velocity and position responses.

Control Characteristics

With the control structure defined, the control characteristics that are associated with the aircraft's response to the individual control inputs can now be considered. The first element of the control system the pilot encounters is the control inceptor, for example, stick, pedals, throttle, and thrust-vector levers. The first impression the pilot forms of the behavior of the aircraft in response to the controls is associated with the first sensation the pilot feels, the control force characteristics of the inceptors. Thus, the features of those controls such as force gradients, breakout forces, and hysteresis, shown as examples in figure 12, are of particular concern. The gradient (the change in control force per unit control deflection) is a primary factor because it provides the pilot with one aspect of the control sensitivity of the aircraft, that is, the amount of force necessary to achieve the initial response. Further, nonlinear characteristics typical of most mechanical control devices must be considered, including hysteresis, breakout force, and changes in the force gradient with control deflection. Too much hysteresis can lead to unpredictable response whereas too much breakout may make precise control difficult to achieve. Considering the nonlinear force gradient shown in the example, as the control is deflected it reaches a point where more force per unit deflection is required to move the control in comparison to that required about the neutral position. Nonlinear gradients of this sort might force the pilot to adapt different control

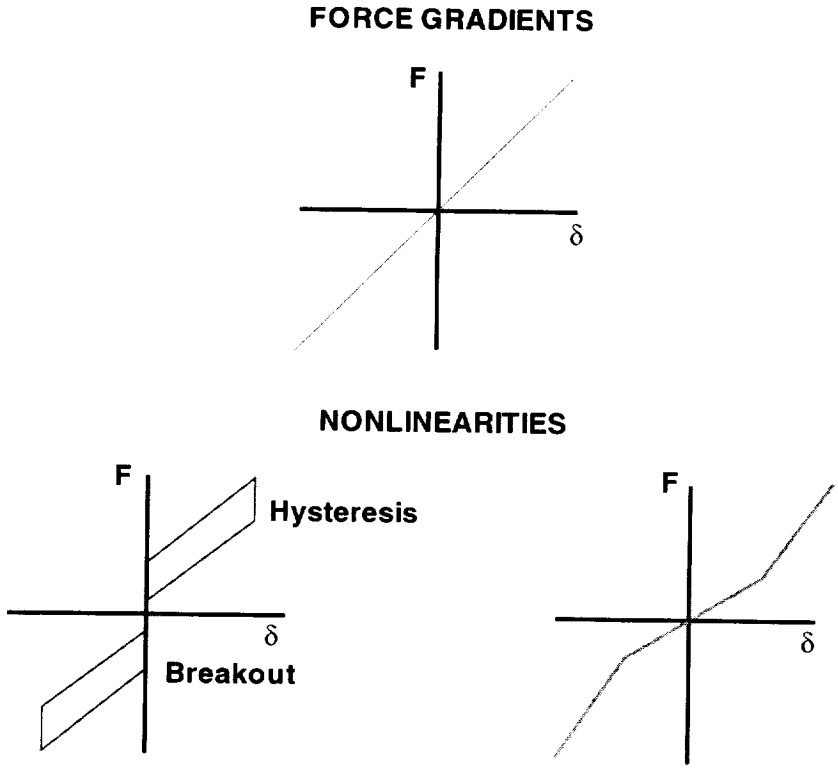

Figure 12. Examples of control force characteristics.

techniques for precise versus large maneuvers. It should also be noted that harmony between the pitch- and roll-control forces, that is the correspondence between the forces in the two axes and the control to be achieved, is important. For example, if the longitudinal forces on a center stick were very heavy and the lateral forces were very light, the pilot could, in applying longitudinal force against the heavy gradient, make inadvertent lateral inputs that could corrupt the aircraft's roll response.

Turning to the aircraft's response to the individual controls, it is appropriate to first consider the response in the steady state before assessing transient response characteristics. These control characteristics are typically covered in a study of aircraft static stability and control. For example, consider an aircraft's longitudinal control requirement versus angle of attack. The gradient, or amount of control required per unit angle of attack, provides an indication of the static stability of the aircraft and, at the limit, indicates the total authority of the pitch control. A related aspect of static stability is the ability to trim the aircraft, to allow it to fly hands-off without need for the pilot to continually adjust the controls to maintain a steady flight condition. This characteristic is referred to as the unattended behavior of the aircraft. It allows the pilot freedom to divert attention to other tasks such as communications and navigation without having to continuously intervene in the aircraft's control. Frequently it is difficult to achieve those characteristics, because aircraft flying at low speed or in hover tend to be unstable and thus require that the pilot constantly stay in the control loop.

Transient response of the aircraft to the controls can be assessed either in the time or frequency domain. These characteristics can be derived from the differential equations that describe the aircraft equations of motion as will be reviewed subsequently. The characteristics of concern in the time domain are illustrated in figure 13 (a). Control sensitivity, which is the initial slope of the aircraft's response to a step control input, is one factor of concern. Sensitivity in either extreme is detrimental to precise control. How quickly the aircraft begins to respond can be characterized by the fraction of time required to reach the intended response, classically the time constant or time to 63 percent of the steady-state response. It provides an indication of how quickly the aircraft will move from the initial state to the final steady-state value that the pilot is seeking. In addition, any delay present in the initial response, such as would be attributed to computational delays or higher-order dynamics in the system, will be perceived by the pilot as potentially detrimental to precise control. Other factors that govern the shape of this response concern how much the transient peak differs from the steady state. The pilot will be very aware of how the aircraft is responding initially. However, if the transient response persists and the pilot's attention is diverted, the response may be entirely different than anticipated from the short-term observation. Thus, factors such as overshoot in the response are important.

Another view of response characteristics is provided in the frequency domain. These characteristics are derived by using the Laplace transform to convert the basic differential equations to functions of the Laplace operator. Then it is possible to consider the amplitude and phase of the aircraft's response as a function of frequency as illustrated in figure 13(b). Characteristics of the magnitude, such as whether the response is amplified at a given frequency, how it decays with increasing frequency, and how it lags in the response as a function of frequency are meaningful to the pilot. Bandwidth of the response is a representative criterion for assessing control characteristics. The system's bandwidth provides an indication of the range of frequencies over which

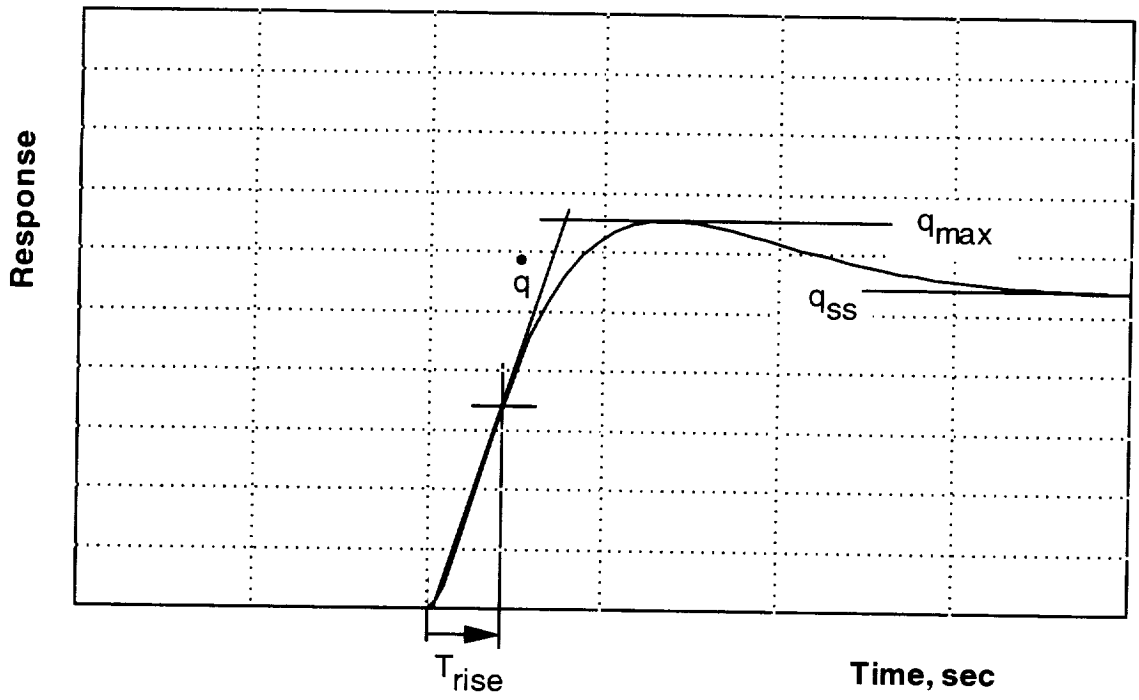

(a) Representative time response.

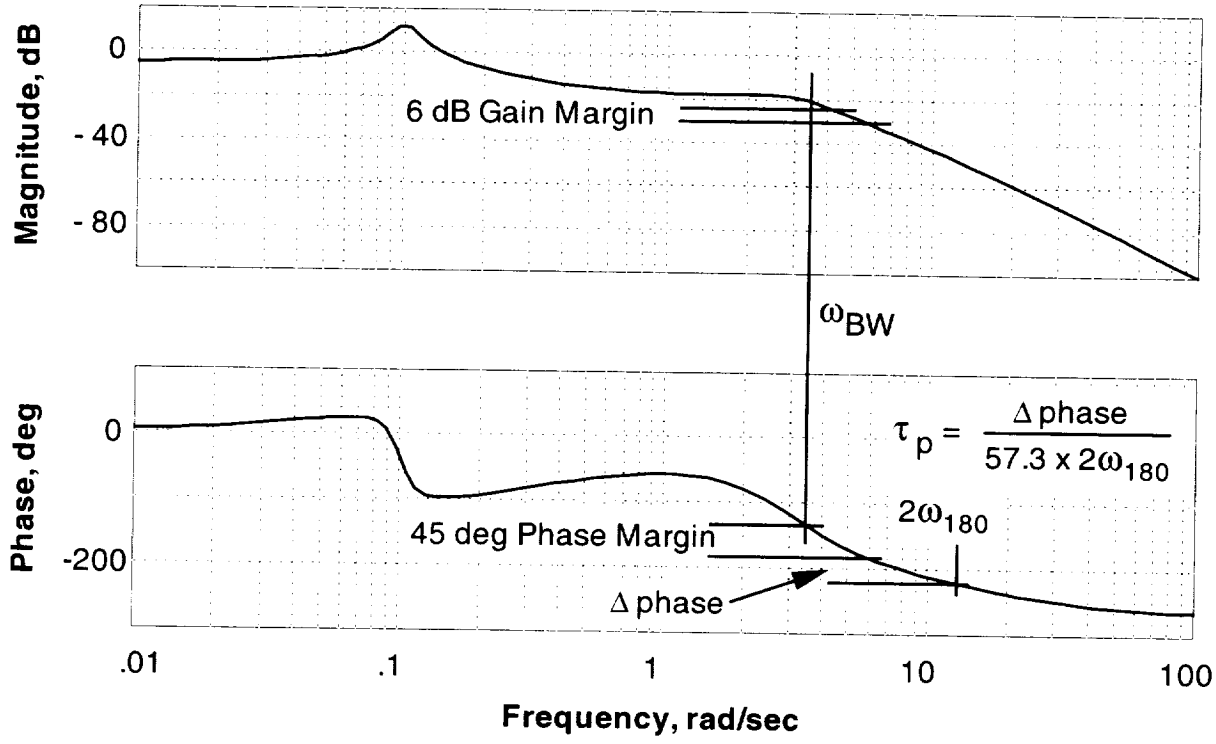

(b) Representative Bode plot.

Figure 13. Examples of time and frequency response characteristics.

the aircraft's response reasonably follows the pilot's control inputs without substantially falling off in magnitude at high frequency or without substantially lagging the pilot's control input. Bandwidth is determined as shown in the figure by the frequency at which a phase margin of at least 45 deg and a gain margin of at least 6 dB are preserved. Phase margin is an indication of the aircraft's stability in the range of frequencies the pilot is trying to control. Gain margin is a measure of the sensitivity of system stability to variations in system gain. The rate of change of phase lag in the vicinity of 180 deg is also of interest as an indicator of the sensitivity of stability to changes in gain at the upper limits of the system's bandwidth. The system's phase delay can be extracted from the change of phase lag in this region as shown in the figure. The time and frequency responses shown are indicative of pitch attitude response to the longitudinal stick in forward flight.

Pilot Models

In order to carry out analyses of the aircraft's flying qualities, it is necessary to have a mathematical representation of the pilot. Pilot models are typically represented in transfer function form that relate the pilot's control output in response to perceived error in the aircraft's response compared to the desired command:

$$Y_p = K_p \frac{(T_L s + 1)}{(T_I s + 1)} \frac{e^{-\tau s}}{(T_p s + 1)}$$

The first element of the transfer function is a constant factor or gain that determines the control input the pilot commands in proportion to the perceived error. The pilot can also perform dynamic compensation such as lead and lag as indicated in the equation. Lead compensation quickens the response of the aircraft by effectively anticipating the amount of control required in response to the error in the aircraft's response. By contrast, lag compensation acts to smooth the control application to high-frequency content or to noise in the error. These are forms of compensation that the pilot consciously applies and can adjust. Elements that cannot be adjusted are associated with the transport delay; they involve visual observation and mental processing of the information. Further, human muscle structure cannot respond instantaneously to commands to move and it exhibits a lag in response which is represented by the first-order term T_p in the equation. There can be high-order terms in this transfer function as well, including shaping factors in both numerator and denominator; they will not be considered further. Although they have been measured, they are not of significance to the control loops of concern in this analysis. For the dynamics of interest, representative values for time delay are of the order of $\tau = 0.2$ sec; the time lag T_p is approximately 0.1 sec. Implications of these delays for pilot-in-the-loop control are noted in the discussion to follow.

The pilot must be able to adjust the control gain over a wide range, to either control the aircraft tightly or loosely, without significant stability implications for control of the aircraft. In instances where system stability limits restrict the gain range, that is, where the pilot must use a very precise control gain, the aircraft's flying qualities will be judged to be poor. When the pilot has a great deal of latitude in adjusting the control gain, the aircraft's response would be considered more favorably. When the pilot is compelled to generate lead or anticipation in control in

response to errors in the aircraft's response, the aircraft's flying qualities will degrade. Mental effort associated with this anticipation increases workload and ultimately causes the pilot to judge that the aircraft has poor control characteristics. The pilot can generate a small amount of lead without unduly penalizing the aircraft's flying qualities, but when the amount of lead approaches a time constant of the order of 1 sec or more, it can be expected that the aircraft's handling will be rated poor. On the other hand, generating lag can be accomplished without penalty; it is performed at low frequency to smooth the aircraft's response and is not conducive to higher workload.

In the sections to follow, the aircraft's response will be analyzed and implications will be drawn concerning the pilot's control required to achieve the desired response. Consideration will be given to the amount of lead compensation the pilot must generate and its likely influence on flying qualities. For an initial assessment, the simplest form of pilot model, a pure gain, will be used to evaluate response characteristics. If simple gain adjustments in the absence of lead compensation can achieve the desired response, the aircraft's flying qualities are likely to be satisfactory. When the response does not meet the desired standards and lead is required to achieve the desired response, judgments must be made as to whether the aircraft's flying qualities will be good or bad based on the amount of lead required. There will be instances where it is necessary to take into account the pilot's higher-order dynamic properties as well. Typically, for analytical purposes, these dynamics will be represented by the transport delay. It is important to include these effects when there is concern with stability margin. If stability margin is low enough to yield pilot-induced oscillations or outright instabilities, then it is essential to take into account the amount of time delay or high frequency lag introduced by the pilot into the system. Under these circumstances, the time delay might be increased to 0.25 to 0.3 sec in order to assess the sensitivity of the control loop to this delay.

The form of the pilot transfer function shown here was identified from laboratory measurements, acquired from human subjects using a simple control manipulator to adjust the error between a reference line and a moving target on an oscilloscope display. By changing the dynamics of the response of the error display to the control input, the characteristics of the human controller were identified. Reference 12 is the historical source for this research, and it provides an excellent compendium of human behavior in single-loop control tasks. The text that follows will not go into further detail on pilot modeling, since the primary emphasis will be on the influence of the aircraft characteristics on the pilot's control tasks. The reader is referred to the literature on manual control for greater depth of treatment of the subject, such as further research by the authors of reference 12 and the research of Hess at the University of California at Davis (e.g., ref. 13).

Pilot Rating of Aircraft Flying Qualities

In the analysis performed with the aircraft and pilot models noted previously, it is possible to make credible predictions of the aircraft's response characteristics. The aircraft's response can also be measured accurately in flight. Pilot workload consists of both the mental and physical effort required to control the aircraft to achieve the desired response. Mental effort, which is difficult to quantify, is associated, for example, with anticipation required to generate lead to compensate for poor aircraft response characteristics. Physical workload can be described as the

work the pilot must expend in deflecting the control inceptors against their resisting force. Reference 14 is the primary source of information for pilot-in-the-loop flying qualities assessment, particularly the evaluation of pilot workload. The principal contribution of that document is contained in the handling qualities rating scale shown in table 2. This scale represents the procedure pilots have used to assess workload for the past 30 years. Similar rating scales were initially devised independently by the authors, George Cooper at NASA Ames Research Center and Robert Harper at Cornell Aeronautical Laboratory. Eventually, the two authors collaborated to create the current version of the scale referenced above.

TABLE 2. COOPER–HARPER HANDLING QUALITIES RATING SCALE

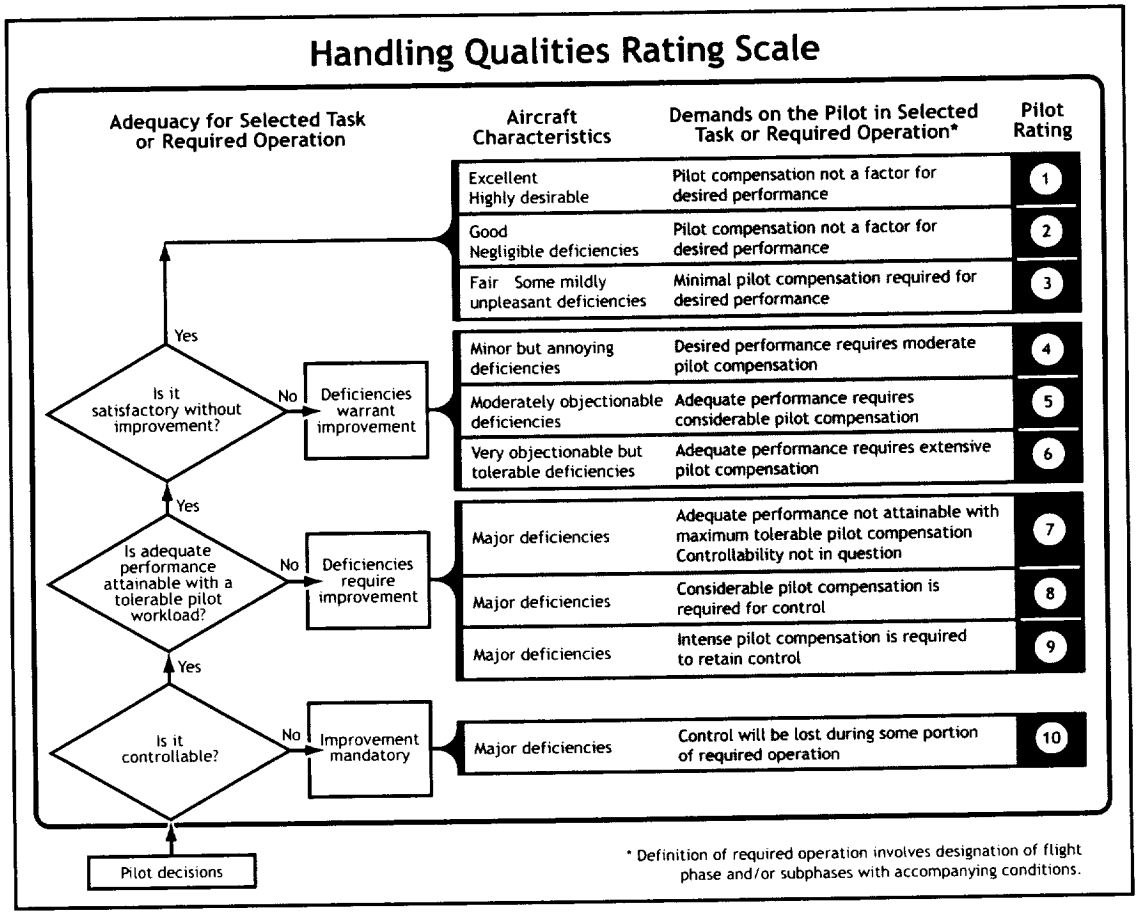

The scale is an adjective-based ordinal scale accessed by a decision tree as seen in the table. Within the table, the pilot must determine if the aircraft can be controlled to the performance demands of a specific task and then assess the level of mental and physical effort required to achieve that level of performance. The first judgment the pilot makes upon entering the decision tree is whether the aircraft is controllable or not. If not, the aircraft is not controllable for the task the pilot must perform, and in some cases the aircraft will crash. As an example, consider a precision shipboard vertical landing. If the aircraft controllability was so poor that the pilot could not safely touchdown on the landing pad and had to abort the landing, the pilot would rate the aircraft not controllable for the task and the rating would be 10, the worst available. If the pilot judges that

the aircraft is controllable in the task, the second decision concerns whether adequate performance can be achieved. Certain performance standards are demanded for a given mission task. For example, adequate performance for a vertical landing on the ship might be considered as touching down within a 10-ft circle while controlling the aircraft's bank angle within 1 deg. If this performance cannot be achieved, although the aircraft can be safely operated in the task, the pilot cannot routinely accomplish the intended objective. Hence, the deficiencies in the aircraft's behavior require improvement before the aircraft can be judged to have acceptable flying qualities for the task. There are further adjective qualifiers that refer to the level of effort the pilot must exert to perform the task, regardless of whether adequate performance can be achieved; these are associated with the numerical ratings of 7, 8, and 9 on the scale. When adequate performance can be achieved, the next decision to be made is whether the aircraft's control is satisfactory without further improvement, that is, whether the pilot can control the aircraft precisely without having to provide compensation to attain desired performance. If the pilot is able to achieve the desired performance from the aircraft with very little mental or physical effort, flying qualities are judged to be satisfactory without need for improvement.

Consider the adjective qualifiers that are associated with achieving desired performance. Using the vertical landing example, desired performance might mean landing within a 5-ft circle. If pilot compensation is not a factor and the pilot intervenes minimally in the control loop, a rating of 1 might be assigned. That rating is rarely assigned, primarily because pilots are never certain that the characteristics are the best that can be achieved. When slightly annoying deficiencies are present in the aircraft's behavior, even though desired performance is still achieved, a rating of 2 would be appropriate; this is frequently the best rating pilots will assign and it still reflects excellent flying qualities. If the pilot is required to generate some compensation, typically in the form of lead or anticipation, some mildly unpleasant deficiencies exist and the pilot would assign the aircraft a rating of 3. However, in all of these cases, the performance of the aircraft for the task intended is very good and the designer is not required to alter the aircraft configuration or control system. If the answer at this juncture in the decision tree is that the aircraft is not satisfactory without improvement, then the pilot must assess the compensation required to achieve performance that is acceptable for the mission or task. If the pilot judges that it requires only moderate compensation to attain desired performance, the flying qualities will be rated a 4. When the pilot is forced to compensate for deficiencies in the aircraft's response to the maximum extent possible to achieve adequate performance, the associated rating is 6.

When the Cooper–Harper scale is used to determine design criteria, the criteria typically refer to "levels" of flying qualities that relate to distinct bands on the scale. In particular, Level 1 corresponds to Cooper–Harper ratings of 3 or better, Level 2 to the range of 4 through 6, and Level 3 to ratings of 7 through 9. A rating of 10 is not considered within these levels of flying qualities since the aircraft would be incapable of performing the designated task. A Level 1 aircraft is easy to fly, and the Cooper–Harper scale shows the adjective rating to be satisfactory without improvement. This aircraft would perform the designated task acceptably without need for modification. A Level 2 rating poses a difficult choice for the designer and operator. The aircraft is not satisfactory for performing the task and has deficiencies that warrant improvement. These deficiencies may range from tolerable to annoying to intolerable. It is within this range of flying qualities where significant design trades are made, typically with regard to the cost required to improve the flying qualities. When the aircraft is a borderline Level 2/Level 3, improvements

are strongly recommended because the pilot would be unable to reliably perform the intended task. If the ratings were borderline Level 1/Level 2, it is reasonable to question whether the deficiencies warrant the cost required for improvement to Level 1. For an aircraft assessed to be Level 3, modifications are mandatory to achieve acceptable flying qualities.

The accuracy of the Cooper–Harper scale has been shown to be quite acceptable for flying qualities design guidance and specification. Although the rating-scale decisions are qualitative, if the pilot's evaluations are performed for a well-defined task and if the pilot understands what must be accomplished, very repeatable results can be achieved. The scatter present in data from properly trained and skilled pilots is typically ±1 rating unit, except at the upper end of the scale. If the task is ill defined or if a trained pilot is not involved in the evaluation, then the data scatter can become excessive. The latter case would be comparable to using an uncalibrated or insensitive force balance in a wind tunnel test. The instrument must be properly calibrated, and in this case the instrument must be a trained and skilled test pilot. In aircraft stability and control design, the Cooper-Harper scale has been one of the enduring technical contributions. It has been tested for 30 years as researchers have attempted to define more quantitative measures of workload. No one has yet been able to arrive at measures that approach the accuracy and the repeatability of this qualitative rating scale.

Example Linear System Analysis

Before proceeding to analyze the characteristics of V/STOL aircraft in order to perform a flying qualities assessment, it is useful to review the proposed analysis methods as they are applied to an evaluation of aircraft dynamics. The example is concerned with linear systems analysis and uses classic root locus, Bode plots, and time histories of the aircraft's response to the controls in the evaluation. Given the equations of motion for the aircraft, the transfer function G(s) that represents the relationship of the response of the aircraft to a control input is

$$\frac{r}{\delta} = G(s)$$

The equation is a function of the Laplace operator s, a complex number having a real part s, and an imaginary part jω. Furthermore, this transfer function can be written in terms of a constant multiplying a numerator polynomial in s divided by a denominator polynomial. The analysis is performed in the frequency domain, because the calculations can be performed algebraically,

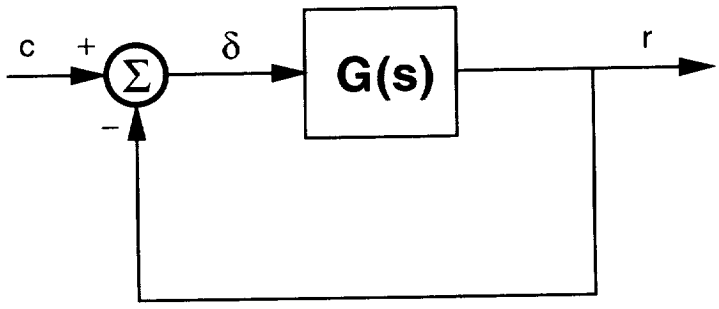

Figure 14. Example system block diagram for pilot-in-the-loop analysis.

allowing simple estimates to be made of the effect of aircraft characteristics on the aircraft's response to the pilot. Further, flying qualities evaluations can be made in the frequency domain using tools such as root locus and Bode plots. The results can be inversely transformed back to the time domain to derive the time solution. The system can be represented graphically in terms of a block diagram (fig. 14). The block G(s) is the open-loop system that relates the response of the aircraft to a control input. It describes how the response of the aircraft to the command input is influenced by the aircraft's aerodynamic, propulsion, control system, and mass distribution characteristics. In the analysis of flying qualities, a loop is closed around the open-loop system to assess the closed-loop behavior of the system. Collecting terms to solve for the closed-loop system response r to the command input c, in terms of the open-loop system G(s) yields

$$\frac{r}{c} = \frac{G(s)}{1 + G(s)}$$

The closed-loop denominator 1 + G(s) is a polynomial in s that describes the characteristic equation of the system, the roots of which determine system stability. The solution of this polynomial determines the values of the roots s of the characteristic equation 1 + G(s) = 0, revealing the influence of the transfer function gain, numerator, and denominator of 1 + KN(s)/D(s) = 0. The location of these roots on the complex plane indicate the nature of the transient response, foremost the stability of the response. For example, if the system consisted of one root that fell on the negative real axis, the system would have a stable exponential response. Conversely, if this root lies on the positive real axis, the response would exponentially diverge. In the case of a solution with a complex pair of roots in the left half of the complex plane, the response would be oscillatory with an exponentially convergent envelope reflecting the negative real part. In contrast, if the real part were positive, this response would be oscillatory and exponentially divergent.

Root locus plots can be used as analytical tools to illustrate the variation of roots of the characteristic equation as a function of a parameter such as a feedback gain or the pilot's control gain K. Figure 15 shows an example root locus plot for a system that has a fifth-order denominator; open-loop roots are indicated by the x's. The use of this plot in inter-

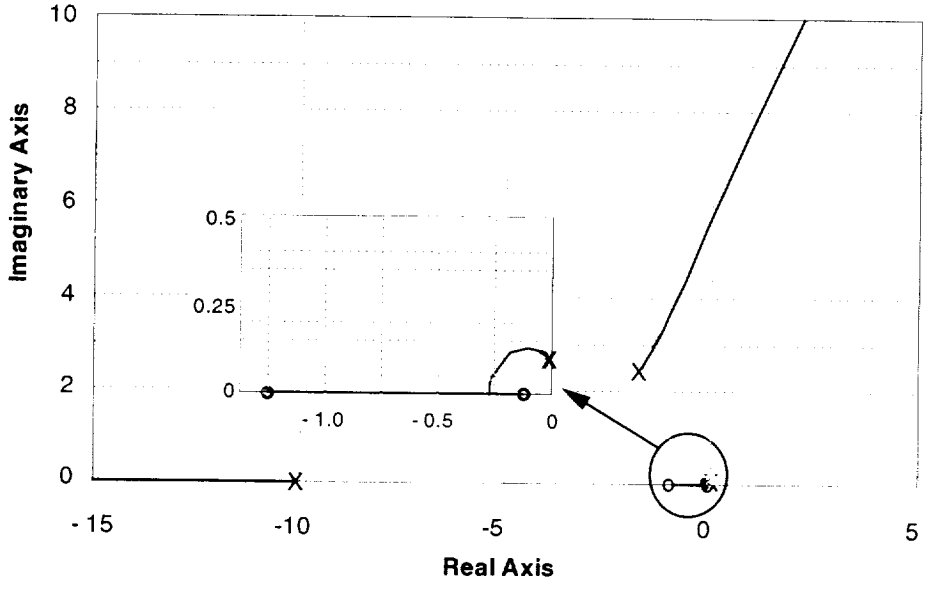

Figure 15. Example root locus plot.

preting closed-loop control characteristics based on the characteristics of the open-loop system, is helpful in interpreting how features of the aircraft influence its closed-loop control by the pilot. However, it should be appreciated that the characteristic roots only partially account for the aircraft's response to controls. Although they determine system stability and the system's characteristic modes, additional and important factors are influenced by the numerator as well. The magnitude and phasing of the response to the pilot's control input are established by the complete closed-loop transfer function.

Another useful analytical tool is the Bode plot of the frequency response characteristics of the aircraft. The example shown in figure 16 is a plot of the open-loop transfer function magnitude and phase, where the magnitude is presented in decibels (dB = 20 $\log_{10}$) and the phase is shown in degrees. Both are plotted as a function of the log frequency in units of radians per second. From linear systems analysis, closed-loop stability of the system exists when the gain of the open-loop transfer function is less than unity for a phase lag greater than (more positive than) −180 deg. The solution of the set of roots for the value of σ and $j\omega$, for which the magnitude is equal to unity for a phase lag of −180 deg (or odd multiples thereof) corresponds to neutral stability and represents the stability boundary. This solution occurs when the roots pass from the left half to the right half of the complex plane. These results apply when the transfer function gain K is positive. When the gain is negative, the solution for neutral stability lies at +1 rather than at −1 and is equivalent to a phase angle of 0 deg (or even multiples of π radians). Although the Bode plot represents the frequency response of the open-loop system, closed-loop characteristics can be inferred from the open loop. If the open-loop gain of G(s) at low frequency is large compared to unity, the gain of the closed-loop transfer function G(s)/[1 + G(s)] will be approximately unity. The latter is sought

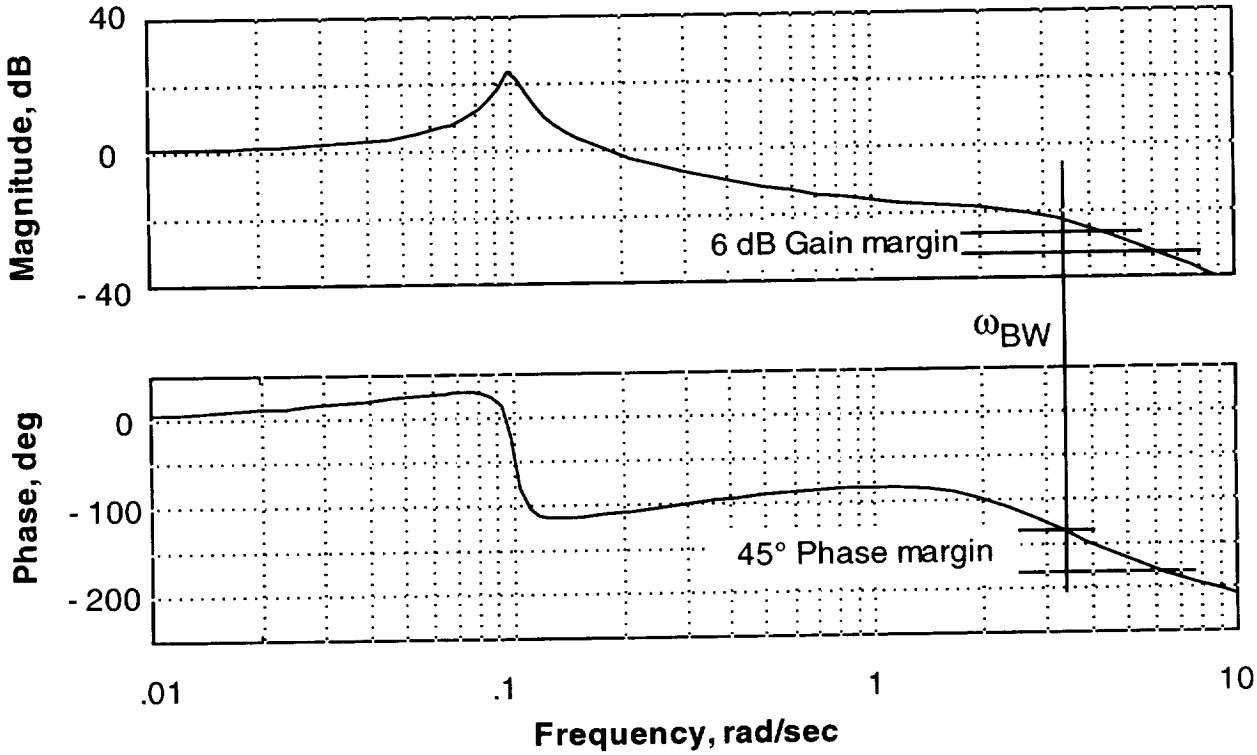

Figure 16. Example Bode plot.

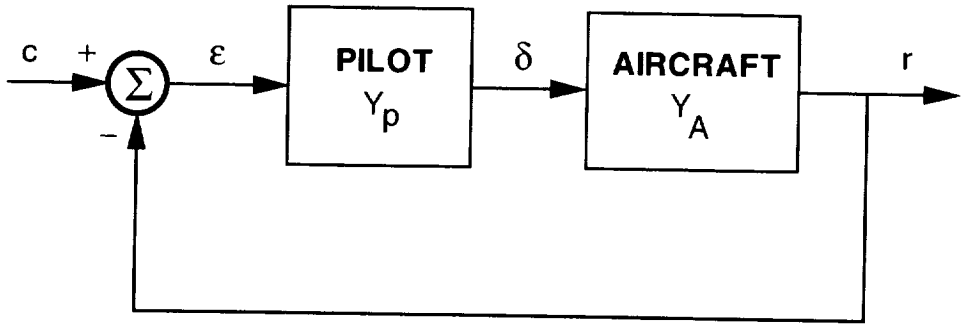

Figure 17. Example block diagram of pilot-in-the-loop control.

to insure good command tracking by the aircraft's response. At high frequency, the open-loop gain is much less than unity, thus the open- and closed-loop characteristics coincide. To insure adequate stability margins at the desired frequency of control for the specified control task (known as the crossover frequency), adequate gain and phase margins from the stability boundary, for example, gain margin > 6 dB, phase margin > 45 deg, must be present. Further, in the region of the crossover frequency ω_{BW}, the slope of the open-loop transfer function magnitude plot should be proportional to the inverse of frequency (i.e., G(s) ~ K/s). This feature provides tolerance to variations in the pilot or system gain or open-loop characteristics over the frequency range important to the pilot's control.

The following example of closed-loop bank-angle control by the pilot will be used to illustrate the application of the analytical methods noted above in the assessment of the aircraft's flying qualities. A similar approach will be taken in the study of V/STOL flying qualities in hover and forward flight. From the closed-loop block diagram of figure 17, the closed-loop response to the pilot's command input is represented by

$$\frac{r}{c} = \frac{Y_p Y_A}{1 + Y_p Y_A}$$

where, in this case, the pilot Y_p will be represented simply by a gain K_p. The aircraft example is for open-loop bank-angle response to lateral control and is given by

$$Y_A = \frac{L_{\delta_A}}{s(s + 1/T_R)}\left(\frac{1}{T_A s + 1}\right)$$

where lateral control sensitivity L_{δ_A}= 1 rad/sec^2/rad, the roll mode time constant T_R = 2 sec, and a control surface actuator has an unusually high time constant T_A = 0.25 sec. Root locus and Bode plots of the system are presented in figure 18(a). From the root locus, it can be seen that the closed-loop roots of the third-order system will become unstable as the pilot's gain increases. In this case, the system reaches neutral stability for a gain of 2.25 at a frequency of 1.4 rad/sec.

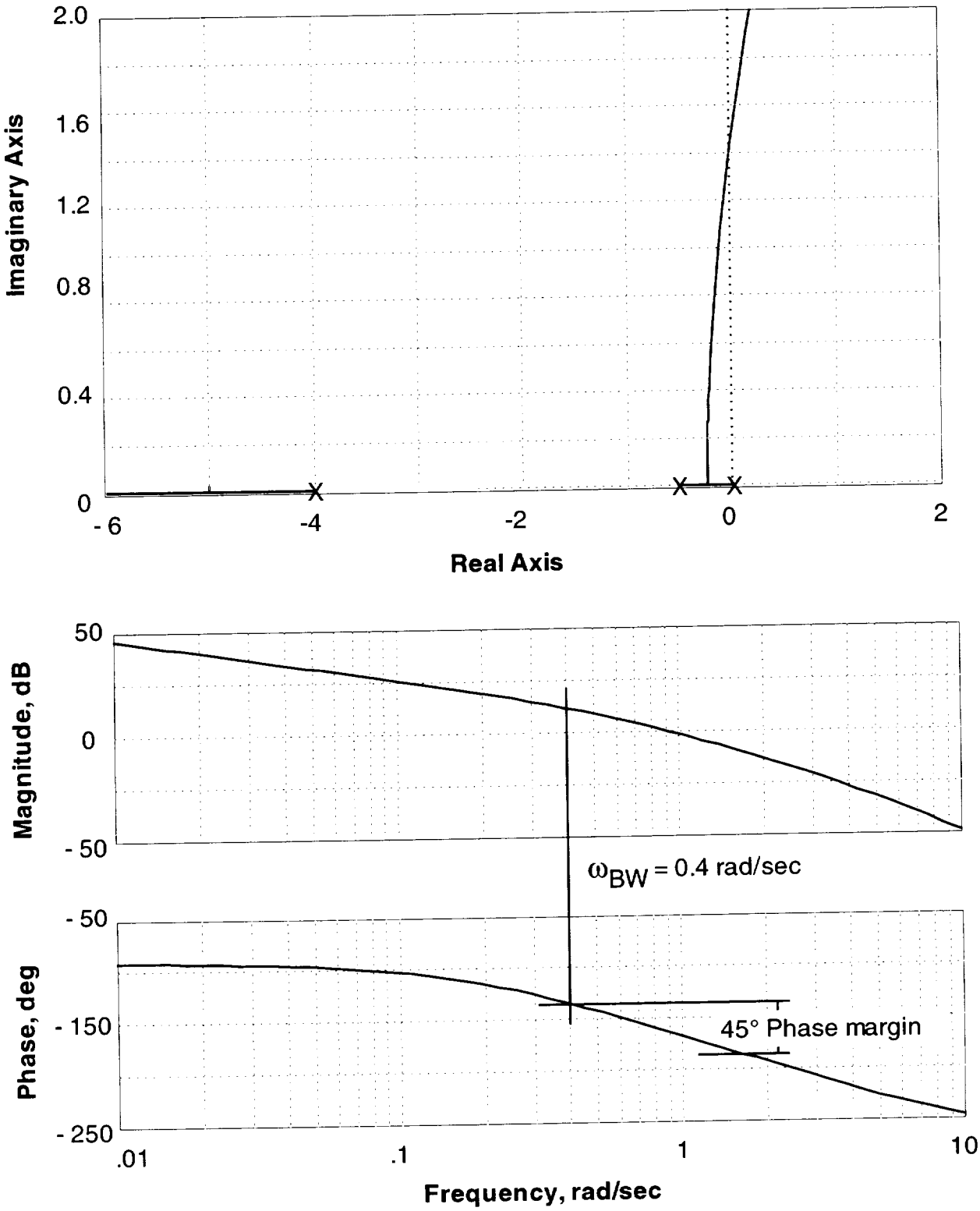

(a) Without pilot lead.

Figure 18. Root locus and Bode plots of bank-angle control.

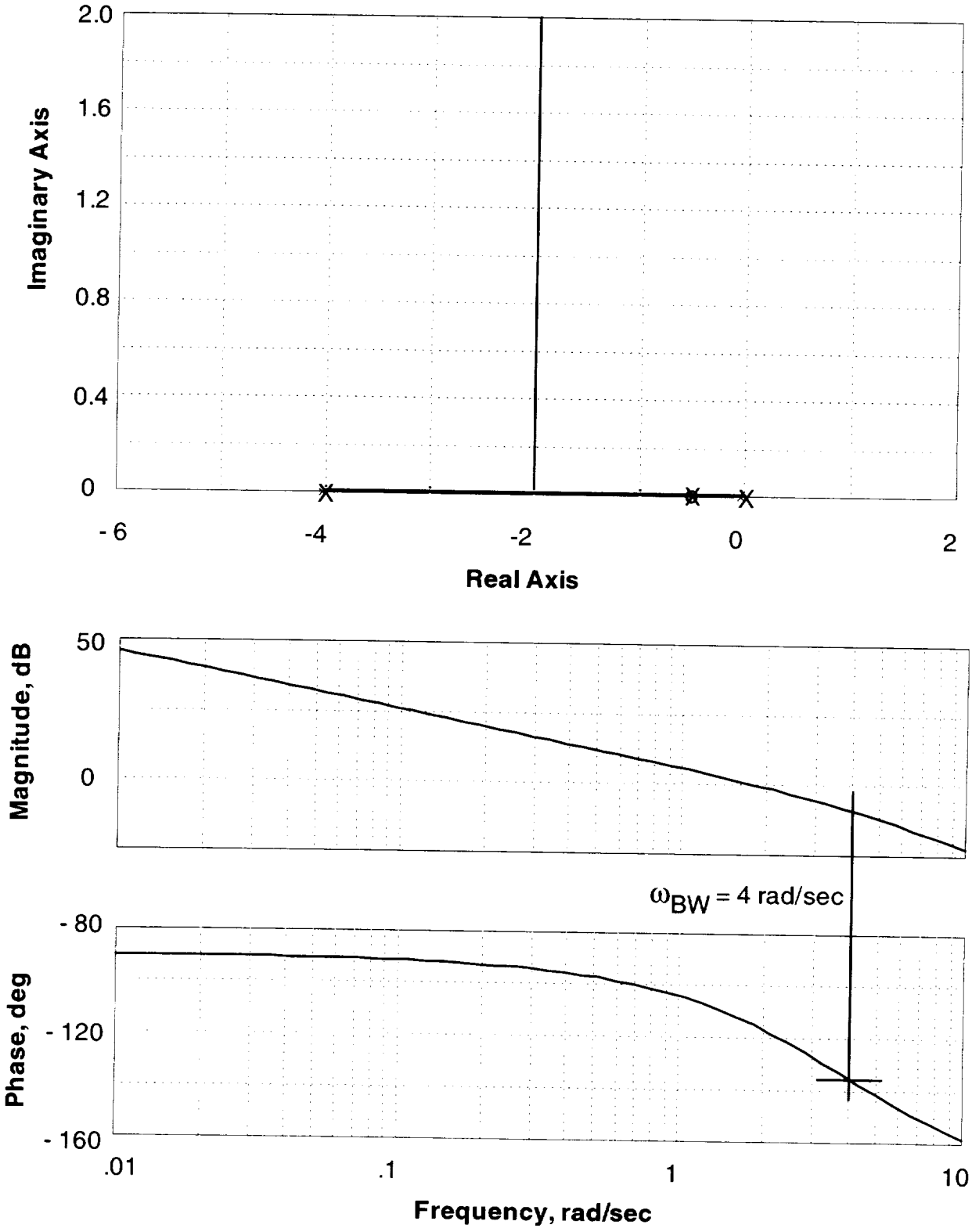

(b) With pilot lead.

Figure 18. Concluded.

This low bandwidth is a consequence of the large roll time constant and sluggish actuator response, both of which were selected to illustrate poor flying qualities and the need for pilot compensation to achieve desirable bank-angle response. From the Bode plot, neutral stability is also evident at a natural frequency of 1.4 rad/sec at which a phase lag of 180 deg is reached. The bandwidth for a stability margin of 45 deg is only 0.4 rad/sec, which is well below that sought for precise roll control. To achieve a desirable control bandwidth of 4 rad/sec with adequate phase margin requires that lead compensation be provided by the pilot. As can be seen from the alternative example in part (b) of the figure, the 4 rad/sec bandwidth can be achieved with a first-order lead time constant of 2 sec. In this case, system stability exists for all pilot gains. However, the lead compensation comes with the penalty of increased anticipation of control inputs by the pilot, hence increased mental effort and workload. Consequently, the roll control flying qualities for the basic aircraft would be judged to be poor.

For use in the flying qualities analyses in the sections to follow, the stability derivatives for five examples of fixed-wing V/STOL aircraft are provided in the appendix; four rotary-wing aircraft cases are included there as a contrast for the fixed-wing counterparts.

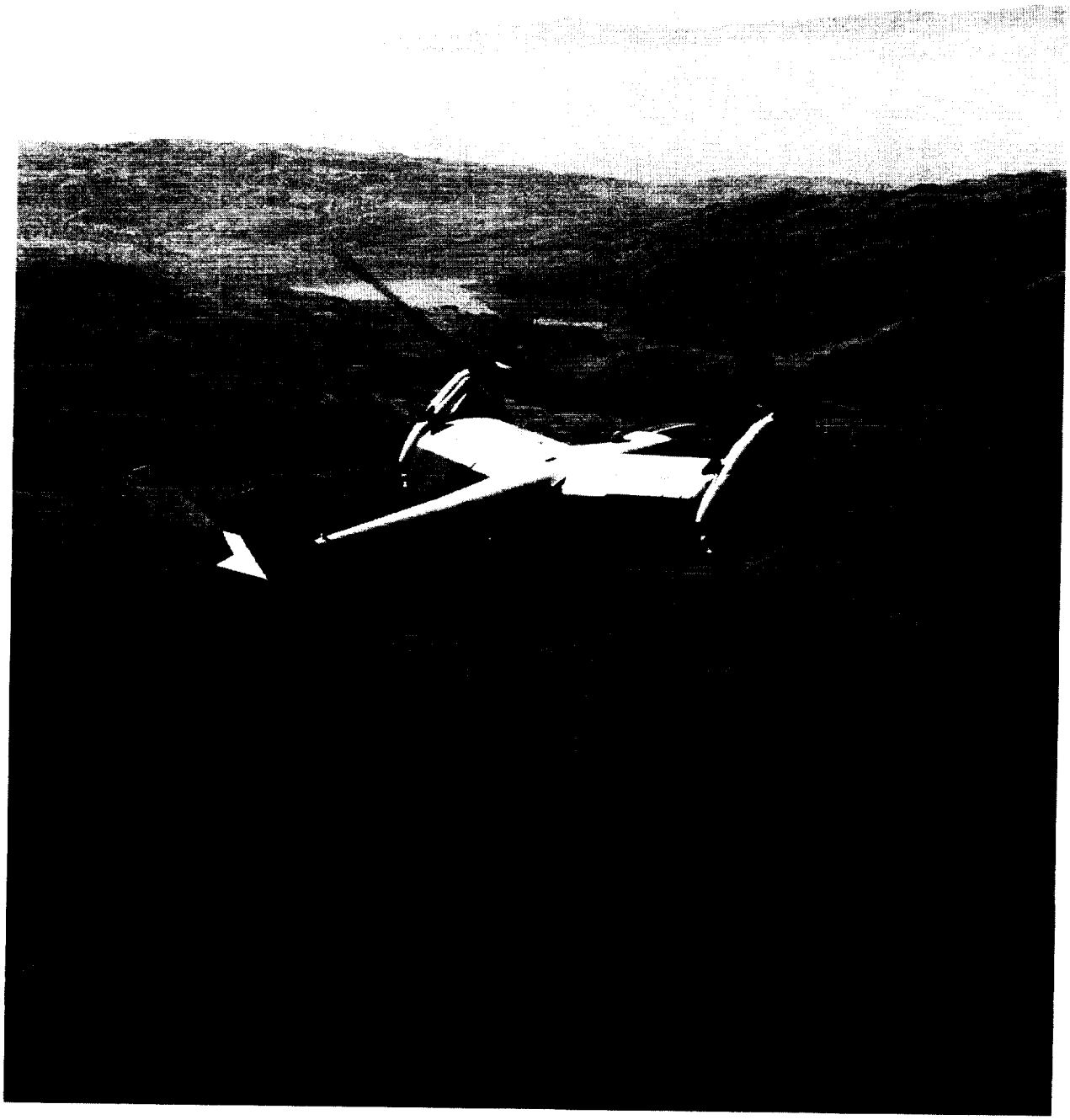

EQUATIONS OF MOTION FOR HOVER AND FORWARD FLIGHT

Before beginning the discussion of V/STOL aircraft flying qualities, it is appropriate to review the equations of motion for hover and forward flight. The aircraft axis system on which the forces, moments, and linear and angular velocities are based is shown in figure 19. It is a right-hand system originating at the center of gravity of the aircraft with the longitudinal or x-axis pointing forward out the nose, the lateral or y-axis pointing out the right wing, and the vertical or z-axis pointing downward. Forces and velocities along the longitudinal axis are positive forward. Rolling moments, angular velocities, and bank angles about the longitudinal axis are positive for right-wing-down rotations. For the lateral axis, forces and velocities are positive out the right wing, and pitching moments about that axis are positive aircraft nose-up as are angular rates and pitch attitude. Along the vertical axis, forces are positive downward, as are vertical velocities. Yawing moments about the vertical axis are positive aircraft nose-right as are angular rates and yaw angles. The axis system can be oriented in the aircraft arbitrarily, for example, with the longitudinal axis along a body reference line or with respect to the relative wind at the initial condition being considered (fig. 20). The latter is known as a stability axis system and is the axis orientation frequently selected for aircraft

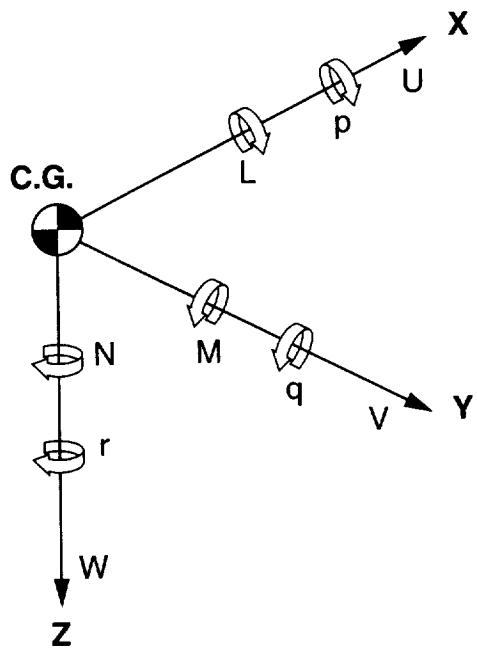

Figure 19. Aircraft axis system.

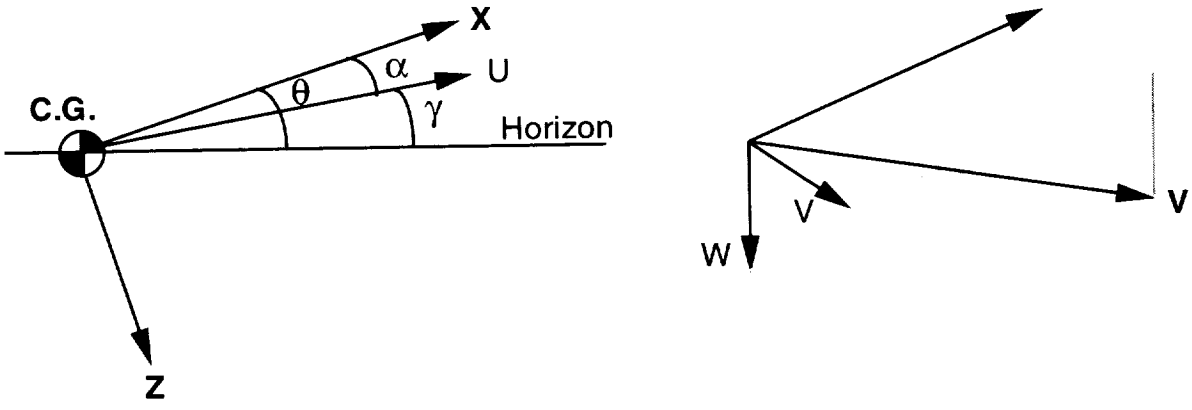

Figure 20. Orientation of the aircraft axis system.

dynamics analyses. The inclination of the velocity vector with respect to the horizon is the flightpath angle, and the angle of attack of the aircraft is the angle between the longitudinal component of the velocity vector and the longitudinal reference axis. Frequently it is desirable to refer to flightpath angle alternatively in terms of aircraft pitch attitude and angle of attack. As shown in the figure, for wings-level flight, $\gamma = \theta - \alpha$. In general, when the velocity vector does not fall in the x-z plane, that is, when the aircraft has some lateral and vertical as well as longitudinal velocity, it can be seen from the figure that angle of attack can be defined in terms of the vertical and longitudinal velocities as the arctangent of their ratio, $\alpha = \tan^{-1}(W/U)$; the sideslip angle is defined by the angle between the lateral velocity and the total velocity vector, $\beta = \sin^{-1}(V/V)$.

The foregoing definitions can be found in reference textbooks on flight dynamics (e.g., refs. 15-17). The equations of motion shown in table 3 come from the same sources. These equations are written in matrix notation in state space form and are the perturbation equations of motion about a steady flight condition. Starting from the top of the matrix, the equations are those for longitudinal force along the x-axis, vertical force along the z-axis, and pitching moment about the y-axis. The next equation relates rate of change of pitch attitude to body-axis rates through the Euler angles for non-wings-level conditions. Following are the side-force equation along the y-axis, the rolling moment equation about the x-axis, and, at the bottom of the matrix, the yawing moment equation about the z-axis. The next to last equation relates rate of change of roll angle with body-axis rates for conditions of nonzero bank angle and nonzero pitch attitude. As written, the equations are in the body-axis reference frame with the initial pitch angle noted. If written in a stability-axis reference frame, the initial angle would instead be flightpath angle and the initial vertical velocity term W_o would be zero. The aircraft state variables are the perturbation velocities along the longitudinal and vertical axes, pitch rate and pitch attitude, lateral velocity, roll rate, bank angle, and yaw rate. On the left-hand side are state rates pre-multiplied by the matrix containing the aircraft inertia properties and the stability derivatives proportional to state rate. The latter are aerodynamic terms that may or may not be significant, but that in general should not be ignored. One is associated with pitching moment as a function of transient vertical velocity that is related to lag in the transmission of the wing downwash to the horizontal tail of a conventional aircraft. Also, there are terms that provide rolling and yawing moments in proportion to rates of change of lateral velocity. Both result from rates of change of sidewash at the vertical tail in relation to sidewash at the center of gravity of the aircraft. As a consequence of these off-diagonal terms, the matrix at the left is not an identity; thus to write these equations in the traditional state space form it is necessary to invert the left-hand matrix and pre-multiply both sides of the equation with it. The terms on the right-hand side of the equality are force and moment contributions due to the aircraft states and to the control input of interest. In this example, the control is a generalized input that could be taken as elevator, aileron, rudder, thrust, or thrust deflection, depending on which is appropriate for the aircraft configuration. This control input will be specific to the examples presented in the application of these equations to a particular problem. The coefficients in these matrixes are dimensional perturbation coefficients that have been divided through by the mass or moments of inertia of the aircraft as appropriate. Thus, as examples, $X_u = (1/m)(dX/du)$ for axial force and $M_u = (1/I_y)(dM/du)$ for pitching moment due to changes in longitudinal velocity.

TABLE 3. SIX-DEGREE-OF-FREEDOM EQUATIONS OF MOTION

$$
\begin{bmatrix}
1 & 0 & 0 & 0 & 0 & 0 & 0 & 0 \\
0 & 1 & 0 & 0 & 0 & 0 & 0 & 0 \\
0 & -M_{\dot{w}} & 1 & 0 & 0 & 0 & 0 & 0 \\
0 & 0 & 0 & 1 & 0 & 0 & 0 & 0 \\
0 & 0 & 0 & 0 & 1 & 0 & 0 & 0 \\
0 & 0 & 0 & 0 & -L_{\dot{v}} & 1 & 0 & -I_{xz}/I_{xx} \\
0 & 0 & 0 & 0 & 0 & 0 & 1 & 0 \\
0 & 0 & 0 & 0 & -N_{\dot{v}} & -I_{xz}/I_{zz} & 0 & 1
\end{bmatrix}
\begin{Bmatrix} \dot{u} \\ \dot{w} \\ \dot{q} \\ \dot{\theta} \\ \dot{v} \\ \dot{p} \\ \dot{\phi} \\ \dot{r} \end{Bmatrix} =
$$

$$
\begin{bmatrix}
X_u & X_w & X_q - W_o & -g\cos\theta_o & X_v & X_p & 0 & X_r + V_o \\
Z_u & Z_w & Z_q + U_o & -g\cos\phi_o \sin\theta_o & Z_v & Z_p - V_o & -g\cos\theta_o \sin\phi_o & Z_r \\
M_u & M_w & M_q & 0 & M_v & M_p & 0 & M_r \\
0 & 0 & \cos\phi_o & 0 & 0 & 0 & 0 & -\sin\phi_o \\
Y_u & Y_w & Y_q & -g\sin\phi_o \sin\theta_o & Y_v & Y_p + W_o & g\cos\phi_o \cos\theta_o & Y_r - U_o \\
L_u & L_w & L_q & 0 & L_v & L_p & 0 & L_r \\
0 & 0 & \sin\phi_o \tan\theta_o & 0 & 0 & 1 & 0 & \cos\phi_o \tan\theta_o \\
N_u & N_w & N_q & 0 & N_v & N_p & 0 & N_r
\end{bmatrix}
\begin{Bmatrix} u \\ w \\ q \\ \theta \\ v \\ p \\ \phi \\ r \end{Bmatrix} +
\begin{Bmatrix} X_\delta \\ Z_\delta \\ M_\delta \\ 0 \\ Y_\delta \\ L_\delta \\ 0 \\ N_\delta \end{Bmatrix} \delta
$$

Several assumptions of significance were made to arrive at these equations. First, the equations originally related the total forces and moments imposed on the aircraft by aerodynamic and gravitational components to their respective translational and angular accelerations. From these equations, the steady-state forces, moments, and kinematics are removed leaving terms associated with perturbations in the aircraft's states and controls. Thus, the motions defined are those fluctuations about the trimmed flight condition of interest. The equations are derived for rigid-body motion of the aircraft and neglect structural flexibility. It is assumed that the aircraft is of constant mass. The equations are Earth-referenced and, for this application, a flat Earth is assumed. They are written in the body-axis reference frame and are defined for straight, though not necessarily wings-level, flight. They are based on small-angle approximations that assume small angles of rotation about the trim conditions. The equations do not display any dynamics associated with the control system such as servo dynamics or dynamics of the propulsion system. These features will be introduced separately as those aspects of the control problem arise.

Many applications permit the simplification of these six-degree-of-freedom equations into two, independent three-degree-of-freedom sets. Considerations of rotorcraft flight dynamics dictate that the six-degree-of-freedom set be retained and even expanded to include the dynamics of the rotor system. For example, pitching moment due to roll rate (and vice versa), pitching moment due to a yaw control application, or yawing moment due to a collective-pitch control application reflect cross-coupling between lateral and longitudinal degrees of freedom that are characteristic of helicopters. Coupling due to the aircraft states and to the controls can exist in general, and examples of these effects will be noted where appropriate. For fixed-wing V/STOL aircraft, it is reasonable to neglect the terms that couple the longitudinal and lateral-directional

motions and to separate the system into two sets of four equations. These two sets correspond to the longitudinal degrees of freedom, including the longitudinal force, the vertical force, and the pitching moment equation, and to the lateral-directional degrees of freedom, including side force, rolling moment, and yawing moment. In these cases, the terms above and below the diagonal in the upper right and lower left quadrants of the full matrix equations are assumed to be insignificant. Furthermore, it is assumed that no control cross-coupling terms exist. These simplifications are based on the assumptions that the aircraft is in wings-level flight and that it has symmetry about the X-Z plane. These assumptions are reasonable for fixed-wing aircraft and, in some instances (though only infrequently) for rotary-wing vehicles. Notice also the absence of terms on the left-hand side, like $X_{\dot{w}}$ and $Z_{\dot{w}}$, whose presence can only rarely be justified by fluid physics. Terms such as Y_p and Y_r are frequently ignored as well, and in some cases $L_{\dot{v}}$ and $N_{\dot{v}}$, particularly near hover, are also neglected.

Longitudinal Hover Equations

Given the preceding background, the simplification afforded by decoupling the longitudinal and lateral-directional equations, particularly for flight in or near hover can be considered. The longitudinal motions are described by the states for longitudinal speed, vertical speed, pitch angular rate, and pitch attitude, and by the longitudinal and vertical force and the pitching moment equations along with the equation to relate pitch attitude and pitch rate:

$$\begin{Bmatrix} \dot{u} \\ \dot{w} \\ \dot{q} \\ \dot{\theta} \end{Bmatrix} = \begin{bmatrix} X_u & 0 & 0 & -g \\ Z_u & Z_w & 0 & 0 \\ M_u & M_w & M_q & 0 \\ 0 & 0 & 1 & 0 \end{bmatrix} \begin{Bmatrix} u \\ w \\ q \\ \theta \end{Bmatrix} + \begin{Bmatrix} X_\delta \\ Z_\delta \\ M_\delta \\ 0 \end{Bmatrix} \delta$$

Note that the derivatives X_w, X_q, and Z_q are neglected and that the hover pitch attitude is zero. Aerodynamic forces near hover are insufficient for these derivatives to be significant in comparison to those terms shown in the matrix. The latter are primarily determined by inlet flow momentum and by jet-induced effects in and out of ground effect.

The influences on stability of the aircraft in hover appear in the longitudinal characteristic equation:

$$s^4 + (-X_u - M_q - Z_w)s^3 + (X_u M_q + X_u Z_w + Z_w M_q)s^2 + (gM_u - X_u M_q Z_w)s + g(Z_u M_w - M_u Z_w) = 0$$

This equation typically factors into two first-order roots and a complex pair of roots. If pitching moment due to vertical velocity is neglected ($M_w = 0$), one of the first-order factors is defined by the aircraft's normal acceleration due to vertical velocity or heave damping:

$$(s - Z_w)\left[s^3 - (X_u + M_q)s^2 + X_u M_q s + gM_u\right] = 0$$

Eventually it will be seen that this term contributes to one of the aircraft's primary modes of motion. The third-order term typically is composed of the other first-order root and the complex

pair. With the additional assumption that pitching moments due to forward velocity are zero ($M_u = 0$), the roots simplify even further to

$$s(s - Z_w)(s - X_u)(s - M_q) = 0$$

with a root at the origin, the first-order heave damping root, and two other first-order roots, one of which is defined by the aircraft's longitudinal acceleration in proportion to longitudinal velocity and its pitch angular acceleration in proportion to pitch rate. If this assumption is valid, the heave damping root would be associated with the aircraft's vertical velocity response, the longitudinal damping with the aircraft's longitudinal velocity response, and the pitch damping term with the pitch response to control inputs. Each response corresponds to an exponential term in the time domain, and the inverse time constants are equal to the three damping derivatives. However, pitching moment due to forward speed typically is not zero and the more complicated form is appropriate.

An example for the Harrier, using the hover characteristics from the appendix, illustrates the points made previously. If pitching moment due to forward speed is zero, the characteristic equation is

$$s(s + 0.031)(s + 0.023)(s + 0.047) = 0 \quad \text{for } M_u = 0$$

whereas if M_u takes on its actual value, the equation becomes

$$(s + 0.031)(s + 0.23)[\, s^2 - 2\,(0.41)(0.19)\, s + (0.19)^2] = 0 \quad \text{for } M_u \neq 0$$

where the notation for the complex pair is $\zeta = 0.41$, $\omega = 0.19$. In either case, the vertical velocity time constant is 32 sec, reflecting the low damping in the vertical axis in hover. Longitudinal and pitch damping are similarly low when pitching moment due to forward velocity is zero. However, if this derivative is nonzero, the location of the roots associated with forward speed and pitch response change substantially. The unstable complex pair of roots appears with a low-frequency oscillatory response at 0.19 rad/sec. Thus the response would not diverge rapidly, although the forward speed and pitch-attitude response would couple in the oscillation. Finally, if pitching moment due to vertical velocity is significant, the roots factor into

$$(s - 0.087)(s + 0.265)[\, s^2 - 2\,(0.19)(0.2)\, s + (0.2)^2] = 0 \quad \text{for } M_u, M_w \neq 0$$

It is apparent that the contribution of M_w has been to create an unstable real root, and that the other first-order root is largely unchanged. The instability of the complex pair is somewhat reduced compared to the case in which M_w is zero.

Root locus plots are useful in visualizing how characteristics of the aircraft influence the characteristic roots. For example, consider the contribution of the effect of pitching moment due to longitudinal velocity. The characteristic equation is rewritten in root locus format to isolate the derivative M_u as a parameter in the equation (with $M_w = 0$):

$$\frac{gM_u}{s(s - X_u)(s - M_q)} = -1$$

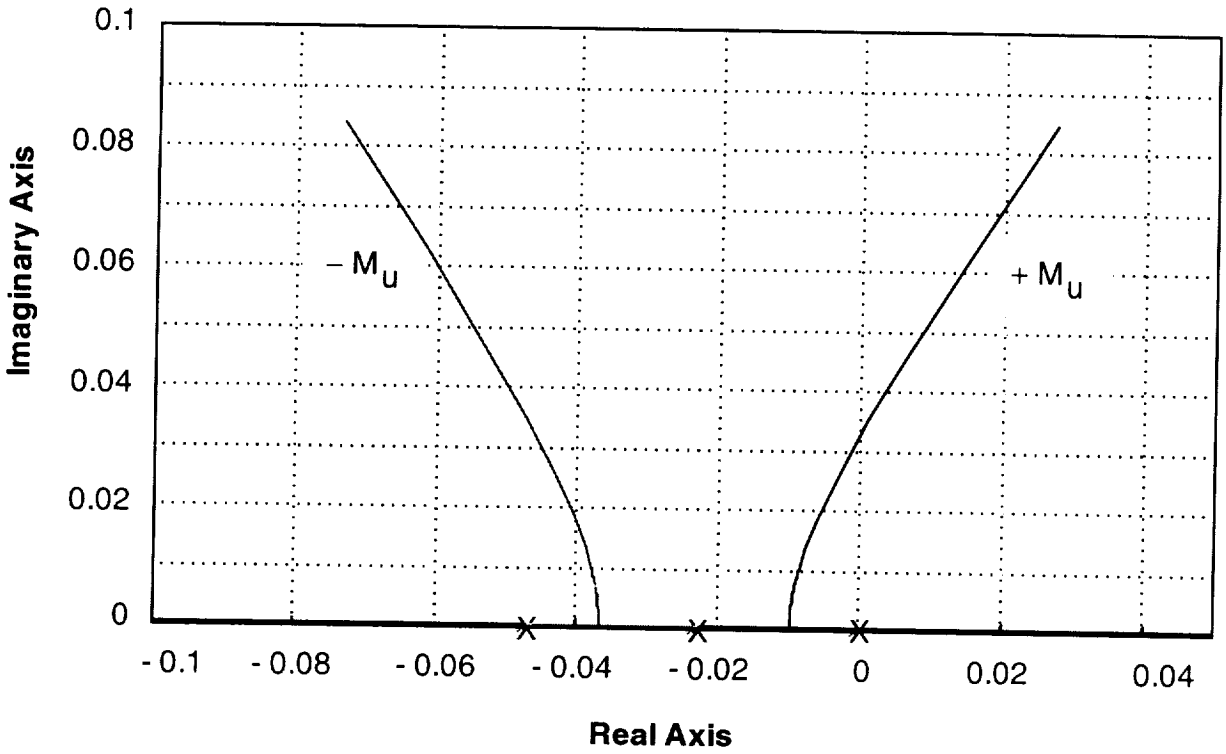

Figure 21. Root locus plot of contributions of M_u derivative to longitudinal characteristic roots.

In the root locus plot of figure 21, the value of M_u varies either positively or negatively, and the characteristic roots migrate as indicated. Starting with the case with no contribution from pitching moment due to longitudinal velocity, the respective roots appear at the origin and at the values for longitudinal velocity damping and pitch damping noted above. With a positive increase in M_u, the roots progress to the unstable complex pair and to two stable real roots. The heave damping root at $-Z_w$ does not move and is not shown on the plot. When M_u is negative, a stable oscillatory pair emerges and the root at the origin moves into the right-half plane. Whatever the value of pitching moment due to forward velocity, the aircraft's overall stability is not improved.

Lateral-Directional Hover Equations

The lateral-directional motions are described by the states for lateral velocity, roll and yaw angular rate, and roll attitude. The lateral-directional equations are composed of the side force, rolling and yawing moment equations, and the equation to relate roll attitude and roll rate:

$$\begin{Bmatrix} \dot{v} \\ \dot{p} \\ \dot{\phi} \\ \dot{r} \end{Bmatrix} = \begin{bmatrix} Y_v & 0 & g & 0 \\ L'_v & L'_p & 0 & L'_r \\ 0 & 1 & 0 & 0 \\ N'_v & N'_p & 0 & N'_r \end{bmatrix} \begin{Bmatrix} v \\ p \\ \phi \\ r \end{Bmatrix} + \begin{Bmatrix} Y_\delta \\ L'_\delta \\ 0 \\ N'_\delta \end{Bmatrix} \delta$$

As in the case of the longitudinal equations for hover, this set is simplified to include only those terms that produce significant aerodynamic or gravitational forces or moments. Note that the cross-product of inertia does not appear in these equations. To simplify the form of the original equations, the inverse of the inertia matrix pre-multiplied both sides of the equation and the product of that inverse and the state and control matrices appear in the form shown above. The "primed" rolling and yawing moment derivatives that appear in the matrices are defined as follows:

$$L' = \frac{L + (I_{XZ}/I_{XX})N}{1 - (I_{XZ}^2/I_{XX}I_{ZZ})} \qquad N' = \frac{N + (I_{XZ}/I_{ZZ})L}{1 - (I_{XZ}^2/I_{XX}I_{ZZ})}$$

If the cross-product of inertia is zero, the unprimed derivatives and their primed counterparts are identical.

The lateral-directional characteristic equation that arises from these equations of motion is fourth-order and consists of a pair of real roots and a complex pair:

$$(s + 1/T_r)(s + 1/T_R)(s^2 + 2\zeta\omega_d s + \omega_d^2) = 0$$

If the derivative L'_r is negligible, the first real root can be approximated by $1/T_r = -N'_r$, the yaw rate damping derivative. The remaining first-order and complex pair of roots includes a contribution from rolling moment due to lateral velocity (dihedral effect). Without the presence of dihedral effect, the equation becomes

$$s(s - N'_r)(s - Y_v)(s - L'_p) = 0$$

which factors into a free s and first-order terms that characterize the yaw, lateral velocity, and roll response of the aircraft. The inverse time constants are defined by the yaw, lateral velocity, and roll damping derivatives. If dihedral effect and roll due to yaw rate are not negligible, then the two real and complex pair of roots appear. Examples for the Harrier follow:

$$s(s + 0.041)(s + 0.029)(s + 0.019) = 0 \text{ for } L'_v, L'_r = 0$$

$$(s + 0.0098)(s + 0.44)[\, s^2 - 2\,(0.45)(0.4)\, s + (0.4)^2] = 0 \quad \text{for } L'_v, L'_r \neq 0$$

With L'_v and L'_r neglected, the three modes are lightly damped as they were in the longitudinal case. Using the actual value of rolling moments due to lateral velocity and yaw rate, the two first-order roots appear along with the unstable oscillatory pair. The latter is at a low frequency of 0.4 rad/sec.

Contributions to Stability Derivatives

The dominant effects on the prominent stability derivatives in hover for a fixed-wing V/STOL aircraft are summarized in table 4.

TABLE 4. EFFECTS OF AIRCRAFT CONFIGURATION ON STABILITY DERIVATIVES

Derivative	Primary Influence of Configuration on Response	
X_u	Longitudinal velocity time constant	Inlet momentum $-\dot{m}_e/m$
Z_w	Vertical velocity time constant	Inlet momentum $-\dot{m}_e/m$
M_q	Pitch rate time constant	Inlet momentum $(-\dot{m}_e/I_y)(X_i + Z_i)^2$
M_u	Phugoid mode stability	Inlet momentum $(-\dot{m}_e/I_y)X_i \sin \theta_o$

The longitudinal force derivative due to longitudinal velocity is the principal contributing factor to the time constant of longitudinal velocity response. For a fixed-wing aircraft in hover, the primary physical contribution to this derivative is due to the momentum of airflow into the engine inlet (fig. 22). There is no airflow of significance over the wings and fuselage that will exert a longitudinal force of consequence on the aircraft relative to that of the inlet flow. The derivative is defined by the mass flow rate into the engine inlets, wherever they are located, divided by the mass of the aircraft; typically, it is a small value of the order of 0.02 sec^{-1}. The vertical velocity damping, pitch-rate damping, and the pitching moment due to forward speed, are the other important effects to consider. For moments, the contributions take into the account the moment arm, in both the X- and Z-axes, of the inlet, or inlets. The moment term also includes the mass flow rate of air into the inlet, in this case divided by the pitch moment of inertia. For the fixed-wing vehicle, the aerodynamic forces and moments are small in comparison to its total mass and inertias. Thus, the aircraft's response in hover will be sluggish with low damping as noted for X_u. Consequently, the pilot must compensate for deficiencies in controlling the vehicle and must be careful to avoid aggressive maneuvers that cannot be easily controlled.

Finally, a phenomenon that must be considered for a fixed-wing aircraft in hover is the influence of ground proximity on its jet-induced aerodynamics. These principally concern the change in lift, pitching, and rolling moments as a fraction of total jet thrust. The number and location of deflected jets on the configuration is a factor determining the magnitude of these forces and moments. The underlying physics are based on the flow of the exiting jet exhaust underneath the wing and fuselage, which creates a negative, or suck-down, force on the vehicle. Typical jet-induced aerodynamic characteristics would show a deficit in lift out-of-ground-effect in proportion to the total jet thrust and the lift would decrease further to large negative values as the aircraft approached the ground (fig. 23). Simple analytical relationships are not available for

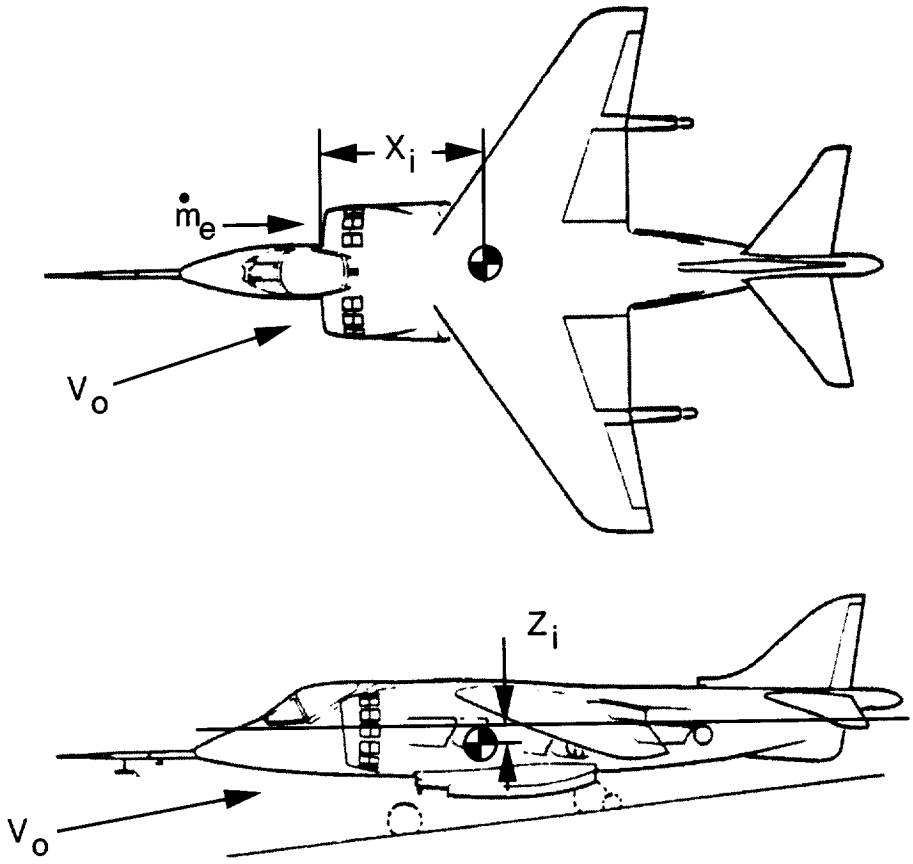

Figure 22. V/STOL aircraft configuration geometry.

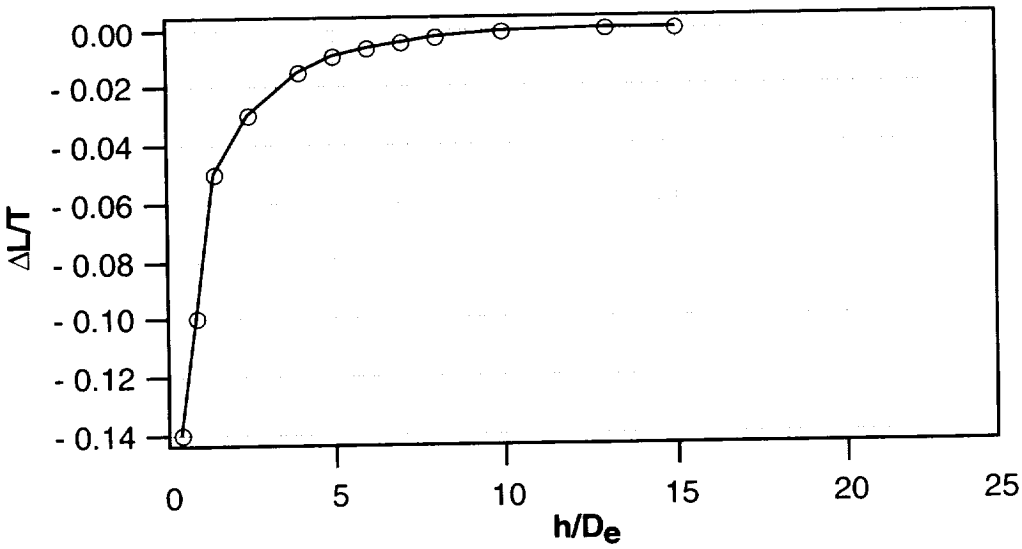

Figure 23. Representative jet-induced lift in the presence of the ground.

these characteristics, although they can be predicted with some complicated empirical methods. More likely, these characteristics will be obtained initially through small-scale wind tunnel tests and will be eventually confirmed with large-scale tests. A more definitive statement cannot be made concerning these effects, but in the absence of specific details of the aircraft configuration, it is important to recognize that these phenomena exist and that they will be important for control of the aircraft in jet-borne flight.

Requirements for Characteristic Roots in Hover

Flying qualities criteria for the longitudinal and the lateral-directional characteristic roots are provided in reference 10. Based on that reference, open-loop characteristic roots for either longitudinal or lateral-directional motions should fall on the complex plane as shown in figure 24. For Level 1 flying qualities in visual meteorological conditions (VMC), the roots must fall to the left of the indicated boundary. This boundary also corresponds to Level 2 for instrument meteorological conditions (IMC). For natural frequencies greater than 1.1 rad/sec, a damping ratio of 0.3 is required. At lower frequencies, neutral stability can be tolerated, and at frequencies below 0.5 rad/sec, a divergent oscillation can be accepted as long as the damping ratio is not less than –0.1.

These characteristics will be acceptable for a hovering vehicle in calm air; however, it will be difficult to achieve operational utility with an aircraft that can only be flown on clear, calm days. The specification indicates that a fair degree of pilot workload would be required to hover this aircraft on instruments with characteristics that fall within the boundary. This assumes cockpit instrumentation that includes at least aircraft attitudes as well as altitude, speed, and heading. Characteristics worse than these make operation in poor visual conditions intolerable. The Level 2 boundary for visual flight allows a time of 12 sec to double amplitude. Longitudinal roots for the Harrier appear in the figure and are indicated by the solid triangles. These characteristics are based on the open-loop aircraft response without stability augmentation devices. For a precision hovering task, this aircraft would be Level 3, implying that these operations cannot be performed by the Harrier. In fact, the Harrier is quite difficult to control without stability augmentation, even in visual flight. This is a consequence of the short time to double amplitude of about 5 sec for the unstable complex pair of roots. It will

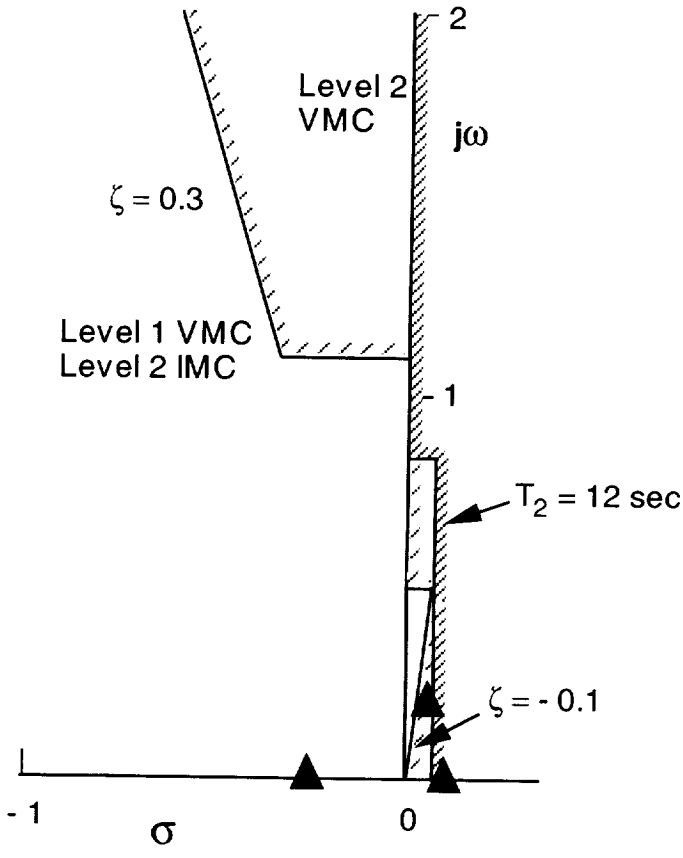

Figure 24. Specifications for longitudinal and lateral-directional characteristic roots in hover.

eventually be seen from an analysis of the pilot's control of hover that these roots can be stabilized easily, although with a requirement for pilot compensation.

The criteria noted are associated with the pitch and roll response in hover. Separate criteria are used for the yaw response, since that axis is typically decoupled from roll and lateral velocity. A first-order root defines the yaw response, and the inverse time constant of that is defined by the vehicle's yaw damping, that is, yawing moment due to yaw rate. Reference 10 criteria indicate that the time constant associated with this root should be 1 sec for Level 1. The time constant increases to 2 sec for Level 2. In no case should the vehicle be allowed to diverge in yaw.

Longitudinal Forward Flight Equations

For forward flight, the longitudinal and lateral-directional equations may be separated and each described by a three-degree-of-freedom set, where the longitudinal equations are

$$\begin{bmatrix} s - X_u & -X_w & g\cos\gamma_o \\ -Z_u & s - Z_w & -(Z_q + U_o)s + g\sin\gamma_o \\ -M_u & -M_{\dot{w}}s - M_w & s^2 - M_q s \end{bmatrix} \begin{Bmatrix} u \\ w \\ \theta \end{Bmatrix} = \begin{Bmatrix} X_\delta \\ Z_\delta \\ M_\delta \end{Bmatrix} \delta$$

These are the equations for longitudinal force, vertical force, and pitching moment; they are written in transfer function form as an example in contrast to the state space format used for the hover case. This format also allows for more obvious treatment of terms such as $M_{\dot{w}}$. The equations are also shown for stability axes, hence the flightpath angle γ appears for the trimmed state. Note that derivatives that did not appear for the hover case are present. These include the longitudinal force derivative as a function of vertical velocity which is strongly influenced by induced drag. For vertical velocity damping where the wing is the primary contributor, lift-curve slope as well as wing loading and dynamic pressure are the principal influence. Longitudinal force due to longitudinal velocity is strongly dependent on the trim level of drag, part of which arises from inlet momentum. The pitching-moment terms will have contributions not only from the wing and tail but from inlet momentum as well. Pitching moment due to vertical velocity is dependent on the static angle-of-attack stability of a vehicle, contributed by both the wing and horizontal tail. The moment term due to rate of change of vertical velocity, or rate of change of angle of attack, is typically determined by the time lag of the wing's downwash reaching the tail. Pitch damping is very strongly influenced by the tail, and may also include an inlet momentum contribution. Control forces and moments can in general arise from contributions of an aerodynamics surface like the tail, but could be a result of the various thrust-producing components of the propulsion system. With deflected jets, jet-induced components can be expected to be present for vertical force and pitching moment. To approximate these derivatives, appropriate sources such as McRuer, Ashkenas, and Graham (ref. 15), Seckel (ref. 16), Etkin (ref. 17), Perkins and Hage (ref. 18), and Roskam (ref. 19) should be consulted for fixed-wing approximations in forward flight where jet flow influences are not present. Kuhn (refs. 20, 21) and Margason (ref. 22) provide useful estimates of jet-induced aerodynamics.

The longitudinal characteristic roots that are derived from the matrix on the left-hand side of the equation are fourth order, and typically factor into two second-order complex pairs of roots:

$$(s^2 + 2\zeta\omega_{sp}s + \omega_{sp}^2)(s^2 + 2\zeta\omega_p s + \omega_p^2) = 0$$

The first pair is known as the short-period mode and the second pair the phugoid mode, where both are defined by their damping ratios and natural frequencies. The short period, as implied by the name, is of short duration and is associated principally with the pitch response of the aircraft to the pitching-moment control. It is usually well damped with frequencies of the order of 2 rad/sec or higher. The other oscillatory pair, the phugoid, is low frequency with very low or even unstable damping ratios. When pitching moment due to angle of attack is low in magnitude or positive in sign, the short period, rather than being a second-order factor, will separate into two first-order roots $(s + 1/T_{s_1})(s + 1/T_{s_2})$.

Approximations can be made that associate frequency and damping of the short period and phugoid modes with an abbreviated collection of stability derivatives that reflect the dominant effect of the aircraft's configuration (refs. 15-19). For the short period, assuming that speed variations are insignificant over the duration of the modal response and that the longitudinal force equation can be ignored for this mode, the natural frequency is predominantly influenced by the aircraft's longitudinal static stability, through the approximation

$$\omega_{sp}^2 \doteq -M_\alpha + Z_w M_q$$

The derivative M_α can also be directly related to the aircraft's static margin and thus to the center of gravity location. The real component of the short-period root, the real damping factor, is affected by vertical velocity damping, pitch damping, and pitch due to rate-of-change in angle of attack, that is,

$$2\zeta\omega_{sp} \doteq -Z_w - M_q - M_{\dot{\alpha}}$$

Pitch damping is governed principally by tail volume, that is, tail size and moment arm, and will vary with flight conditions. When the basic aircraft's pitch damping is deficient, it can be improved by stability augmentation.

It is more difficult to identify a predominant influence on either the frequency or damping for the phugoid mode. Their approximations are

$$\omega_p^2 \doteq \frac{g(M_w Z_u - M_u Z_w)}{\omega_{sp}^2}$$

$$2\zeta\omega_p \doteq -X_u - \frac{M_u(X_\alpha - g)}{\omega_{sp}^2}$$

Note that pitching-moment variations with airspeed influence both frequency and damping of the phugoid. These effects may arise from wing aerodynamics or from moments induced by the propulsion system, and positive values of M_u tend to increase both the frequency and damping. Drag also acts to increase damping for the phugoid through the derivative X_u.

Lateral-Directional Forward Flight Equations

The three-degree-of-freedom lateral-directional equations for forward flight may be written as

$$\begin{bmatrix} s - Y_v & -g/V_o & 1 \\ -L'_\beta & s^2 - L'_p s & -L'_r \\ -N'_\beta & -N'_p s & s - N'_r \end{bmatrix} \begin{Bmatrix} \beta \\ \phi \\ r \end{Bmatrix} = \begin{Bmatrix} Y_\delta / V_o \\ L'_\delta \\ N'_\delta \end{Bmatrix} \delta$$

where the three equations are for side force, rolling moment, and yawing moment. Note that the first state for the side-force equation is sideslip angle rather than lateral velocity, since the pilot typically controls sideslip angle in forward flight. As in the case of the longitudinal equations, this set is expressed in transfer function format. Primed derivatives are used as defined previously in the text. Additional terms appear compared to the hover equations that include cross-coupling between roll and yaw motions arising from angular rates in the two axes. Aerodynamic influences of the wing are dominant in the roll damping and dihedral effect terms. Lesser influences appear in roll due to yaw rate and yaw due to roll rate. The vertical tail contributes strongly to yaw damping and to directional stability. Deficiencies in roll or yaw damping are usually corrected with roll or yaw stability augmentation. Predictions for these characteristics and relationships between them and the aircraft configuration can be found in references 15-19. As in the longitudinal case, estimates of jet-induced aerodynamic influences, in this instance on roll due to sideslip, can be found in references 21 and 22.

Lateral-directional characteristic roots are typically described by two first-order real roots and a complex pair that appear as

$$(s + 1/T_S)(s + 1/T_R)(s^2 + 2\zeta\omega_d s + \omega_d^2) = 0$$

The first of these roots is usually of low frequency and is known as the spiral mode. It is associated with the aircraft's roll and yaw response at low frequency, and can be represented by either a long-time duration convergence or divergence of the response. The second of these first-order modes is known as the roll mode and is almost exclusively associated with the aircraft's roll response to lateral control. Finally, a complex pair known as the Dutch roll, defined by damping ratio and natural frequency, is a low- to intermediate-frequency mode.

The spiral mode can be approximated by

$$1/T_S \doteq \frac{g}{V_o}\left(\frac{L'_r N'_\beta - L'_\beta N'_r}{N'_\beta L'_p}\right)$$

Stability of the spiral mode is determined by the sign of the term in brackets. Although the amounts of directional stability and yaw damping are dictated by Dutch roll modal considerations, dihedral effect provides an independent means of controlling spiral-mode stability. The roll mode is almost exclusively determined by the aircraft's damping in roll, that is, rolling moment due to roll rate, where the inverse time constant is approximated by $1/T_R \doteq -L'_p$. If the aircraft is of low aspect ratio and flying at low speed, this mode may be of lower frequency, causing poor flying qualities at this flight condition. Finally, the Dutch roll approximation for natural frequency is

$$\omega_d^2 \doteq N'_\beta + Y_v N'_r$$

It is strongly influenced by directional stability, that is, yawing moment due to sideslip. Thus, tail size will be important to the natural frequency of this mode. Damping of the Dutch roll is governed by a collection of terms such as lateral velocity damping, yaw damping, and dihedral effect, where

$$2\zeta\omega_d \doteq -(Y_v + N'_r) - \frac{L'_\beta}{N'_\beta}\left(N'_p - \frac{g}{V_o}\right)$$

The dominant contribution typically comes from yaw damping, and is influenced strongly by the aircraft's vertical tail volume. Negative values of rolling moment due to sideslip (positive dihedral effect) can have a destabilizing effect on the Dutch roll. In fact, a conflict exists between the contribution of dihedral effect to spiral and Dutch roll mode stability. Dihedral that is beneficial to one is detrimental to the other.

Contributions to Stability Derivatives

Recall from preceding discussions that jet-induced aerodynamic effects due to deflected jets underneath the wing and fuselage of the vehicle have an effect on lift and pitching moment in hovering flight as a function of height above the surface. These same jet properties, although working through somewhat different physics, will have some influence on the aircraft in forward flight. First, in hovering flight the jets are typically directed straight down, whereas in forward flight they will typically curve back as they exit the exhaust nozzles. They have a strong influence on airflow around the wing and horizontal tail, depending on the location of these lifting surfaces. The jet interaction with wing trailing-edge flaps has a strong influence on lift and pitching moment. Two examples of these influences are shown in figure 25. At the top of the figure, incremental changes in lift are proportional to jet thrust and are a function of the equivalent jet velocity ratio parameter V_e, which is the square root of the ratio of the dynamic pressures in the free stream to those of the jet exhaust. Data from wind tunnel tests will typically collapse when the incremental changes in lift, normalized by the jet thrust, are plotted against jet-velocity ratio. A lift deficit is indicated at hover, which increases substantially with increasing equivalent jet-velocity ratio. This characteristic cannot be generalized, and needs to be predicted with empirical formulas or determined from wind tunnel tests, initially in small-scale and eventually in large-scale tests. Similar behavior appears in rolling moment due to sideslip in forward flight.

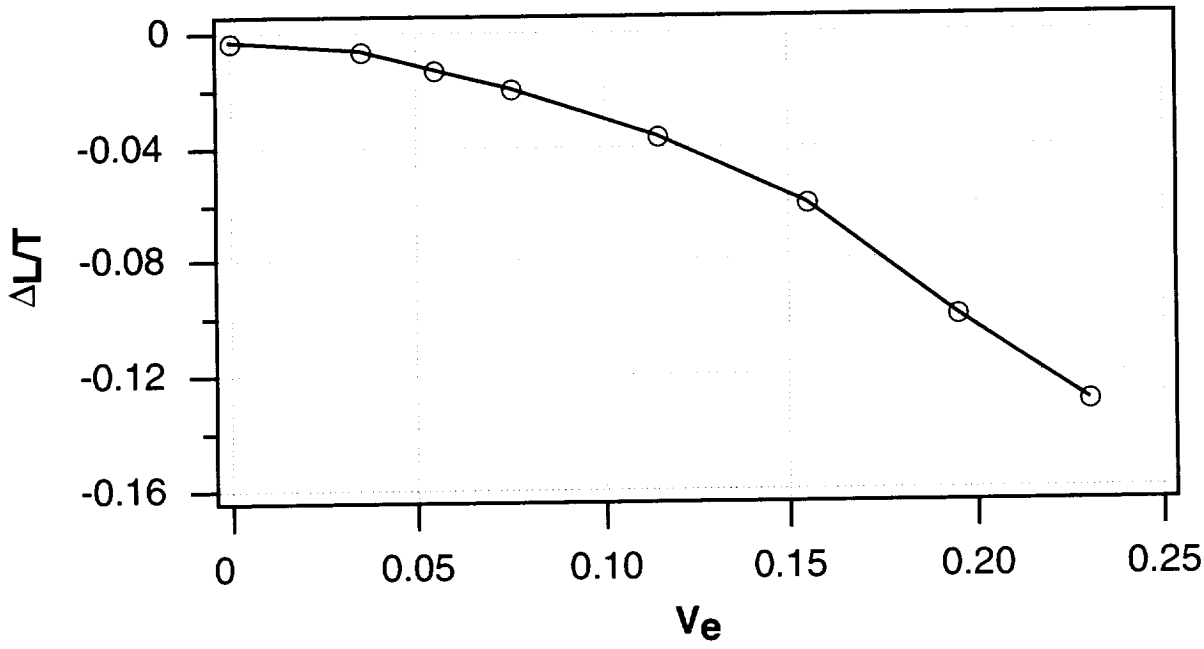

(a) Lift.

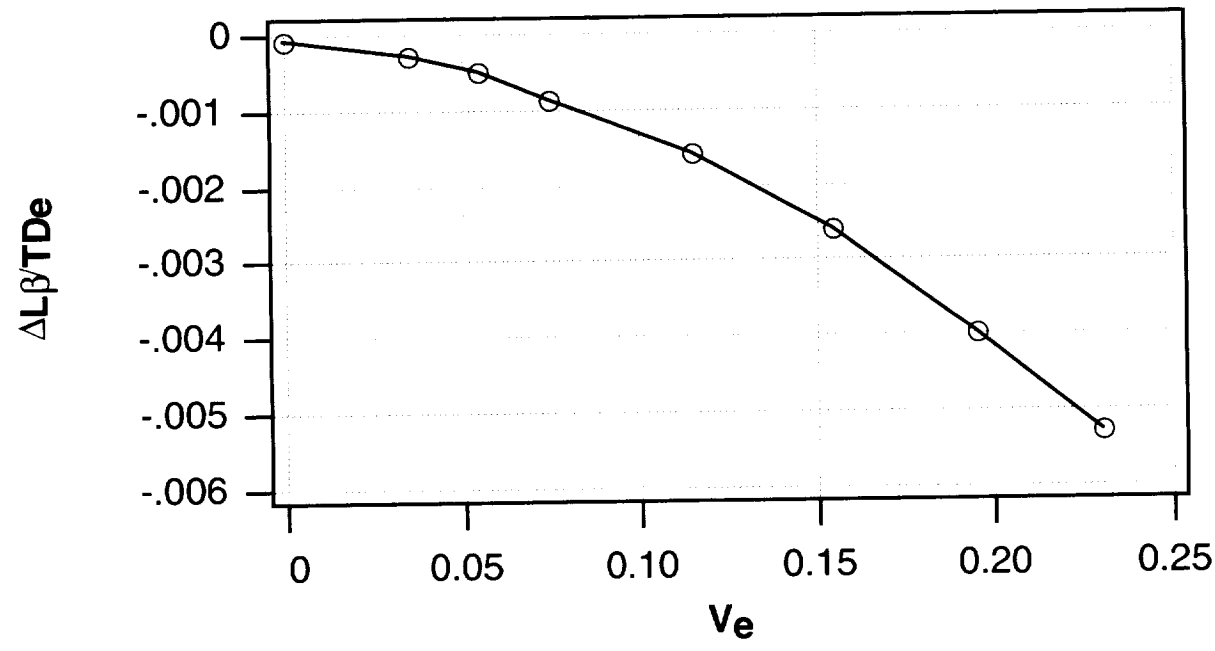

(b) Rolling moment due to sideslip.

Figure 25. Examples of jet-induced aerodynamics in forward flight.

At the bottom of the figure, the change in nondimensionalized rolling moment due to sideslip is plotted against equivalent jet velocity ratio. The phenomenon that produces this rolling moment is related to that which causes lift loss in forward flight. Lift loss is caused by a low-pressure area under the wing in wake of the jet flow. When the airflow approaches the wing asymmetrically, the jet wake is displaced to the downwind side and the area of low pressure moves in that direction, producing a rolling moment as well as lift loss. Thus, the aircraft will tend to roll away from the wind, that is, to roll left for positive sideslip, very much as it would for rolling moment due to sideslip contributed by positive wing geometric dihedral. The magnitude of this effective dihedral can frequently be 2 to 3 times the magnitude of the basic wing characteristics without the jet influence, even for a swept wing aircraft at angle of attack. Thus it is a powerful influence and may well determine the amount of lateral control power required to counteract sideslip in forward flight conditions. This can have a very significant and frequently adverse effect on the aircraft's flying qualities. Thus, it is necessary to consider jet-induced effects in the prediction of the basic stability and control characteristics from which the aircraft's dynamics are derived. References 20-22 should be consulted to make estimates of these effects.

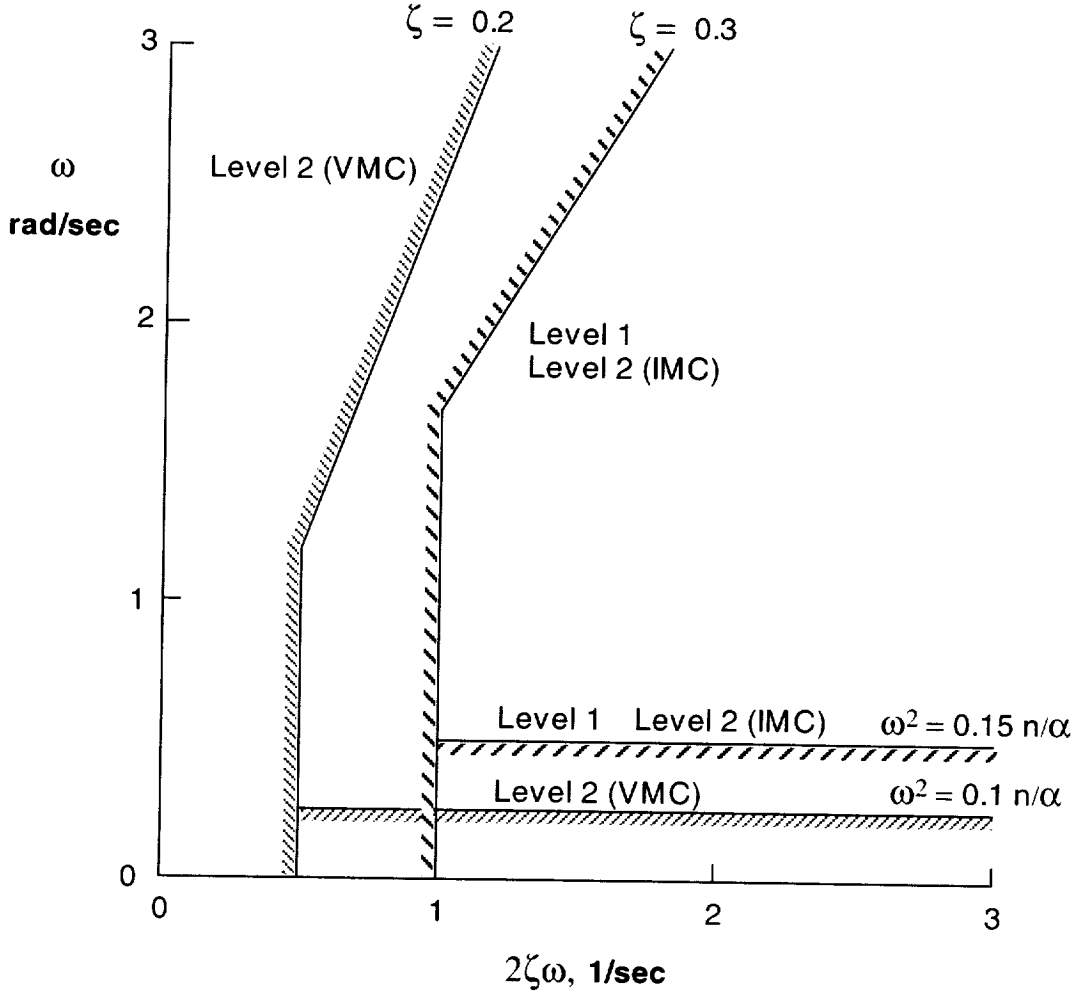

Figure 26. Requirements for longitudinal oscillatory roots.

Requirements for Characteristic Roots in Forward Flight

With this background on the longitudinal and lateral-directional characteristic roots, their requirements for forward flight can be addressed. First, at low frequency, it is necessary that all real or oscillatory roots be stable. This requirement is somewhat more restrictive than for hover, which allowed some instability for very low-frequency, oscillatory roots. In forward flight, it is essential that the aircraft be stable for either VMC or IMC, whereas in hover in visual flight, the pilot should be able to handle a slightly unstable aircraft because good attitude cues are present. For higher-frequency roots such as the short-period modes, additional criteria are imposed. Requirements for natural frequency and damping are provided in reference 10; they are shown in figure 26. For Level 1 characteristics or Level 2 characteristics for instrument flight, the short period must fall inside the boundary, with damping ratios better than 0.3 and $2\zeta\omega$ always greater than 1 rad/sec. There is also a requirement on minimum short-period natural frequency that is proportional to n/α, which is the aircraft's dimensional value of lift-curve slope. This requirement prevents a short period that is too low in frequency and the initial pitch response from being insensitive. For Level 2 in VMC, the short period is allowed to be as low as 0.2 damping ratio and real damping, $2\zeta\omega$, to be as low as 0.5. The natural frequency may reduce somewhat as well. The Harrier does not fall on this plot because it has one unstable real root. Those characteristics do not include stability augmentation, and the Harrier is a difficult aircraft to handle with stability augmentation off in forward flight.

The requirements from reference 10 for lateral-directional characteristics are shown in figure 27. For Level 1 characteristics, the oscillatory or Dutch roll roots must have a damping ratio of at least 0.08, except at low frequencies below 0.5 rad/sec. Dutch roll frequency should not be less than 0.25 rad/sec. For Level 2 characteristics, a neutral or even slightly divergent Dutch roll can be tolerated if the time to double amplitude is not less than 5 sec. Finally, at the lowest frequencies, the damping ratio must not be worse than –0.3. Additional characteristics are noted in the figure for the spiral mode and the roll mode. Note that a slightly divergent spiral mode can be accepted even for Level 1 flying qualities, whereas more stringent requirements for stability are imposed on the roll mode. The value for the roll-mode inverse time constant is 0.7 rad/sec for Level 1. For Level 2, a roll mode as low as 0.33 rad/sec is accepted. The spiral mode for Level 1 is not allowed to double amplitude in less than 20 sec. The Harrier's characteristics noted in the figure show a stable spiral and a reasonably well-damped roll mode. The Dutch roll is slightly divergent and requires control augmentation for normal operation and for instrument flight.

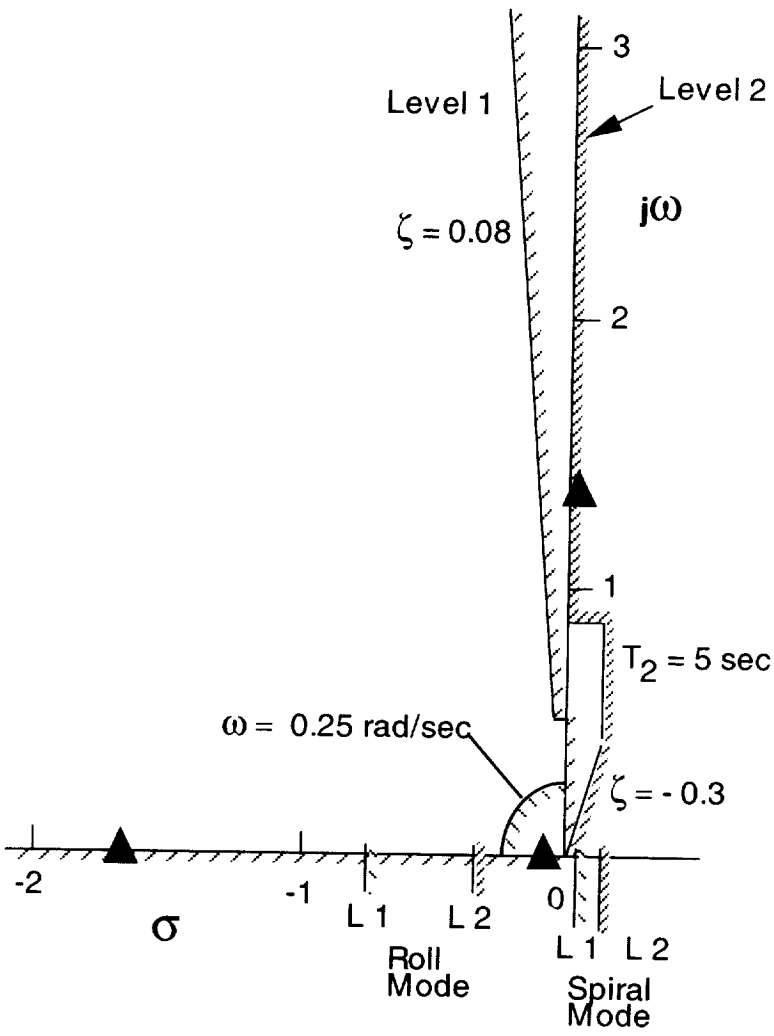

Figure 27. Requirements for lateral-directional characteristic roots.

LONGITUDINAL FLYING QUALITIES IN HOVER

The analyses that follow consider the various responses to the pilot's controls that are pertinent to longitudinal control in hover, along with the important features of the aircraft that influence the response. The aircraft's state variable of interest for the innermost control loop appropriate to the task is pitch attitude. This is the tightest control task the pilot must perform to control the vehicle in hover, including tasks of height control and forward velocity control. Insight into the control task and configuration influences will come from analyzing the control loops in sequence, progressively from the inner loop through the outer loops, such as those that determine the position of the aircraft.

Pitch Attitude Control

First, consider the transfer function that relates aircraft pitch response to the pilot's longitudinal control. It appears with a constant that represents the aircraft's pitch-control sensitivity, two first-order factors in the numerator, and the terms in the denominator consisting of the characteristic roots discussed previously for the hover case

$$\frac{\theta}{\delta_s} = \frac{M_{\delta_s}(s + 1/T_{\theta_1})(s + 1/T_{\theta_2})}{\Delta_{Long}}$$

where

$$\Delta_{Long} = (s + 1/T_{s_1})(s + 1/T_{s_2})(s^2 + 2\zeta\omega s + \omega_p^2)$$

As noted in the previous section, the denominator is fourth order, with two first-order roots and a second-order complex pair. An approximation for the first of the two numerator roots is dominated by the aircraft's axial velocity damping, that is, longitudinal force due to longitudinal velocity:

$$1/T_{\theta_1} \doteq -X_u + M_u \frac{X_\delta}{M_\delta}$$

This approximation is obtained from the complete polynomial in powers of s for the numerator, both in terms of its time constants and of the coefficients in the matrix, and then equating coefficients of like powers of s in the polynomial. Reasonable approximations for the transfer function factors can then be made. The X_u term is associated with inlet momentum on a fixed-wing V/STOL aircraft; it is typically a negative number. If the pitch control produces longitudinal force, which typically will be of small magnitude, it may modify this first-order factor. Overall, this numerator term is typically a small number, about 0.05 sec^{-1}. The second numerator factor is approximately equal to vertical velocity damping, that is,

$$1/T_{\theta_2} \doteq -Z_w$$

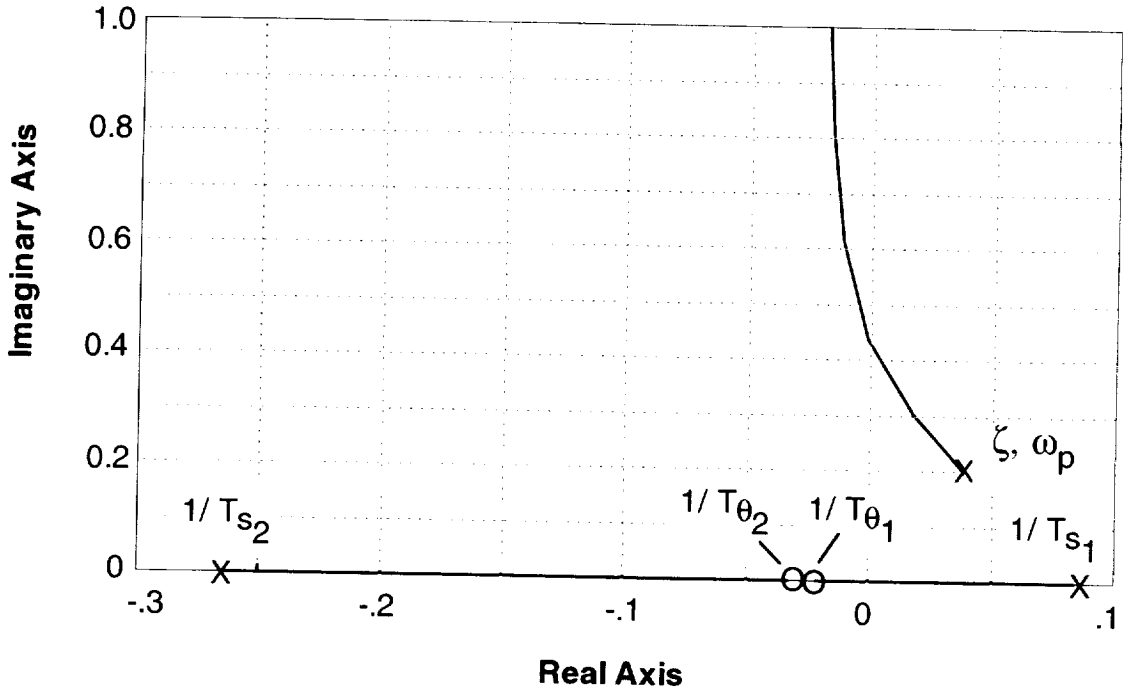

Figure 28. Root locus for pitch-attitude control for the Harrier in hover.

By using this transfer function for pitch-attitude response to the longitudinal control, the pilot's contribution to pitch control can be assessed. As shown previously in the block diagram of figure 17 the pilot's contribution is in cascade with that of the aircraft. Taking the Harrier as an example, a root locus is presented for the pitch-error input to the pilot and the aircraft's response as the output. It is based on the transfer function noted above and uses a loop closure with pilot gain alone (fig. 28). The notation used on the root locus plot represents the characteristic roots with an X and numerator roots with an O. The roots initiate from the unstable complex pair and from the real roots in the left-and right-half plane. As the pilot controls attitude more tightly by increasing the gain, the unstable pair is slightly stabilized while the real roots are driven toward the numerator roots near the origin. The closed-loop roots show very low levels of damping if the pilot closes the loop with a pure gain. It is apparent that desirable closed-loop characteristics cannot be achieved with a simple proportional feedback of the pitch-attitude error to the control.

The combined root locus and Bode plots in figure 29 provide an indication of the pitch-attitude control with lead compensation. First, note in the root locus at the top of the figure that the added numerator root reflects the lead compensation that has been introduced. The value of the lead time constant T_L of 0.5 sec is chosen to provide sufficient phase margin for the loop closure. The substantial improvement in stability for the case with lead compensation is apparent when compared with the previous figure. The complex pair of roots progresses rapidly into the left-half plane and eventually splits into a pair of real roots. Thus by introducing enough lead compensation, the unstable oscillation can be stabilized at the expense of the pilot's effort and anticipation to produce that lead. The consequence of introducing that lead compensation may be increased workload for the pilot, thus degraded flying qualities.

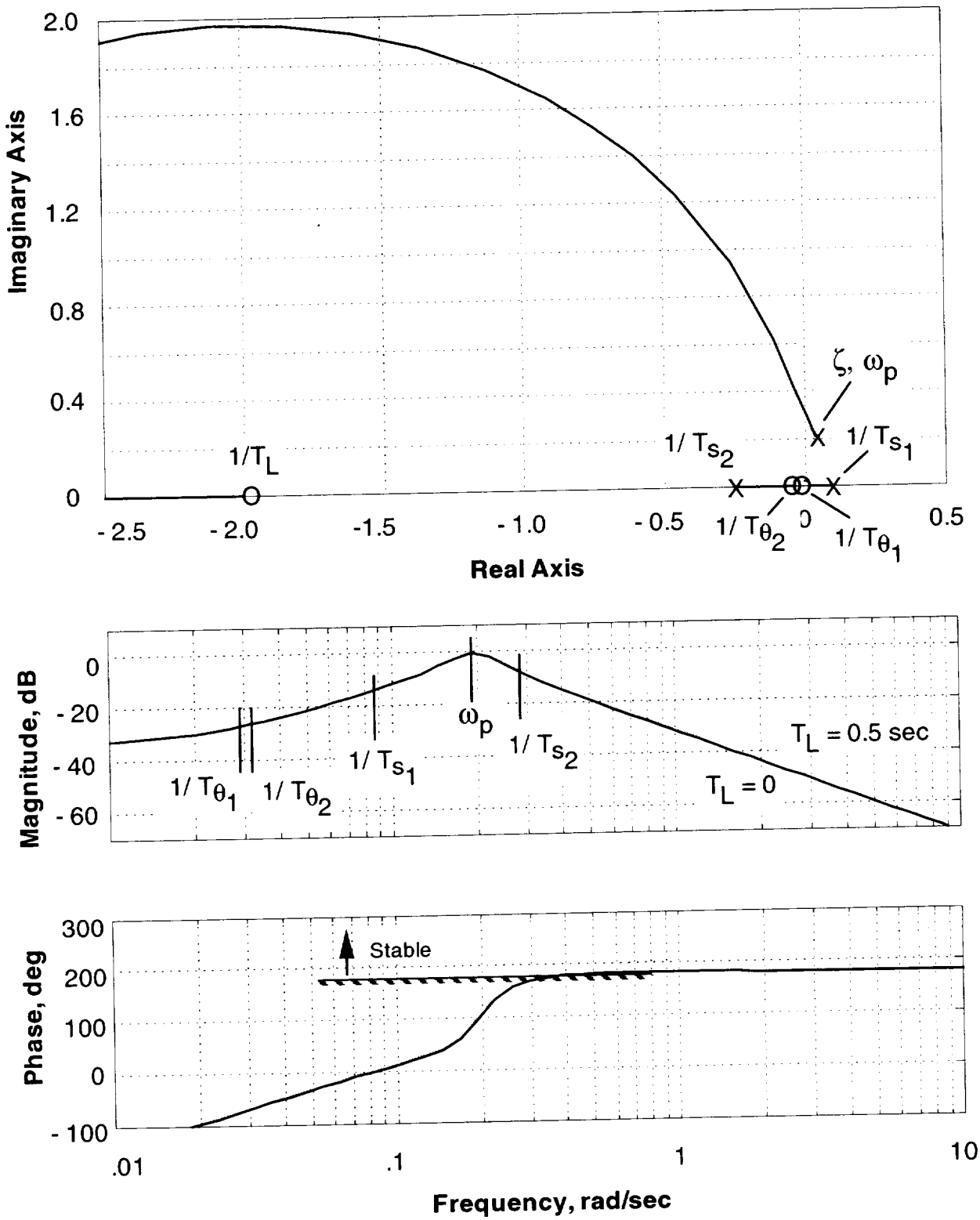

Figure 29. Root locus and Bode plots of pitch-attitude control for the Harrier in hover.

The Bode plot magnitude and phase show these characteristics from the perspective of the open-loop frequency response, with and without lead compensation by the pilot. Locations of the open-loop numerator and denominator roots are noted in the figure. Note that the phase angle for neutral stability is +180 deg. Without pilot lead, stability is not achieved until the pilot's gain is increased sufficiently, and an ample phase margin of 45 deg or better is never reached. With lead compensation, the instability at low gain still exists due to the unstable open-loop roots, but the desired phase margin is achieved at frequencies of 2-3 rad/sec.

Another characteristic to note is the sag or droop in the frequency response plot at low frequency. This will be reflected in overshoot in short-term pitch-attitude response compared with that of the steady state. This overshoot is reflected as well in the time history of pitch response to a step-control command by the pilot which is shown in figure 30. Recall from an

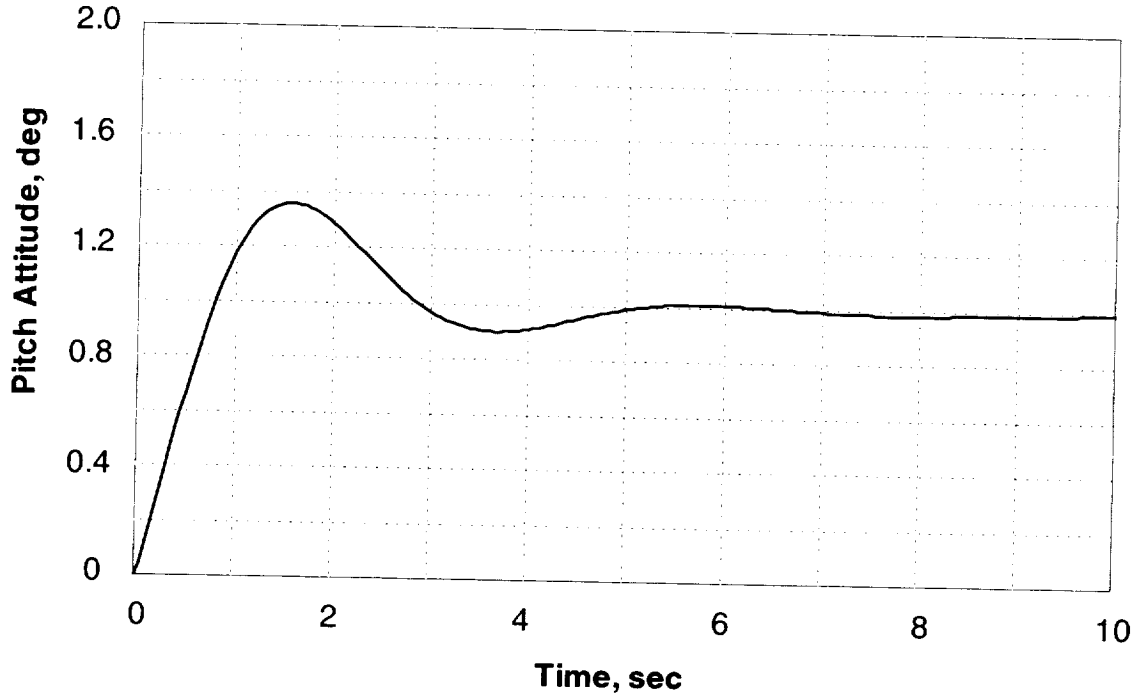

Figure 30. Time history of pitch response to a step command input for the Harrier in hover.

earlier discussion in this report that a large low-frequency gain or magnitude on the Bode plot is necessary if the system is to have good steady-state command following. If the steady-state response to the command is unsatisfactory, the pilot must compensate for that deficiency. This means the pilot must generate gain at low frequency while leaving the higher frequency lead unchanged. To do so, the pilot can introduce lag or integral compensation at low frequency. The total contribution of lead and integral compensation by the pilot would appear as

$$Y_P = \frac{K_\theta (T_L s + 1)(T_i s + 1)}{s}$$

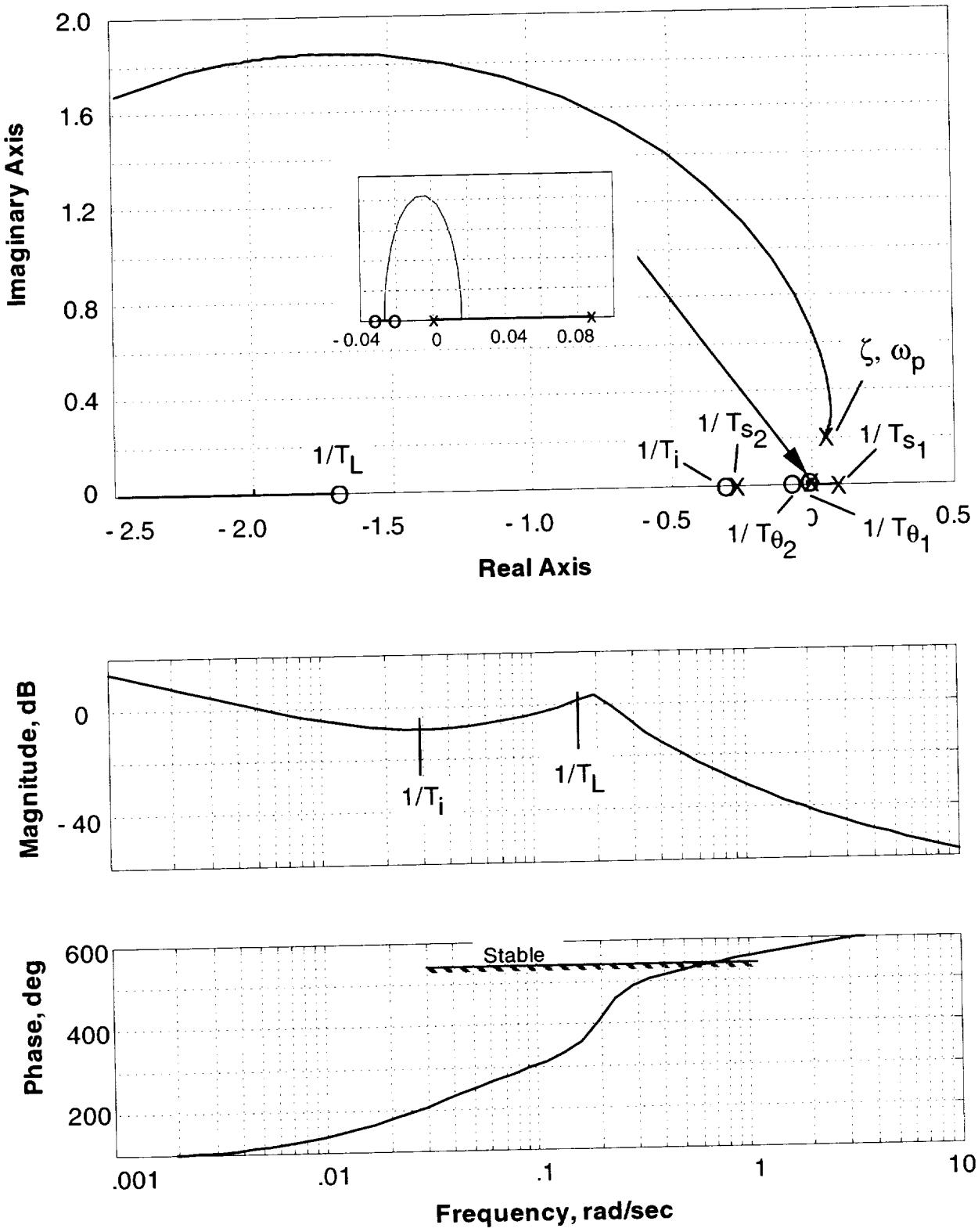

(a) Root locus and Bode plots.

Figure 31. Proportional, rate, and integral compensation for pitch control of the Harrier in hover.

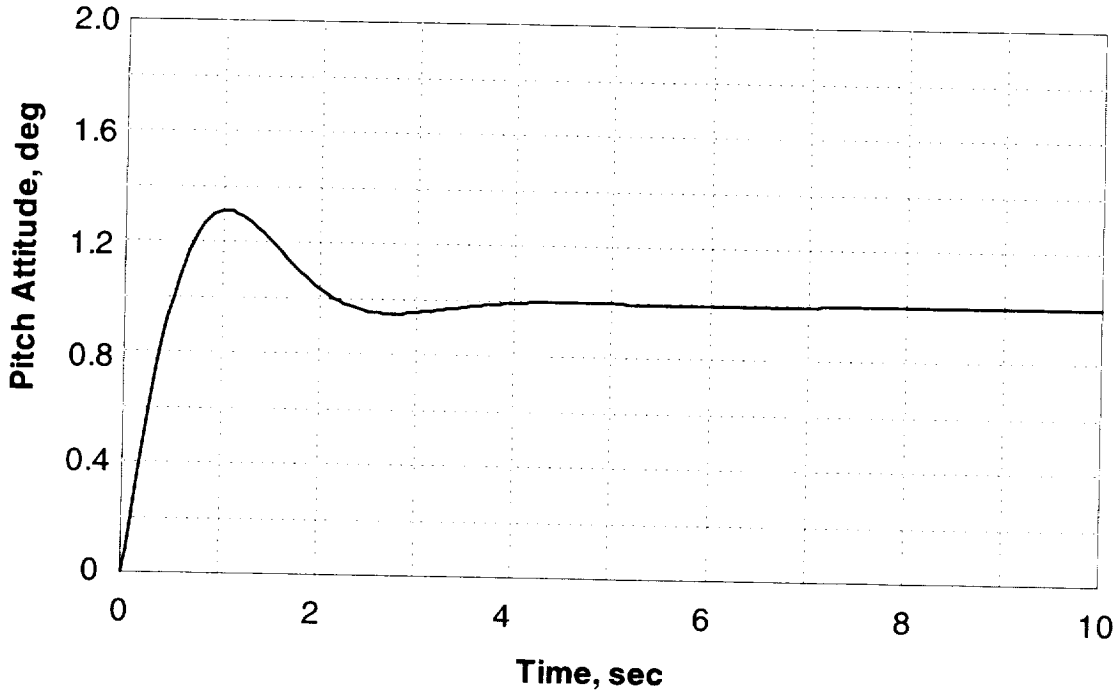

(b) Time history.

Figure 31. Concluded.

The Bode plot in figure 31 includes this compensation, and substantially more gain is evident at low frequency. From the phase plot, lead compensation has generated enough margin for adequate stability in the frequency range of 2-4 rad/sec. This was achieved by selecting the values of the two time constants to give 45 deg of phase margin from the stability boundary over that frequency range. The time response shows that the pitch-response tracks the command well in the steady state.

The necessity to generate lead to provide adequate stability margins may cause the flying qualities to be downgraded. It is not difficult to provide integral compensation, since it is a low-frequency trimming function, and only requires the pilot to gradually move the stick to maintain the steady-state response desired. In practice, that amount of integral compensation does not penalize the flying qualities of the aircraft.

Finally, it should be noted that the basic aircraft's instability is strongly influenced by its total level of damping, including pitch damping and vertical velocity damping. In the example, there is insufficient damping to relieve the pilot of the need to generate lead compensation in order to achieve the desired precision of attitude control. The process for stabilizing pitch attitude is straightforward. The pilot observes the horizon and adjusts the control to establish and maintain the intended visual attitude. This technique is powerful for quickly stabilizing the unstable root. The stick motion per degree of pitch-attitude error required is not substantial. The most objectionable demand on the pilot is to generate lead to provide the phase margin required.

Longitudinal Velocity Control

For the pilot to control longitudinal velocity with the longitudinal stick, the transfer function is

$$\frac{u}{\delta_s} = \frac{X_{\delta_s}\left[s^3 + (-M_q - Z_w)s^2 + \left(M_q Z_w - g\frac{M_{\delta_s}}{X_{\delta_s}}\right)s + g\left(\frac{Z_w M_{\delta_s} - M_w Z_{\delta_s}}{X_{\delta_s}}\right)\right]}{\Delta_{Long}}$$

With the assumption that X_{δ_s} and Z_{δ_s} can be neglected, and given the characteristic roots noted previously, the transfer function simplifies to

$$\frac{u}{\delta_s} = \frac{-gM_{\delta_s}(s - Z_w)}{(s + 1/T_{s_1})(s + 1/T_{s_2})(s^2 + 2\zeta\omega_p s + \omega_p^2)}$$

Based on this transfer function, the root locus plot in figure 32 illustrates the consequences of direct control of longitudinal velocity with the stick. The open-loop characteristic roots for the Harrier, which were previously shown for the pitch-control example, appear here as well. The unstable oscillatory pair is increasingly destabilized as gain is increased for the loop closed with velocity error to the stick. Thus, without appropriate compensation, the pilot will be unable to control longitudinal velocity in this manner. Further, it may not be feasible for the pilot to provide effective lead compensation in this loop because of the lack of strong cues for rate of change of longitudinal velocity.

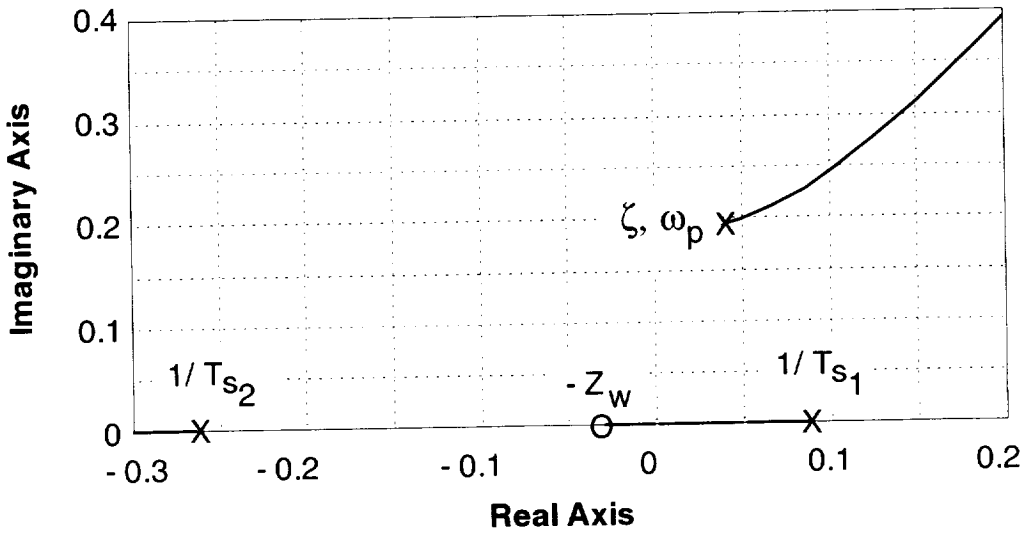

Figure 32. Root locus for longitudinal velocity control for the Harrier in hover.

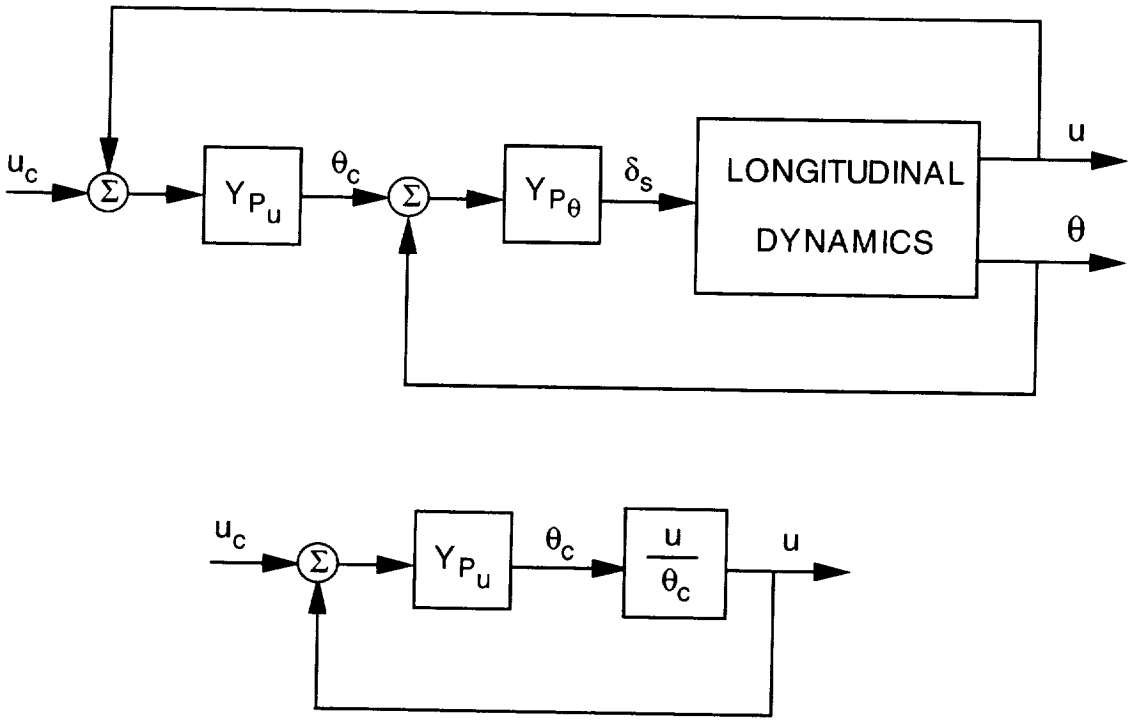

Figure 33. Block diagram of longitudinal velocity control with pitch-attitude loop closed.

The benefit of stabilization of pitch attitude on the control of longitudinal velocity is shown in the next example. Figure 33 presents a block diagram of longitudinal velocity control with the pitch-attitude inner loop closed. The inner-loop pilot transfer function includes the pilot gain and lead compensation developed in the earlier example. The multi-loop structure can be reduced to the single loop closure shown at the bottom of the figure, where the open-loop transfer function for velocity control u/θ_c incorporates the pitch-attitude inner loop. This transfer function is derived using block diagram algebra and is

$$\frac{u}{\theta_c} = \frac{Y_{P\theta}\left(\frac{u}{\delta_s}\right)}{1 + Y_{P\theta}\left(\frac{\theta}{\delta_s}\right)}$$

$$= \frac{Y_{P\theta} N_\delta^u}{\Delta_{Long} + Y_{P\theta} N_\delta^\theta}$$

Thus, velocity response to attitude changes can be expressed by the product of the pilot's transfer function for the attitude loop and the open-loop velocity-to-stick transfer function, divided by the

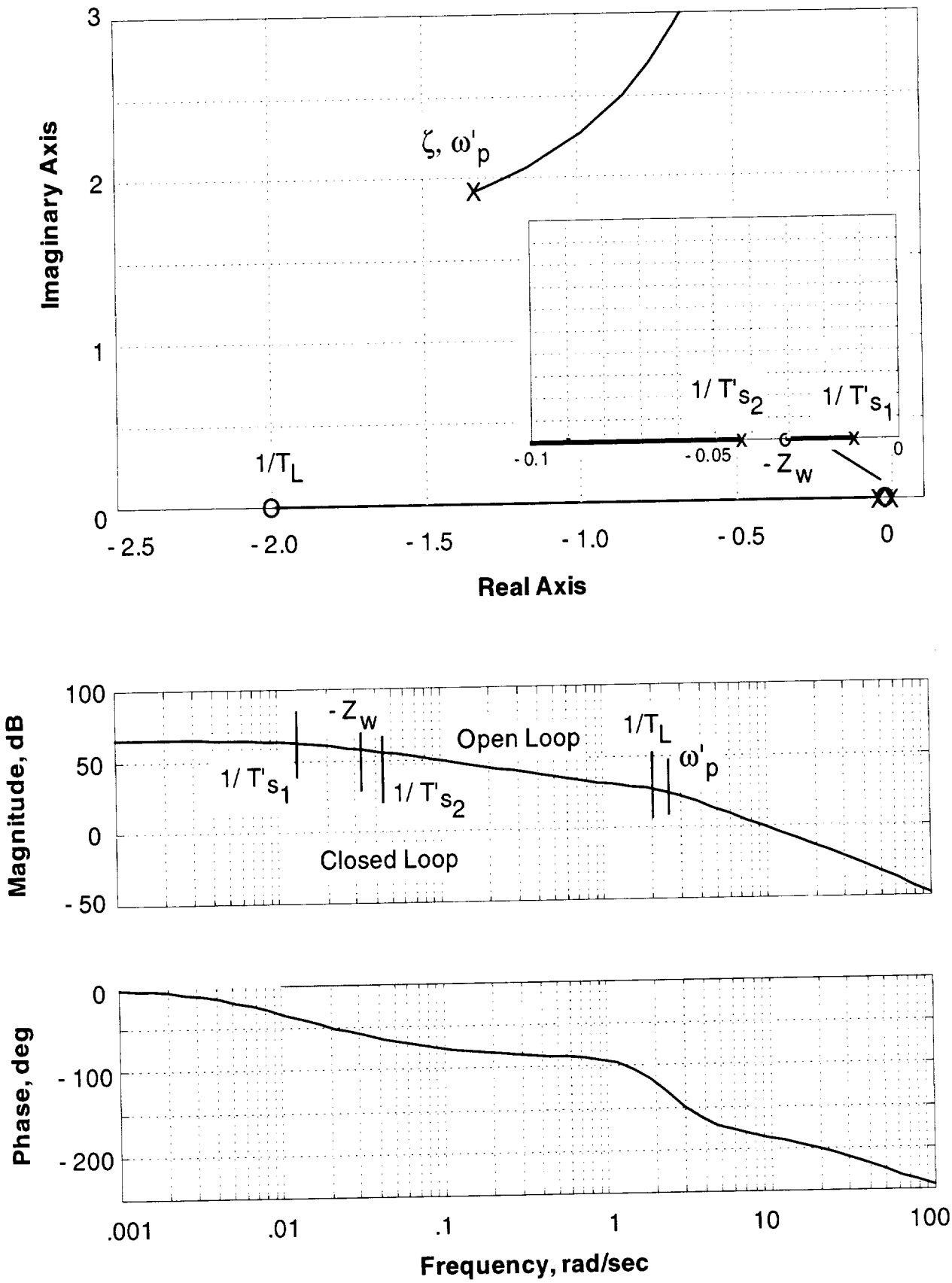

Figure 34. Root locus and Bode plots of longitudinal velocity control for the Harrier in hover.

characteristic roots of the aircraft with the pitch-attitude loop closed. Substituting the appropriate factors for the numerator and denominator terms, the transfer function can finally be written as

$$\frac{u}{\theta_c} = \frac{-gM_{\delta_s} K_\theta (T_L s + 1)(s - Z_w)}{(s + 1/T'_{s_1})(s + 1/T'_{s_2})(s^2 + 2\zeta\omega'_p s + \omega'^2_p)}$$

where the primed notation refers to roots with the attitude loop closed.

The root locus plot in figure 34 shows the progression of the closed-loop roots for velocity control when the attitude loop is closed. The roots initiate at the closed-loop attitude roots shown in the previous section, which are the stable complex pair and the two real roots. Those are roots for the case in which the pilot provides lead compensation for pitch control. For velocity control with feedback gain alone and no other velocity loop compensation, adequate system stability is maintained for a reasonable range of gain. The inner attitude loop has provided the compensation required for stable velocity control. This is illustrated as well by the Bode plot in the figure. Both the open- and closed-loop Bode plots are shown for comparison. The open-loop phase plot shows a phase margin of 45 deg or better out to a frequency of 2.5 rad/sec. Typically, the velocity-loop closures would be made at a bandwidth of the order of one-quarter of that of the attitude loop, which in this case would be approximately 0.5 rad/sec. Thus, the phase margin for closed-loop stability is more than adequate for this example. The Bode plot with the velocity loop closed shows good command tracking out to a frequency of 0.5 rad/sec. A time history of closed-loop speed response to a step command speed change in figure 35 indicates a well damped response.

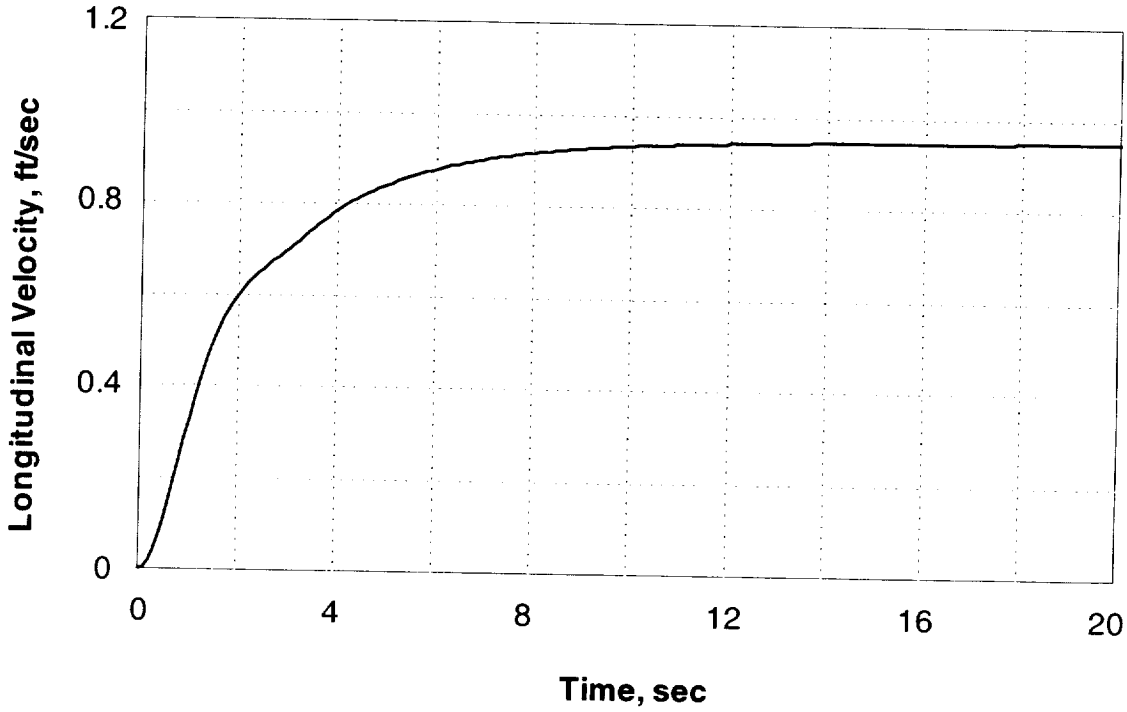

Figure 35. Time history of closed-loop control of longitudinal velocity for the Harrier in hover.

For purpose of understanding the essentials of velocity control dynamics, the equations can be simplified considerably with the assumption of modal separation between changes in aircraft attitude in comparison to response of the aircraft longitudinal velocity. This recognizes that attitude changes take place much more quickly than the aircraft's longitudinal velocity can respond. Thus, the equation of significance is the longitudinal force equation, and pitch attitude is assumed to be the commanded attitude, where commanded attitude becomes the pilot's longitudinal force control. Thus, the longitudinal force equation is now written

$$\dot{u} = X_u u - g\theta_c$$

and the transfer function of velocity to pitch-attitude command is

$$\frac{u}{\theta_c} \doteq \frac{-g}{s - X_u}$$

This very basic relationship shows that the velocity response to changes in attitude are represented by a first-order lag with an inverse time constant of X_u and a control sensitivity that is equivalent to the gravitational constant. Thus the speed response will be sluggish and the steady-state relation of longitudinal velocity to attitude is g/X_u.

Vertical Velocity Control

The remaining topic for the longitudinal axis in hover is vertical velocity control. The appropriate open-loop transfer function for vertical velocity in hover is that for the thrust control, since thrust is the appropriate control effector for the vertical axis. If longitudinal force due to thrust is neglected,

$$\frac{\dot{h}}{\delta_T} = \frac{-Z_{\delta_T}(s + 1/T_{\dot{h}})(s^2 + 2\zeta\omega_{\dot{h}}s + \omega_{\dot{h}}^2)}{\Delta_{Long}}$$

$$= \frac{-Z_{\delta_T}\left[s^3 + (-M_q - X_u)s^2 + (M_q X_u)s + g\left(M_u - Z_u \frac{M_{\delta_T}}{Z_{\delta_T}}\right)\right]}{\Delta_{Long}}$$

The real numerator root lies in the left-half plane and may be approximated by the pitch damping derivative M_q if it is much larger than X_u in magnitude. The complex pair of roots typically lie in the right-half plane, and these in combination with the unstable complex characteristic roots of the basic aircraft result in an unstable control of vertical velocity with thrust. In the presence of pitching moments from thrust, it is necessary to first stabilize pitch attitude before using the thrust control. With the pitch-attitude loop closed, the transfer function of vertical velocity to thrust becomes

$$\frac{\dot{h}}{\delta_T} = \frac{N^{\dot{h}}_{\delta_T} + Y_{p_\theta} N^{\dot{h}\theta}_{\delta_T \delta_s}}{\Delta_{long} + Y_{p_\theta} N^{\theta}_{\delta_s}}$$

where the numerator and denominator have been modified by the pitch-attitude loop closure. The first term in the numerator represents the roots for the open-loop transfer function of vertical velocity to thrust and the last term consists of the pilot transfer function multiplying the coupling numerator:

$$N^{\dot{h}\theta}_{\delta_T \delta_s} = \begin{vmatrix} s - X_u & 0 & 0 \\ -Z_u & -Z_{\delta_T} & 0 \\ -M_u & -M_{\delta_T} & M_{\delta_s} \end{vmatrix} = -Z_{\delta_T} M_{\delta_s} (s - X_u)$$

Reference 15 describes coupling numerators and shows them to be composed of those terms in the determinant associated with the loop closure that add to the basic open-loop numerator. In the same regard, the characteristic roots consist of the open-loop roots modified by the attitude loop closure. The vertical velocity transfer function now becomes

$$\frac{\dot{h}}{\delta_T} = \frac{-Z_{\delta_T} (s + 1/T'_{\dot{h}})(s^2 + 2\zeta\omega'_{\dot{h}} s + \omega'^2_{\dot{h}})}{(s + 1/T'_{s_1})(s + 1/T'_{s_2})(s^2 + 2\zeta\omega'_p s + \omega'^2_p)}$$

and if the pilot closes the attitude loop at sufficiently high gain such that the second of the two terms in the numerator and denominator dominate the transfer function, the transfer function may be reasonably approximated by

$$\frac{\dot{h}}{\delta_T} \doteq \frac{N^{\dot{h}\theta}_{\delta_T \delta_s}}{N^{\theta}_{\delta_s}}$$

$$\doteq \frac{-Z_{\delta_T} (s - X_u)}{(s + 1/T_{\theta_1})(s + 1/T_{\theta_2})}$$

leaving a first-order numerator and two real complex roots to describe the response. As an example, a root locus plot for thrust control of vertical velocity with pitch attitude stabilized is shown in figure 36 for the Harrier. The cancellation of the pole-zero complex pair is evident, and the loop closure produces a stable response with a dominant first-order characteristic root. The figure also shows a time history of vertical velocity response with and without the attitude loop closed. The open-loop divergence is apparent while the response with pitch attitude controlled is stable. Heave damping for the Harrier is low in hover, consequently, the time to reach the steady hover is quite long and, over the period the pilot observes this response, it will appear to be an acceleration-like response.

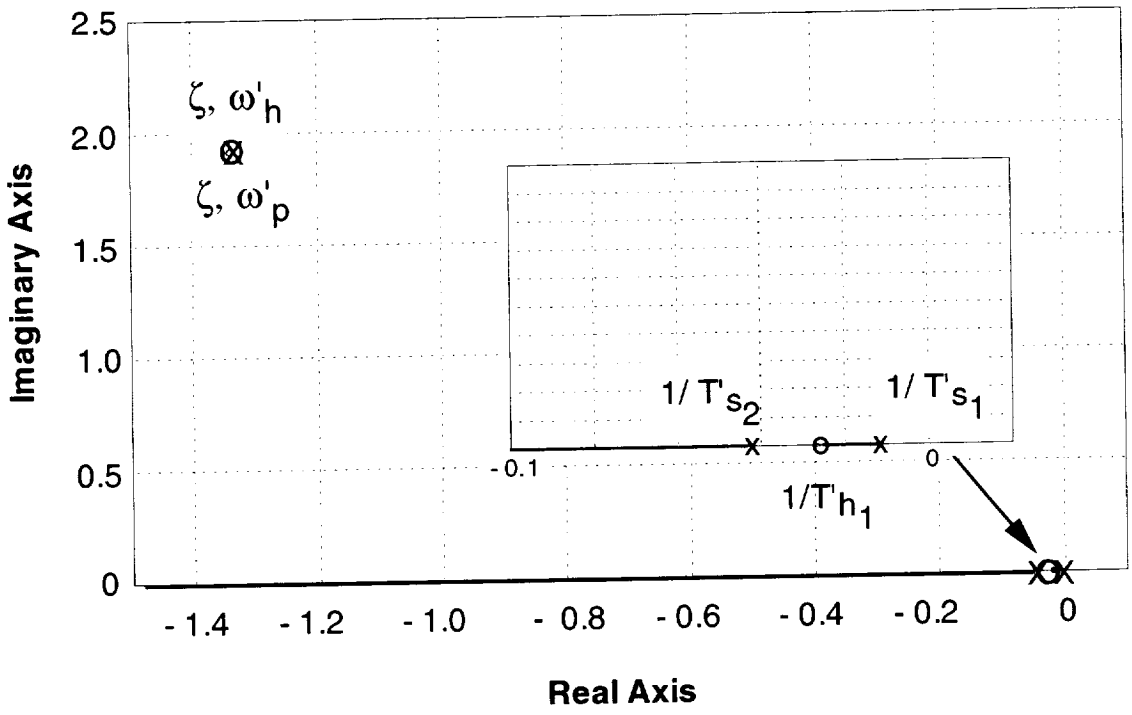

(a) Root locus of vertical velocity control with thrust.

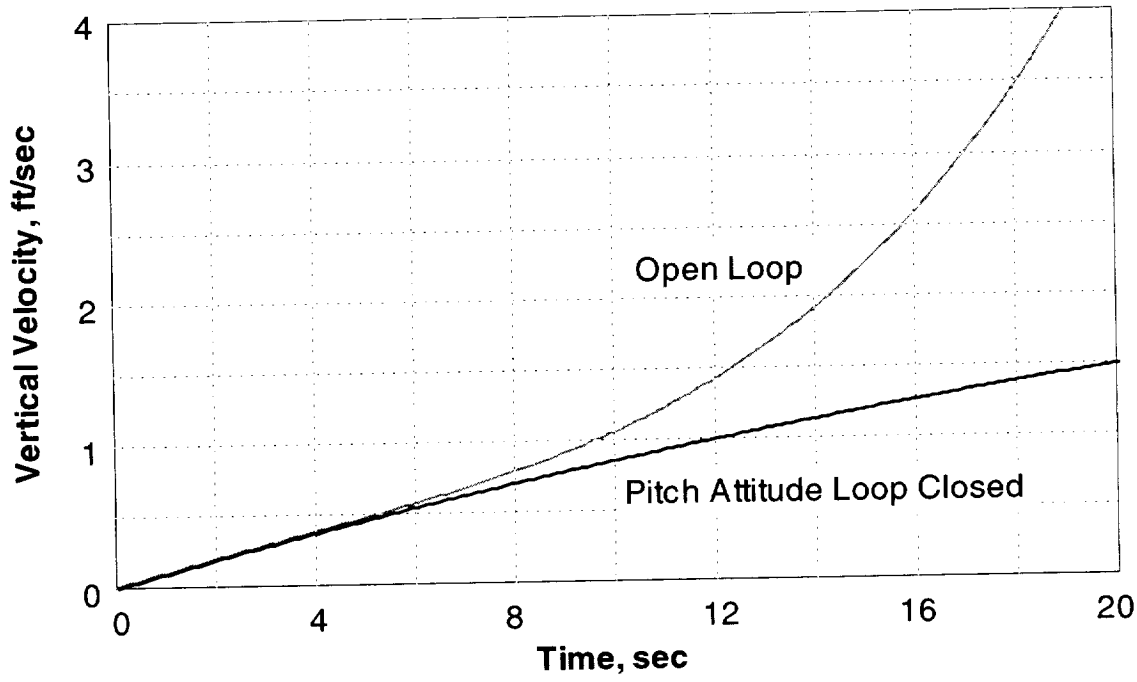

(b) Time history of vertical-velocity response to thrust.

Figure 36. Vertical velocity control with pitch attitude stabilized for the Harrier in hover.

In the absence of significant pitching moments from thrust and vertical velocity in the open-loop transfer function for vertical velocity, the numerator roots cancel like terms in the open-loop characteristic roots, simplifying the thrust control relationship to

$$\frac{\dot{h}}{\delta_T} \doteq \frac{-Z_{\delta_T}}{s - Z_w}$$

The remaining terms in the vertical velocity transfer function are the gain and the first-order root with inverse time constant equal to vertical velocity damping derivative Z_w. This equation describes the nature of vertical velocity control with thrust. The initial response sensitivity is determined by Z_{δ_T} and its steady-state control sensitivity by Z_{δ_T}/Z_w.

FLYING QUALITIES REQUIREMENT	MIL-F-83300 (Ref. 10)	AGARD 577 (Ref. 9)	
	$\theta(1)$ deg	$\ddot{\theta}_{max}$ rad/sec^2	$\theta(1)$ deg
LEVEL 1 Satisfactory Without Improvement	3	0.1 - 0.3	2 - 4
LEVEL 2 Adequate Improvement Warranted	2		

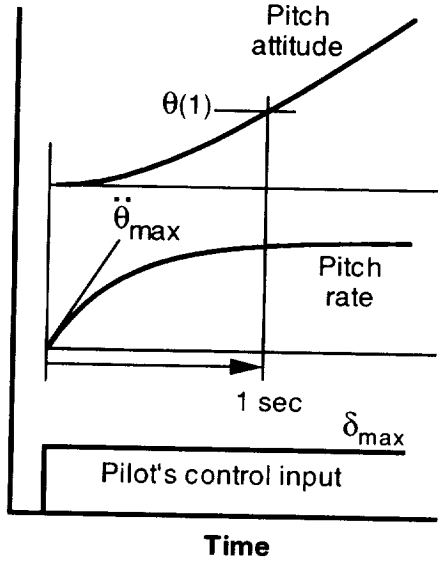

Figure 37. Requirements for pitch-control authority in hover.

Longitudinal Flying Qualities Requirements in Hover

Flying qualities requirements in hover are concerned with demands for control power and dynamic response. Both references 9 and 10 provide suggestions for control power in terms of maximum available angular acceleration or pitch-attitude change in 1 sec. This control authority is based on demands for maneuvering the aircraft for precision hover and for initiating and stopping longitudinal translations. Control used to trim the aircraft is not included. The requirements from reference 9 are only provided for Level 1 flying qualities; those from reference 10 apply to both Levels 1 and 2. Figure 37 contains a graphical description of the attitude change requirement and the required values of angular acceleration and attitude change in response to an abrupt control input taken from both references. The attitude change requirement more nearly reflects operational maneuvers demanded of the aircraft; it accounts for the angular acceleration produced by the control and the restoring moment proportional to angular rate (pitch rate damping) that opposes the control moment. For a pitch response of the rate command type, which can be represented by a first-order time response to a step input, the relationship between angular acceleration and attitude change is shown in figure 38. Based on this relationship, an attitude change of 3 deg in 1 sec and an angular acceleration of 0.2 rad/sec^2 (from refs. 9 and 10) are self-consistent for a rate-response type with a time constant of 0.43 sec. Dynamic-response requirements for attitude control are described in reference 23. These take the form of response bandwidth and phase delay that were covered in general at the

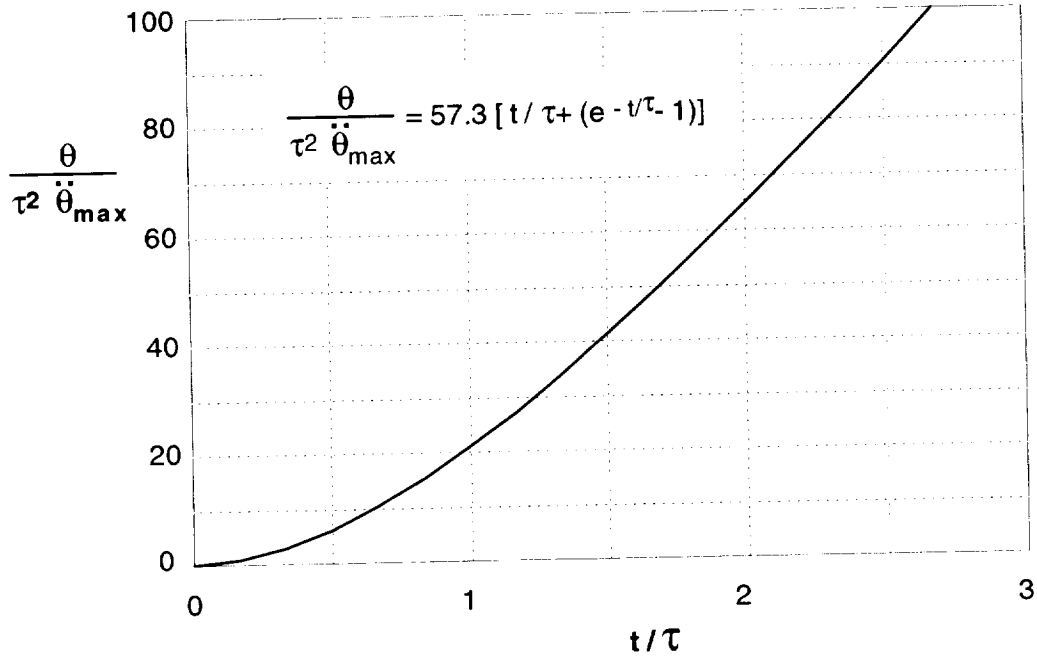

Figure 38. First-order attitude-rate command system response to step control input.

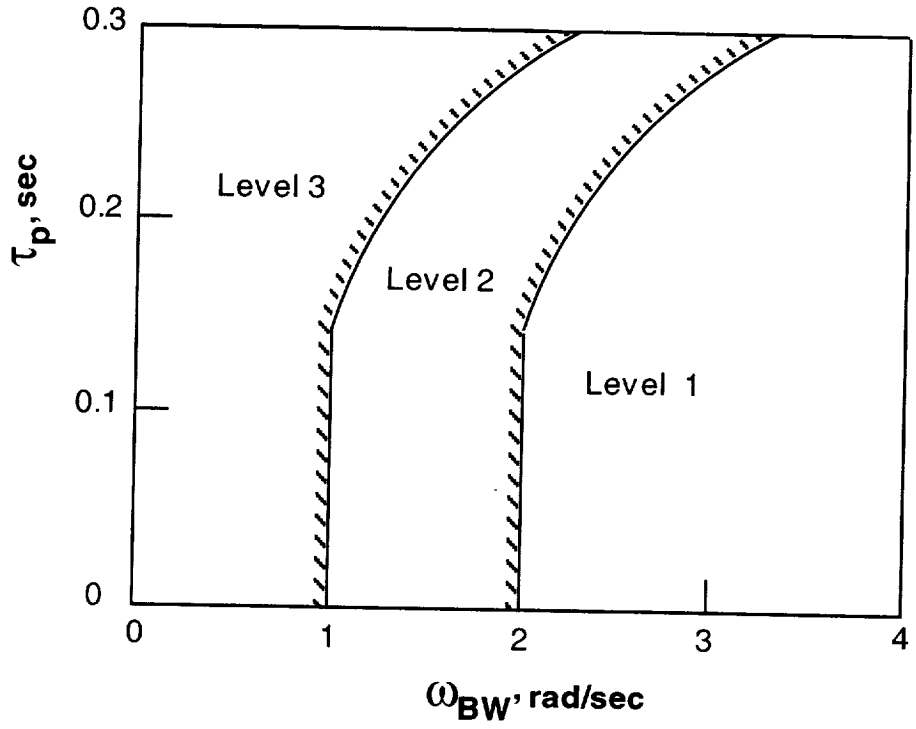

Figure 39. Pitch-attitude dynamic response requirement.

outset of this report. Level 1 and 2 requirements are shown in figure 39. To achieve Level 1 characteristics, attitude-response bandwidths of 2 rad/sec or greater are necessary. These requirements for bandwidth increase as phase delay increases above 0.15 sec.

No formal design criteria exist for longitudinal velocity control. Criteria are provided in both references 9 and 10 for vertical velocity response. For control authority, reference 9 states the requirement in terms of minimum levels of thrust-to-weight ratio or in terms of a minimum rate-of-climb capability, that is, the minimum rate of climb that can be achieved with maximum thrust. Reference 10 bases the requirement on thrust-to-weight or Δg. Figure 40 shows these respective requirements. The minimum requirement for thrust-to-weight for Level 1 is 1.05. An alternative requirement in terms of incremental acceleration calls for 0.1 g vertical acceleration to permit precise height control and to arrest a rate of descent. It may appear that these two requirements are inconsistent. However, a vertical descent requires thrust to be reduced to somewhat less than thrust-to-weight of 1. If enough vertical velocity damping is present, thrust-to-weight may be reduced to around 0.95, leaving a 0.1 Δg margin between 0.95 and 1.05 thrust-to-weight for arresting the sink rate.

At the bottom of the figure, reference 9 indicates that there is some experience indicating that a thrust-to-weight ratio less than 1.1 may be accepted in the presence of higher vertical velocity damping. The reasoning anticipates that less thrust control is required if the pilot does not have to provide so much height damping. Hence, as little as 3 percent thrust margin might be acceptable.

Other research based on simulator and flight data (ref. 23) contends that a minimum level of vertical velocity damping of about –0.3 sec^{-1} is necessary to achieve satisfactory height control characteristics. To realize those levels of damping on fixed-wing V/STOL aircraft having minimal aerodynamic forces in hover requires artificially provided damping through control augmentation.

FLYING QUALITIES REQUIREMENT	MIL-F-83300 (Ref. 10)		AGARD 577 (Ref. 9)	
	T/W_{min}	Δg_{min}	T/W_{min}	$\dot{h}_{min}$ ft/min
LEVEL 1 Satisfactory Without Improvement	1.05	0.1	1.03-1.1	600
LEVEL 2 Adequate Improvement Warranted	1.02	0.05		

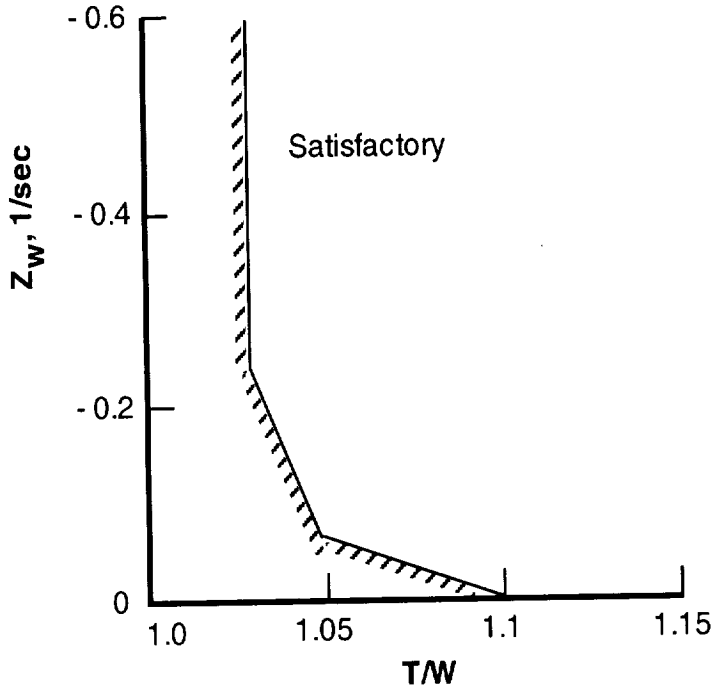

Figure 40. Requirements for heave control authority in hover.

The requirements noted above from references 9 and 10 apply for operations out of ground effect and do not account for the influence of ground-induced disturbances on the aircraft. However, recent NASA research has shown the need to consider the influence of ground effect on the thrust required for the vertical landing. Reference 24 provides criteria for thrust-to-weight ratio as a function of mean ground effect and ingestion. Figure 41 (from ref. 24) presents the criteria, where mean ground effect and ingestion are defined by the integral function and $\Delta L/T$ incorporates jet-induced aerodynamic lift and thrust variations with engine inlet temperature. The range of wheel height over which the mean ground effect and ingestion is based is 0 to 43 ft. Thrust-to-weight to the right of the boundary is acceptable for the landing for a given ground effect and ingestion. The upper part of the boundary for positive ground effect is more appropriately concerned with having enough thrust margin to hover out of ground effect. Note that a thrust-to-weight ratio of 1.03 was found to be acceptable in this case, in contrast to the higher values noted in the earlier work. As ground effect becomes negative, the pilot's primary concern is the ability to arrest a rate of decent at a reasonable decision height. The pilot is unwilling to initiate the descent to landing without the ability to temporarily halt the landing. The boundary was established based on a decision height of 15 ft, which means the aircraft could descend to 15 ft at a nominal landing sink rate of the order of 4 ft/sec, and at 15 ft apply maximum thrust and not touch the surface. Finally, at the far right of the boundary, the main concern is sink rate at touchdown. As the aircraft descends below decision height, the pilot does not want the aircraft to accelerate into ground effect at an unacceptably high sink rate that could damage the landing

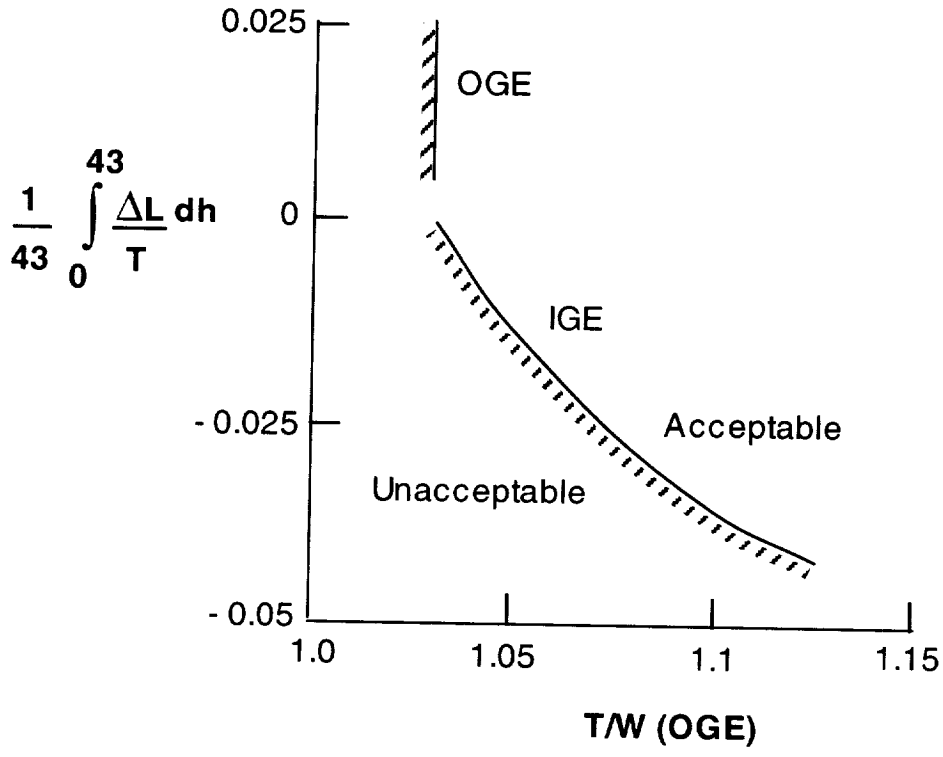

Figure 41. Influence of ground effect and hot gas ingestion on thrust margin for vertical landing.

gear. This boundary is based on moving-base simulation data for the Harrier. It is also based on AV-8B and the AV-8A operational requirements. The AV-8A and AV-8B anchor the curve at the lower right and upper left end points, respectively.

Requirements for dynamic response can be defined in terms of height control bandwidth with the throttle, which includes the contributions of the basic aircraft and propulsion system to height response. For Level 1 characteristics, reference 25 suggests a bandwidth with 45 deg phase margin for altitude response to the throttle of 0.6 rad/sec. From reference 26, the Level 2 requirement is 0.3 rad/sec. The Harrier or any other fixed-wing V/STOL aircraft will fall well below those values and would not meet Level 2 requirements. Precise height control with these aircraft would be difficult. Thus, control augmentation is typically required to achieve satisfactory height control.

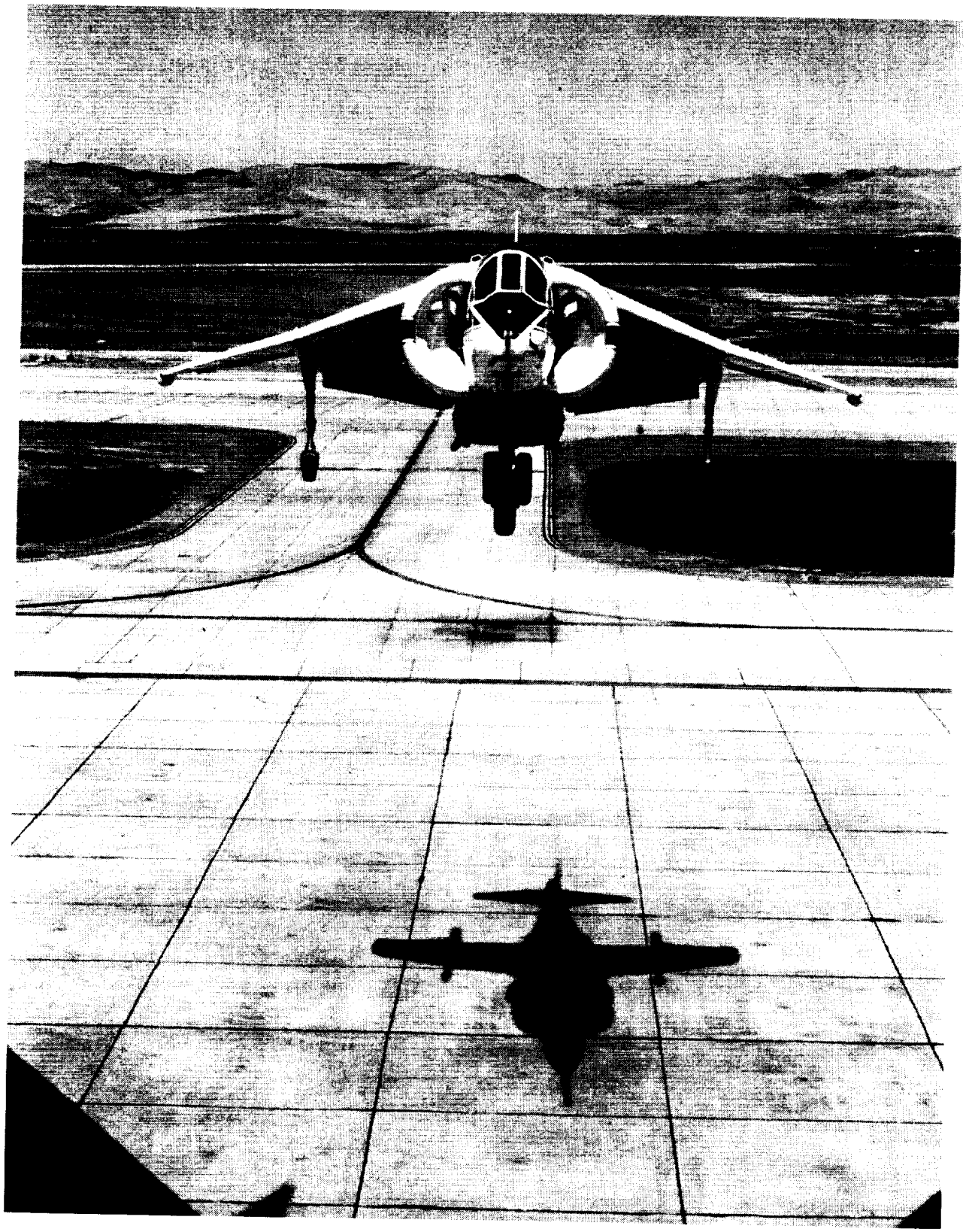

LATERAL-DIRECTIONAL FLYING QUALITIES IN HOVER

Lateral-directional flying qualities in hover are concerned with control of bank angle, lateral velocity, and heading, and their analysis is similar to and symmetric with the longitudinal case.

Bank Angle Control

Inner-loop attitude control is of primary concern in this case as it is for longitudinal control in hover. The transfer function for bank angle to the lateral stick is

$$\frac{\phi}{\delta_s} = \frac{L'_{\delta_s}(s + 1/T_{\phi_1})(s + 1/T_{\phi_2})}{\Delta_{Lat}}$$

where the characteristic equation derived previously is

$$\Delta_{Lat} = (s + 1/T_r)(s + 1/T_R)(s^2 + 2\zeta\omega_d s + \omega_d^2)$$

and consists of two real roots and a complex pair. Terms in the numerator include control sensitivity and two real roots. If roll due to yaw and side force due to the lateral control are negligible, these two roots are given by $1/T_{\phi 1} = -N'_r$ and $1/T_{\phi 2} = -Y_v$. The first term will cancel the like term in the characteristic roots, and the transfer function becomes

$$\frac{\phi}{\delta_s} = \frac{L'_{\delta_s}(s + 1/T_{\phi_2})}{(s + 1/T_R)(s^2 + 2\zeta\omega_d s + \omega_d^2)}$$

A root locus plot with the pilot represented by only a gain reveals the same problem as observed earlier for pitch control (fig. 42). As the loop is closed at progressively higher gain, the unstable

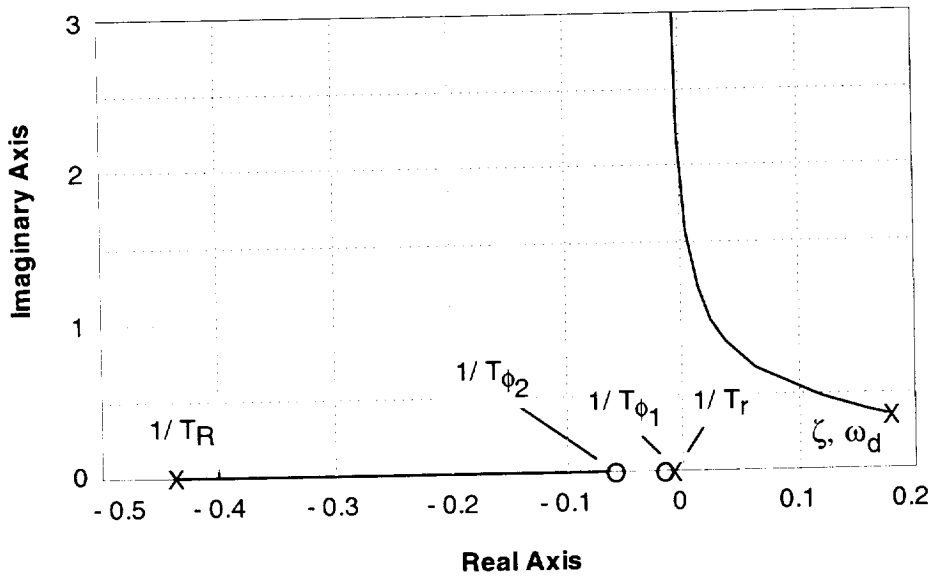

Figure 42. Root locus of bank-angle control for the Harrier in hover.

Dutch roll complex pair is barely stabilized. Thus, it is necessary to introduce lead compensation to achieve a reasonable level of stability. Figure 43 presents an example of a root locus and

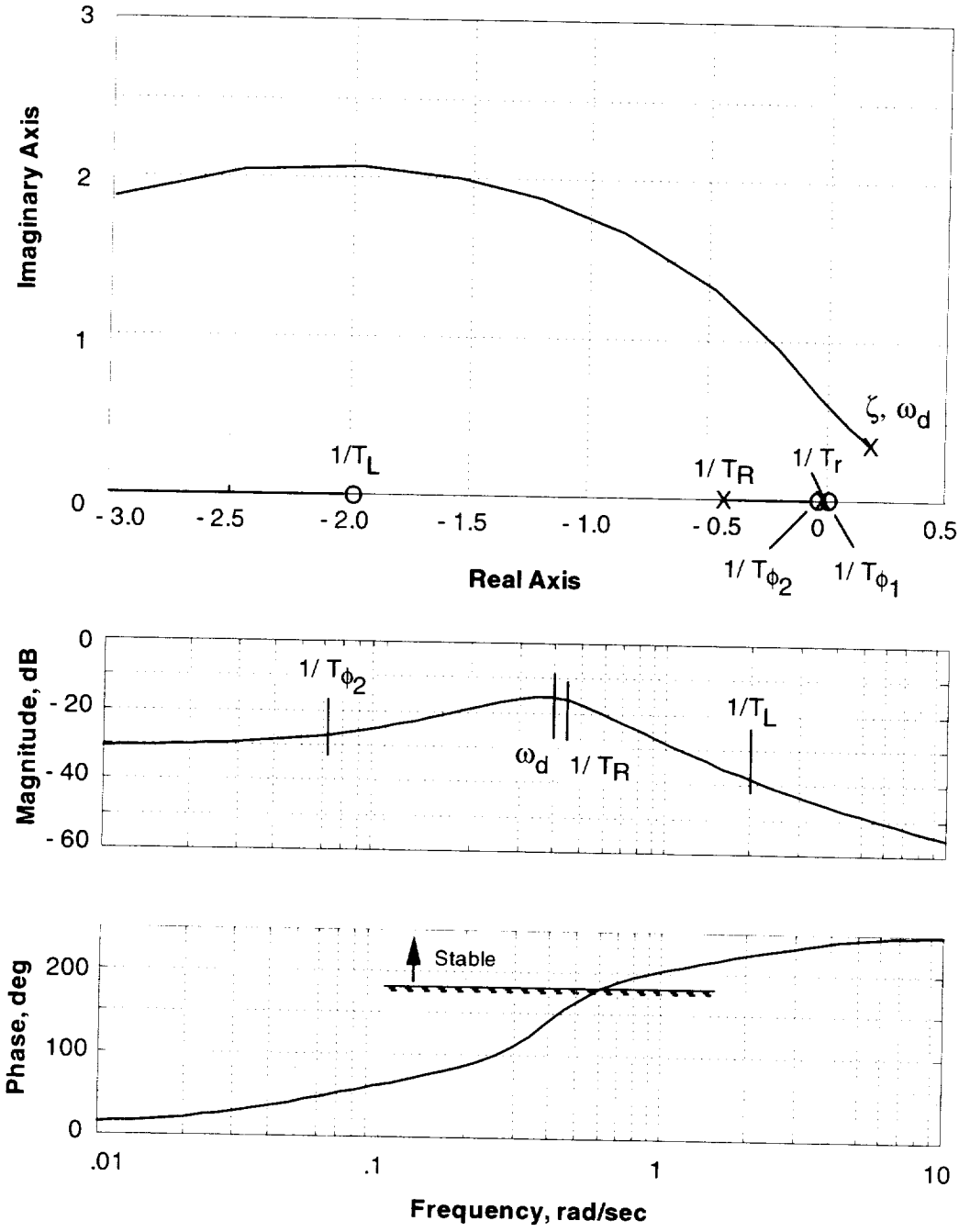

Figure 43. Root locus and Bode plots of bank-angle control for the Harrier in hover.

Bode plot that illustrate the effect of lead compensation. In this situation, the Dutch roll root is readily stabilized; the pilot can accomplish this with good bank angle cues in visual flight by responding with sufficient lateral control to maintain the desired attitude. The open-loop Bode plot indicates that the pilot's gain can be raised sufficiently to stabilize the Dutch roll and achieve adequate phase margin for a bandwidth of 2-4 rad/sec. Note the low-frequency droop in the

magnitude plot, which indicates that the steady-state response will not match its commanded value. This deficiency could be rectified, as in the longitudinal case, with integral compensation.

Lateral Velocity Control

Control of the aircraft's lateral translation is accomplished with changes in bank angle. For most V/STOL aircraft, the aircraft's roll attitude must be used to tilt the thrust vector in order to generate the force component necessary to move the aircraft laterally. The open-loop transfer function of lateral velocity to the lateral control is

$$\frac{v}{\delta_s} = \frac{Y_{\delta_s}(s + 1/T_v)(s^2 - L'_p s + g\frac{L'_{\delta_s}}{Y_{\delta_s}})}{\Delta_{Lat}}$$

When the side force due to lateral control Y_{δ_s} can be neglected, this transfer function becomes

$$\frac{v}{\delta_s} = \frac{gL'_{\delta_s}(s + 1/T_v)}{(s + 1/T_r)(s + 1/T_R)(s^2 + 2\zeta\omega_d s + \omega_d^2)}$$

and if L'_r is negligible, $1/T_v = -N'_r$. The difficulty with direct control of translational velocity with the stick that appeared longitudinally exists for lateral velocity control as well. The root locus plot of figure 44 illustrates this problem, since the basic aircraft is unstable and feedback of

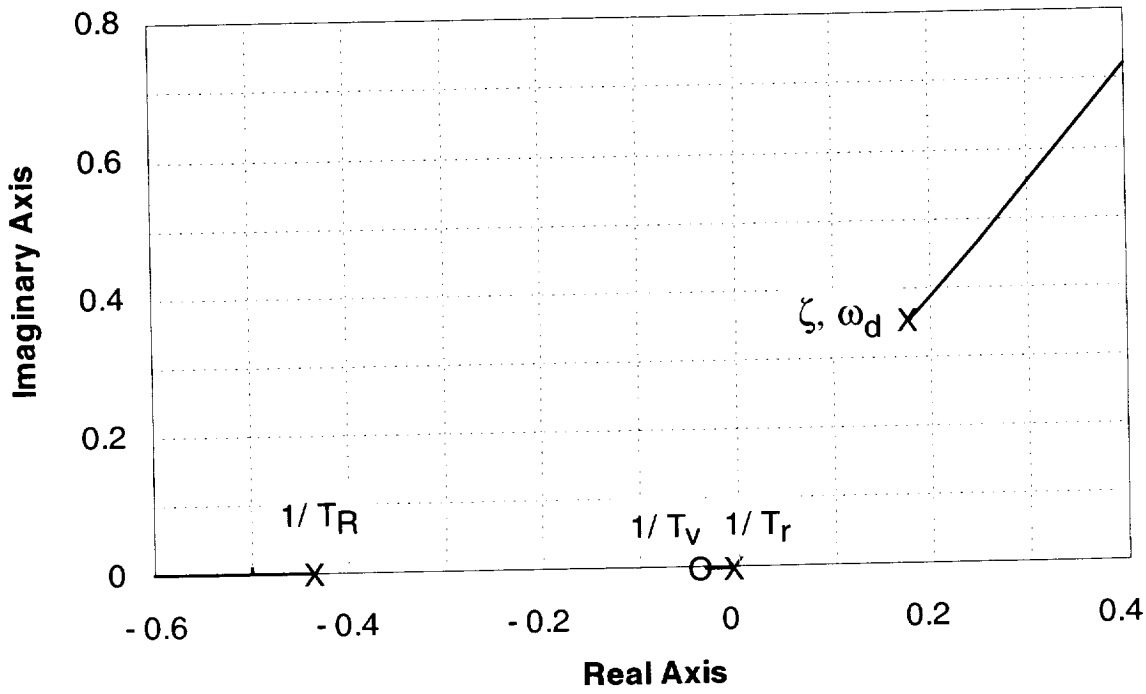

Figure 44. Root locus for lateral-velocity control for the Harrier in hover.

lateral velocity to lateral stick aggravates the instability. As in the longitudinal case, it is essential that the aircraft attitude be stabilized before control of lateral velocity is attempted. An example for the Harrier with the bank-angle inner loop closed is shown in the root locus plot of figure 45. Starting with a stable set of characteristic roots associated with the bank-angle loop

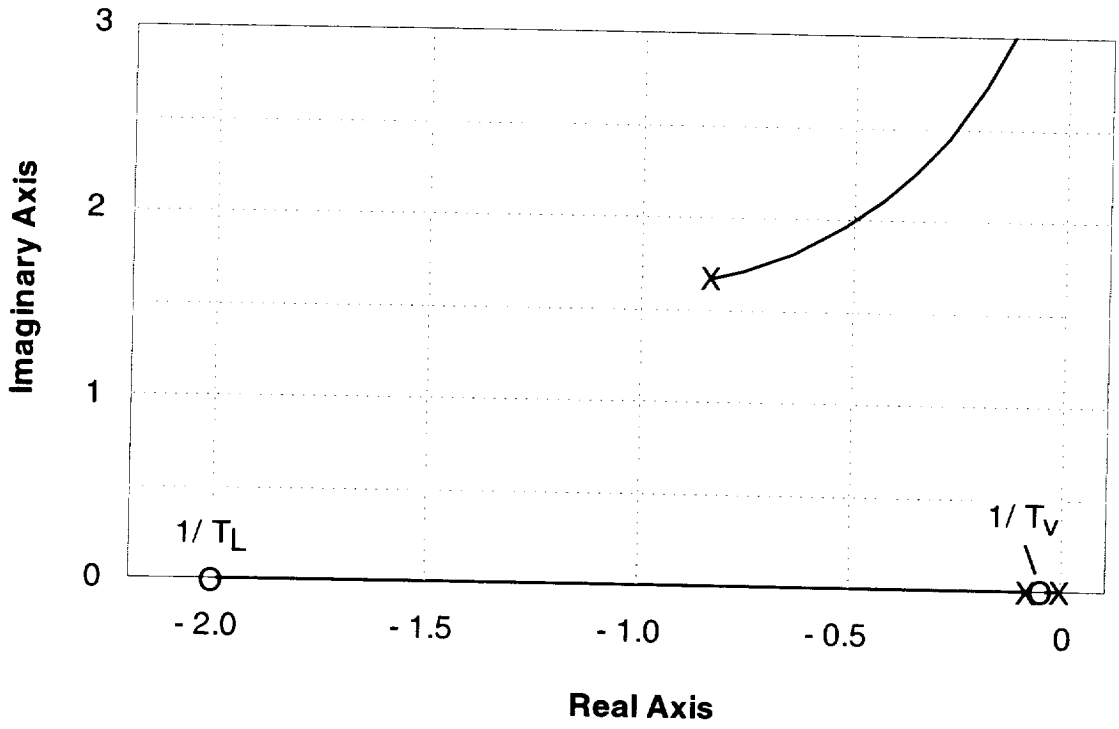

Figure 45. Root locus of lateral-velocity control with bank-angle inner loop for the Harrier in hover.

closure, closure of the velocity loop still leaves the system with adequate stability. Note the presence of the lead compensation numerator root from the bank-angle inner loop. Thus, once the bank-angle loop is stabilized, lateral velocity can be controlled without the need for lead compensation in the velocity-control loop.

A simplified relationship of lateral velocity response to bank angle can be expressed in a form similar to that for longitudinal velocity. The transfer function, derived from the side-force equation is

$$\frac{v}{\phi_c} = \frac{g}{s - Y_v}$$

This assumption is based on modal separation between the bank-angle inner loop and the velocity response and eliminates the yawing- and rolling-moment equations, based on the decoupling of yaw response from roll and lateral velocity. Thus, the control input for the lateral axis can be considered to be commanded bank angle. It relies on tight control of aircraft attitude, where bank-angle changes are made quickly and are followed by lateral velocity response. The inverse

time constant is equal to lateral velocity damping. As in the longitudinal case, this approximation captures the essence of the characteristics of lateral velocity response to the pilot's input.

Yaw Control

The final lateral-directional response to consider in hover is yaw in response to the pedals, which is described by the yaw rate transfer function,

$$\frac{r}{\delta_p} = \frac{N'_{\delta_p}(s + 1/T_r)(s^2 + 2\zeta\omega_r s + \omega_r^2)}{\Delta_{Lat}}$$

The first term is yaw control sensitivity or yaw acceleration due to directional control input. In the absence of significant side force or rolling moments due to the directional control, the first-order and second-order numerator roots combined are identical to the first- and second-order pair in the characteristic roots. With that pole-zero cancellation, the remaining terms are the control sensitivity and the first-order lag associated with yaw damping, and the transfer function becomes

$$\frac{r}{\delta_p} = \frac{N'_{\delta_p}}{s - N'_r}$$

The steady-state yaw rate to pedal is determined by the ratio N'_{δ_p}/N'_r, and the inverse time constant for the lag is defined by the yaw damping derivative N'_r.

Lateral-Directional Flying Qualities Requirements in Hover

Roll-axis flying qualities requirements are similar in form to those for the pitch axis. Control power is again expressed in terms of the ability to change bank angle within a specified time interval. In this case, Level 1 flying qualities noted in reference 10 demand 4 deg of bank angle change in 1 sec; Level 2 requirements are 2.5 deg in the first second. Recent research on more modern V/STOL fighters (ref. 24) indicates that these criteria should be increased to 6 deg in 1 sec for Level 1. For roll-axis dynamics, the bandwidth and phase delay requirements for the pitch axis apply. Flying qualities criteria for the yaw axis relate to control power and the yaw response time constant. Specifically, reference 10 requires a heading change of 6 deg in the first second following an abrupt pedal input if Level 1 flying qualities are to be achieved. For Level 2, a 3-deg heading change in 1 sec is sufficient. The research in reference 24 suggests that the Level 1 requirement could be relaxed to 4 deg in 1 sec. Requirements for yaw dynamics are stated in terms of the yaw inverse time constant, which for Level 1 is 2 rad/sec and for Level 2, 1 rad/sec.


NASA
704

LONGITUDINAL FLYING QUALITIES IN FORWARD FLIGHT

The analysis of longitudinal flying qualities in forward flight involves a loop structure similar to that for hover. That is, the pitch-attitude inner loop is closed first, followed by the airspeed, flightpath, and altitude outer loops. As will be seen shortly, the attitude-loop closure provides compensation that improves the dynamics of the subsequent loop closures.

Pitch Attitude Control

The open-loop transfer function for pitch-attitude response to the longitudinal control in forward flight appears with two real numerator roots and the characteristic equation that was derived in an earlier section:

$$\frac{\theta}{\delta_s} = \frac{M_{\delta_s}(s + 1/T_{\theta_1})(s + 1/T_{\theta_2})}{\Delta_{Long}}$$

where the characteristic roots as derived earlier are

$$\Delta_{Long} = (s^2 + 2\zeta\omega_p s + \omega_p^2)(s^2 + 2\zeta\omega_{sp} s + \omega_{sp}^2)$$

The first of the numerator roots is dominated by longitudinal velocity damping, which is determined in part by the aircraft's trim drag associated with X_u. The approximation is

$$1/T_{\theta_1} \doteq -X_u + Z_u \frac{X_w}{Z_w}$$

This root can be modified by terms that, among other things, include induced drag X_w and vertical velocity damping Z_w. The second factor in the numerator is dominated by vertical velocity damping (determined by lift curve slope, wing loading, and airspeed) and is described by

$$1/T_{\theta_2} \doteq -Z_w + M_w \frac{Z_{\delta_s}}{M_{\delta_s}}$$

It is modified by lift due to the normal force from the longitudinal control, Z_{δ_s}. If this term can be neglected, the numerator factor is determined solely by vertical velocity damping. The values associated with this numerator factor are typically of the order of 0.5 rad/sec over the part of the flight envelope of interest.

In performing maneuvers, the pilot is concerned with the aircraft's short-term pitch response. This response is associated with the short-period mode, for which the pitch rate due to the longitudinal stick can be approximated by the following expression

$$\frac{q}{\delta_s} \doteq \frac{M_{\delta_s}(s + 1/T_{\theta_2})}{s^2 + 2\zeta\omega_{sp} s + \omega_{sp}^2}$$

This representation is found in most aircraft dynamics texts (refs. 15-19) and describes the pitch changes that occur at approximately constant airspeed. Under those circumstances it is reasonable to disregard the drag equation and to rely on the lift and pitching moment equations, based on angle of attack and pitch rate, to describe the motion. From another viewpoint, this approximation relies on separation of the response of the high-frequency (short-period) and low-frequency (phugoid) modes. Thus, neither the phugoid root nor the low-frequency numerator term appears in the transfer function. In this approximation, the short-period frequency and damping govern the bandwidth of pitch control. Further, the position of the numerator root with respect to the short-period frequency determines the amount of overshoot in the response. As noted earlier in the text, short-period frequency is influenced prominently by longitudinal static stability M_α, and short-period damping is determined by pitch damping M_q and by pitching moment due to rate change of angle of attack $M\dot{\alpha}$. The numerator factor, as noted above, is related to vertical velocity damping Z_w. These relationships illustrate the connections between the basic vehicle characteristics and dynamic response that are important to the pilot.

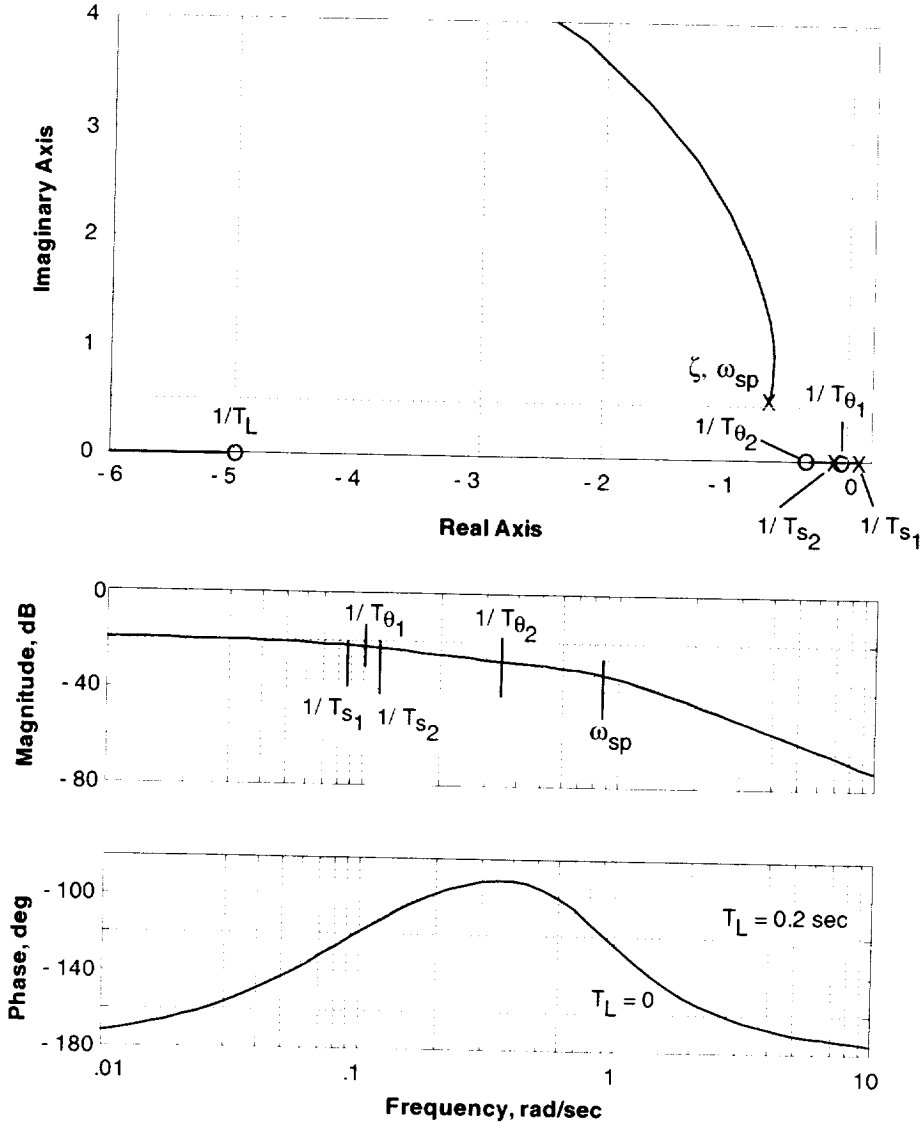

Figure 46. Root locus and Bode plots of pitch-attitude control for the Harrier at 100 knots.

Returning to the complete transfer function for pitch response to the longitudinal control, the characteristics of closed-loop control can be seen in the root locus and Bode plots of figure 46. The root locus shows an example for the Harrier in semi-jet-borne flight at 100 knots that includes lead compensation. The open-loop short period is reasonably well damped, although at a low frequency of about 0.8 rad/sec. The aircraft also has two real roots, which result from the negative value for M_u that has driven the phugoid, normally a low-frequency oscillatory root, into a pair of real roots, one of which is unstable. The two numerator roots for the pitch-to-stick transfer function and the numerator root associated with the pilot lead are also noted. The Bode plot shows inadequate phase margin if lead is not included. However, the modest amount of lead shown (T_L = 0.2 sec) provides more than adequate phase margin in the frequency range from 2-4 rad/sec. The closed-loop Bode plot in figure 47 shows that pitch response extends to 2 rad/sec before falling off. A time history plot (fig. 48) presents open- and closed-loop pitch response to the pilot's input. The open-loop

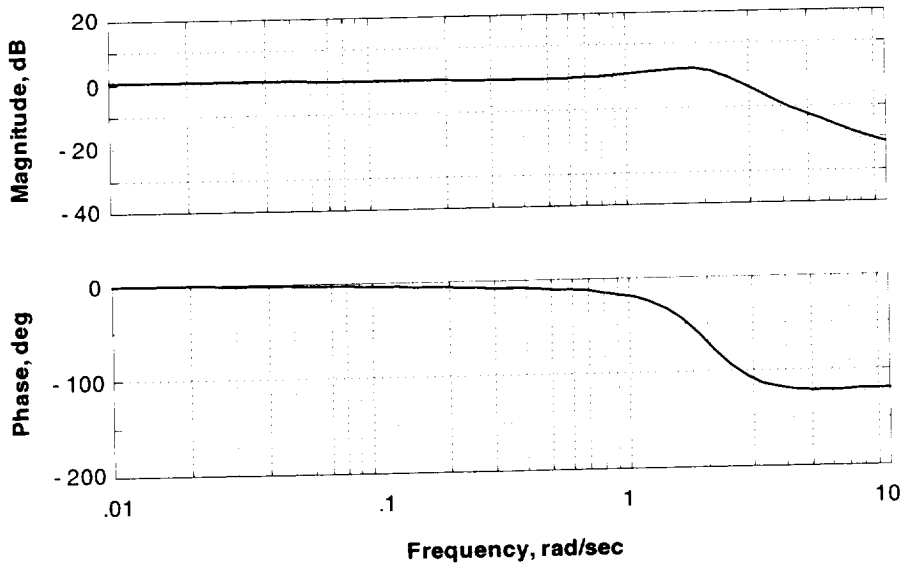

Figure 47. Closed-loop Bode plot for pitch-attitude control for the Harrier at 100 knots.

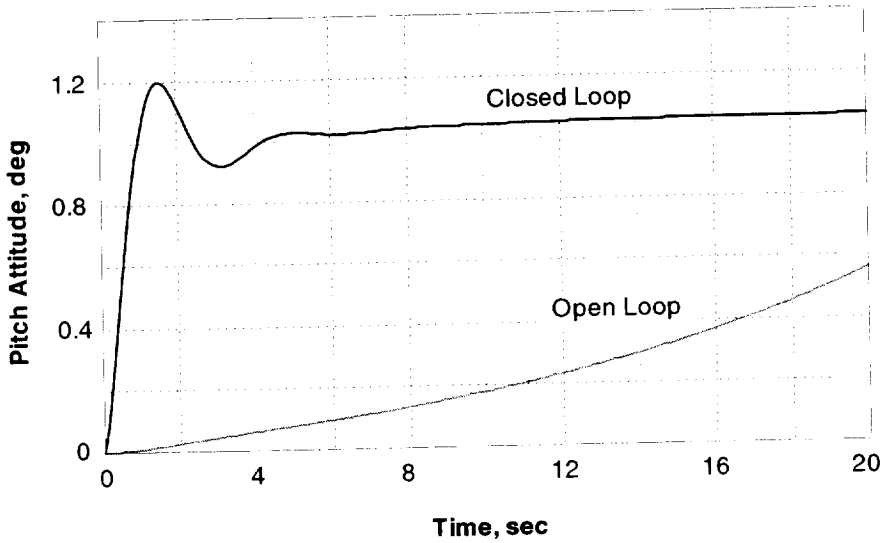

Figure 48. Time history of attitude response for the Harrier at 100 knots.

response clearly shows the exponential divergence associated with the unstable real root. However, the closed-loop response is deadbeat and quick enough to insure responsive as well as accurate pitch control. The level of lead compensation is not excessive and would not be associated with a great deal of pilot effort.

Airspeed Control

In principle, airspeed can be controlled either with the longitudinal stick or with thrust; however, when thrust is partially or completely deflected to augment basic aerodynamic wing lift, it no longer can serve as an effective control for the longitudinal axis. Further, over much of the low-speed flight regime, this class of aircraft operates on the so-called backside of the drag curve and, as will be seen subsequently, this characteristic renders the pitch control ineffective for flightpath control in the long term. Considering pitch control of airspeed, the open-loop transfer function of airspeed to longitudinal stick is

$$\frac{u}{\delta_s} = \frac{X_{\delta_s}(s + 1/T_{u_1})(s + 1/T_{u_2})(s + 1/T_{u_3})}{\Delta_{Long}}$$

The numerator is third order when the longitudinal control force X_δ is present. If that force is negligible, one of the numerator factors will drop out leaving two real roots. The approximation for the low-frequency numerator root is

$$1/T_{u_1} \doteq \frac{-g}{X_\alpha - g}\left(-Z_w + M_w \frac{Z_{\delta_s}}{M_{\delta_s}}\right)$$

and is determined principally by vertical velocity damping if X_α is small. The other root typically is high-frequency and is not a strong influence on the loop closure.

The root locus in figure 49 shows that the loop closure of airspeed to the longitudinal stick causes the real pair of roots to coalesce and move into the right-half plane. As noted earlier for the hover case, it is not feasible to control airspeed without first stabilizing pitch attitude. Without this compensation, the pilot would continually chase airspeed through the poorly damped low-frequency oscillation, and in attempting to control speed tightly would drive the system unstable. Thus, as in the hover case, the attitude loop must be closed first, with airspeed controlled by modulating pitch attitude. The airspeed transfer function with the pitch-attitude loop closure appears as

$$\frac{u}{\theta_c} = \frac{X_{\delta_s} K_\theta (T_L s + 1)(s + 1/T_{u_1})(s + 1/T_{u_2})(s + 1/T_{u_3})}{(s + 1/T'_{s_1})(s + 1/T'_{s_2})(s^2 + 2\zeta\omega'_{sp} s + \omega'^2_{sp})}$$

where θ_c is the attitude command input. The numerator is the same as that for the open-loop airspeed transfer function and includes the pilot's lead compensation in the pitch loop. The characteristic roots are those for the attitude loop closure. The root locus for airspeed control with the pitch inner loop closed (fig. 50) shows that the low-frequency roots associated with

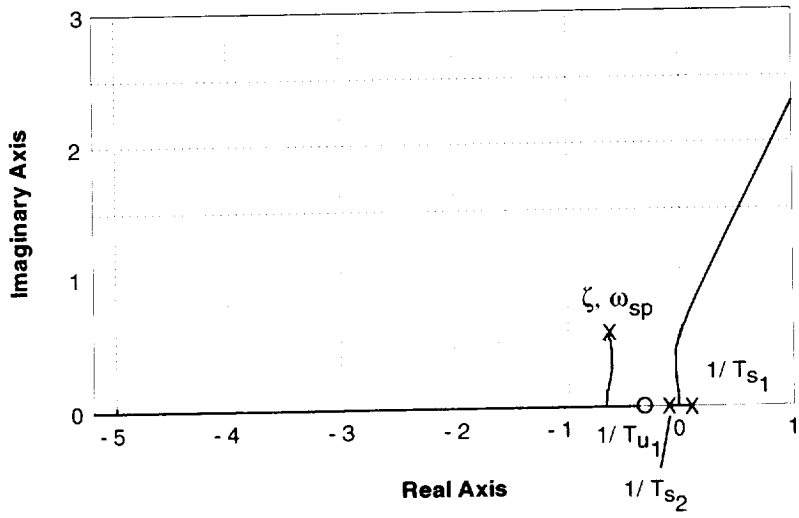

Figure 49. Root locus of airspeed control for the Harrier at 100 knots.

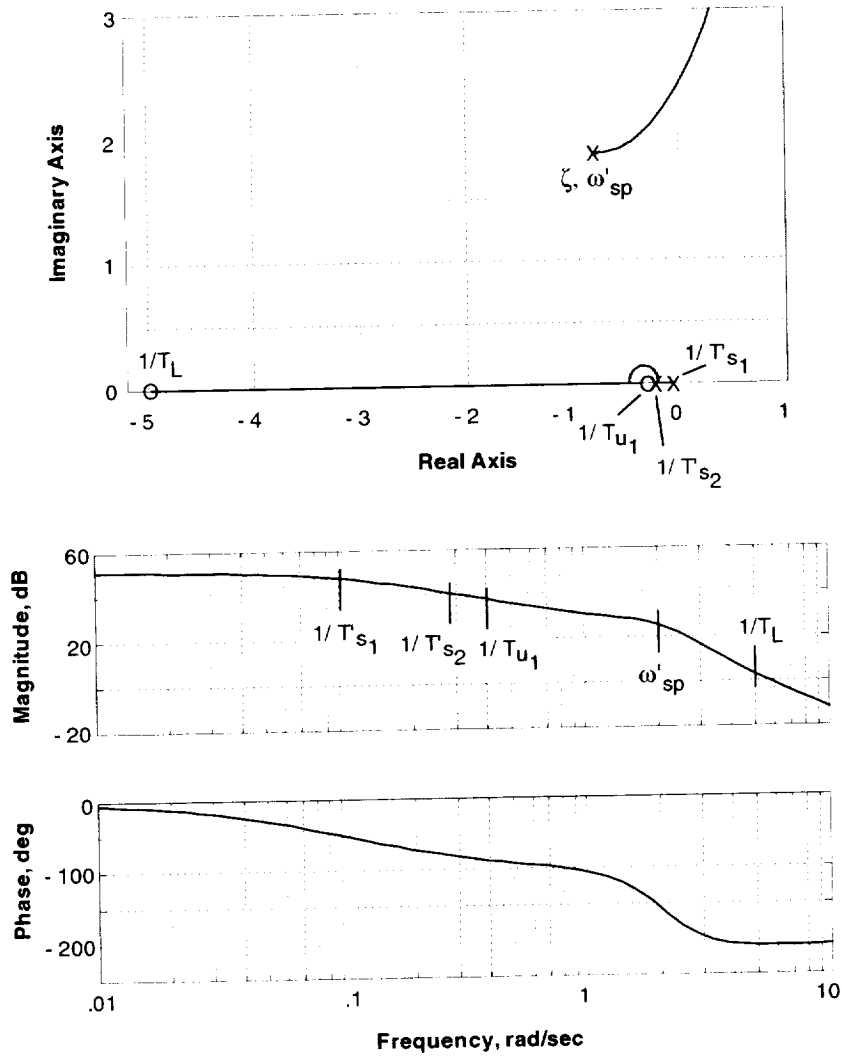

Figure 50. Root locus and Bode plots of airspeed control with pitch-attitude loop closed for the Harrier at 100 knots.

airspeed response are strongly stabilized and that the short-period damping is reduced. The important point is that the speed-loop closure no longer destabilizes the low-frequency roots. The aircraft's airspeed response will take place over a bandwidth associated with the lowest frequency mode.

The Bode plot clearly indicates the significance of the low-frequency root to airspeed control with the roll-off in response at frequencies above the root at $1/T'_{s_1}$. Thus, the essence of airspeed response to changes in pitch attitude can be characterized by the time constant associated with that first-order lag. This simplified view is justified by the time history of airspeed response to attitude shown in figure 51. The variation of airspeed shows an exponential convergence to a new steady-state value with a time constant of the order of 10-15 sec, which is comparable to that of the low-frequency mode at $1/T'_{s_1}$. Further, it is clear that closing the attitude loop has changed the airspeed response from a poorly damped, low-frequency oscillation at phugoid frequencies into an exponential convergence. The airspeed time constant is associated with longitudinal velocity damping X_u. Although the response is not that simply described, it is reassuring to see that such an approximation provides a reasonable indication of the aircraft's behavior.

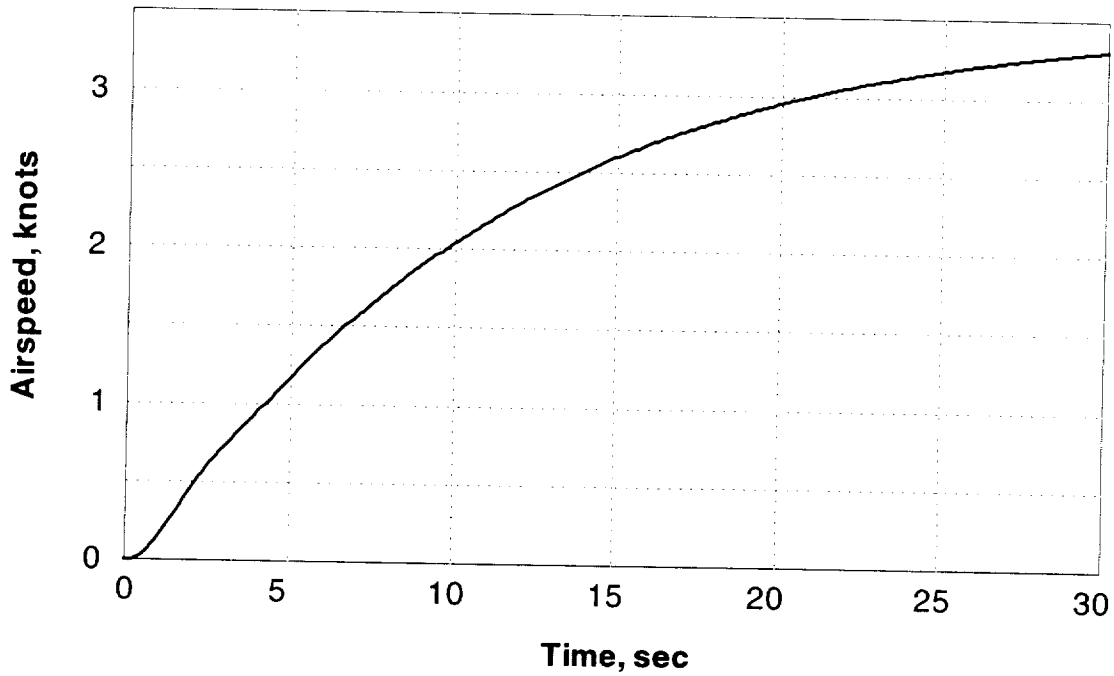

Figure 51. Time history of airspeed response to pitch attitude for the Harrier at 100 knots.

Altitude Control

For altitude control, either of two control techniques may be used depending on the region of the flight envelope in which the aircraft is operating, in particular with regard to the region of the drag versus speed curve. When operating on the frontside of the drag curve, that is, where the aircraft climbs as the nose is raised and airspeed is reduced, control of altitude with the pitch control is appropriate. Conversely, on the backside of the drag curve, the aircraft descends as

airspeed is reduced, and control of altitude must be achieved with the use of thrust. Examining the pitch-control option, first without inner-loop attitude stabilization, the open-loop response of altitude control to longitudinal stick is described by

$$\frac{h}{\delta_s} = \frac{-Z_{\delta_s}(s + 1/T_{h_1})(s + 1/T_{h_2})(s + 1/T_{h_3})}{s\Delta_{Long}}$$

The free s in the denominator arises from the integration of vertical velocity to altitude. The transfer function includes a third-order numerator over a fifth-order denominator. The second and third numerator terms are typically at high frequency, well beyond the range that is appropriate for control of altitude with longitudinal stick. The first root is typically much lower in frequency and is influenced by the trim level of drag and induced drag according to the approximation

$$1/T_{h_1} \doteq -X_u + \frac{Z_u}{Z_w}\left(X_w - \frac{g}{U_o}\right)$$

In the low-speed region of the flight envelope, the relative values of the individual terms in this approximation can cause the sign of this root to be either positive or negative, such that the numerator root can lie either in the left- or right-half plane. Positive values of $1/T_{h_1}$ can be shown to correspond to the portion of the performance envelope lying on the frontside of the drag curve. Conversely, operation on the backside of the drag curve corresponds to negative values of $1/T_{h_1}$ and to non-minimum phase characteristics of the transfer function. Thus, even if the aircraft is stable open loop, with the numerator root in the right-half plane, closed-loop control can become unstable. An example of this behavior is shown in the root locus plot for altitude response to the longitudinal stick for the Harrier in figure 52. Two undesirable characteristics are apparent in the

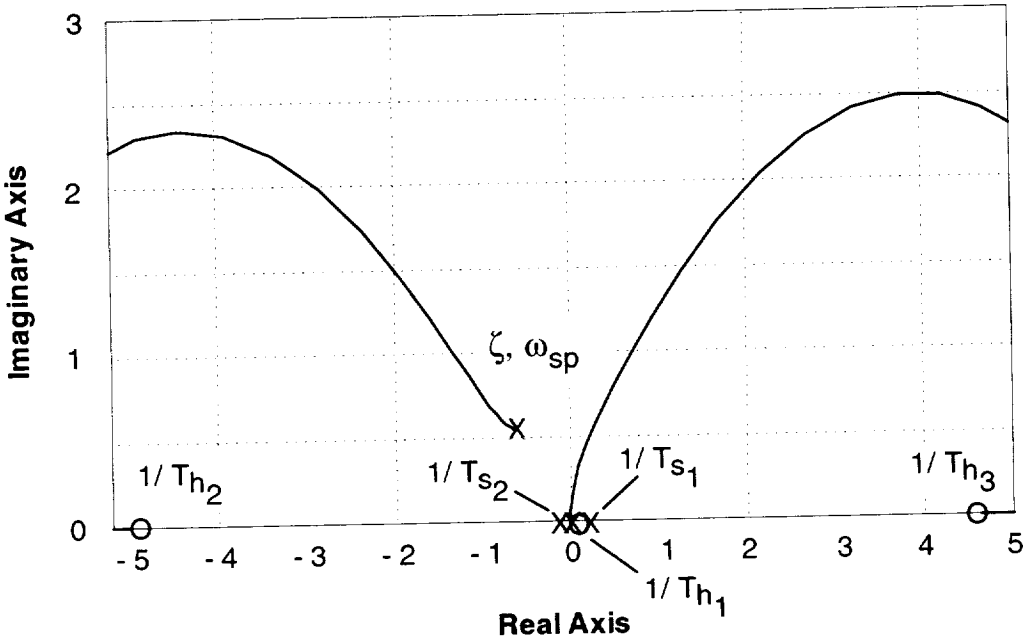

Figure 52. Root locus of altitude control with the longitudinal control for the Harrier at 100 knots.

root locus. First, as was the case for airspeed control, the two low-frequency roots are driven into an unstable complex pair. Thus, in the attempt to control altitude with the longitudinal stick, the pilot will be continually chasing altitude through this unstable oscillation. Further, the low-frequency numerator factor appears in the right-half plane and confines the open-loop unstable root in the right-half plane, producing an exponential divergence in altitude in response to the longitudinal control. If the numerator factor had been in the left-half plane, this low-frequency root could have been stabilized. Both of these issues, that of need for attitude stabilization and the location of the numerator root, must be considered in order to obtain acceptable altitude control at low speed.

The first problem can be resolved, as in the case for airspeed control, by closing the attitude inner loop. Given that pitch attitude is satisfactorily controlled, as demonstrated in the previous section, the roots for altitude response to longitudinal stick are as shown in figure 53. The altitude response to attitude command transfer function is

$$\frac{h}{\theta_c} = \frac{-Z_{\delta_s} K_\theta (T_L s + 1)(s + 1/T_{h_1})(s + 1/T_{h_2})(s + 1/T_{h_3})}{s(s + 1/T'_{s_1})(s + 1/T'_{s2})(s^2 + 2\zeta\omega'_{sp} s + \omega'^2_{sp})}$$

The numerator roots are the same as shown previously for the open-loop altitude response. If the pilot produces lead in the attitude loop, that lead compensation term also appears in the numerator. The denominator is composed of the same closed-loop short-period roots and the two closed-loop real roots that were produced by the attitude inner-loop closure noted earlier. The figure shows that closing the altitude loop does not produce a poorly damped low-frequency oscillation. If this was the only concern, it would be possible to make the aircraft climb to a given altitude by pulling the nose up to a predetermined pitch attitude, allowing the climb to develop, then on approaching the desired altitude, pushing the nose back to the initial trim reference. However, the location of the low-frequency numerator term remains a concern when it lies in the right-half plane. The only recourse will then be to use another control that does not exhibit the non-minimum phase characteristic and attendant problem of closed-loop stability.

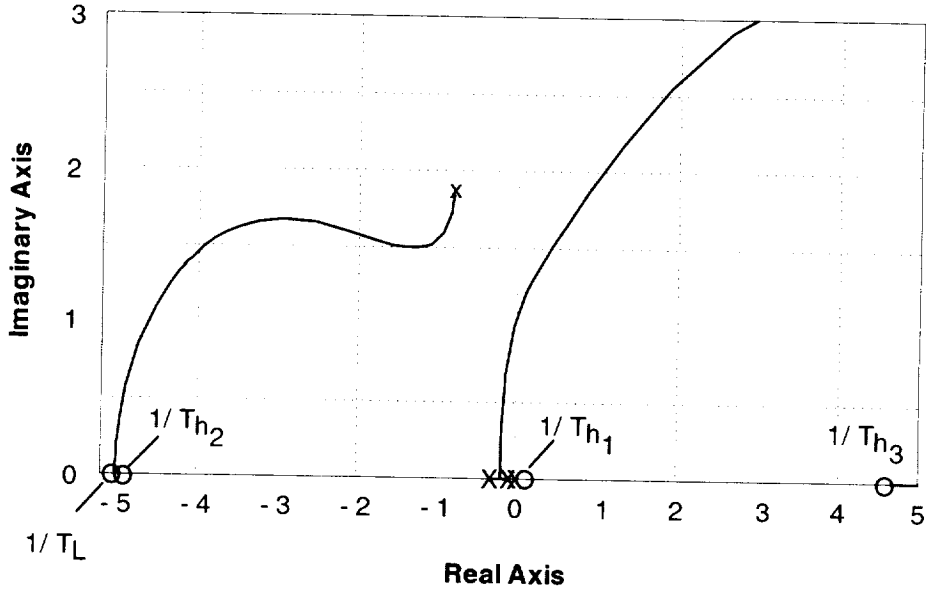

Figure 53. Root locus of altitude control with pitch-attitude loop closed for the Harrier at 100 knots.

Simplified Longitudinal Dynamics: Pitch Attitude Stabilized

Before proceeding further with the longitudinal control analysis, it is useful to simplify this analysis to provide a better understanding of the link between the aircraft configuration and the flightpath and airspeed responses to the pilot. Analysis of pitch-attitude response has been covered earlier in the text. Attitude response takes place at frequencies that are considerably higher than those associated with airspeed or flightpath response (e.g., 2-3 rad/sec vs 0.5 rad/sec). With the assumption that the pilot controls pitch attitude tightly and that attitude response and the associated dynamics are well separated in frequency from those for flightpath and airspeed, it was suggested in reference 27, in accord with the analysis in reference 28, that the removal of the attitude dynamics from consideration of the response of flightpath and airspeed is justified. Returning to the original three-degree-of-freedom open-loop equations,

$$\begin{bmatrix} s - X_u & -X_w & g\cos\gamma_o \\ -Z_u & s - Z_w & -(Z_q + U_o)s + g\sin\gamma_o \\ -M_u & -M_{\dot{w}}s - M_w & s^2 - M_q s \end{bmatrix} \begin{Bmatrix} u \\ w \\ \theta \end{Bmatrix} = \begin{Bmatrix} X_\delta \\ Z_\delta \\ M_\delta \end{Bmatrix} \delta$$

and using the assumptions mentioned, the pitching-moment equation can be eliminated from consideration. Then, the attitude-related terms in the longitudinal and vertical force equations can be transferred to the right-hand side to become control inputs to the two-degree-of-freedom coupled set. With the state variables changed to longitudinal velocity and flightpath angle, the equations above are rewritten as

$$\begin{bmatrix} s - X_u & U_o X_w \\ Z_u / U_o & s - Z_w \end{bmatrix} \begin{Bmatrix} u \\ \gamma \end{Bmatrix} = \begin{bmatrix} U_o X_w - g\cos\gamma_o & X_\delta \\ -Z_w + (g/U_o)\sin\gamma_o & -Z_\delta / U_o \end{bmatrix} \begin{Bmatrix} \theta_c \\ \delta \end{Bmatrix}$$

Flightpath angle, as derived in the original equations of motion, is $\gamma = \theta - \alpha$. The pilot's control inputs are the generalized control δ, which can represent either the thrust magnitude or thrust deflection, and θ_c, the commanded aircraft attitude. This two-degree-of-freedom, second-order set of equations substantially simplifies the analysis of airspeed and flightpath response to the pilot's primary controls. The characteristic roots factor into either a pair of real roots or a complex pair as follows:

$$\Delta_{Long} = s^2 + (-X_u - Z_w)s + X_u Z_w - X_w Z_u$$

$$= (s + 1/T_{\theta_1})(s + 1/T_{\theta_2})$$

or

$$(s^2 + 2\zeta\omega_\theta s + \omega_\theta{}^2)$$

Note that if either one of the two derivatives X_w or Z_u is zero, then the root at $1/T_{\theta_1}$ would be defined by the derivative X_u and the root $1/T_{\theta_2}$ would be represented by Z_w. As X_w and Z_u become significant, the roots migrate away from X_u and Z_w, and eventually combine into a complex pair. The influence on the characteristic roots of these four stability derivatives, which relate to the aircraft's lift and drag, is apparent. Although lift and drag are traditionally associated with aircraft performance, it is evident that they also play a significant role in the dynamic behavior of flightpath and airspeed as perceived by the pilot.

It should also be noted that the approximations for the characteristic roots shown above bear a similarity to the numerator roots of the pitch-attitude transfer function that appeared in the earlier section on pitch control. Recall that closure of the pitch-attitude loop caused the phugoid roots to migrate toward those two numerator roots at $1/T_{\theta_1}$ and $1/T_{\theta_2}$. If the pitch loop is closed tightly, the closed-loop roots will closely approach those numerator factors. Although pitch response is associated with the higher frequency short-period roots, airspeed and flightpath response are associated with the roots $1/T_{\theta_1}$ and $1/T_{\theta_2}$.

In general, the characteristics of flightpath and airspeed control that appear in the following discussion can be expressed by a transfer function of the form

$$\frac{r}{c} = \frac{K(s + 1/T)}{(s + 1/T_{\theta_1})(s + 1/T_{\theta_2})}$$

where response to the command is given by a gain, a first-order numerator root, and the second-order characteristic roots. Some general observations about the aircraft's response can be made for a transfer function of this form. First, in response to a step input, the initial response of the aircraft, which is the control sensitivity, is shown by the initial slope of the time response. This can be derived from the initial value theorem of Laplace transforms to be

$$\left[\frac{\dot{r}(t)}{c}\right]_{t\to 0} = \left[s\frac{sr(s)}{c}\right]_{s\to\infty} = K$$

Further, in the steady state, the Laplace transform final value theorem shows that

$$\left[\frac{r(t)}{c}\right]_{t\to\infty} = \left[s\frac{r(s)}{c}\right]_{s\to 0} = K\left(\frac{T_{\theta_1} T_{\theta_2}}{T}\right)$$

Dynamic response, interpreted either from Bode plots or from time histories, has particular properties as well. For example, in the Bode plot in figure 54, when the numerator root is at frequency well below that for the characteristic roots, the resulting peak in the frequency response translates into a time response that overshoots and then drops back to the steady state. When the arrangement of poles and zeros in the transfer function consists of a low-frequency characteristic root at lower frequency than the numerator root, the frequency response drops off immediately above $1/T_{\theta_1}$, meaning that the substantial part of the vehicle's response takes place at low frequency with a first-order time response as shown in the figure.

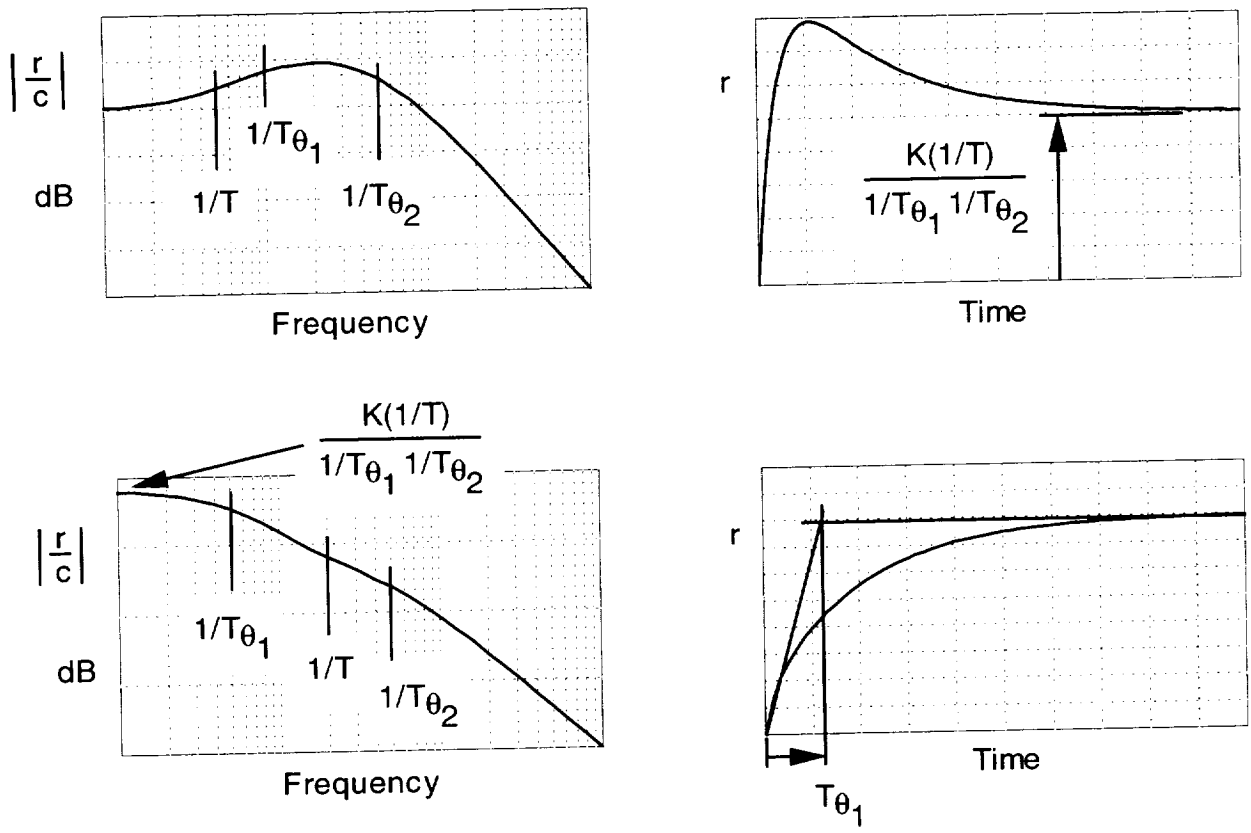

Figure 54. Example Bode plot and time histories for the generalized transfer function.

Airspeed Control

With these simplified equations, airspeed control performed by changing pitch attitude or thrust magnitude can be addressed. For the pitch control the airspeed transfer function is

$$\frac{u}{\theta_c} = \frac{(U_o X_w - g\cos\gamma_o)(s + 1/T_{u_\theta})}{\Delta_{Long}}$$

and is represented by a constant term, which determines the sensitivity of speed response to attitude, and a first-order numerator over a second-order denominator. The first-order numerator is approximated by a term that has a dominant contribution from vertical velocity damping:

$$1/T_{u_\theta} \doteq g\left(\frac{Z_w\cos\gamma_o - X_w\sin\gamma_o}{U_o X_w - g\cos\gamma_o}\right)$$

For reasonable values of these derivatives, which would include positive values of X_w and negative values of Z_w, the numerator root will typically be larger in value than Z_w alone. With a low-frequency root at $1/T_{\theta_1}$, and the numerator and other denominator term at higher frequency

in the region of Z_w, speed response is characterized by a first-order response with an inverse time constant of $1/T_{\theta_1}$. For an aircraft in forward flight, this time constant is ordinarily very long.

Next, consider the response of airspeed to changes in engine thrust. The relevant transfer function is

$$\frac{u}{\delta} = \frac{X_\delta (s + 1/T_{u_\delta})}{\Delta_{Long}}$$

In conventional flight with the thrust vector directed aft, the derivative X_δ is a large number, because most of the engine thrust is then oriented longitudinally. Whereas, with the aircraft in hover and the thrust vector deflected vertically, X_δ is small and possibly negative. The numerator root is given by

$$1/T_{u_\delta} = -Z_w + X_w \frac{Z_\delta}{X_\delta}$$

and contains the vertical velocity damping term and a further contribution based on the sign of X_δ and the ratio Z_δ/X_δ. Because X_w and X_δ are normally positive and because Z_δ is always negative, the second term is generally negative, which will reduce the magnitude of the numerator root compared to Z_w. Thus, the numerator will fall in a frequency range that will influence the nature of the airspeed response to thrust.

Table 5 shows characteristics that describe airspeed response to thrust for different relative values of X_δ and Z_δ, that correspond to different flight conditions. Deflected thrust aircraft, such as the Harrier and tilt rotors and some STOL aircraft, can span a range of these characteristics. When thrust is not deflected, Z_δ is zero, the numerator root reduces to $-Z_w$, and will approximately cancel the higher frequency of the two characteristic roots. Thus, airspeed response to thrust for that condition will be first-order with a long time constant. At the other extreme, with thrust deflected to the vertical, X_δ is zero and the transfer function becomes a constant term over the two characteristic roots. The low-frequency root again will dominate the response so that airspeed response to throttle under these circumstances will again be characterized by $1/T_{\theta_1}$. It should be noted that, with Z_δ negative and X_w positive, the steady-state response to an increase in thrust is negative. This is in contrast to the behavior anticipated in forward flight where increasing thrust results in an increase in airspeed. Finally, there is a particular case when the ratio of the derivatives X_δ/Z_δ is in the same proportion as X_w/Z_w and no steady-state change in speed occurs in response to thrust. In this situation, the pilot can use thrust to control flightpath without disturbing airspeed; this would reduce control workload when constant airspeed is desired such as during a slow-speed approach to a short field or confined landing site.

TABLE 5. EFFECTS OF THRUST DEFLECTION ON AIRSPEED CONTROL CHARACTERISTICS

$Z_\delta = 0$	$\frac{u}{\delta} \doteq \frac{X_\delta}{s + 1/T_{\theta_1}}$	Cruise configuration; no thrust deflection
$\frac{X_\delta}{Z_\delta} = \frac{X_w}{Z_w}$	$\frac{u_{ss}}{\delta} = 0$	Thrust deflection to decouple speed from thrust
$X_\delta = 0$	$\frac{u}{\delta} = \frac{Z_\delta X_w}{\Delta_{Long}}$	Adverse speed coupling

Some examples of airspeed response characteristics for the Harrier illustrate the points made above. Figure 55 shows a frequency response plot of airspeed response to pitch attitude, thrust magnitude, and thrust deflection. In each case, the numerator root and the characteristic root at $1/T_{\theta_2}$ essentially cancel and the response can be seen to fall off above the low-frequency root at $1/T_{\theta_1}$. Time histories of airspeed response for the Harrier to inputs from three different controls

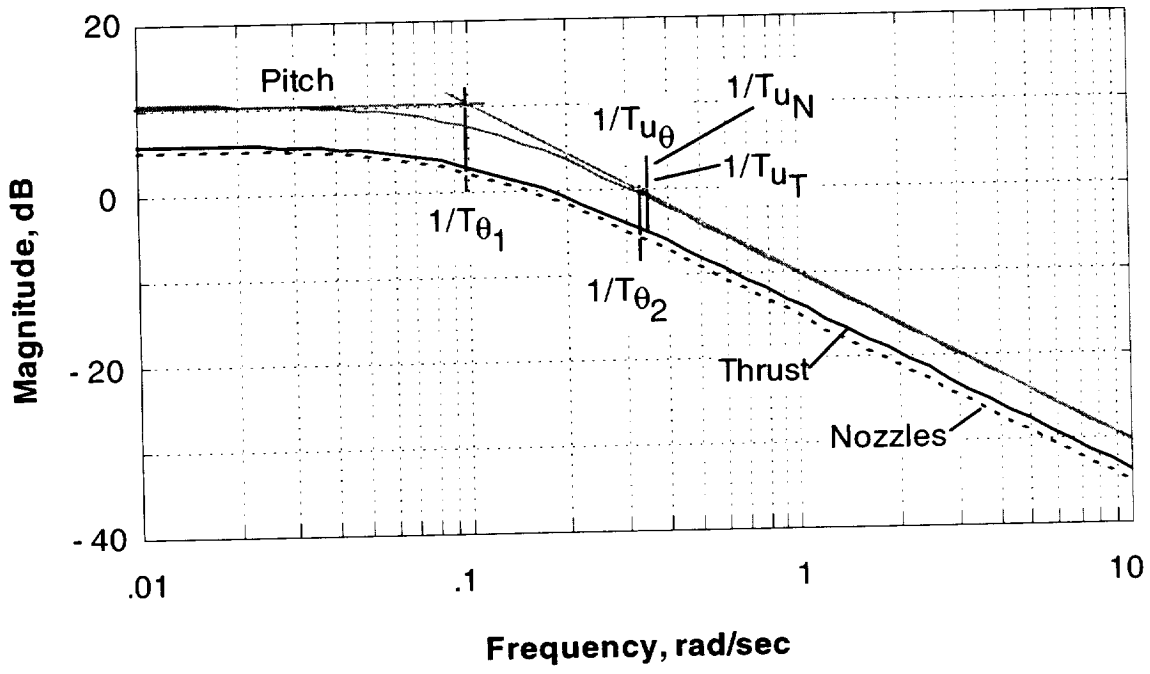

Figure 55. Bode plot of airspeed response to pitch attitude, thrust, and nozzle deflection for the Harrier at 100 knots.

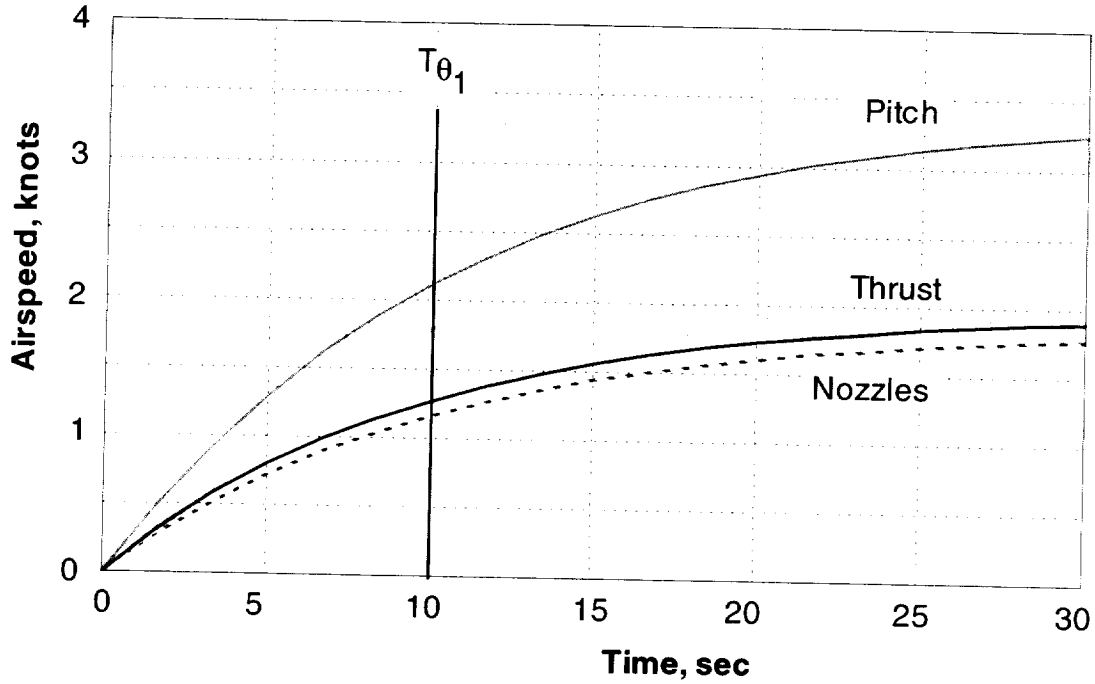

Figure 56. Time histories of airspeed response to pitch attitude, thrust, and nozzle deflection for the Harrier at 100 knots.

appear in figure 56. One shows response to a 10 deg nose-down change in pitch attitude, another to a 1 percent increase in thrust, and a third to a 1 degree aft rotation of the thrust vector. The flight condition is at 100 knots with the thrust deflected initially at 60 deg. Note that all three responses are characterized by a first-order lag with a time constant of about 10 sec. Although not exact, the first-order lag with a time constant close to T_{θ_1} is a reasonable approximation of the response.

Flightpath Control

Flightpath response is also considered for changes in aircraft attitude or thrust. Flightpath response to aircraft attitude is represented by the transfer function

$$\frac{\gamma}{\theta_c} = \frac{(-Z_w + \frac{g}{U_o}\sin\gamma_o)(s + 1/T_{\gamma_\theta})}{\Delta_{Long}}$$

where vertical velocity damping Z_w appears as the dominant element of control sensitivity and the numerator root is approximated by

$$1/T_{\gamma_\theta} = -X_u + Z_u\left(\frac{U_o X_w - g\cos\gamma_o}{U_o Z_w - g\sin\gamma_o}\right)$$

Note that this is similar to the approximation for the low-frequency numerator root of the aircraft's altitude response to longitudinal stick shown previously. Its magnitude may be similar to that for $1/T_{\theta_1}$ or less, depending on the specific values of the individual derivatives. Further, it can be either positive or negative, that is, in either the right- or left-half plane. The derivative X_u is negative and is related to the level of trim drag, and Z_u and Z_w are both negative; X_w is typically positive, but can vary substantially depending on the overall level of induced drag. Its magnitude, in comparison to the gravity term, determines whether the second term in the approximation is positive or negative, that is whether the aircraft is flying on the front or backside of the drag curve. Flightpath response will tend to take place at frequencies of the order of the higher-frequency characteristic root that is associated with the derivative Z_w. Thus, the flightpath response to changes in pitch attitude are tied to the change in lift generated by changing angle of attack and are thus governed by lift-curve slope, wing loading, air density, and airspeed. Further, with the numerator root positive (frontside of the drag curve), when the pilot makes a positive (nose-up) change in attitude, the aircraft will establish a steady climb. When the numerator is negative (backside operation) the nose-up attitude change will eventually lead to a descending flightpath in the steady state. In either situation, the initial response will be to climb. However, the consistency of the short-term and long-term response is important in determining the pilot's control technique.

Flightpath response to thrust is described by

$$\frac{\gamma}{\delta} = \frac{-Z_\delta}{U_o} \frac{(s + 1/T_{\gamma_\delta})}{\Delta_{Long}}$$

where the control sensitivity is determined by Z_δ and the numerator is approximated by

$$1/T_{\gamma_\delta} = -X_u + Z_u \frac{X_\delta}{Z_\delta}$$

The numerator root is determined by the derivative X_u and by the relative values of longitudinal and normal force associated with the thrust control, X_δ and Z_δ. The importance of these two derivatives to flightpath response, as related to thrust deflection, is noted in table 6. For the cruise configuration, the thrust vector is directed aft and the vertical force component in response to changes in thrust is zero. In this case, the numerator root vanishes, and flightpath response is dominated by the lower frequency of the two characteristic roots with time constant T_{θ_1}. It is intuitive physically that the aircraft will not respond quickly in the vertical axis to thrust when thrust is directed along the longitudinal axis. At the other extreme, when the thrust vector is deflected vertically, the first-over-second-order transfer function form applies and the numerator factor is defined by X_u. Typically $1/T_{\theta_1}$ is somewhat larger than X_u. Thus, the transfer function will have a lower frequency numerator root and two higher-frequency characteristic roots. If this numerator factor is substantially less than the characteristic roots, the frequency response characteristics will show a significant peak and flightpath response will have amplification in the frequency range corresponding to the characteristic roots. Hence, overshoot in the response to a step thrust input will be present, with flightpath reaching a peak followed by a drop back to the steady-state condition. This discrepancy between the short- and long-term response can be

objectionable to the pilot in that the response appears to be unpredictable. The intermediate thrust deflection case corresponds to the decoupled airspeed response to thrust shown previously. When the ratio of X_δ to Z_δ is equal to the ratio of X_w to Z_w, the numerator root cancels the low-frequency characteristic root at $1/T_{\theta_1}$. Flightpath response is represented by a first-order lag at $1/T_{\theta_2}$. This condition provides the best flightpath and airspeed response characteristics for the pilot, since the two are decoupled and flightpath response to thrust is readily predictable.

TABLE 6. EFFECT OF THRUST DEFLECTION ON FLIGHTPATH RESPONSE CHARACTERISTICS

$Z_\delta = 0$	$\frac{\gamma}{\delta} = \frac{X_\delta Z_u}{(s+1/T_{\theta_1})(s+1/T_{\theta_2})}$	Cruise configuration; $1/T_{\theta_1}$ determines bandwidth
$\frac{X_\delta}{Z_\delta} = \frac{X_w}{Z_w}$	$\frac{\gamma}{\delta} = \frac{-Z_\delta}{U_o}\left(\frac{1}{s+1/T_{\theta_2}}\right)$	Deflected thrust; speed decoupled; $1/T_{\theta_2}$ determines bandwidth
$X_\delta = 0$	$\frac{\gamma}{\delta} = \frac{-Z_\delta}{U_o}\left[\frac{s+1/T_{\gamma_\delta}}{(s+1/T_{\theta_1})(s+1/T_{\theta_2})}\right]$	Deflected thrust; γ overshoot

Bode plots for flightpath response to attitude, thrust magnitude, and thrust deflection for the Harrier at the 100-knot forward flight condition are shown in figure 57. First, for the response to

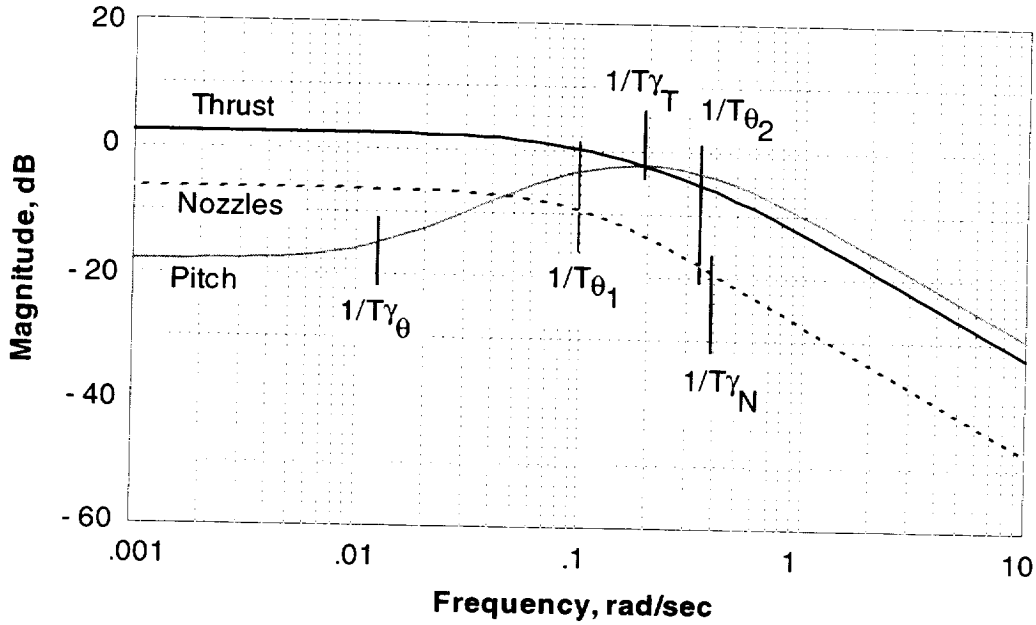

Figure 57. Bode plots of flightpath response to pitch attitude, thrust, and nozzle deflection for the Harrier at 100 knots.

attitude, note the peaking that indicates overshoot in the flightpath response. This occurs because the numerator and lower-frequency denominator roots are widely separated. The further significance of the numerator root location is noted in the time history to follow. Response to thrust is reasonably flat out to the frequency at $1/T_{\theta_2}$. Flightpath time histories for pitch attitude, thrust magnitude, and nozzle deflection inputs appear in figure 58. Interesting differences are

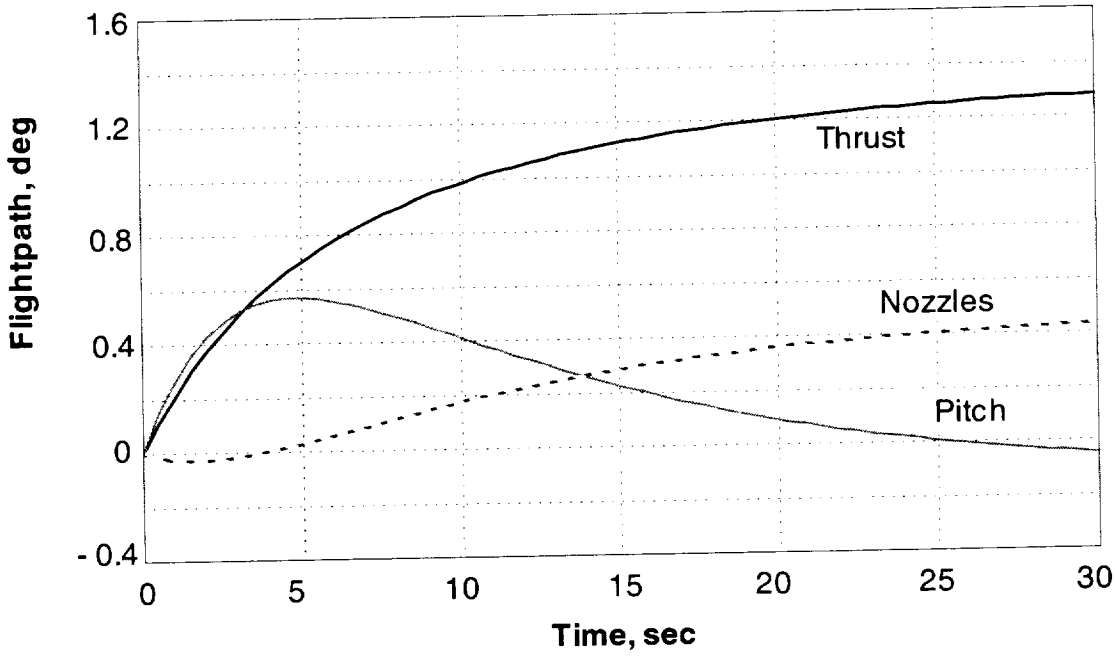

Figure 58. Time histories of flightpath response to pitch attitude, thrust, and nozzle deflection for the Harrier at 100 knots.

evident in these responses. Following a 1 deg nose-up change in attitude, flightpath initially climbs quickly, then in the long-term becomes a shallow descent. This occurs because the Harrier is flying on the backside of the drag curve at 100 knots due to its large induced drag. This reversal in flightpath response (its non-minimum phase character) is anticipated by the right-half plane flightpath numerator root. Flightpath response to a 1 percent increase in thrust has a reasonable first-order character with a time constant of approximately 10 sec. For the thrust deflection example, the thrust vector is retracted 1 deg from the initial 60 deg setting. This control input causes the aircraft to speed up and in the long term to climb. Note that the initial flightpath settles; this occurs because rearward deflection of the jet lift reduces the vertical component of thrust, which causes a non-minimum phase response that makes thrust vector deflection poorly suited for tight control of flightpath.

To summarize this section, a second-order set of differential equations has provided a simple dynamic analysis that offers a wealth of information about the aircraft's response in flightpath and airspeed and about the links to characteristics of the aircraft that govern that behavior. The underlying physics are associated with the generation of lift and drag that will be discussed next.

Influences of Lift and Drag

Lift and drag characteristics determine aircraft performance, as has been noted, but they also are the dominant influence on flying qualities associated with flightpath and airspeed control. Several of the factors that have been defined previously to influence flying qualities can be extracted from a steady-state analysis of flightpath and airspeed characteristics. To appreciate these influences, an understanding of the effects of the aircraft's lift and drag on these characteristics is necessary.

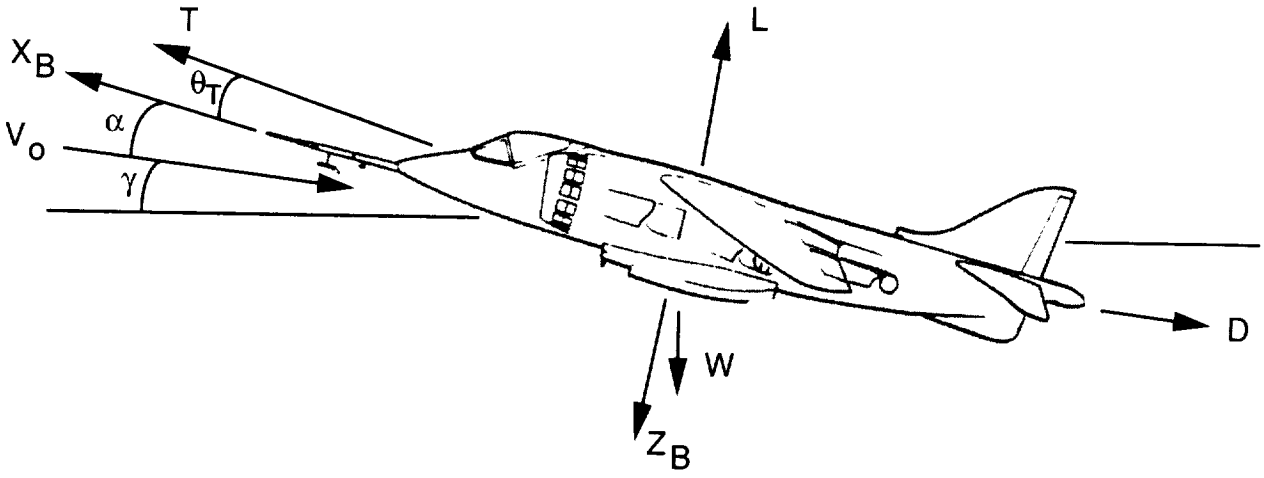

Figure 59. Stability axis system.

Lift and drag are oriented with respect to stability axes, that is, along and normal to the velocity vector. The diagram of the Harrier in figure 59 illustrates this axis system and includes the orientation of the thrust vector. Thrust is inclined from the aircraft's body axis through an angle θ_T. The longitudinal axis is aligned with the free-stream velocity vector, which is inclined from the horizontal plane by the flightpath angle γ. The aircraft's body axis is further inclined from the flightpath by the angle of attack α. Using this axis system, the definitions of the longitudinal (axial) and vertical (normal) force equations are

$$\text{Axial force} \qquad T\cos(\alpha + \theta_T) - D = W\sin\gamma$$

$$\text{Normal force} \qquad T\sin(\alpha + \theta_T) + L = W\cos\gamma$$

The solution for flightpath follows from the axial force equation where

$$\gamma = \sin^{-1}\left[\frac{T\cos(\alpha + \theta_T) - D}{W}\right]$$

Airspeed is extracted from the relationship of lift to its nondimensional coefficient

$$L = C_L \frac{\rho}{2} V^2 S$$

The normal force equation can then be rewritten to solve for airspeed in terms of thrust, lift coefficient, weight, angle of attack, and flightpath angle:

$$V = \sqrt{\frac{2[W\cos\gamma - T\sin(\alpha + \theta_T)]}{\rho C_L S}}$$

In the solution for flightpath, drag must be defined, in this case in terms of its nondimensional coefficient as was done for lift, where

$$D = C_D \frac{\rho}{2} V^2 S + \dot{m}_e V$$

The second term, ram drag, arises from the momentum of the mass of the air entering the engine inlet. Inlet momentum drag is included in the net thrust calculation for aircraft with conventional propulsion systems; however, for powered-lift aircraft, gross thrust and ram drag are typically treated separately in the force equations. If the effects of jet-induced lift are negligible, the aircraft's drag coefficient can be defined in terms of parasite drag and induced drag by

$$C_D = C_{D_f} + \frac{C_L^2}{\pi A e}$$

This relationship, known as the drag polar, relates drag to lift and is extracted from wind tunnel data as would appear in the general form indicated in figure 60, which shows drag increasing with lift as a function of increasing angle of attack. With the lift coefficient derived from the normal force equation by

$$C_L = \frac{2[W\cos\gamma - T\sin(\alpha + \theta_T)]}{\rho V^2 S}$$

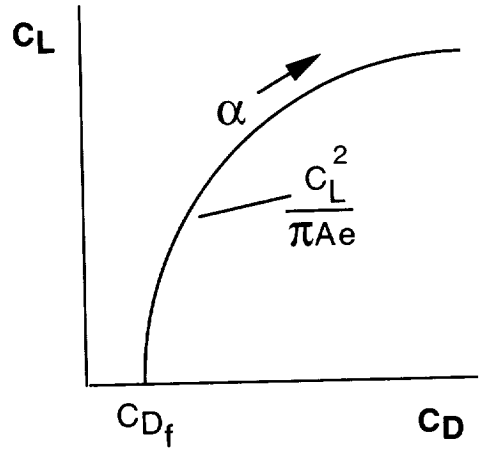

Figure 60. Example drag polar.

all of the individual terms in the flightpath equation can now be included and flightpath can be shown as a function of airspeed to be

$$\gamma = \sin^{-1}\left\{\frac{T}{W}\cos(\alpha+\theta_T) - \left[\frac{C_{Df}\rho}{2W/S}\right]V^2 - \left[\frac{\dot{m}_e}{W}\right]V - \left[\frac{2[W\cos\gamma - T\sin(\alpha+\theta_T)]^2}{\pi\rho SWAe}\right]\frac{1}{V^2}\right\}$$

where individual terms appear in proportion to airspeed, the square of airspeed, and the inverse square of airspeed. Note that the last three terms in the equation are those from the drag contribution. A plot of the drag terms as a function of airspeed, shown in figure 61, reveals a parabolic shape, where the drag increase at low airspeed is in proportion to the inverse square of airspeed and the increase at high speed is proportional to the square of airspeed. The segment of the parabola at the left is referred to as the backside of the drag curve and is associated with induced drag; the right segment is known as the frontside and is associated with parasite drag.

Using the normal and axial force equations, the aircraft lift and drag characteristics can be mapped into flightpath and airspeed and can be used to interpret aspects of the pilot's control of the aircraft. A family of curves of flightpath versus airspeed, derived from lift and drag for variations in thrust, with lines of constant pitch attitude, is shown in figure 62. This plot is divided into two regions, one associated with the frontside, the other with the backside of the drag curve. Note the change in slope of flightpath as a function of velocity between the frontside and backside regions. On the frontside, as airspeed increases the flightpath angle is reduced, which is consistent with lowering the nose to descend while maintaining constant thrust. On the backside of the drag curve, however, with increasing airspeed the flightpath angle increases, and, conversely, as airspeed is reduced the aircraft descends. From the previous linear analysis of flightpath dynamics, this variation of flightpath with airspeed can be defined as well. The

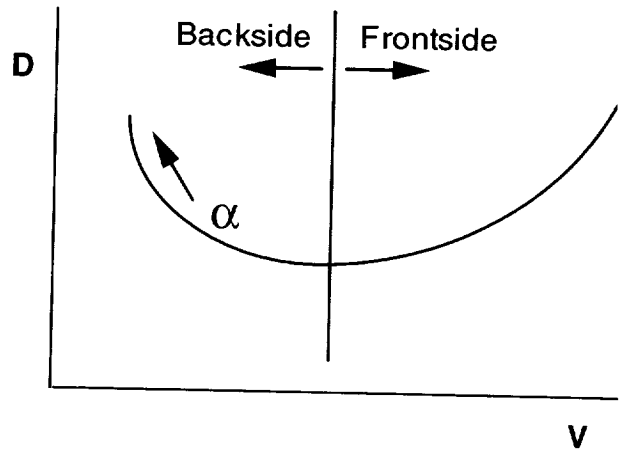

Figure 61. Example plot of drag as a function of airspeed.

derivative of flightpath with respect to airspeed can be derived from the ratio of the transfer functions of flightpath and airspeed in response to pitch attitude in the steady state:

$$\left(\frac{d\gamma}{dV}\right)_{ss} = \frac{(\gamma/\theta)_{ss}}{(V/\theta)_{ss}}$$

$$= \frac{(-Z_w + \frac{g}{U_o}\sin\gamma_o)(s + 1/T_{\gamma\theta})}{(U_o X_w - g\cos\gamma_o)(s + 1/T_{u\theta})}$$

which for small γ can be reduced to

$$\left(\frac{d\gamma}{dV}\right)_{ss} = -\frac{1}{g}(1/T_{\gamma\theta})$$

Note that the slope of flightpath with respect to airspeed is directly proportional to the low-frequency numerator term in the transfer function for flightpath to pitch attitude. Thus, when $1/T_{\gamma\theta}$ is positive, the gradient of flightpath with airspeed $(d\gamma/dV)_{ss}$ is negative, as associated with frontside operation, and is confirmed by referring to figure 62. Similarly, operation on the backside corresponds to negative values of $1/T_{\gamma\theta}$ and positive gradients of flightpath with airspeed $(d\gamma/dV)_{ss}$. Thus, the transfer function numerator factor indicates not only the slope of these curves, but also what the initial and final response of the aircraft's flightpath will be with changes in airspeed that are produced by changes in pitch attitude.

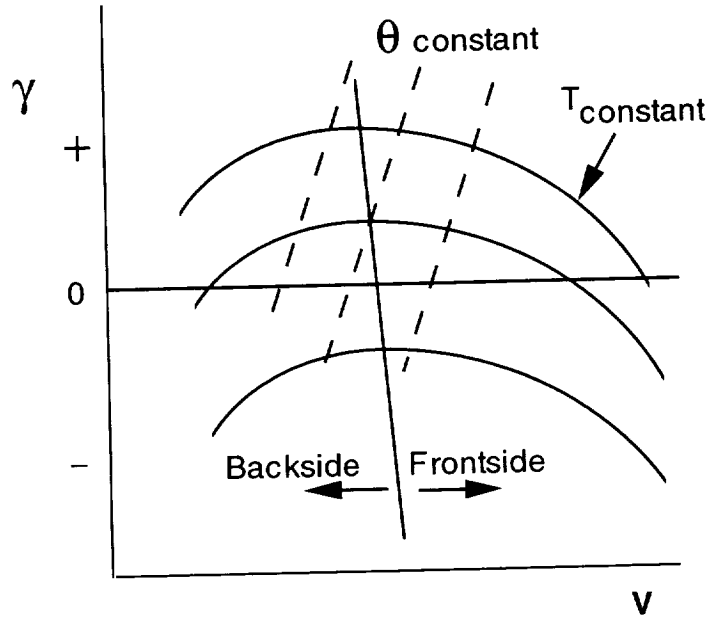

Figure 62. Example plot of flightpath angle as a function of airspeed, thrust, and pitch attitude.

This example provides an illustration of flightpath control characteristics that can be extracted from aircraft performance characteristics plotted in variables that are meaningful to the pilot. Other characteristics that are apparent in this plot are control sensitivity, such as the change in airspeed and flightpath achieved for a unit change in pitch attitude or thrust.

Figure 63 presents an example of the relationship between the lift-drag polar and flightpath-airspeed plots for the Harrier at low airspeed. These data are presented for a semi-jet-borne case with the thrust vector deflected 55 deg; the lift and drag were extracted from large-scale wind tunnel tests of a full-scale model of the aircraft. The lift-drag polars are shown for angles of attack from –4 to 16 deg, over a range of equivalent jet velocities from 0.16 to 0.34. Equivalent jet velocity is the nondimensional parameter describing the range of thrust settings, and specifically it is the square root of the ratio of free-stream dynamic pressure to dynamic pressure in the engine's jet exhaust. It is proportional to the square root of the inverse of the thrust coefficient. The effect of increasing thrust (reducing jet velocity ratio) to increase lift is evident, and is due not only to the direct contribution of the deflected jet exhaust, but also to the jet-induced airflow around the wing. The basic wing aerodynamic lift may either increase or decrease depending on the configuration and airspeed. Mapping these characteristics into the flightpath-airspeed plane using the equations derived above, yields the plots of flightpath and airspeed variation with pitch attitude and thrust at the bottom of the figure. In the intermediate airspeed region, the Harrier can fly on either the frontside or the backside of the drag curve. The Harrier typically operates on the backside, except at high power settings, and it is not appropriate to use pitch attitude to control the flightpath in this part of the

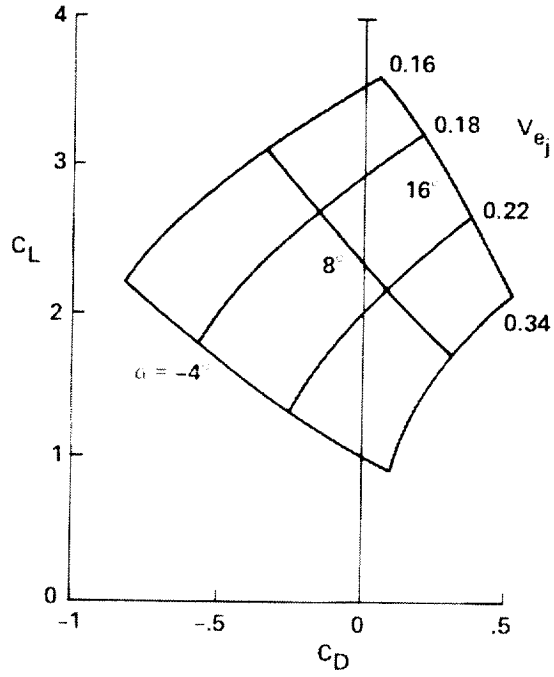

(a) Lift-drag polar.

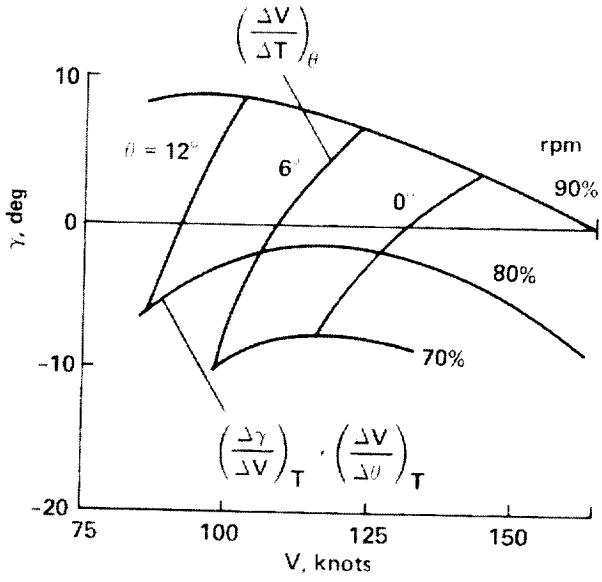

(b) Flightpath-airspeed.

Figure 63. Lift-drag polar and flightpath-airspeed relationships for the Harrier at low airspeed.

envelope. However, flightpath control with thrust is effective for this thrust-vector deflection. Another point to note relates to the lines of constant aircraft pitch attitude, shown at 0, 6, and 12 deg. Increasing thrust with the pitch attitude fixed increases airspeed. Thus, when the pilot uses thrust to control flightpath, airspeed will also change, requiring the pilot to compensate by changing aircraft pitch attitude. This coupling is a source of increased workload on the pilot and one that should be alleviated with a different thrust vector deflection.

TABLE 7. EFFECT OF THRUST DEFLECTION ON PILOT'S CONTROL TECHNIQUE

	Flightpath	Airspeed
$Z_\delta = 0$ $d\gamma/dV$ (–)	Pitch control for short and long term	Thrust control for long term
$Z_\delta = 0$ $d\gamma/dV$ (+)	Pitch control for short term Thrust control for long term	Pitch control for long term
$X_\delta = 0$	Thrust control for short and long term	Pitch control for long term

To summarize, because either pitch or thrust can be used to control flightpath and airspeed, it is important for the pilot to know which control should be considered primary for each response. Table 7 provides a summary of aircraft characteristics and their implications for the pilot's control technique. Time history plots for flightpath and airspeed response to the pitch and thrust controls shown in figure 64 provide supporting evidence for the comments in the table. First, consider the conventional aircraft configuration with thrust undeflected ($Z_\delta = 0$). If the operation is on the frontside of the drag curve ($d\gamma/dV$ negative), with the flightpath and airspeed response as shown in the figure, control of flightpath with pitch attitude for both the short-term and long-term response is appropriate. The pilot can achieve quick initial flightpath response and then sustain that response in the long term. Flightpath response to thrust is too sluggish for rapid path corrections. The response of airspeed to either pitch attitude or thrust is reasonable; however, pitch is the primary flightpath control, thus thrust should be the primary airspeed control. This priority of control is typical for an aircraft in conventional flight, particularly when the aircraft is flown tightly and precisely. For flight with the thrust vector undeflected while operating on the backside of the drag curve ($d\gamma/dV$ positive), the roles of the pitch and thrust controls are reversed. This situation exists when the aircraft decelerates to a lower airspeed without the thrust being deflected. In this case, although flightpath initially responds quickly to pitch attitude, in the long term the flightpath change cannot be sustained. Airspeed response to attitude is still reasonable. The character of flightpath response to thrust has not changed and is still sluggish. Airspeed response to thrust is also essentially unchanged. Thus, the pilot finds this operation to be more complicated than for the frontside condition. The only way to achieve quick flightpath response is with the pitch control; however, it is essential to follow up promptly with a change in thrust to

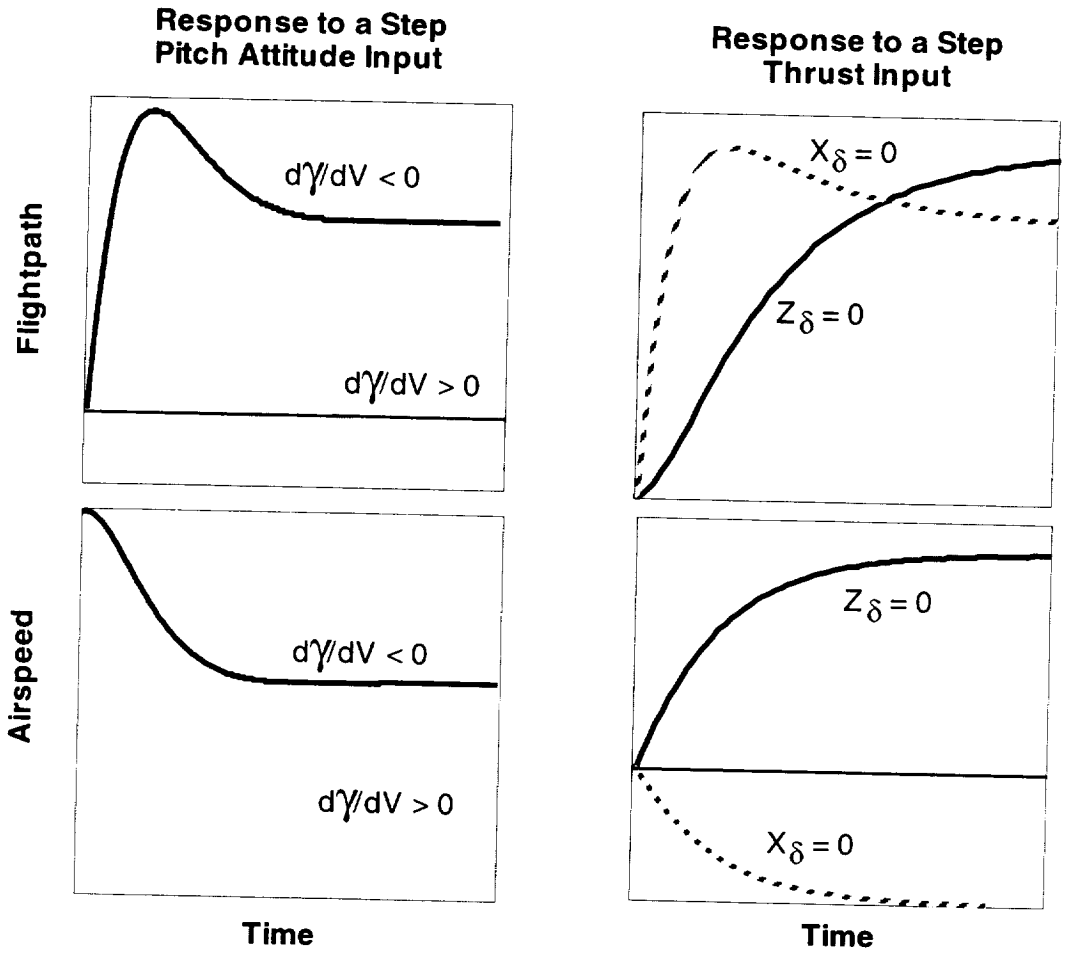

Figure 64. Example time histories for flightpath and airspeed response to pitch attitude and thrust.

sustain the flightpath correction. Then pitch attitude may need to be readjusted to maintain the desired airspeed. This is a complicated, coupled control technique that, nevertheless, is unavoidable for these characteristics and operating conditions. Further, if these characteristics become exaggerated, the aircraft's flying qualities will degrade significantly. When the thrust vector is deflected to the vertical position, the response characteristics and control choices are unambiguous. Flightpath response to aircraft attitude still corresponds to the backside characteristics and relegates attitude to the task of airspeed control. However, with the thrust vector deflected vertically, flightpath response to thrust is rapid enough for precise control. The only concern is whether the flightpath sags excessively in the long term. Thus, with the aircraft configured for V/STOL flight, the pilot should use thrust to control flightpath and pitch attitude to control airspeed. To avoid a confused control situation for intermediate thrust vector deflections, before the aircraft decelerates to airspeeds on the backside of the drag curve, the pilot should deflect the thrust vector sufficiently that the V/STOL control technique can be employed. Experience shows that is the best technique for use with the Harrier; STOL aircraft are flown that way as well.

Longitudinal Flying Qualities Requirements in Forward Flight

Different criteria for pitch-control power in forward flight were adopted in references 9-11. References 9 and 11 draw from STOL aircraft experience and propose criteria either in terms of maximum pitch angular acceleration or attitude change in 1 sec. Angular acceleration capability of 0.05 to 0.2 rad/sec^2 is suggested or, as an alternative, an attitude change in 1 sec of 2-4 deg is proposed. The STOL data relate to the use of attitude to control flightpath and airspeed, to rotate the aircraft for takeoff, and to perform maneuvers in wing-borne flight. A different approach, applied more frequently in V/STOL practice (ref. 10), assures that the control required to trim does not exceed half of the total control available. Figure 65 provides examples of the trim

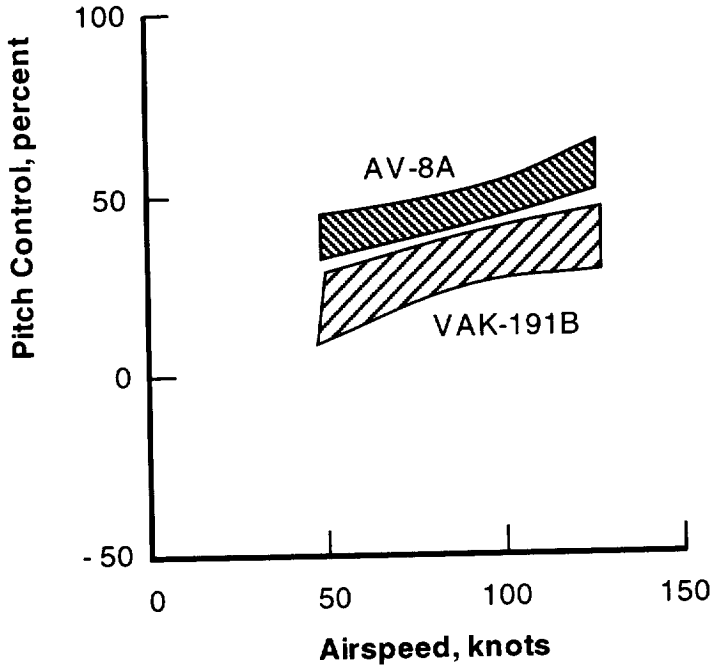

Figure 65. Control required to trim for the AV-8A and VAK-191B.

required for the AV-8A Harrier and VAK-191B jet-lift aircraft. The AV-8A was recognized to have pitch-control limitations for coping with large changes in thrust or thrust deflection at low speed, for example, during short takeoff. In the figure, the nose-down trim demands over the semi-jet-borne speed range are 50 percent or more of the total nose-down control. Both aircraft shown were considered unsatisfactory for pitch-control authority in this flight regime. The AV-8B design has reduced this trim demand to nearly neutral and is considered to have satisfactory pitch-control authority.

Requirements for pitch dynamics, as in hover, call for a bandwidth of 2 rad/sec with at least 45 deg phase margin for Level 1 characteristics and 1 rad/sec bandwidth for Level 2. For either the hover or forward flight tasks, the pilot must be able to control and stabilize the aircraft over the same frequency range, that is, to quickly generate well-damped attitude changes.

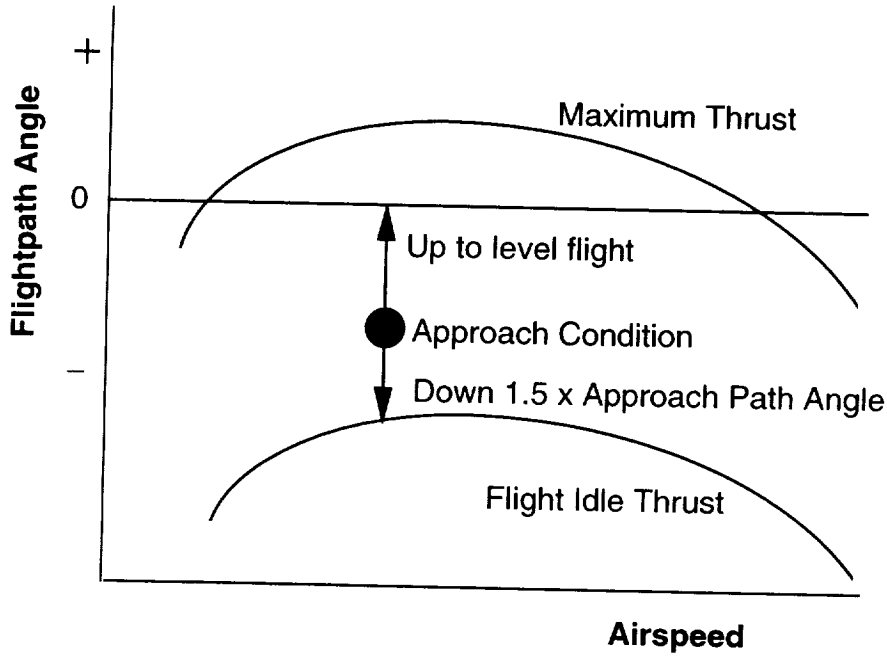

Figure 66. Flightpath control authority criteria.

With the appropriate assignment of primary controls for flightpath and airspeed, it is possible to establish criteria for control authority and dynamic response. Figure 66 presents a flightpath versus airspeed plot with guidelines for climb and descent capability for control about a designated approach-path angle. These guidelines were drawn from research NASA conducted with the Federal Aviation Administration into design requirements for commercial powered-lift transports (ref. 29). They are associated with a precision instrument approach, which is a demanding phase of operation requiring precise approach-path control. The approach-path angle is selected by the aircraft's operator; for example, conventional transport aircraft fly a 2.75 degree descent; V/STOL and STOL aircraft have operated at approach angles as steep as 7.5 deg. To be able to control to the designated approach path and to be able to temporarily arrest the rate of descent, the pilot must be able to achieve at least level flight with the application of maximum allowable thrust. Typically, more ascent capability can be achieved if the flaps are retracted or the thrust vector deflection is reduced. Further, it is necessary to be able to descend at least 50 percent more steeply than the nominal approach path. These requirements are intended to accommodate operations in a reasonable level of wind and turbulence. These performance requirements may size the propulsion system and determine the allowable aircraft configuration, in terms of flaps and thrust deflection, that can be used during the landing approach. These demands on the design are strongly influenced by the overall drag of the aircraft, where one of the difficult design objectives is to obtain sufficient drag for the required descent and deceleration capability. An additional criterion suggested in reference 9 concerns flightpath authority in terms of normal acceleration, and recommends a capability of ±0.1 g for path control. This latter criterion may be excessive in light of experience with the Harrier and advanced STOVL designs that suggest incremental normal acceleration of 0.03 to 0.05 g may be acceptable.

Dynamic response criteria are defined for STOL aircraft in reference 30, and are based on data extracted from flight tests of steep approaches. Although STOL aircraft are not capable of hovering, the control requirements for both flightpath and airspeed in semi-jet-borne flight are appropriately defined by the STOL data. Results suggest that a flightpath rise time in response to a step change in thrust should be 2 sec for conducting an instrument approach to breakout. This rise time is defined as the time required to reach 50 percent of the peak response, which, for a first-order response, is related to altitude response bandwidth by $\omega_{BW} T_{.5\Delta\gamma max} = 0.693$. Thus, the desired altitude response bandwidth for a rise time of 2 sec would be 0.35 rad/sec. Rise time in excess of 4 sec would be expected to produce inadequate flying qualities. Note that the overall control bandwidth must also include the propulsion system response to the pilot's throttle input. When the thrust dynamics for the aircraft's engine are included in the previous results, an additional 0.2 sec could be added to the 2 sec rise time, and the corresponding bandwidth would be reduced to 0.32 rad/sec.

Another characteristic of concern is the throttle control sensitivity, or the rate of change of flightpath that is generated initially in response to a step throttle input. Expressed in terms of incremental normal acceleration per unit control, desired values range from 0.1 to 0.2 g/in.; if it is much less than 0.1 g/in., the pilot will consider the response to be insensitive; whereas, with 0.3 g/in. or greater, the initial response will be too sensitive. The amount of flightpath overshoot, that is, the maximum change in flightpath compared to the steady-state response, should be not greater than 2 for satisfactory flying qualities. When overshoot is greater than 3, flightpath control will degrade significantly. Ideally, no overshoot is desired.

Returning to the flightpath versus airspeed plot, limits are imposed on the slope of the curve for backside operation. Desired values for $d\gamma/dV$ should be less than 0.06 deg/knot; for adequate flying qualities, however, the slope can be as large as 0.15 deg/knot. When the slope is too steep, changes in airspeed quickly erode flightpath control capability and strongly couple flightpath and airspeed response. Rather than force a change in the aircraft design, which would require a change in the induced-drag characteristics, this requirement restricts operation to speeds at which the slope is not objectionable. Recall that this slope is tied to values of the numerator of the flightpath response to pitch-attitude transfer function. Thus, comparable values for the numerator for these slope restrictions would be greater than –0.05 for adequate characteristics or greater than –0.02 for desired characteristics.

Airspeed control for V/STOL aircraft can either involve maintaining a stable speed associated with a slow approach to landing, deceleration of the aircraft continuously from forward flight to hover, or accelerating to forward flight. These maneuvers must be performed without complicated procedures for the pilot and with acceptable levels of acceleration and deceleration capability. Figure 67 presents a flight envelope for the XV-15 in terms of the acceptable airspeed range for variations in engine nacelle tilt. The envelope corresponds to level flight, and the boundaries describe the aircraft's flight envelope within which acceleration from hover to forward flight or deceleration from forward flight to hover can be performed. Typically, the limits are determined by structural restrictions at high speed and by stall, buffet, or flow separation at low speed. Within the envelope, combinations of aircraft attitude, thrust, and nacelle tilt exist for a given airspeed or for varying airspeed. A wide corridor is desired for ease of control. If the

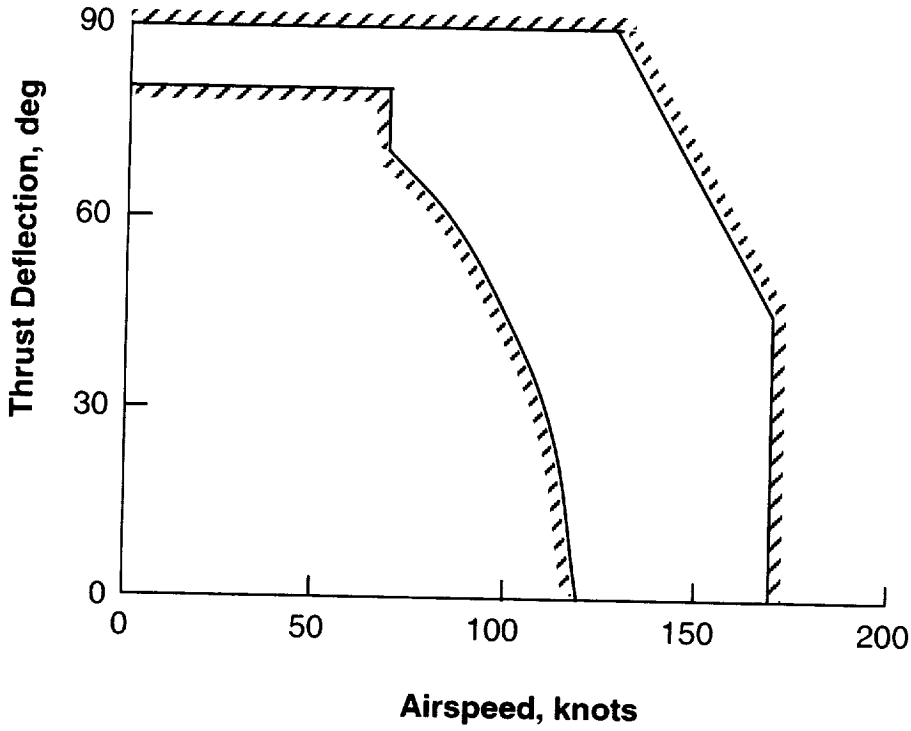

Figure 67. Typical transition flight envelope for the XV-15 Tilt Rotor.

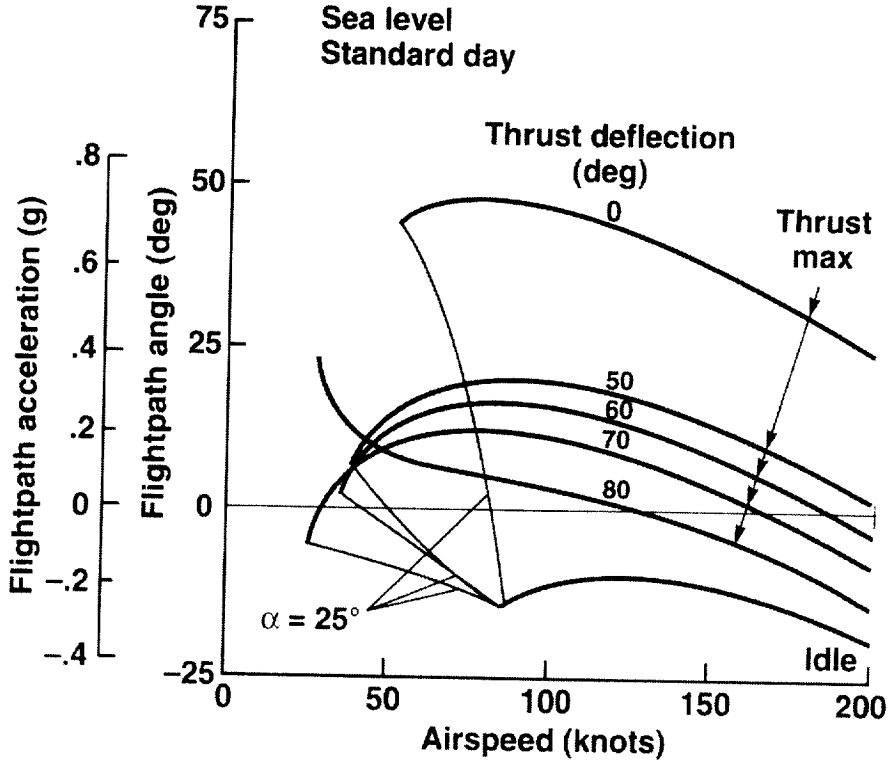

Figure 68. Example transition envelope.

corridor were narrow, the pilot would be required to adhere to a tightly prescribed combination of nacelle tilt, thrust magnitude, and aircraft attitude to perform the transition. A complex technique may render the task impossible to fly under instrument conditions. An aircraft like the XV-15 or the Harrier typically has a generous envelope, and aircraft that do not have the capability to fully deflect their thrust generally have a narrower corridor.

Another view of the transition envelope is presented in figure 68. This figure shows a family of curves generated for a conceptual STOVL fighter design. The upper boundaries correspond to maximum thrust and, at the bottom, to the flight idle thrust condition. The flightpath that can be sustained at maximum thrust depends on the amount of thrust deflection, with examples shown for the thrust vector ranging from horizontal to deflections of 80 deg. Starting with a generous flight envelope with no thrust deflected, the maximum climb capability reduces progressively with thrust deflection and reaches a minimum in an intermediate speed region. In this region, the aerodynamic characteristics are typically dominated by jet flows under the wing, which reduce lift and hence require more thrust to maintain equilibrium flight. A proposed criterion defines the minimum climb capability that can be sustained at constant speed or, alternatively, the longitudinal acceleration capability that can be achieved in level flight (ref. 31). This acceleration capability should preferably be at least 0.13 g and should not be less than 0.08 g. Converted to flightpath angle through the relationship $\dot{u} = g\gamma$, those capabilities would be 7.4 deg climb desired and 4.6 deg minimum acceptable at constant speed. During the transition, the pilot's technique for controlling airspeed is to adjust the thrust deflection to maintain a margin from the envelope boundary until the aircraft passes through the confining portion of the corridor.

Consideration must be given to the means for deflecting thrust to control the transition. For aircraft like the Harrier, the total thrust vector can be continuously deflected from 1.5 deg through 100 deg with respect to the aircraft's waterline, 16.5 deg forward of the vertical for the normal hover attitude of 6.5 deg. To accelerate the aircraft away from hover, the thrust vector is rotated aft and thrust is increased to make up for the vertical component lost through the cosine of the rotation angle. The cosine effect is small, and as the vector is rotated to accelerate the aircraft, only a small increase in thrust is required to support the weight of the aircraft. A substantial change in longitudinal acceleration can be produced with a modest increase in thrust. In contrast, an aircraft that can only transfer thrust between aft-oriented (cruise) and vertically-oriented (lift) nozzles is much less efficient in the use of thrust throughout the transition. To accelerate from hover, the longitudinal thrust must be added to that required to support the aircraft's weight, meaning an increase in total engine thrust of 13 percent of weight to achieve the desired acceleration. Figure 69 provides an indication of the relationship between thrust-vectoring efficiency and thrust-to-weight ratio for acceptable and minimum levels of acceleration capability. Vectoring efficiency is defined by the expression

$$\text{Vectoring efficiency} = \frac{\sqrt{F_X^2 + F_Z^2}}{F_{total}}$$

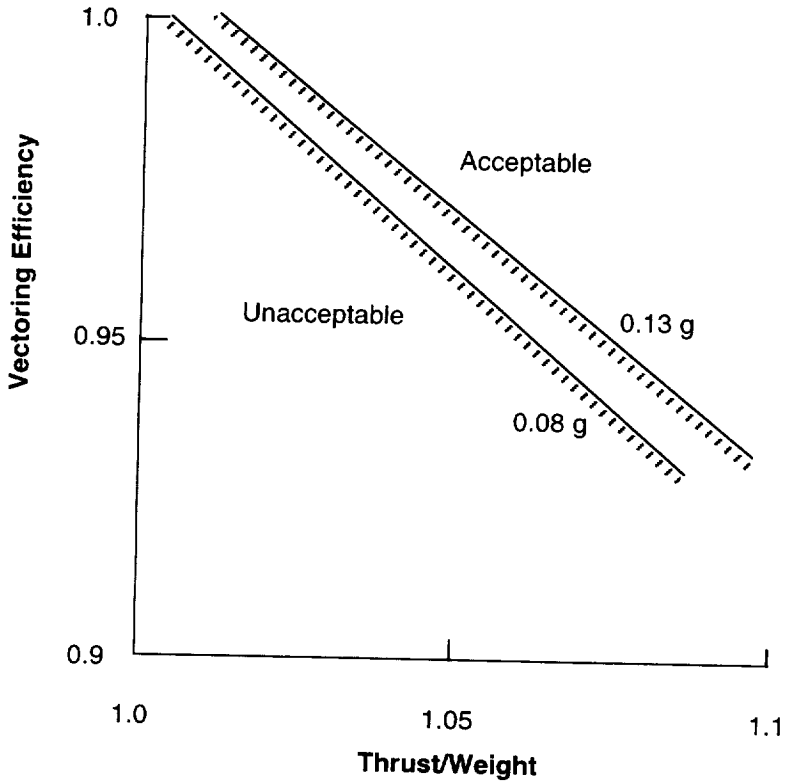

Figure 69. Relationship of vectoring efficiency to required thrust to weight.

which is the ratio of the vector sum of the longitudinal and vertical thrust components to the total thrust required of any particular design to perform this transition. For full thrust-vector deflection, $F_X = F_{Total} \cos \theta_j$; $F_Z = F_{Total} \sin \theta_j$, and the vectoring efficiency is 1. The figure shows that as vector efficiency is reduced, a significant increase in thrust is required. At the extreme, the aircraft that cannot deflect thrust and can only transfer thrust between lift and cruise nozzles ($F_X + F_Z = F_{Total}$) requires a thrust-to-weight ratio of 1.13 to perform the level flight acceleration, with an associated vectoring efficiency of 0.89. Thus, the designer is motivated to achieve a concept that is as close to a fully vectoring configuration as possible to avoid driving the propulsion system size to extremes. The designer may have to compromise, that is, to accept a solution that only partially vectors thrust, but it would be desirable to avoid a design that can only transfer thrust between components.

Finally, a bandwidth of the order of 0.3-0.4 rad/sec is a reasonable objective for speed control. Specific requirements for dynamic response for speed control have not been defined.

Response to Wind and Turbulence

In the analysis of hover flying qualities, the response of the aircraft to external disturbances caused by ground effect was discussed. In forward flight, when aerodynamic forces are significant, the disturbances of the air mass due to winds and atmospheric turbulence are important

influences on flying qualities. The response of the aircraft to a gust input can be expressed in terms of the gust transfer function, which is derived from the equations

$$\begin{bmatrix} s - X_u & -X_w & g\cos\gamma_o \\ -Z_u & s - Z_w & -(Z_q + U_o)s + g\sin\gamma_o \\ -M_u & -M_{\dot{w}}s - M_w & s^2 - M_q s \end{bmatrix} \begin{Bmatrix} u \\ w \\ \theta \end{Bmatrix} = \begin{Bmatrix} X_{wg} \\ Z_{wg} \\ M_{wg} \end{Bmatrix} w_g$$

The matrix on the left is associated with the state variables of longitudinal velocity, vertical velocity, and pitch attitude; on the right, the stability derivatives are associated with the gust component being considered. In this example, a vertical gust is multiplied by the appropriate stability derivatives to produce longitudinal and vertical forces and pitching moments. The nature of the atmospheric disturbance can be a discrete gust, such as a step or 1-cosine input, or a ramp to represent wind shear. It can also be in the form of a random input representative of atmospheric turbulence.

Turbulence is treated as randomly occurring waves in the atmosphere. As the aircraft traverses the turbulence field, it experiences the spatially distributed disturbance as a time varying input with a frequency content based on the periodicity of the wave field. The time variation of the disturbance depends on the speed at which the aircraft penetrates the turbulence field. The turbulence input is treated analytically as filtered random noise, and the analysis is conducted in the frequency domain. Power spectral density is used to describe the gust over the frequency spectrum; it reflects the power contained in the wind disturbance at a given frequency. More detailed background material concerning the application of random process analysis to aircraft dynamics is given in reference 15.

Once the power spectral density of vertical gusts is known, the power spectral density of the aircraft's response can be derived from the expression

$$\Phi_\theta(\omega) = |\,\theta/w_g\,|^2\,\Phi_{w_g}(\omega)$$

where pitch attitude is the aircraft state used as an example. The pitch power spectral density is the product of the square of the magnitude of the transfer function of pitch attitude to vertical gusts and the power spectral density of the vertical gust. The spectral characteristics for vertical gusts are given by

$$\Phi_{wg} = \sigma^2\left(\frac{L_w}{\pi V_o}\right)\left\{\frac{3\left(\frac{\omega L_w}{V_o}\right)^2 + 1}{\left[\left(\frac{\omega L_w}{V_o}\right)^2 + 1\right]^2}\right\}$$

This spectral form for turbulence was derived by Hugh Dryden, based on his research in random turbulence. The Dryden spectrum provides an adequate description of the features of the air mass that influence the aircraft's response. Both reference 15 and 17 discuss turbulence response, and reference 17 devotes a chapter to the characteristics of atmospheric turbulence. In the Dryden spectrum, the constant factor scales the magnitude of turbulence, where σ is the standard deviation of the vertical gust (mathematically the square root of the integral of the power spectral density for all positive values of ω). Standard deviations from 2 to 5 ft/sec provide representative levels of turbulence ranging from light to moderate that are normally used for flying qualities assessments. The variable L_w is the scale length representative of the turbulence wavelength, and V_o is the velocity at which the aircraft traverses the turbulence field. The numerator is first-order and the denominator is second-order; both roots occur at a frequency proportional to V_o /L. Thus, the turbulence intensity tends to roll off at frequencies above V_o /L. Representative values for scale length in the lower atmosphere are 1,500 ft for altitudes above 1,500 ft; below 1,500 ft the turbulence scale varies in direct proportion to altitude.

The aircraft transfer function for response to turbulence can be derived from the three-degree-of-freedom set of equations above where, for example, the pitch-attitude response to vertical gusts is represented by

$$\frac{\theta}{w_g} = \frac{-M_{w_g} s(s + 1/T_{\theta w_g})}{\Delta_{Long}}$$

Note first that the free s in the numerator indicates no steady-state change in pitch to a step vertical gust. The magnitude is determined by the pitching moment derivative due to vertical velocity. The first-order numerator root is approximated by

$$1/T_{\theta w_g} = -X_u + M_u \frac{X_w}{M_w}$$

and is dominated by the longitudinal velocity damping, X_u. The characteristic roots represent either open-loop or closed-loop control, and both cases should be considered in analyses of the aircraft's turbulence response. The open-loop response will provide an indication of the extent to which pilot-in-the-loop control will be required.

Figure 70 shows an example of the components that make up the power spectral density of attitude response, that is, the turbulence spectra and the attitude to vertical gust transfer function. The vertical gust spectrum diminishes above the corner frequency at V_o /L_w and the magnitude scales with σ^2, the mean-squared value of turbulence. The mean square as noted previously is the integral of the power spectral density as a function of frequency, that is, the area under the spectral curve. The turbulence spectrum is multiplied by the square of the aircraft's pitch-to-vertical-gust transfer function. Two factors can be seen to influence the magnitude and frequency content of the pitch response, one being the shape of the aircraft transfer function and the second the bandwidth of the turbulence spectrum. If the turbulence spectrum rolls off at low frequency,

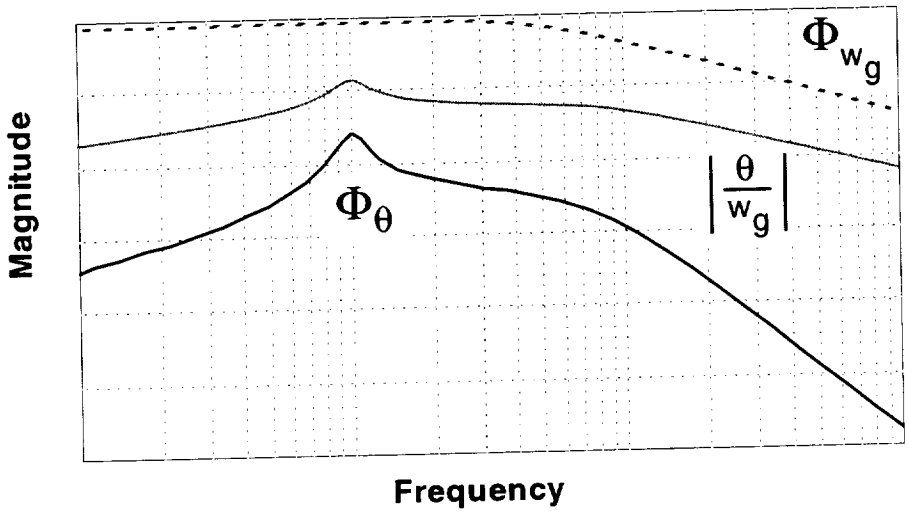

Figure 70. Components of turbulence response power spectrum for pitch attitude due to vertical gusts.

there will be insufficient energy in the gust field to excite the peak in the aircraft's mode. However, if this gust has energy beyond the phugoid frequency, it will excite the aircraft's phugoid. If the closed-loop response were considered, the phugoid peak would be eliminated by stabilizing pitch attitude, and that would act to suppress the gust response at low frequency.

It is also important to consider the aircraft's response to a discrete gust. An example to consider is flightpath and airspeed response to changes in the longitudinal component of the wind or wind shear. The appropriate equations are

$$\begin{bmatrix} s - X_u & U_o X_w \\ Z_u / U_o & s - Z_w \end{bmatrix} \begin{Bmatrix} u \\ \gamma \end{Bmatrix} = \begin{bmatrix} -X_u \\ Z_u / U_o \end{bmatrix} \{u_g\}$$

which apply when pitch attitude is stabilized. Then the transfer functions of flightpath and airspeed are

$$\frac{\gamma}{u_g} = \frac{Z_u}{U_o}\left(\frac{s}{\Delta_{Long}}\right)$$

$$\frac{u_A}{u_g} = \frac{-s(s + 1/T_{u_A})}{\Delta_{Long}}$$

where u_A is airspeed response to longitudinal gusts and is given by $u_A = u - u_g$; the gust is defined as positive along the positive x-axis. Thus, a tailwind carries a positive sign. Flightpath response has a simple numerator that is scaled by the derivative of normal acceleration with

respect to airspeed divided by the aircraft's trimmed forward speed, and contains a free s term. Airspeed response is characterized by a first-order numerator root defined by $1/T_{u_A} = -Z_w$, the vertical velocity damping derivative. Since the characteristic roots consist of a lower-frequency root associated with longitudinal velocity damping and a higher-frequency root associated with vertical velocity damping, approximate pole-zero cancellation will occur in the airspeed transfer function, and the response will be associated with the lower-frequency mode. Flightpath response will also fall off for frequencies above the low-frequency mode. The free s terms in both transfer function numerators indicate that no steady-state flightpath or airspeed changes will occur for a step gust input. However, a ramp gust, as characterizes wind shear, will create steady-state variations in both responses.

An example of response to wind shear is shown in figure 71. The time history includes both flightpath and airspeed for the ramp wind input shown at the bottom of the figure. The inertial speed variation, u, is presented as well. The wind shear corresponds to an increasing tailwind or decreasing headwind. The steady-state change of flightpath is first of all defined by 1/g, which corresponds to 3 deg/knot/sec of wind shear. A wind gradient of 1 knot/sec is not particularly

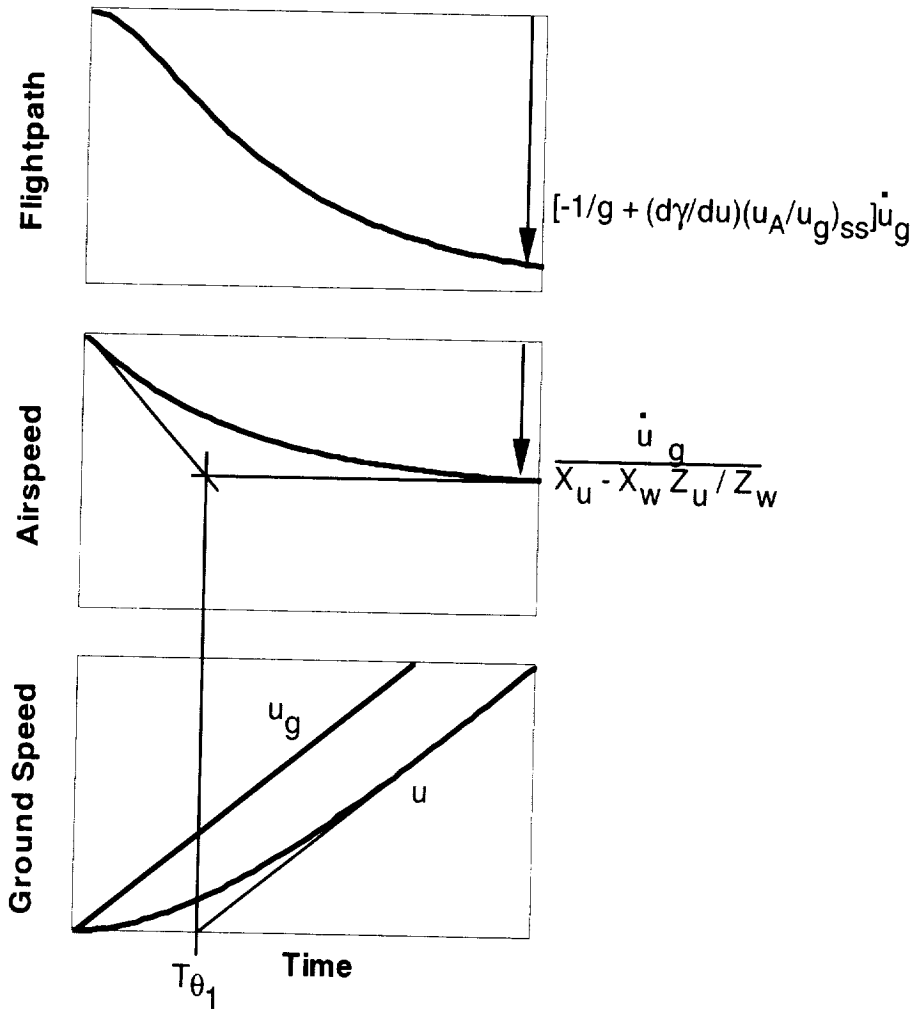

Figure 71. Flightpath and airspeed response to wind shear.

large, whereas a gradient of 2 to 3 knots/sec is a significant disturbance to an aircraft. That value is modified to account for the effect of airspeed variations on flightpath through the flightpath-airspeed coupling that can be seen on a plot of flightpath versus airspeed. The additional term indicates that backside operation ($d\gamma/dV$ positive), combined with an airspeed loss in the wind shear, will further increase the flightpath disturbance. The magnitude of the airspeed loss is indicated in the figure. The lower frequency root of the characteristic roots, T_{θ_1}, represents the time response of both flightpath and airspeed as anticipated. Thus, these responses occur over a relatively long time, although for V/STOL aircraft, especially for flight in a high-drag condition, the time constant may be less than it would be for a conventional aircraft. Further, the V/STOL aircraft with no thrust deflected and flying at 200 knots could be substantially different in its response to wind shear than it would at lower speeds. At lower speeds these responses can take place more rapidly, perhaps 2 to 3 times quicker than at the higher speed conditions.

LATERAL-DIRECTIONAL FLYING QUALITIES IN FORWARD FLIGHT

Lateral-directional flying qualities in forward flight are concerned with control of bank angle, heading, and sideslip. Comparable to the case for hover, inner-loop control of bank angle must be considered before outer-loop control of heading can be undertaken.

Bank-Angle Control

The transfer function for bank-angle control with the lateral stick is

$$\frac{\phi}{\delta_s} = \frac{L'_{\delta_s}(s^2 + 2\zeta\omega_\phi s + \omega_\phi^2)}{\Delta_{Lat}}$$

It is represented by lateral control sensitivity, a second-order numerator and the lateral-directional characteristic roots

$$\Delta_{Lat} = (s + 1/T_S)(s + 1/T_R)(s^2 + 2\zeta\omega_d s + \omega_d^2)$$

Recall that the spiral mode is typically very low frequency and can be either stable or unstable. The roll mode is of short duration and the Dutch roll root is an oscillatory pair that typically is present in the roll and yaw response. The aspects of the aircraft that influence the characteristics of the numerator have common links with those same characteristics for the Dutch roll. In particular, the numerator damping and natural frequency are defined by

$$2\zeta\omega_\phi = -(Y_v + N'_r) + L'_r \frac{N'_{\delta_s}}{L'_{\delta_s}}$$

$$\omega_\phi^2 = N'_\beta \left(1 - \frac{L'_\beta N'_{\delta_s}}{N'_\beta L'_{\delta_s}}\right)$$

Note that two of the factors that determine the damping of the numerator are lateral velocity damping and yaw damping, both of which contribute to damping of the Dutch roll. The additional term comes from yawing moment due to lateral control, and it can significantly alter the numerator root location in relation to the Dutch roll. The numerator frequency is associated first with directional stability, which again was one of the contributions to the Dutch roll. However, this term is also modified by yaw due to lateral control. The magnitude of this modifying term is also related to dihedral effect and to directional stability. Depending on the magnitude and sign of dihedral effect, in combination with lateral-control yaw, the frequency of the numerator roots may be considerably different from that of the Dutch roll. The location of the numerator roots with respect to the Dutch roll is a significant influence on excitation of the Dutch roll in the aircraft's roll response and on the pilot's ability to control bank angle. A substantial separation of the numerator and Dutch roll will produce oscillatory roll response that leads to increased work-

load for bank-angle control. Further, if the frequency of the numerator exceeds that of the Dutch roll, the bank-angle loop closure will result in reduced stability for the Dutch roll mode. This circumstance most frequently occurs with positive values of yawing moment due to the lateral control, N'_{δ_s}.

The example for the Harrier shown in figure 72 illustrates problems encountered with roll control in forward flight. The time response at the top of the figure is completely dominated by the presence of the unstable and highly excited Dutch roll response. The spiral mode convergence is apparent although not relevant in the presence of the large roll oscillations. The root

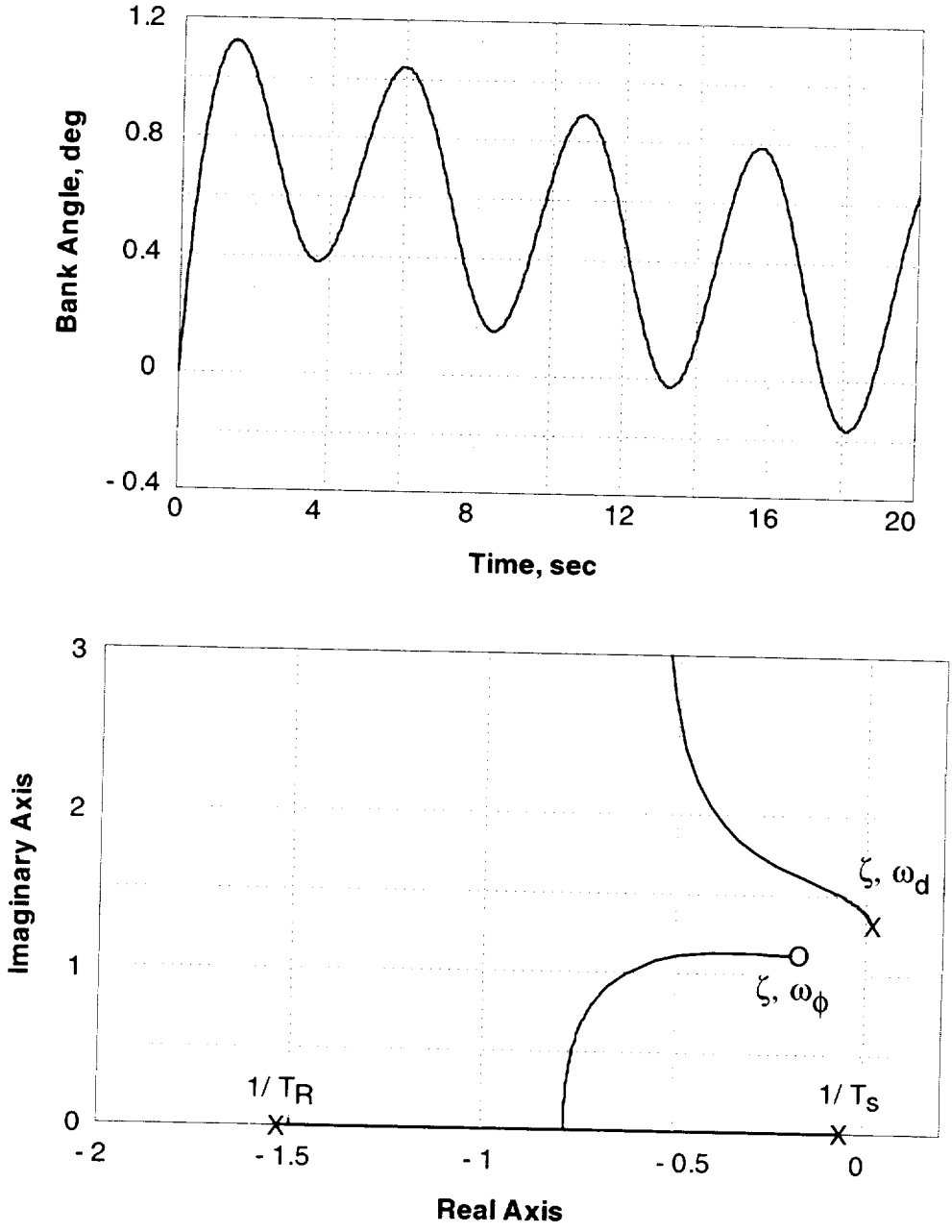

Figure 72. Open-loop time history and root locus for bank-angle control for the Harrier at 100 knots.

locus at the bottom of the figure reinforces these observations. Note that the unstable Dutch roll mode violates open-loop criteria and will immediately lead to roll-control problems. The roll mode is reasonably well damped, and the spiral mode is slightly stable. Considerable pole-zero separation is present between the Dutch roll and roll numerator roots, where in this case the numerator is lower in frequency than the Dutch roll. The root locus shows that closed-loop control will be poor, due first to the low-frequency roll mode, and second to the poorly damped, although slightly stable Dutch roll. This behavior will force the pilot to compensate for the deficiencies in the response, with adverse consequences for flying qualities.

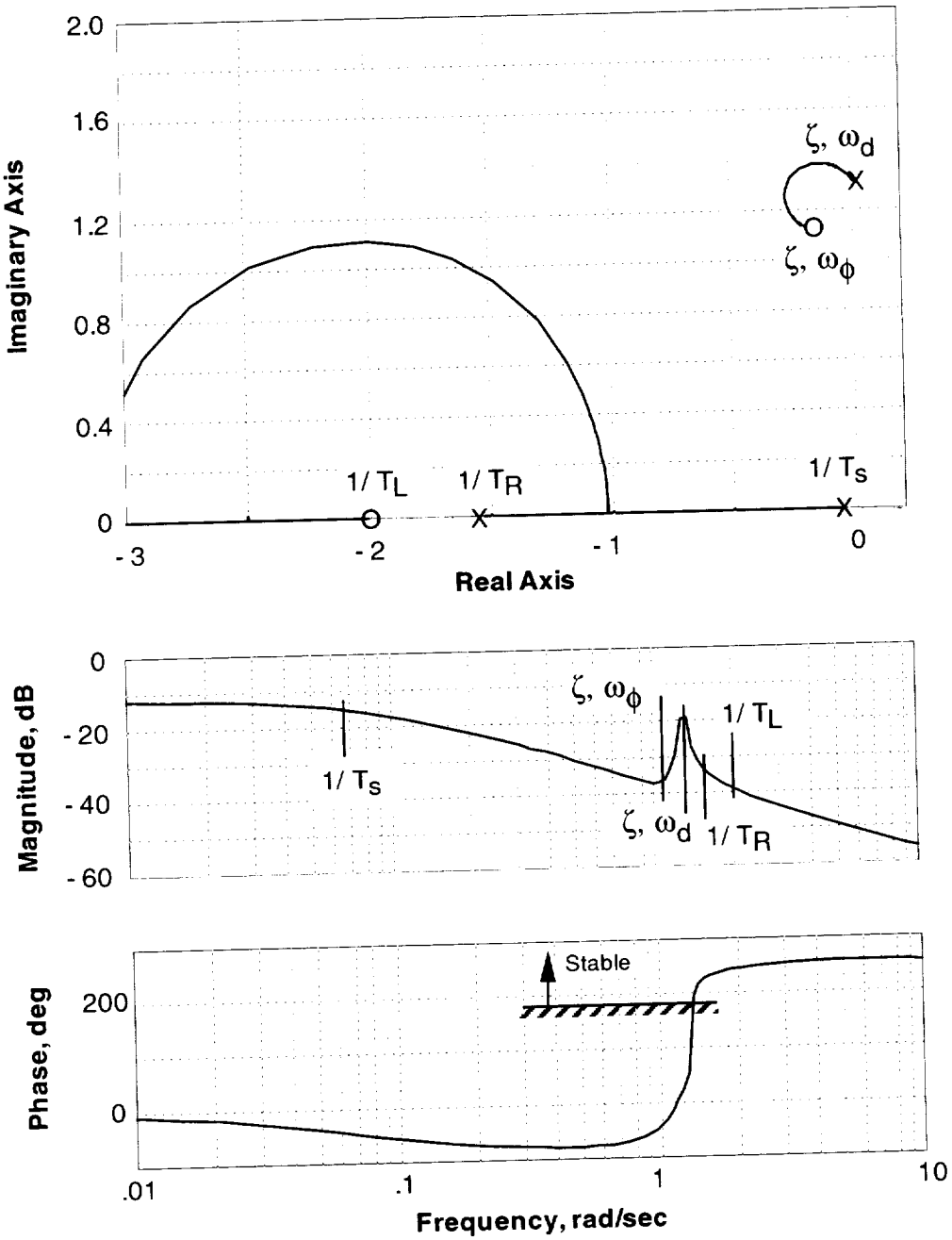

Figure 73. Root locus and Bode plot of bank-angle control with lead compensation for the Harrier at 100 knots.

The effects of lead compensation on roll control are shown in figure 73. In the root locus plot, the pilot's lead appears in the numerator root at $1/T_L$. As the pilot closes the bank-angle loop, both the spiral and roll mode progress further into the left-hand plane and increase the bandwidth of roll response. The unstable Dutch roll is also stabilized and migrates toward the numerator root, although Dutch roll oscillations will still appear in the roll response. The Bode plot indicates that adequate phase margin is present for roll control at 2-3 rad/sec. However, it will be necessary to suppress the Dutch roll without placing further demands on the pilot. Experience has shown that this will require augmentation of Dutch roll damping and a reduction in the amount of Dutch roll in the roll response by artificial means. Examples will be covered at a later point in the text.

Yaw Control

In controlling the aircraft's heading, the pilot will roll the aircraft to a bank angle so that the lateral component of lift can curve the flightpath in the horizontal plane, allow the aircraft to turn, then roll to level the wings after achieving the desired heading. If the pilot were to control heading directly, the equation that relates heading response to the lateral stick is

$$\frac{\psi}{\delta_s} = \frac{N'_{\delta_s}(s + 1/T_\psi)(s^2 + 2\zeta\omega_\psi s + \omega_\psi^2)}{s\Delta_{Lat}}$$

The numerator is third-order with a gain term, the yawing moment due to lateral control, that determines the direction the aircraft yaws initially in response to the lateral control. The presence of the free s in the denominator relates the response to heading instead of yaw rate. The first-order numerator root is approximately equal to the roll mode $1/T_\psi = 1/T_R$ so the pole-zero combination cancels for heading response. The complex pair is characterized by damping and natural frequency,

$$2\zeta\omega_\psi = -Y_v\left(1 - \frac{N'_p L'_{\delta_s}}{L'_p N'_{\delta_s}}\right) - \omega_\psi^2 T_\psi$$

$$\omega_\psi^2 = \frac{gL'_\beta}{V_o L'_p}\left(\frac{N'_\beta L'_{\delta_s}}{L'_\beta N'_{\delta_s}} - 1\right)$$

where the damping is typically low and potentially negative, which would place these numerator roots in the right-half plane. The frequency scales with dihedral effect. When yaw due to lateral control is absent, as it is in the case of the Harrier example, the numerator becomes

$$L_{\delta_s} N'_p\left(s^2 - Y_v + \frac{gN'_\beta}{V_o N'_p}\right)$$

and factors into two real roots, one in the right-half, one in the left-half plane at $\pm\sqrt{\frac{-gN'_\beta}{V_o N'_p}}$.

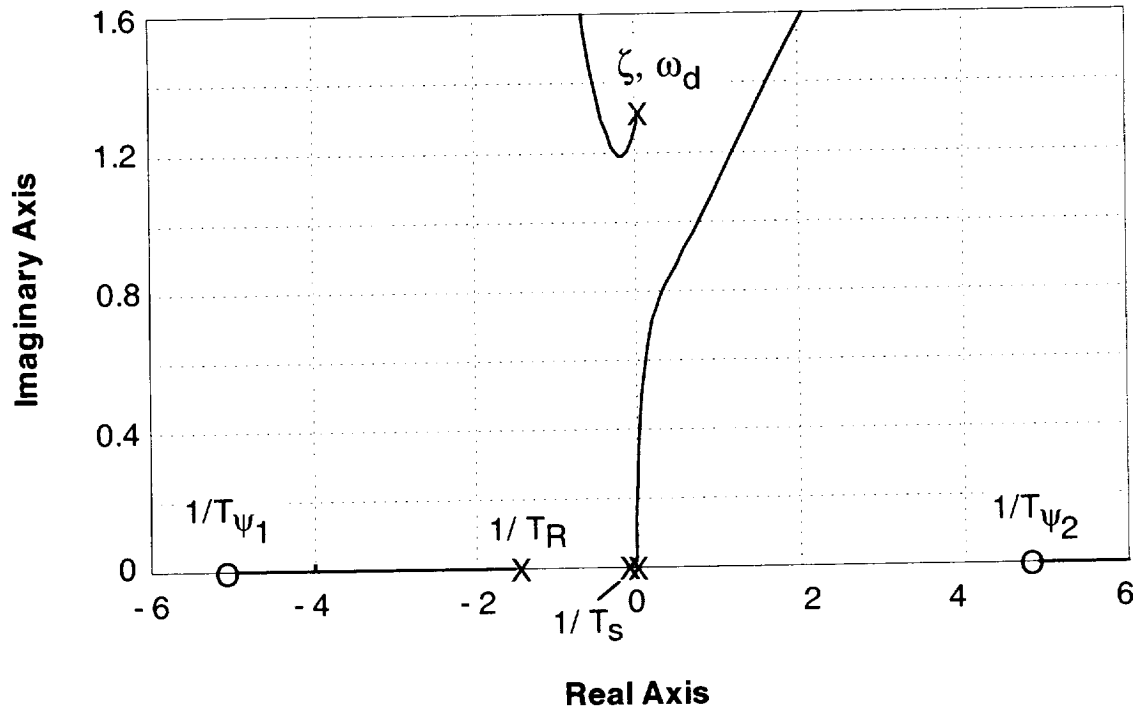

Figure 74. Root locus of heading control with the lateral stick for the Harrier at 100 knots.

An example of the effect of closed-loop heading control with the lateral stick in the absence of bank-angle control is shown in the root locus of figure 74. Note the roots progressing from the origin and the spiral mode, coalescing and moving into the right-half plane at low frequency. Thus, closed-loop control of heading with the lateral stick will quickly drive the aircraft unstable. The appearance to the pilot would be a long-period oscillatory wandering in heading similar to the case for altitude or airspeed control in the absence of pitch-attitude control. As in the longitudinal case, this problem can be resolved by first stabilizing the attitude inner loop, and then controlling heading through changes in bank angle. The transfer function of heading to bank-angle command is represented by

$$\frac{\psi}{\phi_c} = \frac{N'_{\delta_s} K_\phi (s + 1/T_\psi)(s^2 + 2\zeta\omega_\psi s + \omega_\psi^2)}{s(s^2 + 2\zeta\omega'_R s + \omega'^2_R)(s^2 + 2\zeta\omega'_d s + \omega'^2_d)}$$

where the closed-loop roots that were initially associated with the spiral, the roll mode, and the Dutch roll are now the closed-loop counterparts. The example root locus in figure 75, with the spiral and roll modes modified by the bank-angle closure, shows a stable progression of roots at low frequency. Note that it is possible to drive the Dutch roll unstable; however, adequate heading-control bandwidth will have been achieved before the point of instability is reached. It can be observed on the Bode plot that adequate phase margin exists for control to a bandwidth of 1 rad/sec; bandwidths for control of heading without the bank-angle inner loop closed are half that value or less.

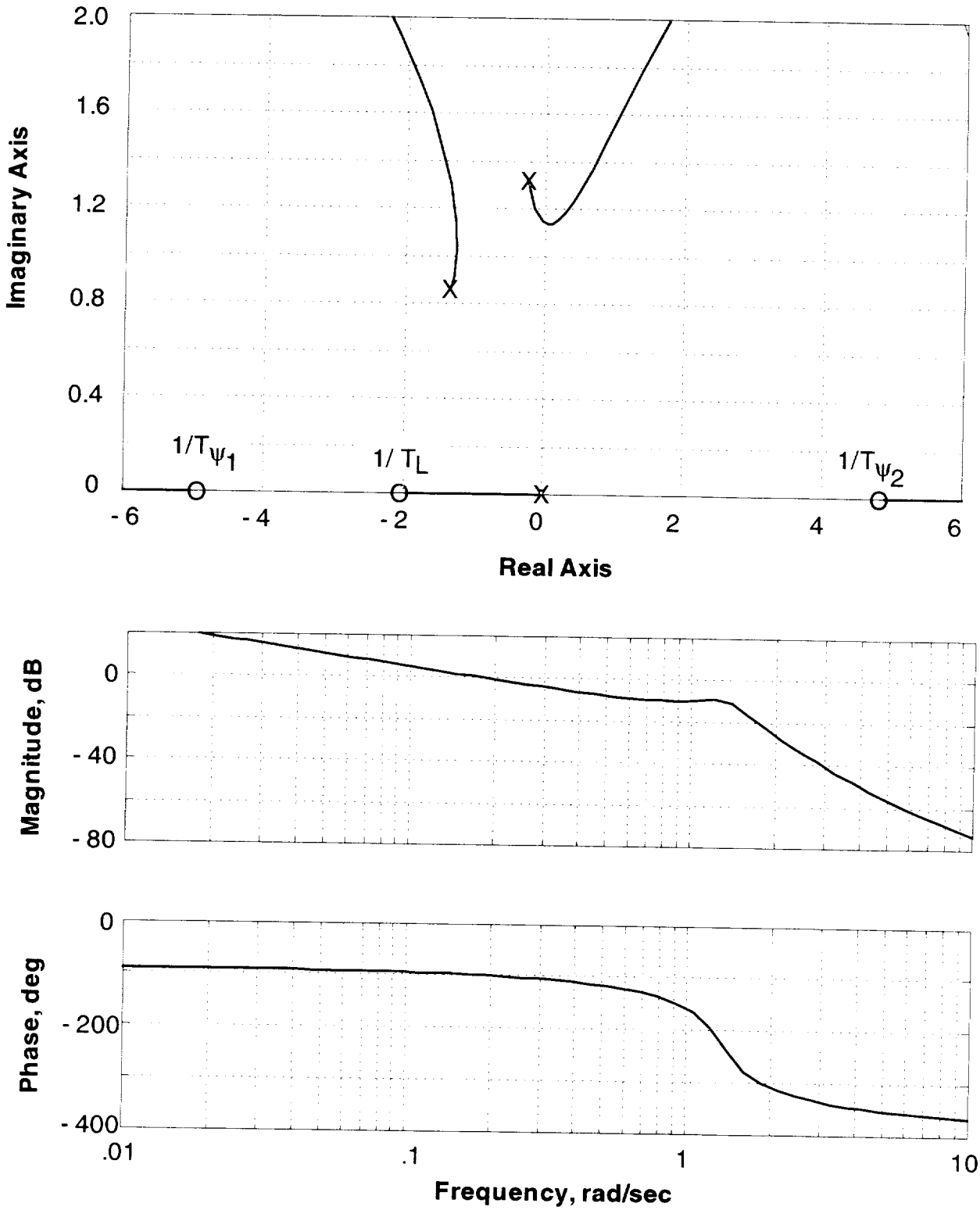

Figure 75. Root locus and Bode plot of heading control with the bank-angle loop closed with lead compensation for the Harrier at 100 knots.

Another means of controlling yaw is through the directional control. In this case, the yaw rate transfer function is

$$\frac{r}{\delta_p} = \frac{N'_{\delta_p}(s + 1/T_r)(s^2 + 2\zeta\omega_r s + \omega_r^2)}{\Delta_{Lat}}$$

Control sensitivity is defined by yawing moment due to the directional control, and the first-order numerator term is again approximately the same as the aircraft's roll mode, $1/T_r = 1/T_R$. The second-order roots are approximated by

$$2\zeta\omega_r = -Y_v + \frac{Y_{\delta_p} N'_\beta}{V_o N'_{\delta_P}} - \omega_r^2 T_r$$

$$\omega_r^2 = \frac{gL'_\beta}{V_o L'_p}$$

The yaw rate to pedal root locus in figure 76 does not presume a bank-angle inner loop closure, thus the root locations are those for the open-loop aircraft. Reasonably good closed-loop control can be achieved unless the loop is closed at such a high gain as to destabilize the Dutch roll. Adequate yaw-rate control does not require high bandwidth; as a result the Dutch roll stability

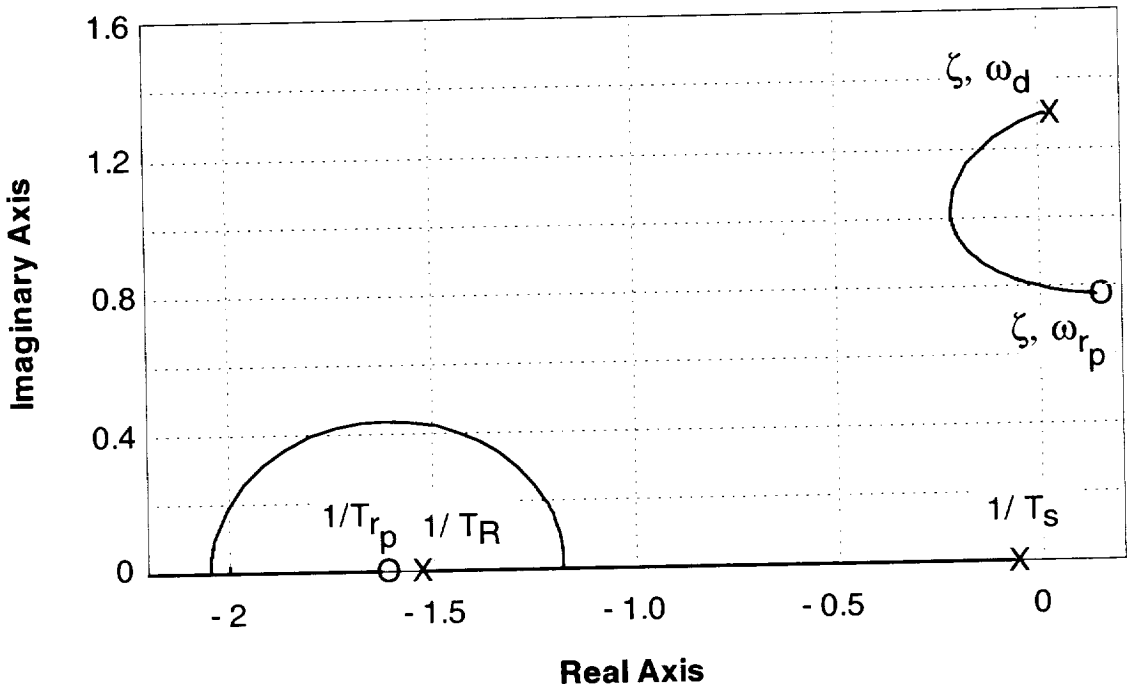

Figure 76. Root locus of yaw-rate control with the directional control for the Harrier at 100 knots.

would not be compromised. This control technique would be employed by the pilot to suppress unwanted yaw excursions rather than to execute steady turns.

A simple yaw damper commands the directional control in proportion to yaw rate. In later discussions of control augmentation, an example of a yaw damper for the Harrier will be noted, including some different approaches to the design other than using yaw rate alone.

Sideslip Control

A final consideration for lateral-directional control in forward flight concerns control of sideslip. Sideslip excitation with the lateral control during roll and turning maneuvers has the potential to degrade lateral-directional flying qualities. Ideally, the pilot would like turning maneuvers to be performed in coordinated flight, which is with minimal sideslip while entering and exiting the turn. Thus, during the roll into the turn, the nose will immediately move in the direction of the turn without any lag or dynamic oscillations. If the aircraft is poorly coordinated, control of heading may be difficult. Recall that in the heading-to-lateral-stick transfer function the leading term was yawing moment due to lateral control. When that control derivative is negative, the aircraft will initially yaw in the direction opposite to the turn. If the pilot is trying to make a small heading change and the nose moves initially away from the turn, precise heading control will be difficult.

Before considering control of sideslip, it is necessary to determine to what extent sideslip is excited by the lateral control. Sideslip response to the lateral control is described by the transfer function (assuming no side force from the lateral control)

$$\frac{\beta}{\delta_s} = \frac{N'_{\delta_s}(s + 1/T_{\beta_1})(s + 1/T_{\beta_2})}{\Delta_{Lat}}$$

For the open-loop response, yawing moment due to lateral control is the scaling factor and determines the initial response. Even in the absence of this initial yawing moment, sideslip will not necessarily be eliminated dynamically, even in the steady state. With lateral-control yaw present, the transfer function consists of a second-order numerator over the classic fourth-order denominator. One of the numerator roots tends to be at low frequency, and the other root falls in a frequency range that will be of interest to sideslip control. This root can be approximated by

$$1/T_{\beta_1} = -L'_p + \frac{L'_{\delta_s}}{N'_{\delta_s}}\left(N'_p - \frac{g}{V_o}\right)$$

The dominant contribution comes from roll damping; however, the second term can significantly alter the numerator location. This transfer function is used to determine the amount of sideslip generated and whether the sideslip presents a difficulty for heading control. If the aircraft generates objectionable levels of sideslip, then the pilot must use the directional control to attempt to null the sideslip during the course of the maneuver.

If it is necessary for the pilot to control sideslip directly, sideslip response to the directional control is described by

$$\frac{\beta}{\delta_p} = \frac{Y_{\delta_p}}{V_o}\left[\frac{(s+1/T_{\beta p_1})(s+1/T_{\beta p_2})(s+1/T_{\beta p_3})}{\Delta_{Lat}}\right]$$

The gain factor is side force due to the control, divided by the steady-state airspeed at that flight condition. The numerator is third-order with one term at high frequency that can be ignored for the frequency range of interest. Another tends to be at low frequency and without a good approximation, although it does not significantly affect closed-loop sideslip control. An intermediate root that is of significance to the pilot's control of sideslip can be approximated by

$$1/T_{\beta p_2} = -L'_p + \frac{L'_{\delta_p}}{N'_{\delta_p}}\left(N'_p - \frac{g}{V_o}\right)$$

This root is typically close to the aircraft's roll mode unless the ratio $L'_{\delta_p}/N'_{\delta_p}$ is large because of a considerable rolling moment generated by the directional control. Otherwise, the roll damping term dominates this root, and it would cancel with the roll mode in the characteristic equations.

As noted in reference 32, use of this control to coordinate the aircraft during lateral maneuvers can be described by

$$\left(\frac{\beta}{\delta_s}\right)\delta_s + \left(\frac{\beta}{\delta_p}\right)\delta_p = 0$$

Although it is not necessary that sideslip be nulled at all times during the maneuver, it is worth understanding the pilot's control actions that are required to counteract sideslip. The transfer function that describes use of the yaw control follows from the preceding equation:

$$\frac{\delta_p}{\delta_s} = -\frac{\left(\frac{\beta}{\delta_s}\right)}{\left(\frac{\beta}{\delta_p}\right)}$$

$$= -\frac{N'_{\delta_s}}{N'_{\delta_p}}\left(\frac{s+1/T_{\beta_1}}{s+1/T_{\beta p_2}}\right)$$

where the higher-frequency terms are ignored. Although there is a lower-frequency term in the directional-control transfer function, it also is removed so as to consider only the characteristics

that complicate the control process. A low-frequency denominator root would appear as a long-term trimming function and would not increase the complication for the pilot. The ratio of control sensitivities provides the scaling between the yaw and roll controls. Dynamics of the yaw-control input are derived from the ratio of the two first-order roots. The resulting time response for yaw control in response to the roll control becomes

$$\delta_p \sim 1 + \left(\frac{T_{\beta p_2}}{T_{\beta_1}} - 1 \right) \left(1 - e^{\frac{-t}{T_{\beta p_2}}} \right)$$

The important features in the time domain are determined by the ratio of the two time constants and by the rate of subsidence in the exponential factor associated with the denominator root $1/T_{\beta_{p2}}$.

The time histories in figure 77 show the directional control required for a number of different ratios of the time constants $T_{\beta_{p2}}/T_{\beta_1}$. They are also shown for either sign of yaw due to the lateral control N'_{δ_s}. For the simplest of these examples, which would represent a typical conven-

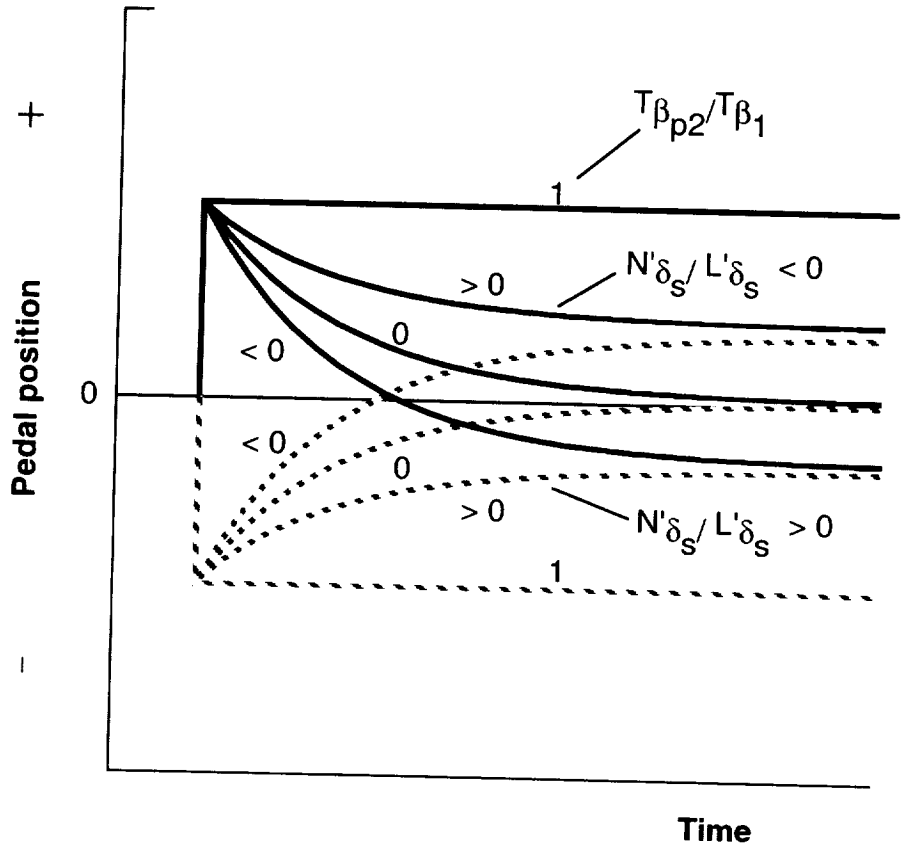

Figure 77. Example time history plots of directional control required to minimize sideslip during roll maneuvers.

tional aircraft, the two time constants can be assumed to be equal. Then the yaw control required with the lateral control is simply a step input that carries the sign of the yaw due to the lateral control. That is the easiest form of control coordination, a proportional crossfeed from the lateral control to the directional control, and one that may not degrade flying qualities. It is a control technique that can be readily learned and eventually applied subconsciously by the pilot. When the two time constants are not equal, the control compensation becomes more difficult. To maintain good coordination, when $T_{\beta_{p2}}$ is zero, the pilot must initially apply yaw control and eventually remove it entirely as the maneuver proceeds. Should $T_{\beta_{p2}}$ and T_{β_1} be of opposite sign, the pilot would reverse the directional control during the maneuver. When complicated dynamic control applications are required, the pilot's mental workload increases and degrades flying qualities. With unfavorable roll-sideslip phasing that requires such complicated control coordination, very little sideslip can be tolerated.

An example time history of a turn entry maneuver for the Harrier is shown in figure 78. The pilot has applied a pulse input to roll the aircraft over to approximately a 10 deg bank and the resulting sideslip excitation is about 2 deg. The amount of Dutch roll excitation and sideslip excursion in comparison to roll make this behavior unsatisfactory to the pilot.

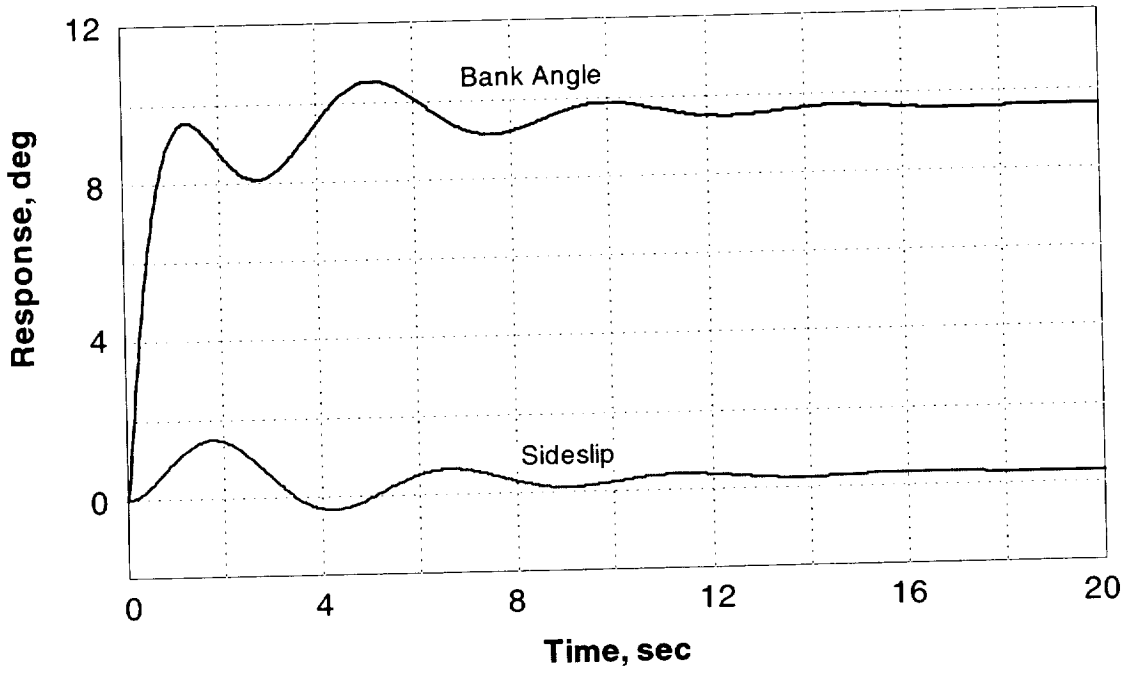

Figure 78. Time history of roll and sideslip response for the Harrier at 100 knots.

Lateral-Directional Flying Qualities Requirements in Forward Flight

Design criteria for roll control concern control power, control bandwidth, and residual oscillations arising from Dutch roll excitation; they are noted in reference 10. Control power in forward flight is based on the time required to reach a 30 deg bank angle. For a highly maneuverable aircraft like a fighter in the approach and landing, Level 1 flying qualities demand 30 deg of bank in 1 sec, with the time increasing to 1.3 sec for Level 2. Somewhat less roll performance is needed for a heavy aircraft like a transport. In that case, 2.5 sec time to 30 deg of bank is needed for Level 1 or 3.2 sec for Level 2. These control power demands will size the lateral control effectors such as ailerons or propulsion system components that produce rolling moments during powered-lift operations. Considering dynamic response, appropriate values for characteristic roots for the roll and spiral modes were covered previously in the text. Roll bandwidth requirements are the same as those for pitch attitude, that is, 2-4 rad/sec for Level 1 and 1 rad/sec for Level 2. A final concern is the amount of Dutch roll that can be allowed in the roll response. Figure 79 shows the allowable level of roll oscillations in proportion to the average roll response

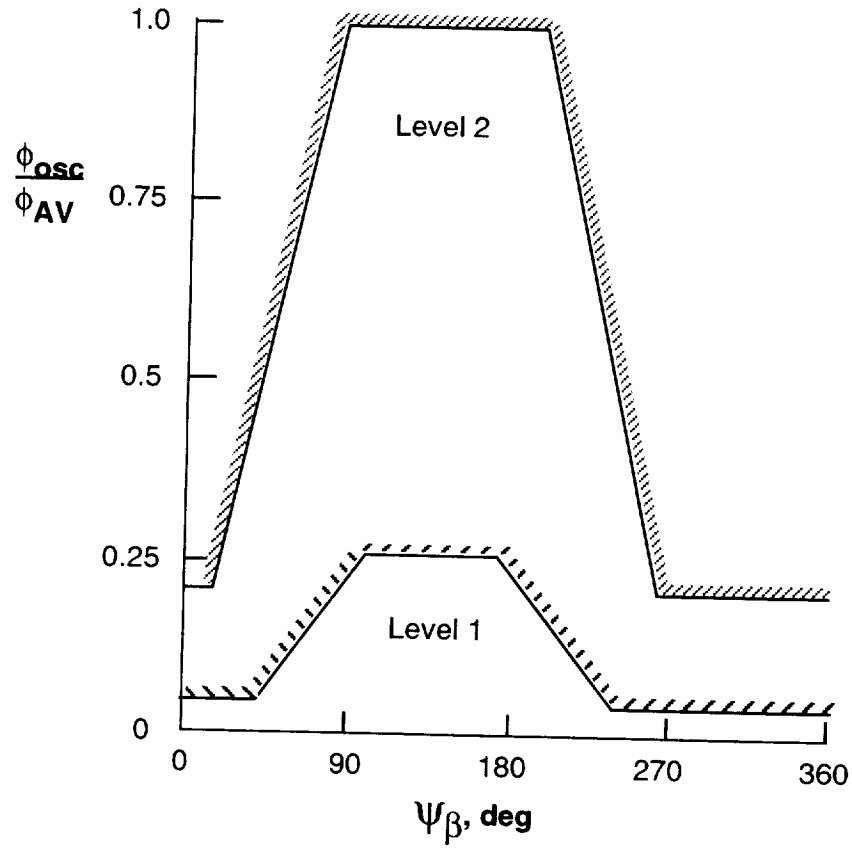

Figure 79. Allowable Dutch roll in the roll response to lateral control.

for Levels 1 and 2 flying qualities. For Level 1 the oscillatory response should not be more than about 25 percent of the average, whereas for Level 2 that ratio increases to 1:1. The allowable roll-response envelope is a function of a phasing parameter for sideslip in relation to roll and is described below in the paragraph on sideslip response.

Flying qualities criteria for the magnitude of transient sideslip excursions indicate whether the open-loop response is acceptable. The criteria are based on the peak change in sideslip that occurs during the roll into the turn (fig. 80). The incremental change in sideslip is scaled in proportion to the magnitude of the rolling maneuver. The criteria are shown in two parts at the top and bottom of the figure and depend on the magnitude of roll excitation in relation to sideslip excitation in the Dutch roll. To enter either plot it is necessary to define the phase angle parameter

$$\psi_\beta = 360[(n - 1) - (t_{n_\beta}/T_d)]$$

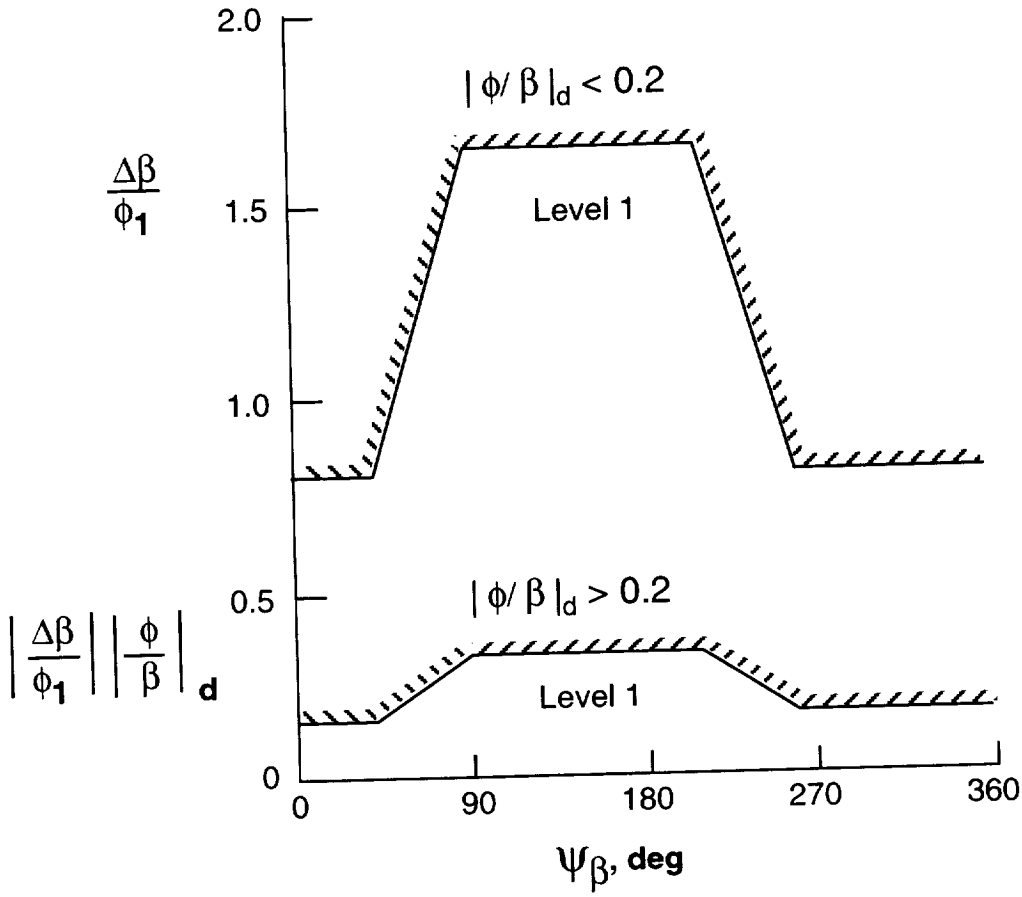

Figure 80. Open-loop sideslip design criteria.

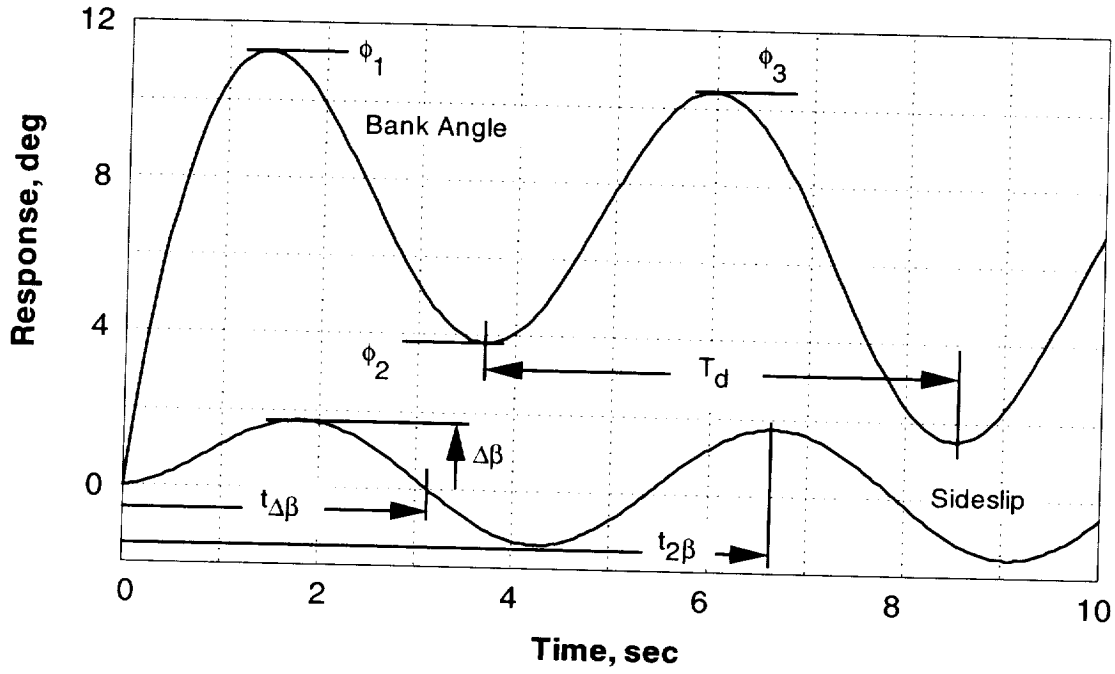

Figure 81. Example roll and sideslip response for definition of sideslip phase.

where the Dutch roll period T_d and the phasing period $t_{n\beta}$ are noted in figure 81. Bank angle, roll rate, and sideslip are shown in response to a lateral control pulse. The first peak in bank angle divided into the peak change in sideslip is one element of the criteria. The amount of roll occurring in the Dutch roll compared to sideslip is derived from the relative magnitudes of this oscillatory envelope of the two responses. Finally, the Dutch roll period and the phasing period are noted on the figure. The phase-angle parameter is a measure of the sideslip phasing with respect to bank angle. The criterion is more forgiving for Level 1 characteristics depending on the sideslip phasing. If the sideslip peak is sufficient for the Level 1 boundary to be exceeded, it will be necessary to use the yaw control to reduce the sideslip excursions. The pilot's technique with the yaw control to suppress the sideslip depends on the phasing of the two.

The criterion for yaw control power is expressed in terms of heading change in 1 sec after application of the directional control. For Level 1 and Level 2, these values are 6 deg and 3 deg, respectively. These are comparable to those for the hover case and, for semi-jet-borne flight, are reasonable for sizing the yaw control.

CONTROL AUGMENTATION AND COCKPIT DISPLAYS

To this point, the discussion of V/STOL flying qualities has focused on the pilot's control of the basic aircraft in hover and forward flight. The balance of the text will cover control augmentation systems and displays and their implications for flying qualities for V/STOL operations.

Need for Control Augmentation and Displays

As should be clear from the foregoing discussion, the inherent characteristics of an aircraft at low speed and hover generally do not provide for ease of handling by the pilot. There are limits in the ability of the basic configuration of the aircraft or the propulsion systems to provide enough damping and stability and to minimize coupling in the control response. Aerodynamic surfaces are ineffective at low speed, and the propulsion system must provide forces and moments for control. Therefore, it is necessary to devise other means of improving the control of the aircraft. These demands lead to use of the control systems to provide the stability and controllability necessary to achieve good flying qualities.

The following example is useful to illustrate the benefit of control augmentation during hover. Recall the longitudinal equations of motion from the discussion earlier in the text:

$$\begin{Bmatrix} \dot{u} \\ \dot{w} \\ \dot{q} \\ \dot{\theta} \end{Bmatrix} = \begin{bmatrix} X_u & 0 & 0 & -g \\ Z_u & Z_w & 0 & 0 \\ M_u & M_w & M_q & 0 \\ 0 & 0 & 1 & 0 \end{bmatrix} \begin{Bmatrix} u \\ w \\ q \\ \theta \end{Bmatrix} + \begin{Bmatrix} X_\delta \\ Z_\delta \\ M_\delta \\ 0 \end{Bmatrix} \delta$$

If the stability and damping terms are small enough to have no apparent effect on the pilot's control in hover, the equations can, for purposes of discussion, be simplified to

$$\dot{u} = -g\theta$$
$$\dot{w} = Z_{\delta_T}\delta_T$$
$$\ddot{\theta} = M_{\delta_s}\delta_s$$

so that longitudinal acceleration is proportional to the inclination of the vertical axis, vertical acceleration is generated by the thrust of the propulsion system, and pitch angular acceleration arises from the moment generated by the pitch control. For a task of moving the aircraft from one position to another in hover, consider the control of pitch attitude and the subsequent use of pitch attitude to control longitudinal position. As indicated in the block diagram of figure 82, the pilot initiates the maneuver with a control input that generates a pitch angular acceleration, which in turn is integrated twice to obtain pitch attitude. Pitch attitude in turn produces a longitudinal acceleration by tilting the thrust vector, which is integrated twice to give longitudinal

position. To control pitch attitude the pilot must anticipate the aircraft's response and control attitude through two integrations. The pilot has no immediate indication of the control needed to reach a steady-state pitch attitude. This process requires mental effort and is compounded by the need to control through two additional integrations to achieve the change in longitudinal position. Height control requires control through two integrations. Whenever the pilot cannot directly anticipate the response that the control input will produce, the result will be increased mental effort, hence workload, and will inevitably lead to poor flying qualities.

Another view of the hover control process that illustrates the benefits of control augmentation is presented in the time history in figure 83. This situation concerns control of longitudinal position as mentioned in the previous example.

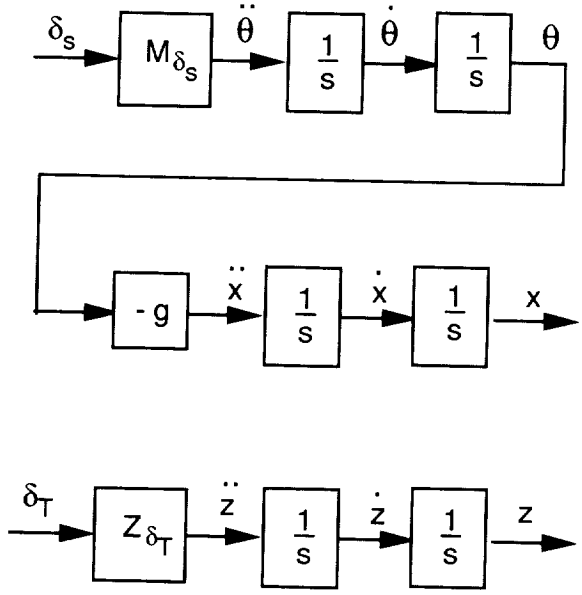

Figure 82. Simplified block diagram of attitude and position control in hover.

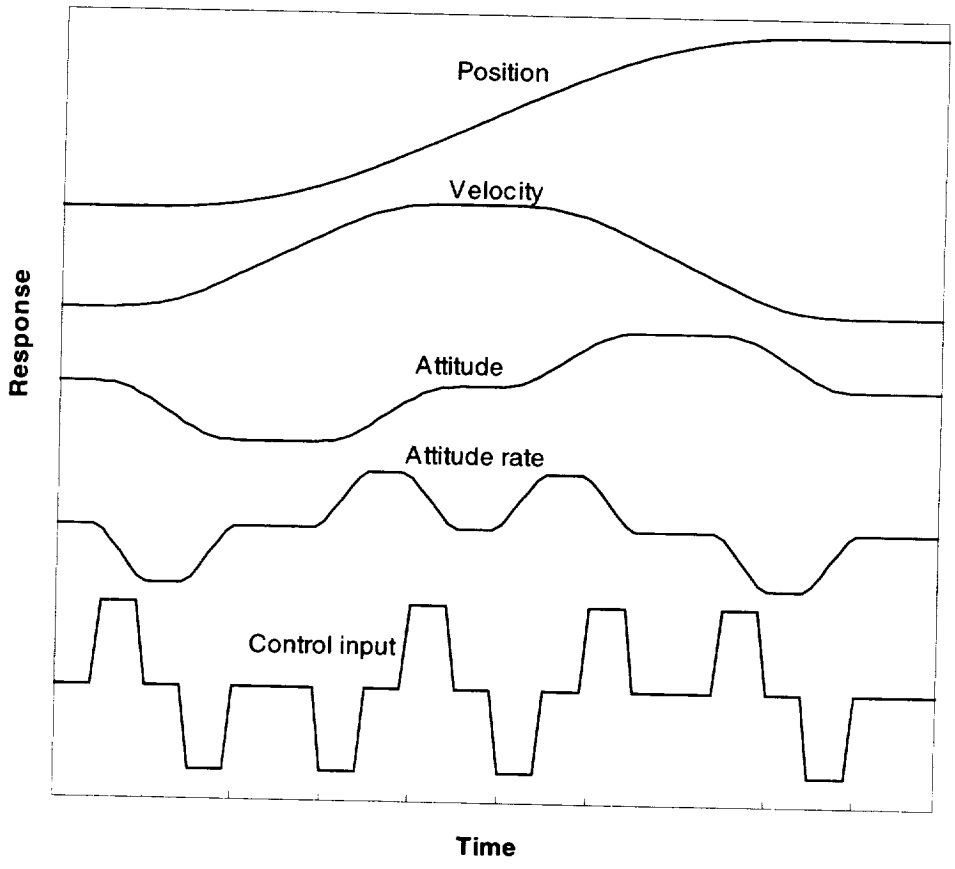

Figure 83. Example time history of longitudinal position control.

The pilot's control input appears at the bottom and the sequential response of pitch rate, pitch attitude, longitudinal velocity, and longitudinal position proceed up the page. The pilot's task is to translate the aircraft from an initial to a final position. The time responses are highly stylized and, as in the previous example, assume that no aerodynamic damping or stability are present. The maneuver is initiated with a forward input of the longitudinal control that lowers the nose to generate longitudinal acceleration that will move the aircraft forward. The pilot then removes that input to establish a steady pitch rate. With the nose moving down at a constant rate, the pilot reverses the input to reduce the pitch rate to zero in order to establish a steady attitude. To achieve a steady forward velocity, the pilot must completely reverse the sequence of control inputs by bringing the nose up at a steady pitch rate, then reducing the rate to zero to restore the aircraft to a level attitude to establish the steady translational velocity. Finally, to bring the aircraft to a halt at the desired position, the entire control process must be reversed again. The pilot raises the nose to arrest the forward velocity and then brings the nose back to level to stop the aircraft at this new position. This time history summarizes a sequence of control inputs that occurs over a period of several seconds and is a reasonable representation of the control process involved with typical hover response characteristics for the basic airframe. In reality, more inputs will likely be required if the pilot's judgment of control sizing and timing is not precise. Thus, the example is probably as simple as the control process can be made.

To appreciate how the pilot's control effort could be reduced, assume the pilot can command pitch rate instead of pitch acceleration. Then the time history for pitch rate would represent the pilot's control inputs, in contrast to the time history shown at the bottom of the figure, and the number of control applications would be cut in half. Further, if the pilot's control could command pitch attitude, the attitude trace would show an even simpler control task. Finally, if the control could command longitudinal velocity, the pilot's task would be reduced to its simplest form. Manual control research has consistently shown that position control by the human operator is best achieved using a control system that provides command of rate of change of position. Thus, for attitude control, an attitude-rate command system works best. For hover position control, a translational rate control is superior. This graphic representation of the control process presents a compelling reason to investigate higher levels of control augmentation for V/STOL aircraft.

Another motivating factor in designing control systems and displays is the requirement that aircraft operate in adverse weather, particularly in winds and turbulence under poor visibility conditions. A description of visibility conditions, the associated visual cues, and their significance, as suggested in reference 23, appear in figure 84. The scale at the top of the figure relates outside visual cues (OVC) to conditions ranging from visual meteorological conditions (VMC) to fully instrument meteorological conditions (IMC). The accompanying adjectives describe the cues that are associated with the ability to visually perceive aircraft attitude or changes in aircraft position and velocity. Thus, OVC 1 indicates that the horizon is clearly visible to provide good attitude cues, and that movement and position over the surface could be clearly perceived. As visibility degrades to OVC 2, the horizon would be somewhat obscured, requiring a good deal of concentration to determine the aircraft's attitude. Movement over the surface can still be clearly observed. Degrading visibility further to partial instrument conditions implies the inability to extract attitude information, although adequate cues for position over the ground, though not

easily obtained, would still be available. However, the ability to observe fine detail of the surface texture that provides rate of motion with respect to the surface would be impaired. Note that the ability to perceive and control the rate of motion is important for providing aircraft damping. Finally, the full instrument flight condition is reached where the visual cues are not adequate to support hovering flight.

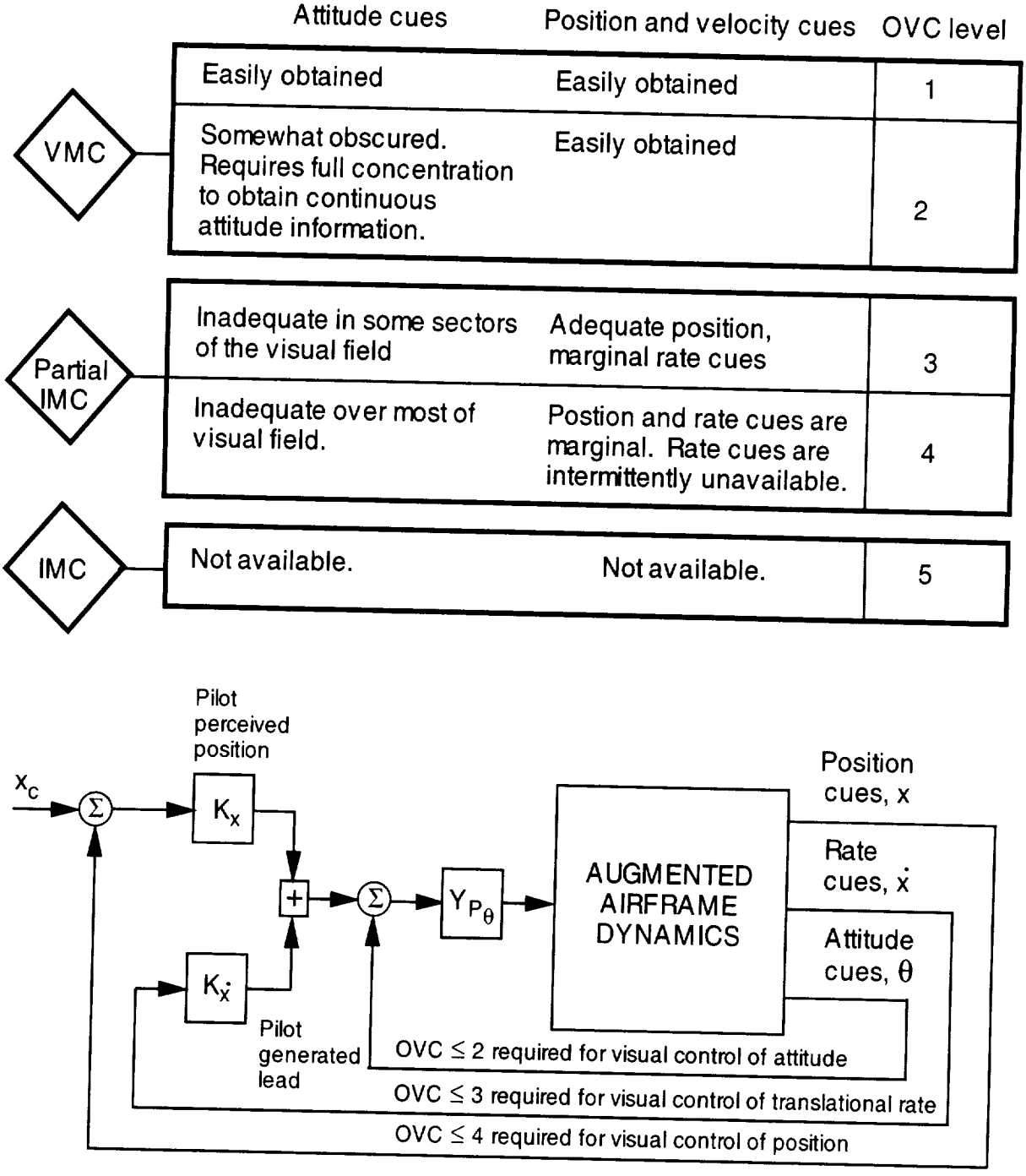

Figure 84. Visual cue scale.

The block diagram at the bottom of the figure indicates the control augmentation required, based on the level of outside visual cues available to the pilot. The diagram links these visual cue ratings to the necessary conditions for manual loop closure for hover position control. To be able to fly the aircraft visually, assuming that the aircraft is otherwise easily controlled, the pilot needs an OVC of 2 or better for attitude control. With poor attitude cues, the pilot will need assistance with the attitude-control loop, perhaps through attitude stabilization, as well as an artificial attitude display. As the visibility degrades further, the pilot requires assistance in perceiving and controlling aircraft rate of motion over the surface. In full instrument conditions, the display must be capable of presenting all the attitude, rate, and position information that would otherwise be available from the external scene. Extension of this conceptual link between the visual cue environment to control augmentation requirements is developed for rotary-wing aircraft design in reference 33.

Benefits of Control Augmentation and Displays

Given this background for the need for control augmentation, examples of pilot evaluations of control augmentation such as those noted in the foregoing discussion can be understood. The benefits of control augmentation for hover and landing operations on land and aboard ship can be seen in figure 85. This is a summary of pilot ratings for vertical landing in VMC for a range of demanding landing tasks. One task involves landing on a 100- by 100-ft pad; another task corresponds to recovery aboard an assault carrier of the LHA class, a ship used for Harrier and

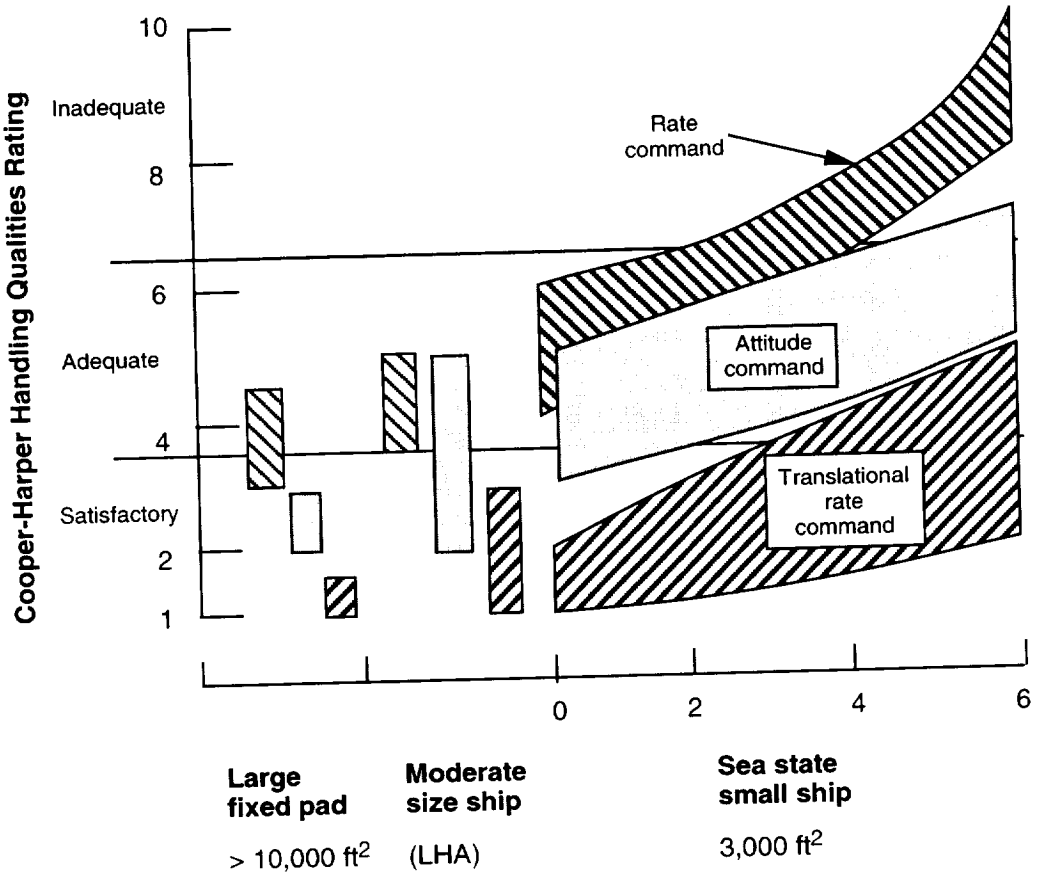

Figure 85. Influence of control augmentation on vertical landing.

helicopter operations; and the final task involves landing aboard a frigate-class ship with a landing pad aft of a hangar enclosure toward the stern of the vessel. Sea conditions from 0 to 3 are encompassed for the LHA class; they ranged from 0 to 6 for the frigate. This information is extracted from a number of reports covering simulation and flight experience; they are summarized in reference 34. These data show pilot assessments of three different control-response types of control augmentation systems. One system provided attitude rate command similar to pitch and roll augmentation on earlier versions of the Harrier; another was pitch and roll attitude command; and a third system provided longitudinal, lateral, and vertical translational velocity command.

The results show that when the landing task is not aggressive, as would be typical of land-based operations or aboard a very large platform at sea, even simple control augmentation can provide marginally satisfactory flying qualities. However, the task involves enough physical and mental effort that stabilization of the aircraft's attitude relieves some of the pilot's workload. The task can be made simple to accomplish with use of the velocity command system. For a moving platform with a reasonably sized landing pad such as the LHA in conditions up to sea state 3, flying qualities begin to degrade to the point where the rate command system is no longer Level 1 and attitude command is considered marginal Level 1. Ratings for the velocity command system remain solid Level 1. However, in an environment of a small moving platform and accompanying sea state, wind, and air-wake disturbances around the platform, substantial differences in flying qualities are evident for the different control systems. Rate-command systems are no longer capable of providing satisfactory flying qualities, even in quiescent conditions. Attitude-command systems can provide borderline satisfactory flying qualities in benign conditions, but in sea states of any significance flying qualities are only adequate. Results show, however, that the translational velocity command system demonstrates satisfactory flying qualities over a wide range of sea conditions up until it is impossible to capture the deck itself. Upon reaching those conditions, the operational limits are reached for recovery to the ship. From this set of results, the improvement in flying qualities and the ability to desensitize the aircraft to a wide range of operational conditions is apparent for the more sophisticated control systems.

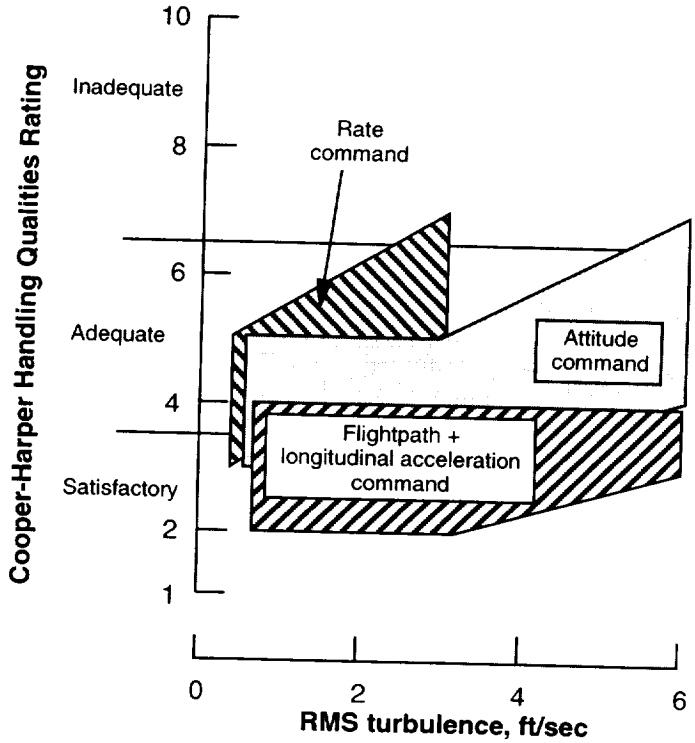

Figure 86. Influence of control augmentation on the instrument decelerating approach.

A comparable result is obtained during the deceleration from forward flight to hover under IMC. The deceleration is carried out on instruments beginning at airspeeds around 200 knots. In figure 86 a range of results is shown for rate command, attitude command, and velocity command,

where velocity command specifically includes flightpath command plus command of the deceleration along the flightpath. Flightpath and deceleration are decoupled in response to the pilot's controls. The related displays present the aircraft's flightpath and deceleration along the flightpath, integrated in a format that does not require the pilot to scan several instruments in order to assimilate information on the aircraft's situation. These display modes are designed to be compatible with their associated control mode, a subject of control and display design to be covered later in this section. For the instrument transition, poor aerodynamic stability and the need to continually adjust thrust-vector angle, thrust setting, and pitch attitude to perform the deceleration creates a high workload task. The figure shows that when the pilot has no assistance in control of the aircraft other than attitude rate command, flying qualities are borderline inadequate. With the addition of attitude stabilization, flying qualities are improved somewhat. With decoupled flightpath-deceleration command, fully satisfactory flying qualities are achieved. Thus, for an instrument transition from cruise to hover, a progressive improvement in flying qualities accompanies the increased capability in the controls and displays for the pilot.

Control Augmentation Systems

With the preceding background and motivation, the following examples illustrate the various types of control augmentation concepts, how they are designed and the design criteria that are involved.

Rate Command System

A rate command system is presented in the simplified example of roll control in hover in figure 87. The block diagram represents the aircraft without any aerodynamic forces imposed. The pilot's lateral stick input generates roll angular acceleration, which is then integrated to roll rate and finally to roll attitude. To construct a system that provides roll-rate command, it is necessary to feed back roll rate to combine with the pilot's control input. A rate gyro sensor provides a roll-rate signal that is multiplied by a gain factor chosen to produce the desired level of roll damping and hence roll control bandwidth. The time history of roll-rate response to a step control input at the bottom of the figure illustrates these design features. It represents a first-order system, where the two characteristics of the response that are important from a designer's point of view are the time constant and

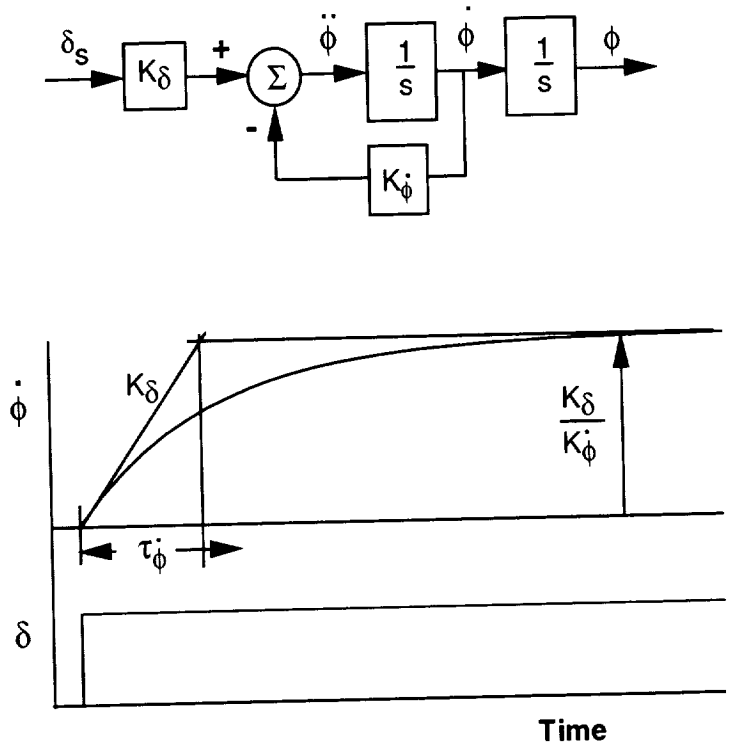

Figure 87. Roll-rate command system.

control sensitivity. The rise time to 63 percent of the steady-state roll-rate response defines the time constant, which in this case is the inverse of the feedback gain $K_{\dot{\phi}}$. Control sensitivity, which is the amount of roll acceleration versus the magnitude of the control input, is proportional to the control-input gain. The steady-state roll-rate response to the pilot's command is the ratio of the control input gain to the rate feedback gain. The choice of time constant is dictated by the roll-attitude bandwidth requirement in hover noted earlier in the text. An attitude bandwidth defined by a 45-degree phase margin would correspond to a 45-degree phase lag in the roll-rate response, which occurs at the frequency of the inverse time constant. Thus for an attitude bandwidth of 3 rad/sec, which would satisfy the Level 1 roll bandwidth requirement, the feedback gain $K_{\dot{\phi}}$ will be 3 sec^{-1}. Requirements for roll-control sensitivity suggest at least 0.3 rad/sec^2/in. If this value for sensitivity is chosen, the steady-state roll-rate response to the control input will be 0.1 rad/sec/in. or approximately 6 deg/sec/in.

The rate-command system for the Harrier follows the preceding diagram and provides a rate feedback that combines with the mechanical input from the control stick. This system includes a roll-rate gyro, whose output is multiplied by a gain factor in a simple computer, and then input to a servo actuator that moves a mechanical summing linkage along with inputs from the pilot's control stick. An example design for the Harrier is shown in figure 88. Note the open-loop aircraft characteristics, the unstable Dutch roll, the roll mode, and the numerator root near the origin. The resulting root locus shows a Dutch roll that is barely stable and that would only meet Level 2 criteria. The Harrier can be flown on instruments with this system, but it has Level 2 bordering on Level 3 flying qualities at low speed because of this poor level of stability. In the short term, the response appears as rate command; however, it is not sustained in the long term because of the low-frequency droop that appears in the Bode plot. This simple rate command provides some improvement over the basic aircraft, but it will be necessary to further augment the control characteristics to achieve significant improvement in hover flying qualities. In principle, the development of pitch-rate and yaw-rate command systems would be accomplished with the same concept, while employing the criteria appropriate for the individual axes.

Yaw Damper-Turn Coordinator

Yaw dampers and turn coordinators are intended to improve the Dutch roll damping and control of heading in forward flight. The Harrier has revealed the need for both, as indicated in previous examples of sideslip excitation during roll maneuvers. In a classic yaw damper, yaw rate is fed back to the directional control through a washout, where the latter is used to eliminate a rudder input during steady turns. The washout is selected so as not to interfere with damping of the Dutch roll mode. Bank-angle and lateral-acceleration feedback, along with roll and yaw rate can be used to synthesize a feedback of rate-of-change of sideslip. This is derived from the contributions to the lateral acceleration measurement, which are

$$a_y = \dot{v} + ru - pw - g\cos\Theta\sin\Phi$$

and since $\dot{v} \doteq V_0\dot{\beta}$ the lateral acceleration equation can be used to estimate sideslip rate. If the objective is to damp the Dutch roll to eliminate unwanted sideslip excitation, sideslip rate is a very effective contribution.

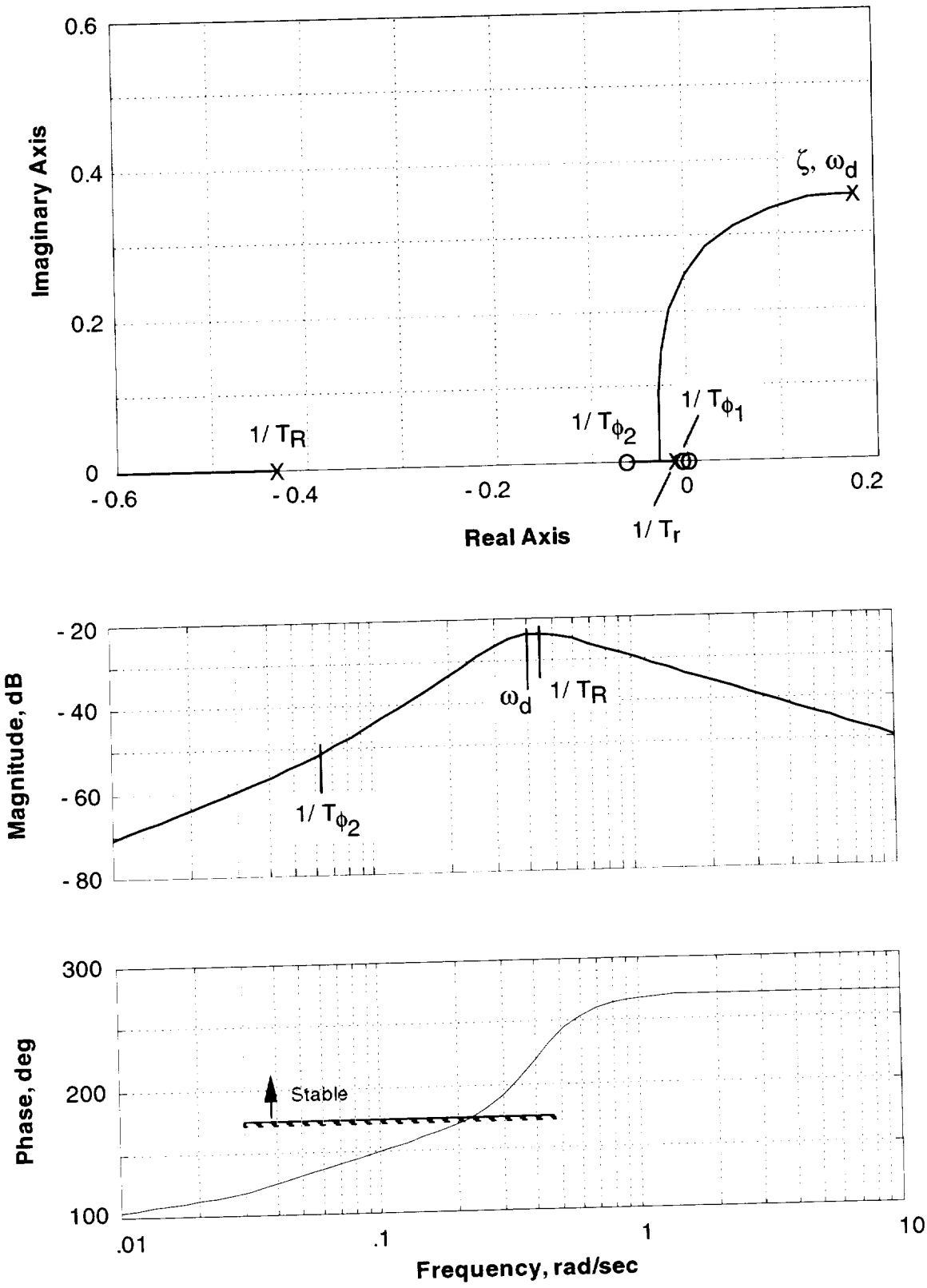

Figure 88. Root locus and Bode plots for a rate-command system for the Harrier in hover.

Considering a washed out feedback of yaw rate to the directional control, the root locus plot shown in figure 89 indicates some Dutch roll stability can be achieved. When yaw-rate feedback is increased, the Dutch roll is initially stabilized, but it eventually migrates to the non-minimum phase numerator root. The maximum Dutch roll damping corresponds to a damping ratio of 0.1. That level of damping provides a marginal improvement in Dutch roll excitation; its robustness is in question if the anticipated stability derivatives are in error.

Feedback of the synthesized sideslip rate noted above is an effective means of damping the Dutch roll as shown in the root locus of figure 90. Dutch roll damping is increased markedly,

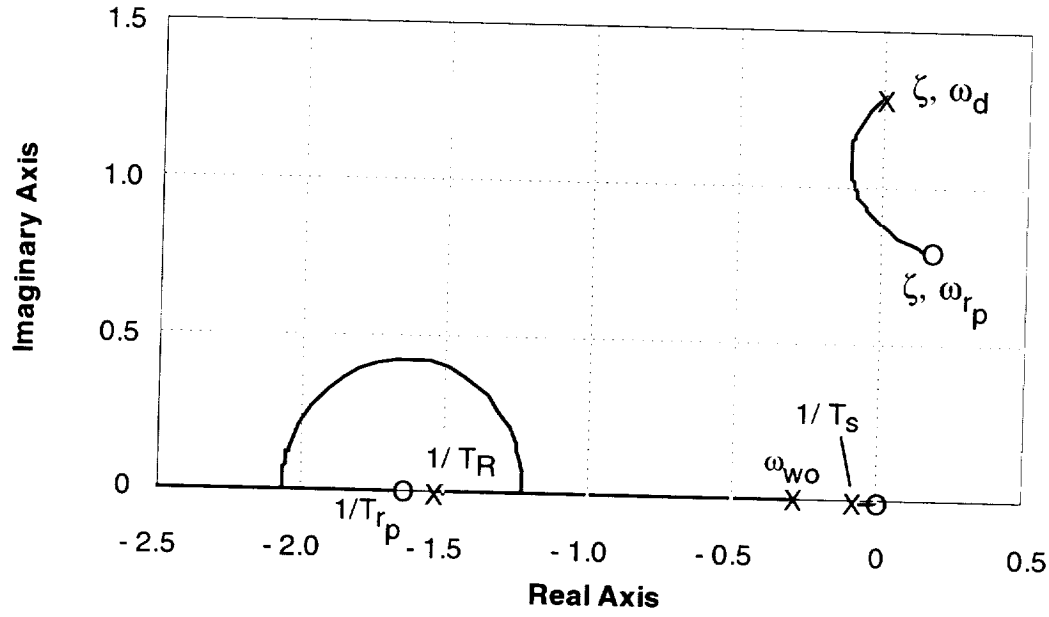

Figure 89. Root locus of washed out yaw rate to the directional control for the Harrier at 100 knots.

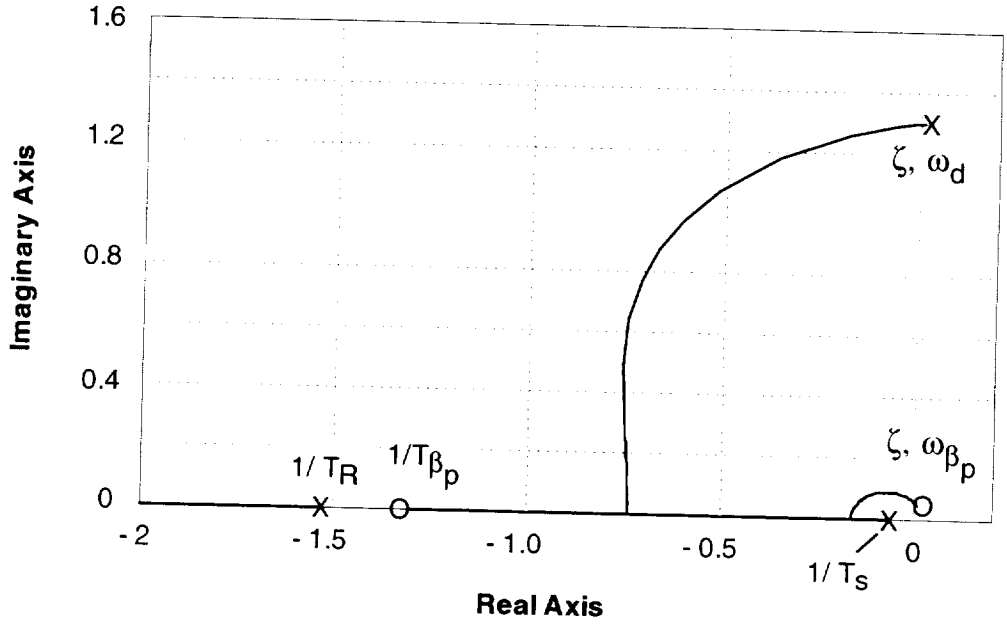

Figure 90. Root locus of sideslip rate to the directional control for the Harrier at 100 knots.

and modest increases in roll and spiral stability occur as well. In figure 91, the bank-angle and sideslip time histories show that Dutch roll excitation is absent and that sideslip response is negligible and would easily meet the yaw-axis flying qualities requirements.

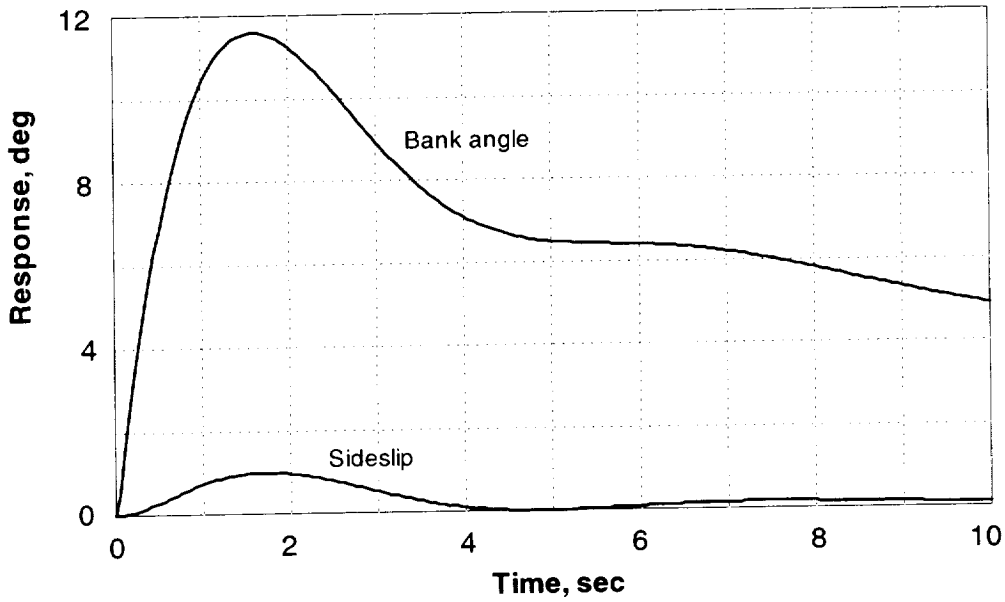

Figure 91. Time history of bank-angle and sideslip response to the lateral control for the Harrier with sideslip rate damping at 100 knots.

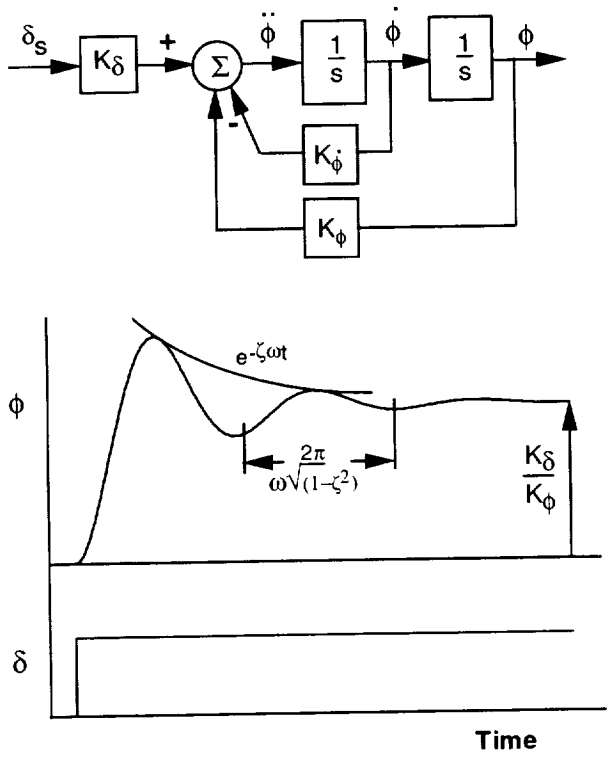

Figure 92. Attitude command system.

Attitude Command System

The next system in the control augmentation hierarchy is the attitude command system. The example to be considered is for bank-angle control; the same approach can be applied to pitch control. Note from the block diagram in figure 92 that the rate command structure is still present and that a feedback of roll attitude has been added. This input is derived from an attitude gyro or from the inertial measurement unit, then fed through a gain and summed with the rate feedback and the pilot's control input. The design criteria are complicated somewhat by the added feedback, which determines the natural frequency of the second-order system. This gain, in concert with the rate feedback, will establish the attitude-command bandwidth. Specifically, the gains are $K_{\dot{\phi}} = 2\zeta\omega$ and $K_{\phi} = \omega^2$ where the natural frequency for a damping ratio of 0.7 will be half the required bandwidth for a phase margin of 45 deg. The steady-state bank-angle response per unit lateral control is the ratio of the control sensitivity and the attitude feedback gain. As previously noted, a roll-control bandwidth of 2-4 rad/sec is appropriate. Note that for a pitch-attitude command system, integral compensation will likely be needed to prevent steady-state attitude biases in response to pitching moment disturbances.

Attitude command will make a marked improvement in hover flying qualities and will contribute improvements to the transition from cruise to hover. In the latter case, the deficiencies in flying qualities come in part from the pitch axis, a result of poor stability and damping and large trim changes with thrust and thrust deflection. Attitude stabilization provides the needed stability and suppresses pitch disturbances from the trim changes.

Application of attitude command to the Harrier is shown in the root locus and Bode plot in figure 93. Lead compensation from the rate and attitude feedback, along with the open-loop poles and zeros, are indicated. The numerator root ($1/T_L = K_{\phi}/K_{\dot{\phi}}$)is located to provide the desired phase margin of 45 deg at 3 rad/sec. The closed-loop gain is chosen for a 3-rad/sec bandwidth. The closed-loop characteristics appear in the Bode and time history plots in figure 94. The frequency response in the closed-loop Bode plot of bank angle to bank-angle command shows the desired phase margin at 3 rad/sec. The time history for an attitude command is well damped with minimum overshoot and maintains the desired attitude in the steady state. Attitude command systems work well in holding the commanded attitude; however, if the pilot is forced to continually change attitude to control the aircraft's hover position, then attitude command alone may not be sufficient for good flying qualities.

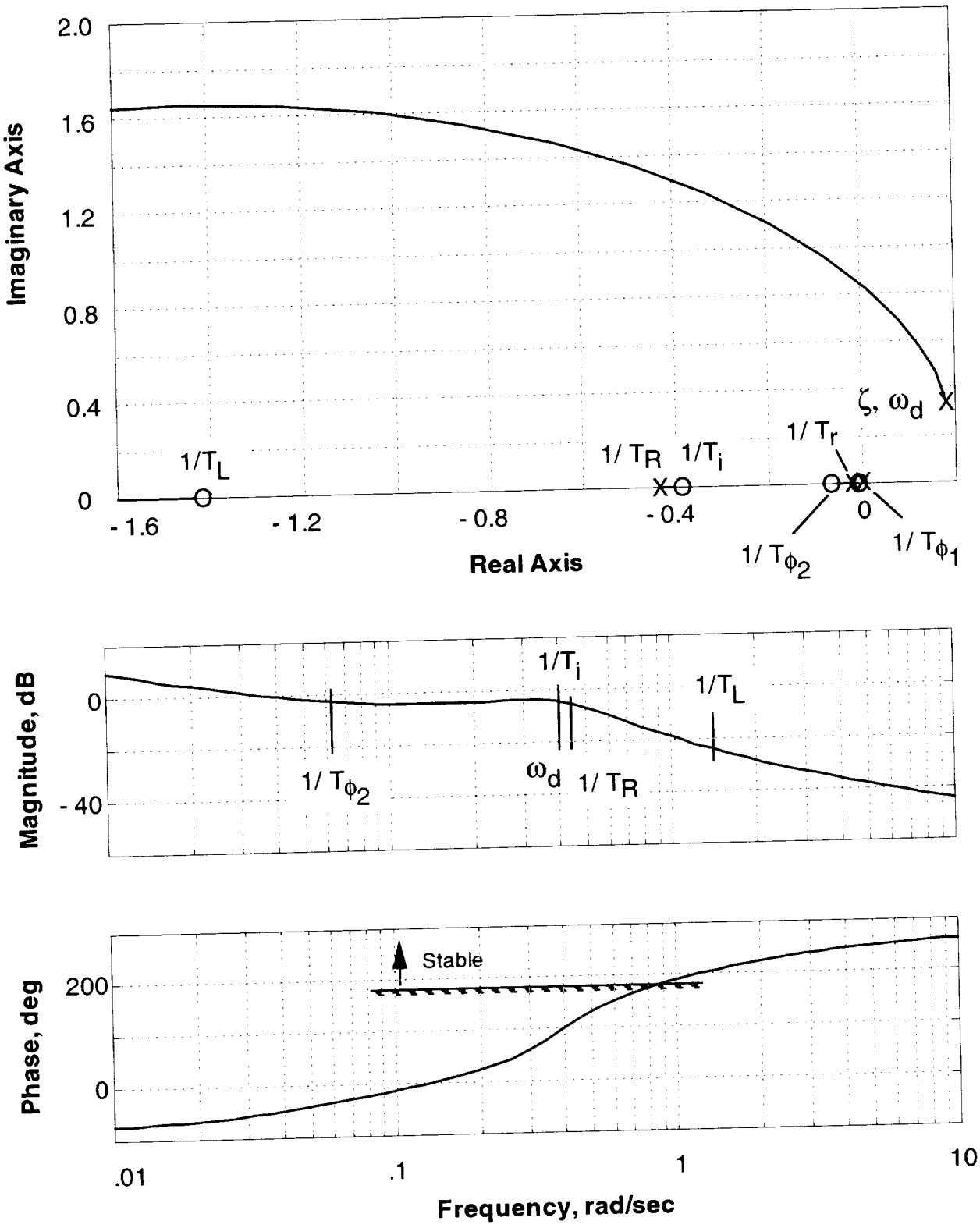

Figure 93. Root locus and Bode plots for attitude command system design for the Harrier in hover.

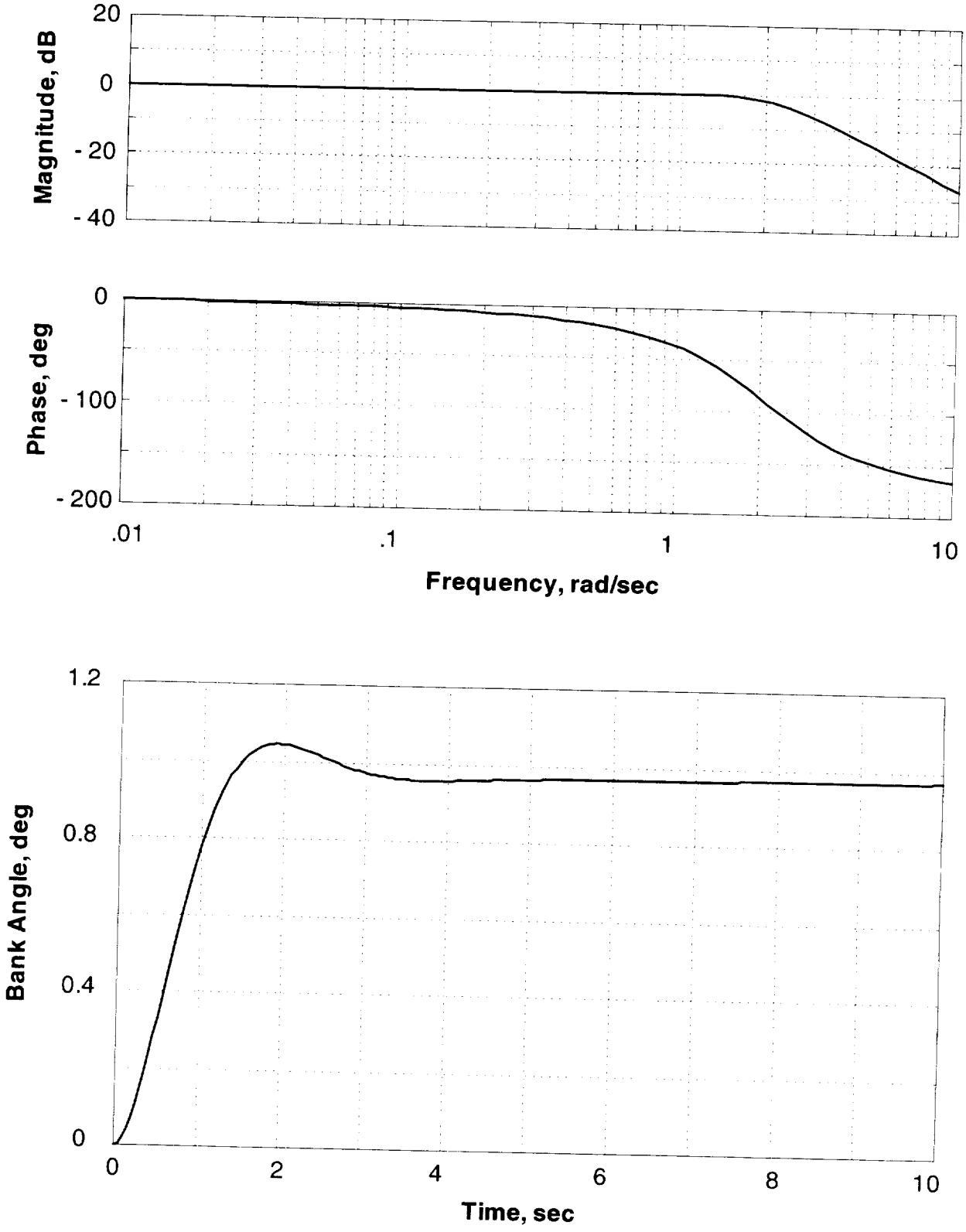

Figure 94. Closed-loop Bode and time history plots for attitude command system for the Harrier in hover.

Vertical Velocity Command System

The first of the velocity command systems to consider is that for vertical-velocity control. Based on previous discussions it was noted that vertical-velocity response to the throttle or the thrust control was typically very sluggish in hover. The transfer function exhibited poor damping, with the response appearing more as a vertical acceleration than a steady vertical velocity. The time response was defined by a time constant that was the inverse of the height rate damping Z_w. The response can also be aggravated by lags in thrust response, and the combination of these two characteristics leads to a poor response for hover height control. The simplest approach for overcoming these deficiencies involves sensing vertical velocity and feeding it back through a servo to sum with the pilot's throttle input to form the thrust command to the propulsion system. A block diagram of this type of system is shown in figure 95. The aircraft is represented by a first-order transfer function for vertical velocity response to thrust, and the propulsion system is represented by a first-order lag in engine thrust. Note that the system concept is comparable to that for the rate-command system discussed previously.

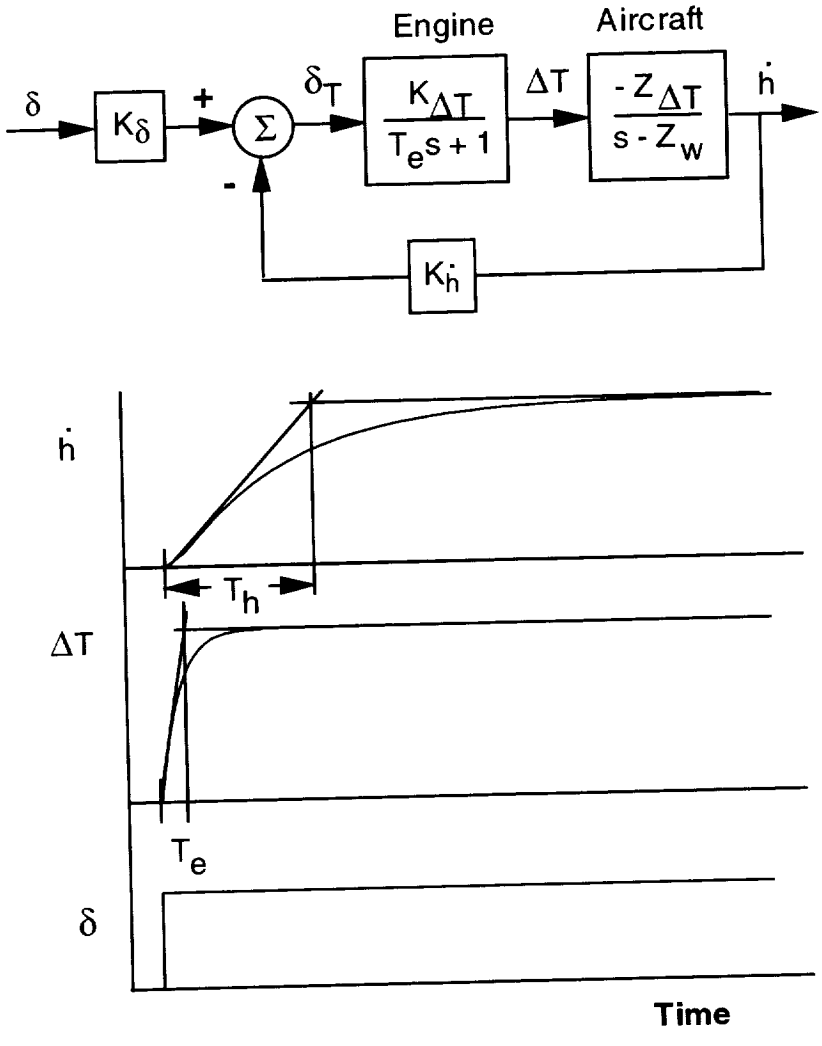

Figure 95. Vertical-velocity command system.

Design characteristics for the vertical-velocity command system are illustrated in the figure. They are the pilot's control sensitivity, the vertical-velocity feedback gain, the engine response time constant, and the aircraft's vertical velocity damping. The time history example at the bottom of the figure shows the contribution of each of these factors. The thrust response shows the effect of the first-order engine lag, and the vertical velocity response shows the initial delay associated with the thrust transient, followed by the first-order lag associated with the aircraft's heave damping as augmented by the vertical velocity feedback. Design criteria for these systems show that the engine response time constant should not be greater than 0.3 sec for Level 1 and no more than 0.6 sec for Level 2. According to reference 25, the overall response of engine and aircraft for Level 1 should produce an altitude control bandwidth of 0.6 rad/sec, based on 45 deg phase margin for the altitude control loop. This should occur without excessive equivalent time delay, hence the importance of the engine's response. A sluggish thrust change would produce a sluggish change in normal acceleration and would give the pilot the impression of time delay in the response. Reference 26 suggests that equivalent time delays not exceed 0.3 sec. The pilot derives useful and informative feedback from the initial response of the aircraft associated with the initial change in thrust. This information comes to the pilot through two paths. Normal acceleration due to the thrust change is a proprioceptive cue felt in the seat of the pants. Further, the pilot senses the change in engine sound level that is associated with thrust change. Appreciable delays in either cue following a throttle input will be perceived by the pilot as a delay in the control loop.

In the vertical-velocity command system design, two variables are available to establish the control sensitivity and bandwidth. The control input gain, K_δ, should be picked for a control sensitivity from 0.1 to 0.2 g/in. of throttle movement. This sensitivity refers to the initial slope of the vertical-velocity response per unit throttle input. The vertical-velocity feedback $K_{\dot{h}}$ is used to meet the bandwidth criteria, and will be sufficient to do so unless the engine response does not meet the criteria stated above. If the engine is not designed to meet reasonable time response requirements, typically the internal design of the engine or the fuel control must be altered to quicken the transient thrust response. Vertical velocity response will typically be second-order (two real roots) with

$$\frac{1}{T_h}+\frac{1}{T'_e}=\frac{1}{T_e}-Z_w \text{ and } \frac{1}{T_h T'_e}=-\frac{Z_w+K_{\dot{h}}Z_{\Delta T}K_{\Delta T}}{T_e}$$

The choice of $K_{\dot{h}}$ should be made so that the lowest frequency of the two roots ($1/T_h$) is at least 0.6 rad/sec. The steady-state vertical velocity per unit throttle input will be approximately the ratio $K_\delta/K_{\dot{h}}$.

Longitudinal Velocity Command System

Longitudinal-velocity command can be achieved either through control of pitch attitude or thrust vector deflection. Examples of both appear in the block diagrams in figure 96. When the control is accomplished using pitch attitude, as shown at the top of the figure, the inner loop represents the attitude-command system described above. The feedback for longitudinal velocity is closed around that attitude-command system, multiplied by a gain, and combined with the pilot's input and the other feedbacks of pitch rate and attitude as inputs to the pitch-control servo. The alternative approach to longitudinal velocity command deflects the thrust vector directly to produce the longitudinal force component while maintaining constant pitch attitude. In this case, the inertial velocity feedback is combined with the pilot's control input and fed to the servo actuator for thrust deflection, as seen in the middle diagram in the figure.

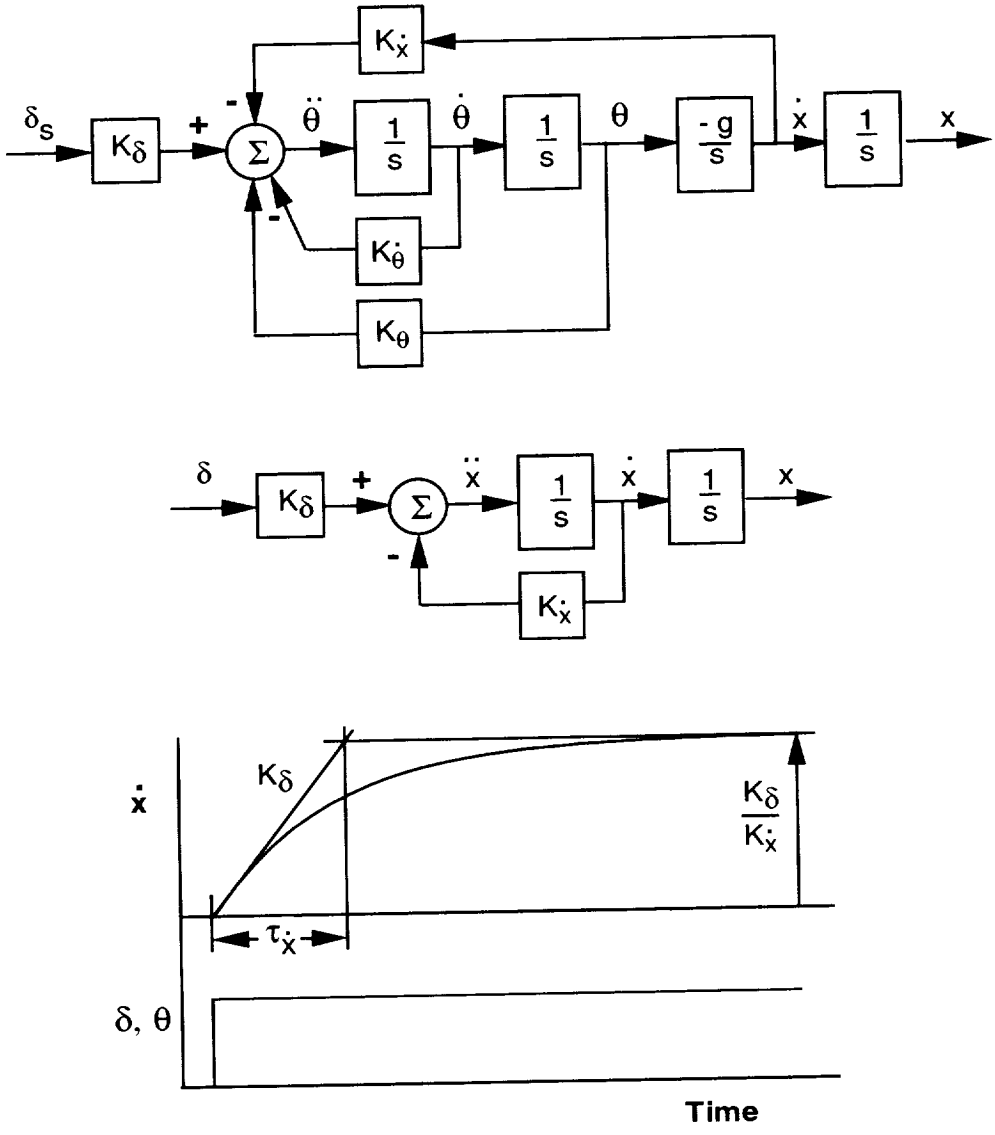

Figure 96. Longitudinal-velocity command.

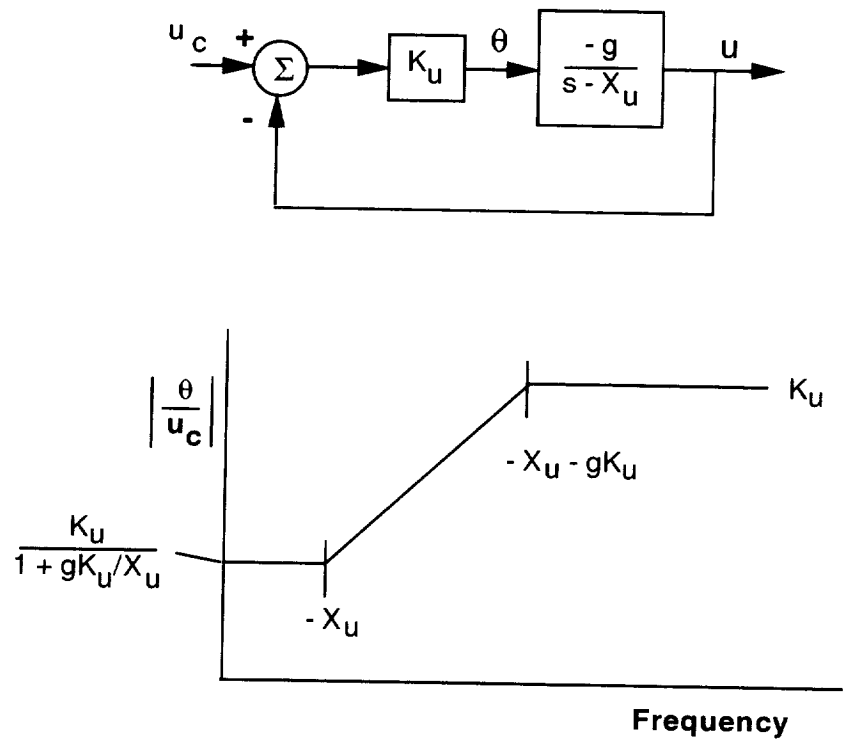

Figure 97. Simplified longitudinal-velocity control with pitch attitude.

To develop design criteria for the system using attitude control, it is useful to simplify the equations of motion to relate translational velocity response to pitch attitude, as previously noted for control of longitudinal velocity in hover. The block diagram in figure 97 shows the simplified system in which the transfer function between longitudinal velocity and commanded pitch attitude is represented by a first-order lag. Then the closed-loop longitudinal velocity response is given by

$$\frac{u}{u_c} = \frac{-gK_u}{s - X_u - gK_u}$$

The response is characterized by a first-order transfer function with bandwidth defined by $\omega_{BW} = -(X_u + gK_u)$, which is the bandwidth at 45-degree phase margin for longitudinal position control. Representative criteria for this control, given in references 25 and 26, indicate the desired bandwidth to be 0.3 rad/sec.

A design concern for the system using pitch-attitude control is the amount of attitude change required to achieve the proper dynamics for velocity command. If there is reasonable consonance between the amount of attitude change and the change in translational velocity, the system will be acceptable to the pilot. If the attitude changes are large and abrupt, the pilot may find them objectionable. Attitude response to the velocity command is described by

$$\frac{\theta}{u_c} = \frac{K_u(s - X_u)}{s - X_u - gK_u}$$

The attitude-response transfer function includes a term in the numerator that will be of considerably lower frequency than that for the denominator root. The Bode sketch at the bottom of the figure shows the significance of the numerator and denominator root locations. The elevated response at high frequency is indicative of overshoot in the short-term attitude response. This high-frequency response is used to quicken the longitudinal velocity response relative to that associated with the basic aircraft. The ratio of the peak attitude change to the steady state can be approximated by the ratio of the high-frequency to the low-frequency Bode gains, giving

$$\theta_{max}/\theta_{ss} \doteq 1 + g\, K_u/X_u$$

Thus, as the velocity feedback is raised to increase the bandwidth for velocity control, the overshoot in pitch attitude increases correspondingly. Combining this equation with that for bandwidth shows the contribution of overshoot:

$$\omega_{BW} \doteq -X_u\, (\theta_{max}/\theta_{ss})$$

In order to move the aircraft quickly, more longitudinal acceleration is required, and that in turn is produced by larger changes in aircraft attitude. A design trade-off must be made between the control bandwidth needed by the pilot to perform the hover positioning task and the pilot's acceptance of large, abrupt attitude excursions.

The velocity-command system using thrust-vector deflection is a straightforward arrangement. The relation of bandwidth to velocity feedback is the same as for the attitude control ($\omega_{BW} = -X_u - gK_u$). The transient response shown previously in figure 96 is characterized by the time constant and control sensitivity. The performance of this system is determined by the ability to deflect thrust rapidly enough to achieve the necessary control bandwidth. Although thrust deflection is necessary to perform the transition from conventional flight to hover, that rate of deflection may not be sufficient for a velocity command system in hover.

Lateral Velocity Command System

Lateral-velocity control is achieved using bank angle to translate the aircraft and follows the same concept discussed for longitudinal-velocity control with pitch attitude. An example for lateral-velocity command appears in figure 98 with the lateral-velocity feedback closed around the existing attitude-command system. Proportional plus integral compensation is included in the forward loop. The system can also be described by the equations of motion, including the control-system equation and the appropriate feedbacks:

$$\begin{bmatrix} s - Y_v & 0 & -g & 0 \\ -L'_v & -L'_r & s^2 - L'_p s & -L'_\delta \\ -N'_v & s - N'_r & -N'_p s & -N'_\delta \\ K_v(Ks + K_i) & 0 & (Ks + K_i)(K_{\dot{\phi}} s + K_\phi) & s \end{bmatrix} \begin{Bmatrix} v \\ r \\ \phi \\ \delta \end{Bmatrix} = \begin{Bmatrix} 0 \\ 0 \\ 0 \\ K_v(Ks + K_i) \end{Bmatrix} V_c$$

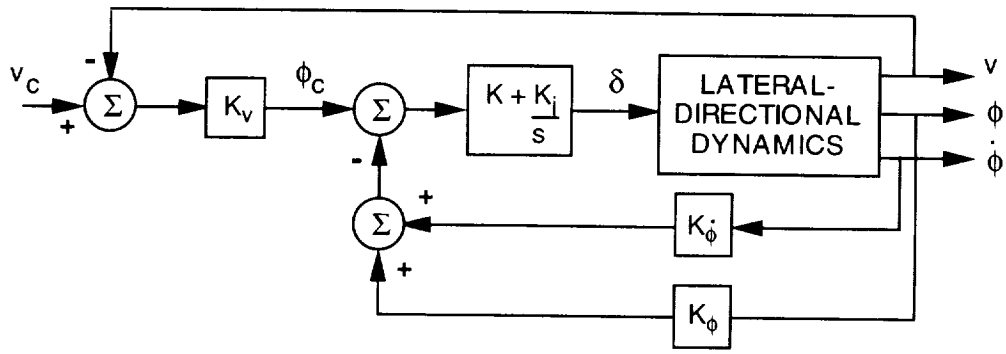

Figure 98. Lateral-velocity command.

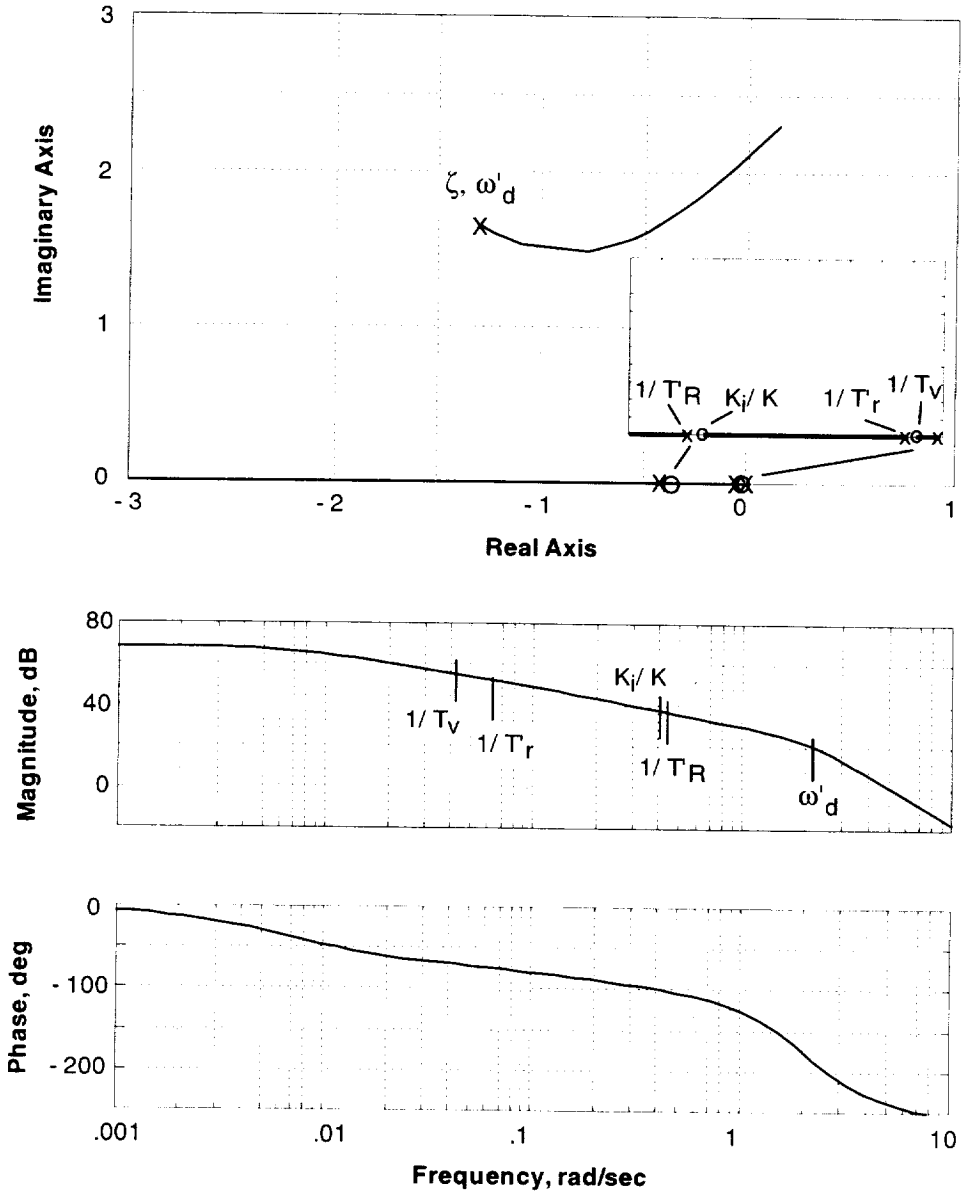

Figure 99. Root locus and Bode plots of lateral velocity command for the Harrier in hover.

The proportional and integral gains were chosen, in combination with the roll-rate and bank-angle gains, to provide an attitude bandwidth of approximately 3 rad/sec. For lateral-velocity command systems, criteria of references 25 and 26 suggest that the bandwidth be 0.37 rad/sec for lateral position response to the pilot's control. Figure 99 shows the root locus and Bode plots for lateral velocity. The closed-loop roots are associated with the bank-angle loop closure and include the modified Dutch roll and roll modes. At high enough gain, the Dutch roll will be destabilized; however, the velocity-control bandwidth is satisfied at much lower gains. The Bode plot at the bottom shows sufficient phase margin at frequencies well in excess of the design bandwidth. No additional compensation is required in the velocity feedback loop.

The Bode plot of the closed-loop system in figure 100 shows characteristics associated with bandwidths for the system ranging from 0.1 to 0.4 rad/sec. Velocity response magnitudes are flat and a phase lag of 45 deg is present at the design bandwidth. This velocity-response phase lag corresponds to a 45 deg phase margin for lateral position control. Time histories in figure 101 show the lateral-velocity and bank-angle excursions in response to a step-command input for the 0.1 and 0.4 rad/sec systems. The differences in the initial velocity response are dramatic, as are the attitude changes that produce the velocity response. The 0.1-rad/sec case would be too sluggish for the pilot, and the 0.4-rad/sec case would probably be somewhat quicker than the pilot would require. The effect of the higher bandwidth on the peak change in bank angle, compared to that required in the steady state to maintain that steady lateral velocity, is dramatic. Note that the lateral velocity is achieved with only 0.4 deg of bank angle in the steady state, since the Harrier has very low lateral-velocity damping and requires little lateral force to maintain a steady lateral velocity in hover. For the higher bandwidth example, the magnitude of short-term bank angle compared to the steady state is substantial. If the peak response approached 10 deg, the pilot would complain about the magnitude and the consonance of this initial attitude change. By contrast, much less change in attitude is required for the lower bandwidth case.

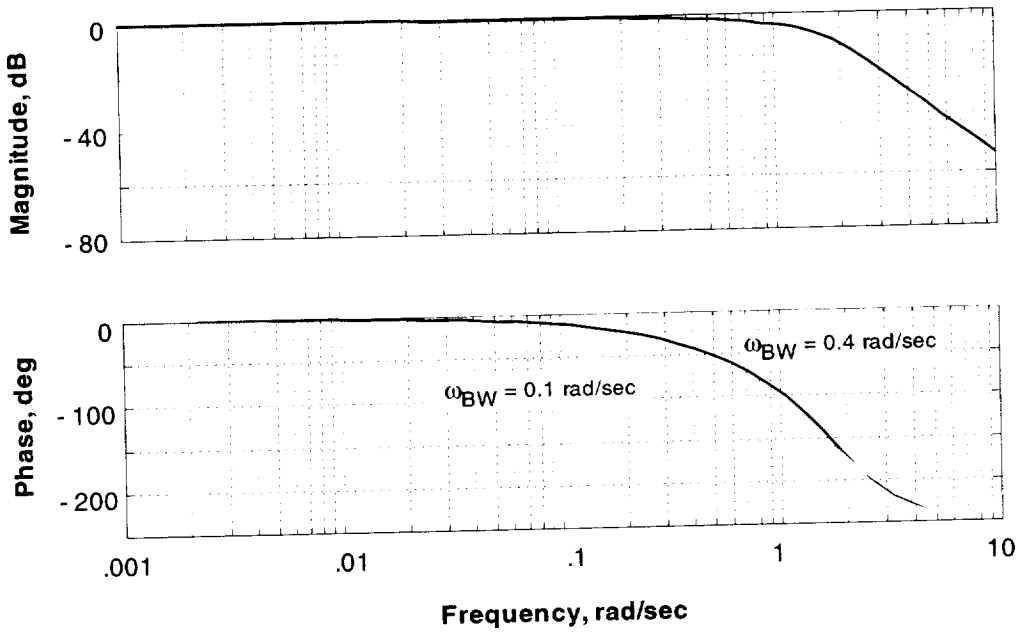

Figure 100. Bode plot of closed-loop lateral velocity command for the Harrier in hover.

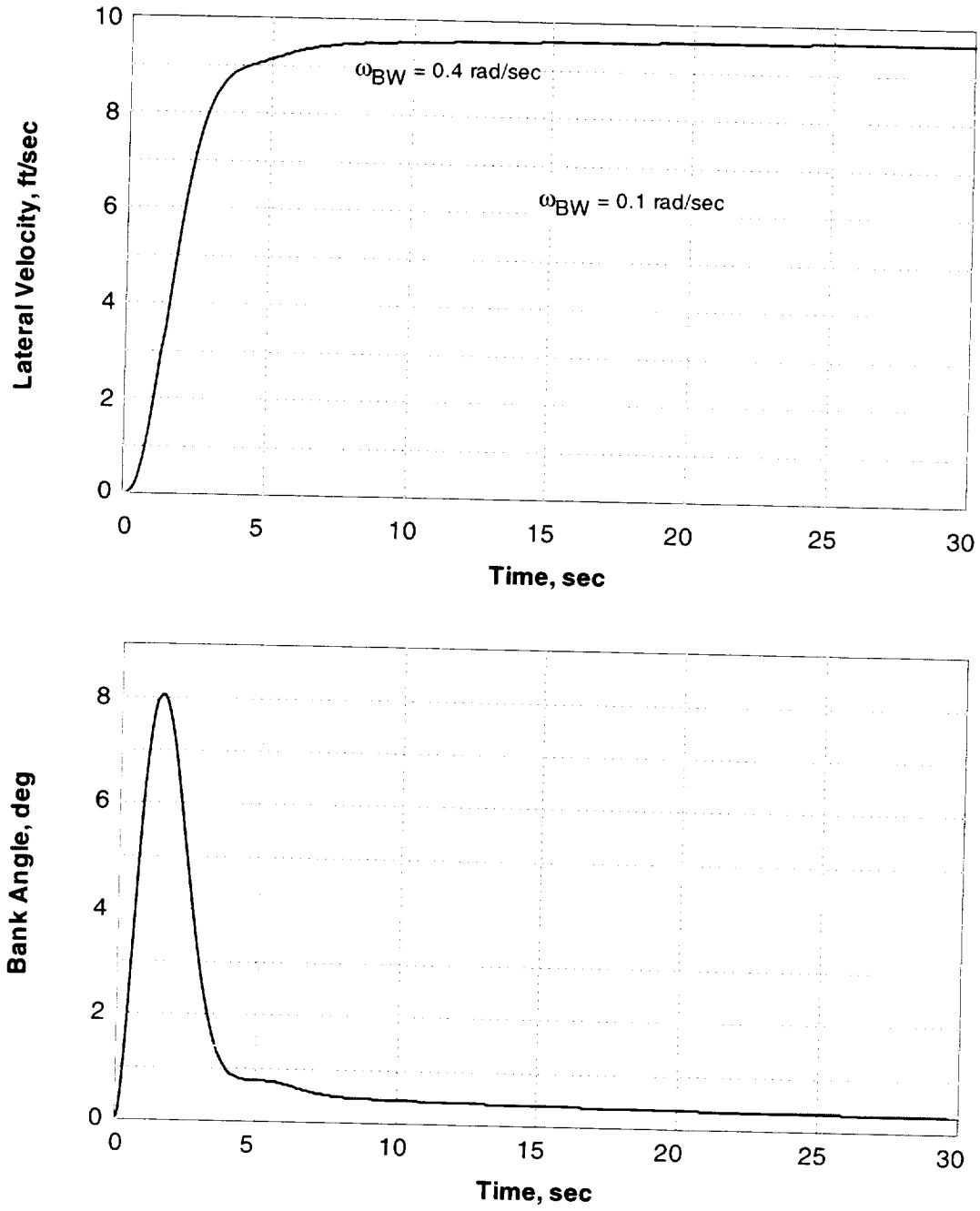

Figure 101. Time histories of lateral-velocity command for the Harrier in hover.

Commands to the Control Effectors

The design of the control system to implement the variety of control laws covered in the previous discussion would be relatively simple if a single control effector (aerodynamic surface or propulsion system thrust-producing component) generated the force or moment on the aircraft necessary to achieve the desired response and if the aircraft characteristics were linear. In general, that is not the situation for a V/STOL aircraft configuration, especially during transition from wing-borne to jet-borne flight. In that flight regime it is necessary to use both the aerodynamic surfaces and propulsion system components to obtain the control authority required. In addition to the associated control redundancy, it is necessary to account for strong nonlinearities in the aerodynamic and propulsion system characteristics to achieve the desired response. To this point, the discussion of rate, attitude, and velocity-command systems has concentrated on the generation of the various response types, that is the sensed input and feedback variables and the selection of gains for the command inputs and feedbacks needed to meet design criteria. The next step in the design involves connecting the response types to the control effectors to achieve the desired response.

To deal with these complicated characteristics, nonlinear inverse and control-effector blender design methods have been employed for a variety of V/STOL designs. An example of this design approach applied to a vertical- and longitudinal-velocity command system for transition and hover is shown conceptually in figure 102. At the left of the figure, commanded accelerations result from the response-type command, sensor feedbacks, and regulator. The nonlinear inverse block represents a nonlinear model of the aircraft whose outputs are the accelerations produced on the aircraft. This model, constructed from analytical predictions and experimentally derived estimates of the aircraft's aerodynamic and propulsion characteristics, yields the current accelerations based on the aircraft's current states (e.g., angles of attack and sideslip, dynamic pressure, angular rates). The difference between the commanded accelerations and the accelerations fed back from the nonlinear inverse represent the commands to the control effectors. The control selector acts on these acceleration commands and turns them into effector outputs. For a simple example, this could correspond to a command for engine thrust to yield a specific vertical acceleration.

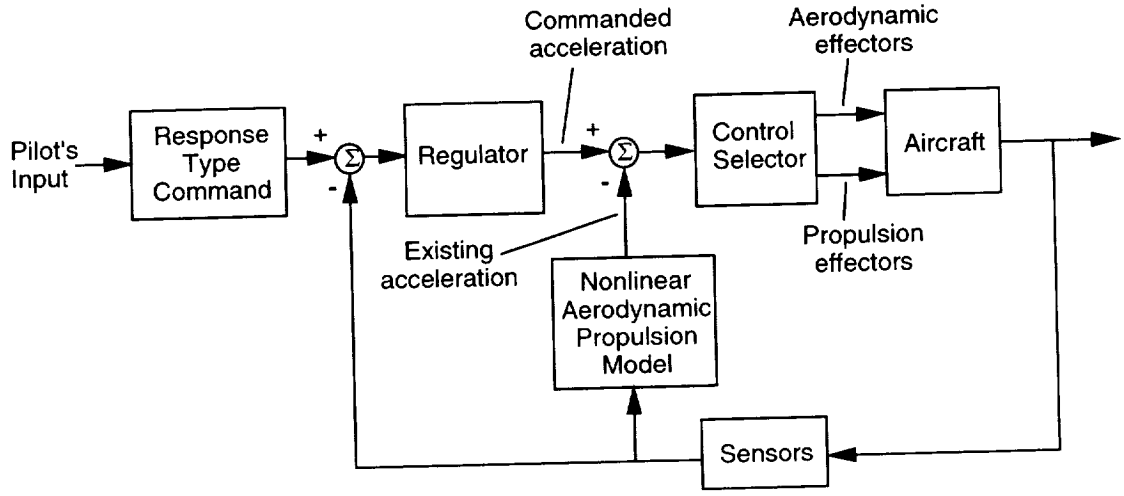

Figure 102. Nonlinear inverse control concept.

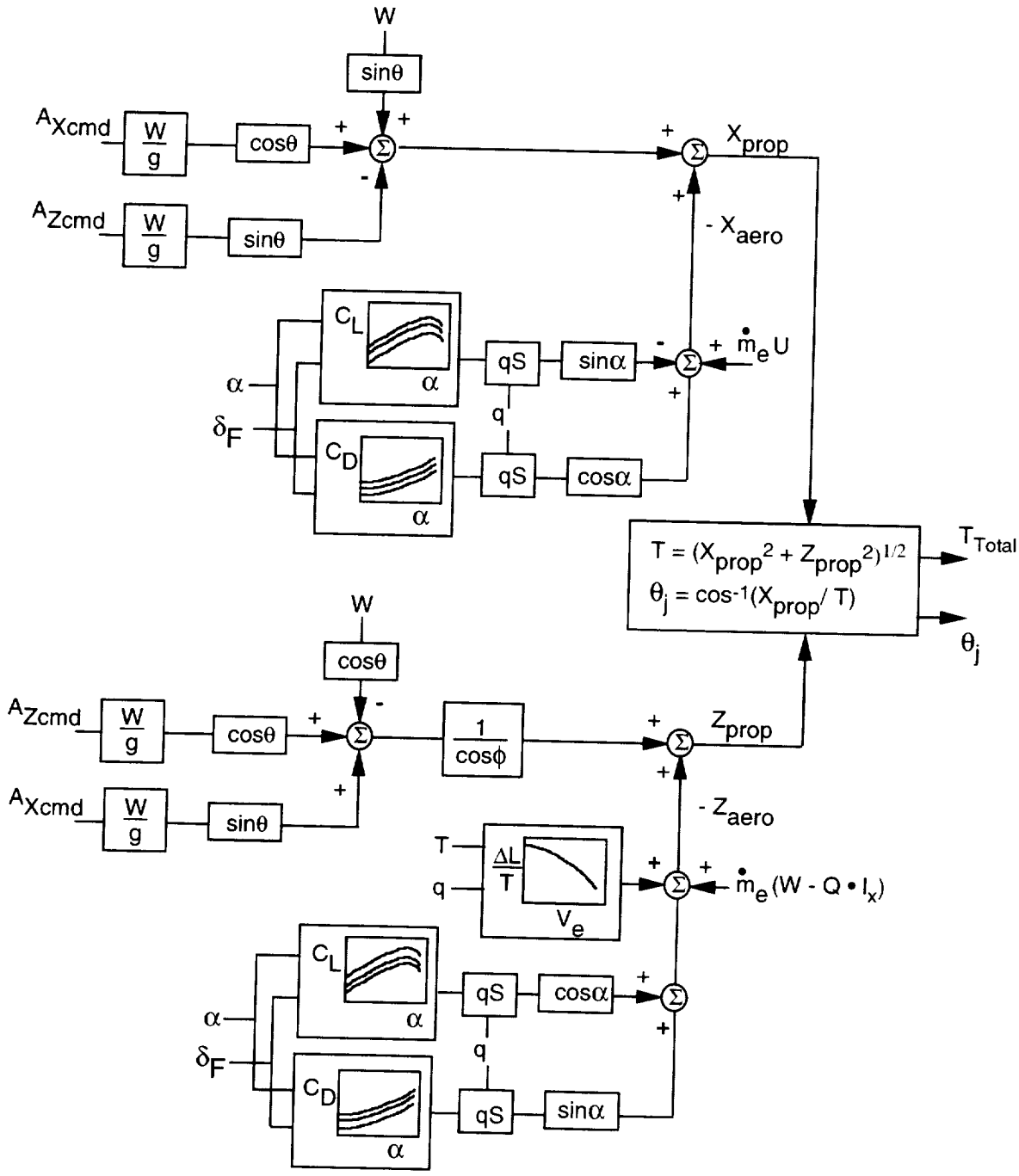

Figure 103. Nonlinear inverse control laws for longitudinal and vertical velocity command.

A block diagram illustration of velocity-command control laws in the longitudinal and vertical axes for a Harrier-type aircraft is shown in figure 103. The commands for the control selector are derived from the longitudinal and vertical force equations in body axes,

$$m\,AX_{cmd} = X_{aero} + X_{prop} - W\sin\theta_{cmd}$$

$$m\,AZ_{cmd} = (Z_{aero} + Z_{prop})\cos\phi + W\cos\theta_{cmd}$$

where the AX_{cmd} and AZ_{cmd} command inputs come from the longitudinal and vertical-velocity command control laws, and where the weight component is resolved into body axes through the commanded pitch attitude. If the aircraft characteristics were linear functions of the aircraft states, the inverse block could be simply described by the matrix of linear stability derivatives multiplied by their respective states (i.e., [A]{x}). When the aerodynamic terms are not so simply represented, the nonlinear inverse is composed of the complete nonlinear expressions,

$$X_{aero} = [-C_D(\alpha_c, \delta_f)\cos\alpha_c + C_L(\alpha_c, \delta_f)\sin\alpha_c]qS - \dot{m}_e U$$

$$Z_{aero} = [-C_L(\alpha_c, \delta_f)\cos\alpha_c - C_D(\alpha_c, \delta_f)\sin\alpha_c]qS - \frac{\Delta L}{T}(V_e, h/d) - \dot{m}_e\,(W - Q \bullet l_x)$$

where the lift and drag coefficients are functions of angle of attack and flap position and are resolved into body axes. They typically are obtained from tabular data derived from wind tunnel tests. The jet-induced lift is a nonlinear function of equivalent jet velocity and nondimensional height above ground and is based on powered-model tests. With the individual terms defined, these equations may be solved for the propulsion system force commands to the control selector, X_{prop} and Z_{prop}.

If the effector characteristics were linear, the control selector block in the figure could simply be the inverse of the linear control effectiveness matrix ($[B]^{-1}$). For a vectored-thrust aircraft such as the Harrier, the thrust magnitude and deflection are related to the longitudinal and vertical propulsion components by nonlinear equations that define the vector sum and orientation:

$$T_{total} = \sqrt{(X_{prop})^2 + (Z_{prop})^2}$$

$$\theta_j = \cos^{-1}(X_{prop}/\sqrt{(X_{prop})^2 + (Z_{prop})^2})$$

The conceptual approach to nonlinear inverse control shown in figure 102 can be applied as well to the pitch, roll, and yaw axes. In these cases, the inverse block models the nonlinear pitch, roll, and yaw accelerations produced by the aircraft, based on wind tunnel data and analytical predictions. The control selector is composed of demanded accelerations mapped into control effector positions, again largely based on wind tunnel data. For a more detailed discussion of the nonlinear inverse control method applied to V/STOL aircraft, the reader should consult reference 35.

Guidance and Control Displays

This study of V/STOL aircraft control and flying qualities has concentrated so far on the pilot's interactions with the basic aircraft and with control augmentation systems that are intended to modify the response of the aircraft in order to improve its flying qualities. This control process is based on the assumption that the pilot perceives the intended and actual response of the aircraft in carrying out its mission. The pilot uses that information to generate commands to the control system to make the aircraft respond as desired. An important aspect of this control process is the means by which the pilot perceives the intended and actual response. These perceptions and interpretations of the commands and response errors must be considered of equal importance to

the aircraft and control system as elements of the control loop. This information can be derived from the external visual scene observed through the wind screen, from instruments on the control panel, from sensing aircraft motion, from audio sensing of engine performance and airspeed, and from feeling the forces and motions of the aircraft's cockpit control inceptors. Visual cues are powerful influences on aircraft control and are used for inner- and outer-loop control. Orientation of the visual horizon gives the pilot a very sensitive measure of aircraft attitude. During flight close to the ground, speed and position relative to objects on the surface are readily extracted from the external view. Accelerations are perceived through the semicircular canals in the inner ear and through pressures and forces on limbs and extremities. This process of observation is a dynamic element in the control loop that contributes, along with the other system elements, to the overall performance of the closed-loop system. It is equally deserving of attention in the consideration of an aircraft's flying qualities.

One of the most difficult tasks for the pilot to perform is instrument flight, particularly during an approach to landing. It is necessary to consider the appropriate information content and presentation that will make tasks such as these easy for the pilot to accomplish. They are an important part of the control loop, and if they are designed or used improperly, the good features of the basic aircraft or control augmentation may be rendered useless to the pilot.

In principle, there should be a trade-off between the capability of the control system and control and guidance displays to influence closed-loop system dynamics. A hypothetical relationship between the two was proposed in reference 36 and is shown graphically in figure 104. Assuming that the aircraft's characteristics are fixed, the figure indicates that providing increasingly sophisticated capability in the display or in the control system can provide improvement in flying qualities by reducing the pilot's need for compensation in the control loop. In particular, there are iso-opinion lines that cut across the plot that represent a constant level of flying qualities and show the trade-off of contributions by the control system and display. The range of control sophistication is represented by control augmentation schemes that have been covered earlier in the text; it encompasses rate dampers, attitude-command systems, velocity-command systems, and, ultimately, fully automatic modes coupling the guidance to the control

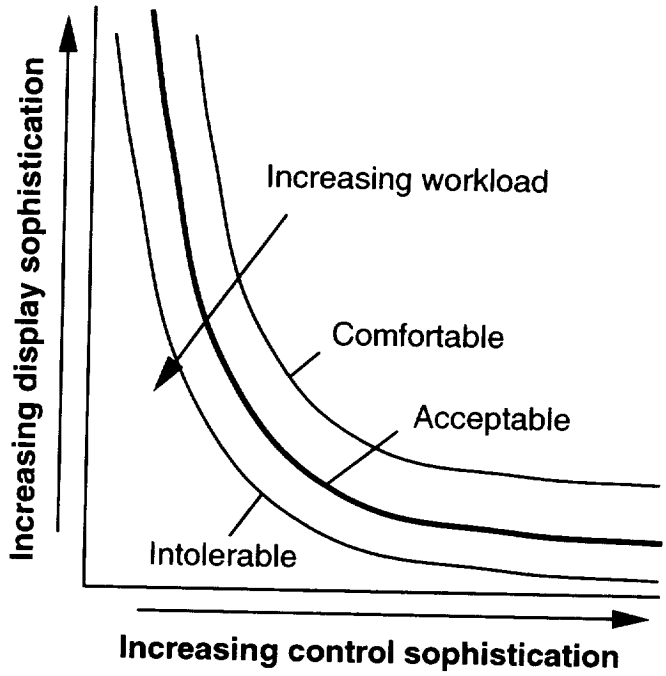

Figure 104. Trade-off between display and control sophistication.

system as in an autopilot. Correspondingly, display sophistication encompasses unprocessed situation information of the aircraft's state ("raw data") shown on a variety of instruments, flight directors that will process some of this information and provide the pilot control commands, and fully integrated situation and command information, perhaps shown on a single display. Applying this to an example aircraft suggests options either of providing the pilot with good flying qualities through augmented controls with minimal displays or presenting a display that allows the pilot to overcome difficult flying qualities for a minimally augmented aircraft. Experience gained over the years has shown that some reasonable level of sophistication of both controls and displays is necessary to achieve acceptable flying qualities in operational use. Without sufficient and easily assimilated information on the aircraft's response, even a well-stabilized aircraft will be difficult to fly in a demanding task. Similarly, displays that provide commands for stabilization of an otherwise poor flying aircraft still require considerable control effort by the pilot. Further, they require the pilot to continually pay attention to the display in order to perform the stabilization task. If the pilot's attention is diverted, for example, to consult a map, tune or communicate on the radio, or to perform a mission task unrelated to flying the aircraft, control may be lost due to lack of attention. This situation is particularly acute when the basic aircraft is unstable. If the control system stabilizes the aircraft, however, the pilot will be free to attend to these diversionary tasks while still extracting useful information from the displays. An appropriate design guideline would seem to be to correct any control deficiencies with control augmentation and to display command and situation information that can be readily assimilated by the pilot in performing the intended task while keeping the pilot continually aware of the aircraft's state.

Control and Guidance Display Concepts

A review of examples of cockpit displays provides a useful perspective from which to elaborate from the designer's view. A picture of a classic approach to cockpit layout is shown in figure 105. This instrument panel includes electromechanical or fully mechanical displays placed in an arrangement that is known as a basic aircraft T. It presents aircraft attitude through the attitude director indicator at the intersection of the T. Heading is presented by the horizontal situation indicator, which is like a compass card presented in the vertical plane, located at the bottom of the T. These instruments in the central part of the display are most frequently scanned by the pilot because they provide the information used for inner-loop control. Completing the top of the T are airspeed on the left and altitude on the right. Added to those are vertical speed or rate of climb and a radar altimeter on the right. Then instruments are included that give the pilot the ability to follow a vertical path and a ground track. Cross-pointers on the horizontal situation indicator indicate whether the aircraft is above or below glideslope or right or left of course. To fly the aircraft precisely using these instruments, the pilot must pay continued attention to the attitude indicator. Vertical speed information is used to track the glideslope, although the mechanics of the instrument introduce significant lags in the control loop. Heading is used to correct to and maintain a steady ground track. This display arrangement persists today in modern aircraft cockpits that now make use of computer-drawn formats on a cathode ray tube or flat panel displays.

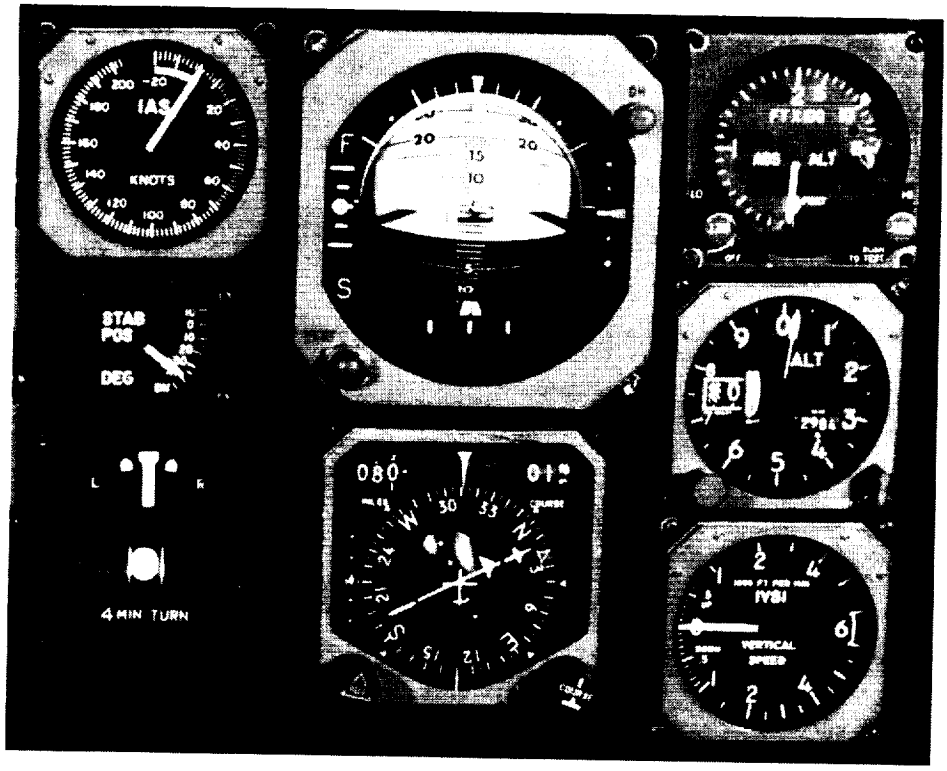

Figure 105. Primary flight instruments.

To fly a precise task under IMC, the pilot must visually scan these instruments and assimilate the necessary information. In performing this task, the pilot determines the aircraft's displacement from the desired flightpath via the pointer displacement from center and applies control inputs that not only compensate for this error but also provide lead compensation to improve the dynamics of the loop closure. The pilot must perceive attitude and close that loop; perceive vertical rate and close that loop; perceive displacement from the path as presented on the cross pointers and null that error. Thus, the pilot is extracting and mentally processing information from all of these displays to fly the aircraft precisely. This task is very demanding of the pilot and, even if the aircraft's control characteristics are Level 1 in visual flight, the workload associated with assimilating that displayed information and judging how to manipulate the controls to make the aircraft follow the commanded path would lead to Level 2 flying qualities. Older jet transports that use this instrument arrangement, although easy to fly in clear air, have Level 2 flying qualities in IMC, especially in the presence of turbulence. With modern generation displays, the situation is not improved unless the information content in the display includes more sophisticated command information for the instrument flight task.

Flight Director Display

The next step in level of sophistication is a flight director for precision path control, shown in schematic form in figure 106. The flight director concept is shown in the diagram at the bottom of the figure, in comparison to the cross-pointer error display at the top of the figure, as referred to in the previous paragraph. By contrast, the flight director combines the aircraft states in a command that requires the pilot to null the error shown by the director needles. It is necessary for the display designer to tailor the flight director to the characteristics of the aircraft so that the dynamics of the closed-loop system meet the control criteria demanded by the precision instrument task. It should be noted that the pilot cannot afford to concentrate solely on nulling the director needles to accomplish the task. It is also essential that the pilot be aware of the basic aircraft states, particularly altitude, airspeed, course along the ground, and the actual errors from the desired flightpath so as to be certain that the flight director is issuing proper commands. All of the information that drives the two director needles is an assimilation of information that is presented on the other displays, and the pilot must be certain that the two forms of information are consistent and that the flight director is performing properly. Thus the pilot still must continually scan all the other instruments and accept the associated mental effort.

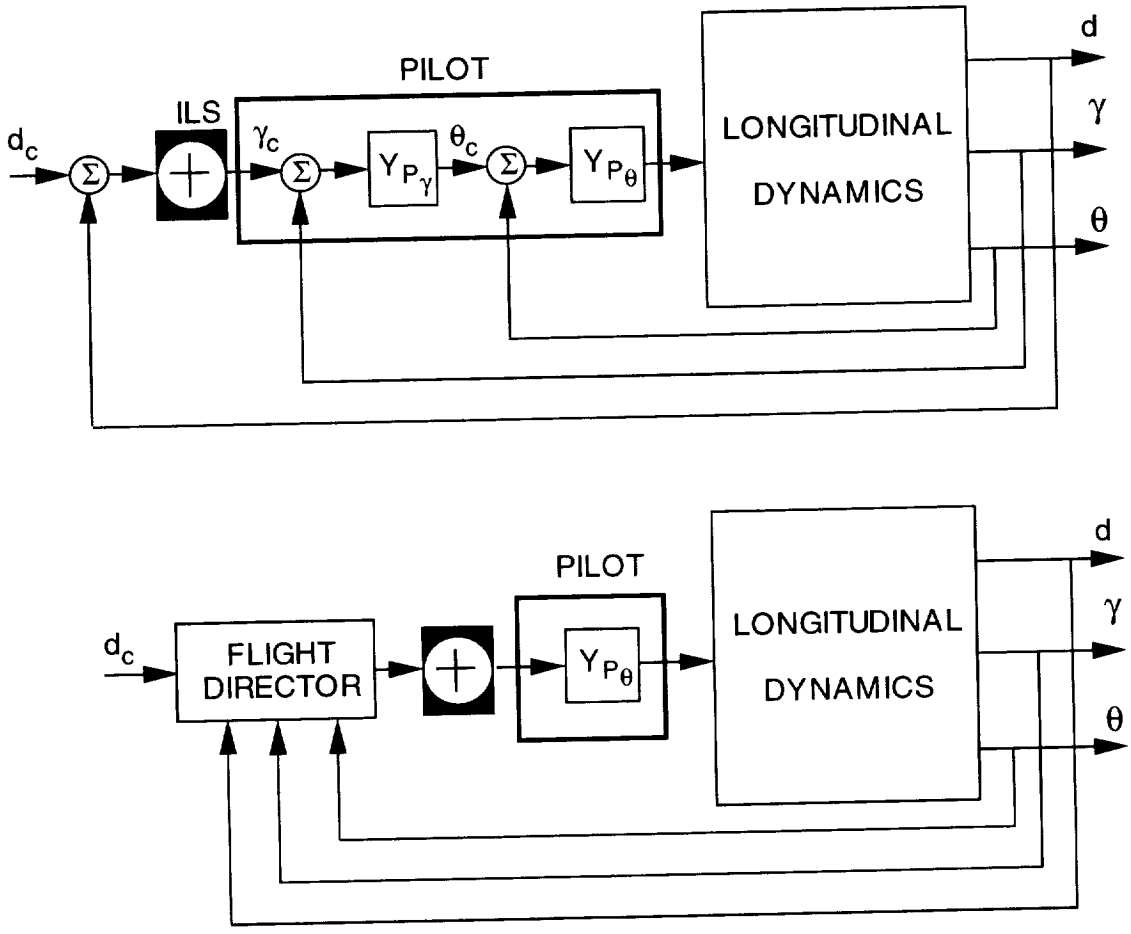

Figure 106. Flight director conceptual diagram.

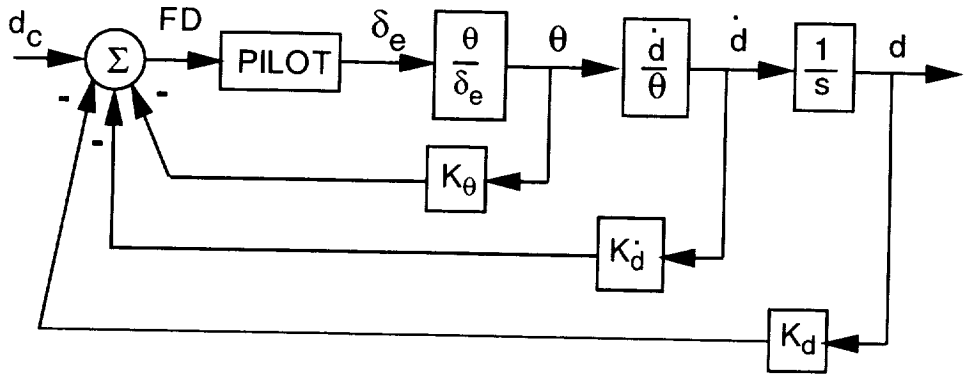

Figure 107. Flight director for vertical path control.

Principles of flight-director design have been understood for some time and are described in detail in reference 37. Given the general loop structure shown in the previous figure, an example of a flight director can be constructed, in this case for vertical path tracking. A block diagram of this specific design is shown in figure 107. In this example, vertical path tracking is performed with the pitch control, assuming operation on the frontside of the drag curve. Thus, the pilot's inputs are through the longitudinal stick in response to the flight director error presentation. Appropriate feedback variables for the flight director are pitch attitude, path deviation, and rate of deviation. Vertical rate with respect to the flightpath can be derived from the transfer function of vertical-rate to pitch-attitude. Assuming the attitude loop has been stabilized by the pilot or by an augmentation system, the pitch attitude to control input (θ/δ_e) can be represented by a second-order transfer function with a 2-rad/sec bandwidth for purposes of this analysis. The example will be constructed with a series of loop closures starting with the path deviation loop first, and then progressively adding loops for deviation rate and pitch attitude to illustrate the improvement they provide in dynamics of vertical path control.

The loop closure for only path-deviation feedback illustrates the system dynamics and difficulties in control associated with flying the path-deviation pointers without any benefit of vertical speed information or aircraft attitude. The characteristics of the flight director response to the pilot's control input are of interest and are described by the following transfer function when $K_\theta = K_{\dot{d}} = 0$:

$$\frac{FD}{\delta_e} = -K_d\left(\frac{d}{\delta_e}\right)$$

$$= -\frac{K_d}{s}\left[\frac{U_o Z_w (s + 1/T_{\gamma_\theta})}{(s + 1/T_{\theta_1})(s + 1/T_{\theta_2})}\right]\left(\frac{\theta}{\delta_e}\right)$$

where if $T_{\gamma_\theta} = T_{\theta_1}$

$$\frac{FD}{\delta_e} = -\frac{K_d}{s}\left(\frac{U_o Z_w}{s + 1/T_{\theta_2}}\right)\left(\frac{\theta}{\delta_e}\right)$$

The transfer function includes a first-order numerator, two first-order denominator roots, and the (θ/δ_e) second-order transfer function with 2-rad/sec bandwidth. Making the indicated assumption for the aircraft's flightpath response to simplify the problem leads to pole-zero cancellation as noted. Then the flight director response to the pilot consists of an integrator and cascaded first-order and second-order lags. The bandwidth of this system will be dominated by the first-order root, which is approximately that for the aircraft's vertical velocity damping. The control bandwidth is unlikely to be sufficient for precise glideslope tracking.

To extend the flight director loop bandwidth, path-deviation rate is added and the resulting transfer function is

$$\frac{FD}{\delta_e} = -K_d\left(\frac{d}{\delta_e}\right) - K_{\dot{d}}\left(\frac{\dot{d}}{\delta_e}\right)$$

$$= -K_d\left(\frac{K_{\dot{d}}}{K_d}s + 1\right)\left(\frac{d}{\delta_e}\right)$$

where if $T_{\theta_2} = -1/Z_w$

$$\frac{FD}{\delta_e} = -\frac{K_d}{s}\left(\frac{K_{\dot{d}}}{K_d}s + 1\right)\left(\frac{U_o}{T_{\theta_2}s + 1}\right)\left(\frac{\theta}{\delta_e}\right)$$

and if $K_{\dot{d}}/K_d = T_{\theta_2}$,

$$\frac{FD}{\delta_e} = -\frac{K_d U_o}{s}\left(\frac{\theta}{\delta_e}\right)$$

A first-order numerator root is introduced with a time constant that is the ratio of gains for path-deviation rate to path deviation. Adjusting this ratio for further pole-zero cancellation with the root at $1/T_{\theta_2}$ extends the K/s slope beyond $-1/Z_w$ and increases the bandwidth to about 1 rad/sec.

To extend the bandwidth further, pitch-attitude feedback is included. The transfer function with path-deviation, deviation-rate, and attitude feedback is

$$\frac{FD}{\delta_e} = -\frac{K_d U_o}{s}\left(\frac{\theta}{\delta_e}\right) - K_\theta\left(\frac{\theta}{\delta_e}\right)$$

$$= -\left(\frac{K_\theta s + K_d U_o}{s}\right)\left(\frac{\theta}{\delta_e}\right)$$

Lead compensation again appears in terms of the ratio of the path-deviation to attitude-feedback gains. If that ratio is chosen to produce an inverse time constant of 2 rad/sec, the bandwidth can be increased to that of the attitude control of the aircraft. As noted in reference 37, it is necessary to washout the pitch attitude feedback to control steady-state errors in the presence of vertical gusts and horizontal wind gradients. Inclusion of the pitch washout gives

$$\frac{FD}{\delta_e} = -\frac{K_d U_o}{s}\left(\frac{\theta}{\delta_e}\right) - K_\theta\left(\frac{s}{s+\omega}\right)\left(\frac{\theta}{\delta_e}\right)$$

$$= -\left[\frac{K_\theta s^2 + K_d U_o s + K_d U_o \omega}{s(s+\omega)}\right]\left(\frac{\theta}{\delta_e}\right)$$

Choosing the pitch feedback gain and washout so that the numerator roots cancel the denominator of the θ/δ_e transfer function allows the flight director loop to be closed at the washout frequency. The washout will fall between 1 and 2 rad/sec, resulting in a bandwidth for the flight director that will be satisfactory for vertical path tracking.

A Bode plot of the flight director to the longitudinal control is shown in figure 108. With only path-deviation and no error rate or attitude feedback, the bandwidth that can be achieved for a phase margin of 45 deg is only 0.4 rad/sec. If the pilot tightens control to achieve quicker

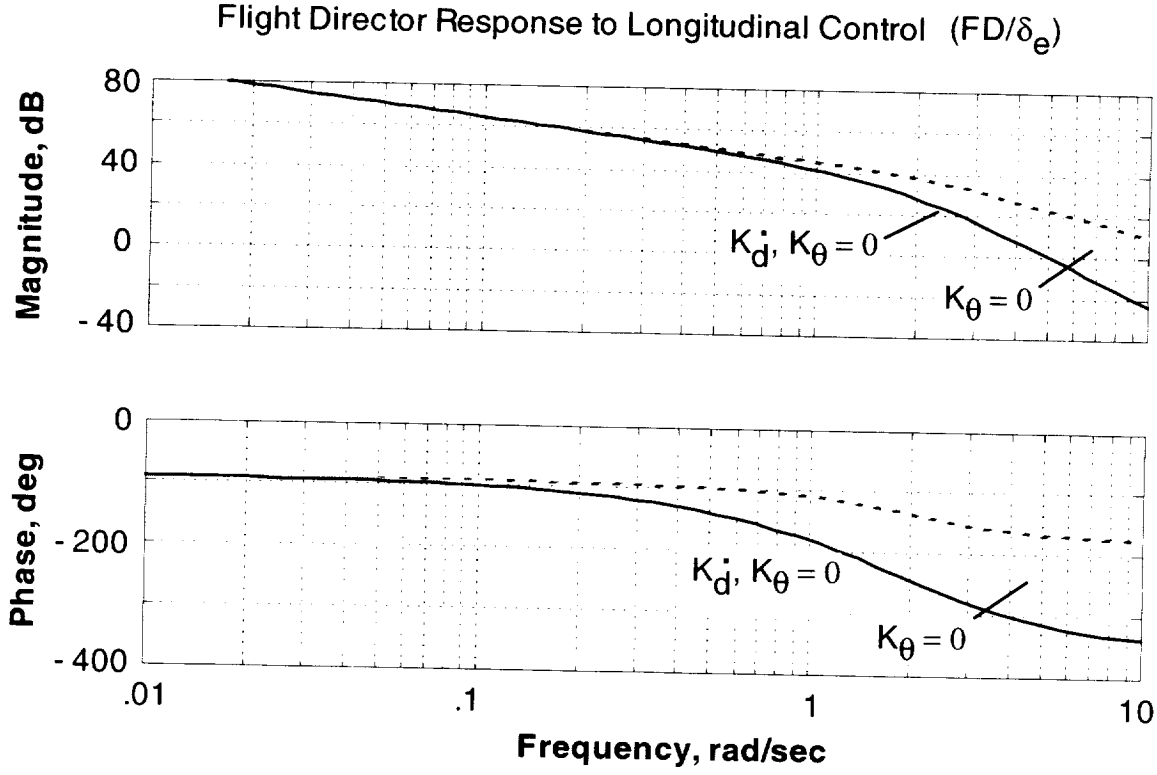

Figure 108. Bode plot of flight director for vertical path control.

response, the system will be driven unstable at about 1 rad/sec. If path-deviation rate feedback is included, the bandwidth is increased to 1 rad/sec with adequate phase margin, which will still show sluggish response to the pilot. When the pilot moves the control, immediate response of the flight director is desired. With the inclusion of attitude feedback, a bandwidth in excess of 2 rad/sec can be achieved and the flight director will respond to the pilot's command with very little perceptible lag.

The same design principles hold for a flight director used to track course in the horizontal plane. Similar state information is used and includes horizontal deviation from the ground track, cross-track velocity, and bank angle for the inner-loop attitude control.

Pursuit Tracking Display

Recall that the flight director produces a command for the pilot to follow that represents the error between the desired path and the path the aircraft is currently following. Another approach to display design provides predictive information that includes the necessary commands and integrates information on the situation of the aircraft as well. Figure 109 presents a comparison of this display concept, called a pursuit-tracking display, with the flight director. The pursuit-tracking concept shown at the bottom of the figure includes a flight status predictor. The function of the predictor is to process the aircraft state information to remove dynamic lags from the flightpath response so as to provide a nearly instantaneous indication to the pilot of the aircraft's response to control inputs. Also included, in contrast to the flight director, is a direct indication of the task the pilot intends to perform, which presents the reference path that the aircraft is commanded to follow. As an example, this path might include a curved approach or a complex descending profile to a runway. In addition to the desired flight profile, the display also shows the aircraft's displacement error from that profile, analogous to that presented in the flight director shown above. Thus, the predictor display gives the pilot information to anticipate changes in the profile so that it is not necessary to wait for errors to develop and then correct for them. It also provides a direct indication of the aircraft's situation with respect to the intended path and perhaps to a final objective such as a runway or landing pad.

Original research on the pursuit-tracking display concept for commercial transport applications was reported in reference 38. The objective of its design is to present a display that is analogous to visual flight, including a precise indication of the aircraft's flightpath. The pilot's task is to follow a leader aircraft on the display that is a predetermined distance ahead. The display is flightpath-centered and flightpath is the controlled element, where dynamic conditioning of the flightpath symbol is provided to enable it to be controlled easily and precisely. The leader (ghost) aircraft follows the desired path through space, and its symbol is driven by raw data derived from navigational aids. The display presentation is heads-up and is conformal with the external scene to the extent possible. Conformality may be lost with strong crosswinds. At low airspeed, typically less than 60 knots, scaled vertical and lateral velocities are presented by the flightpath symbol.

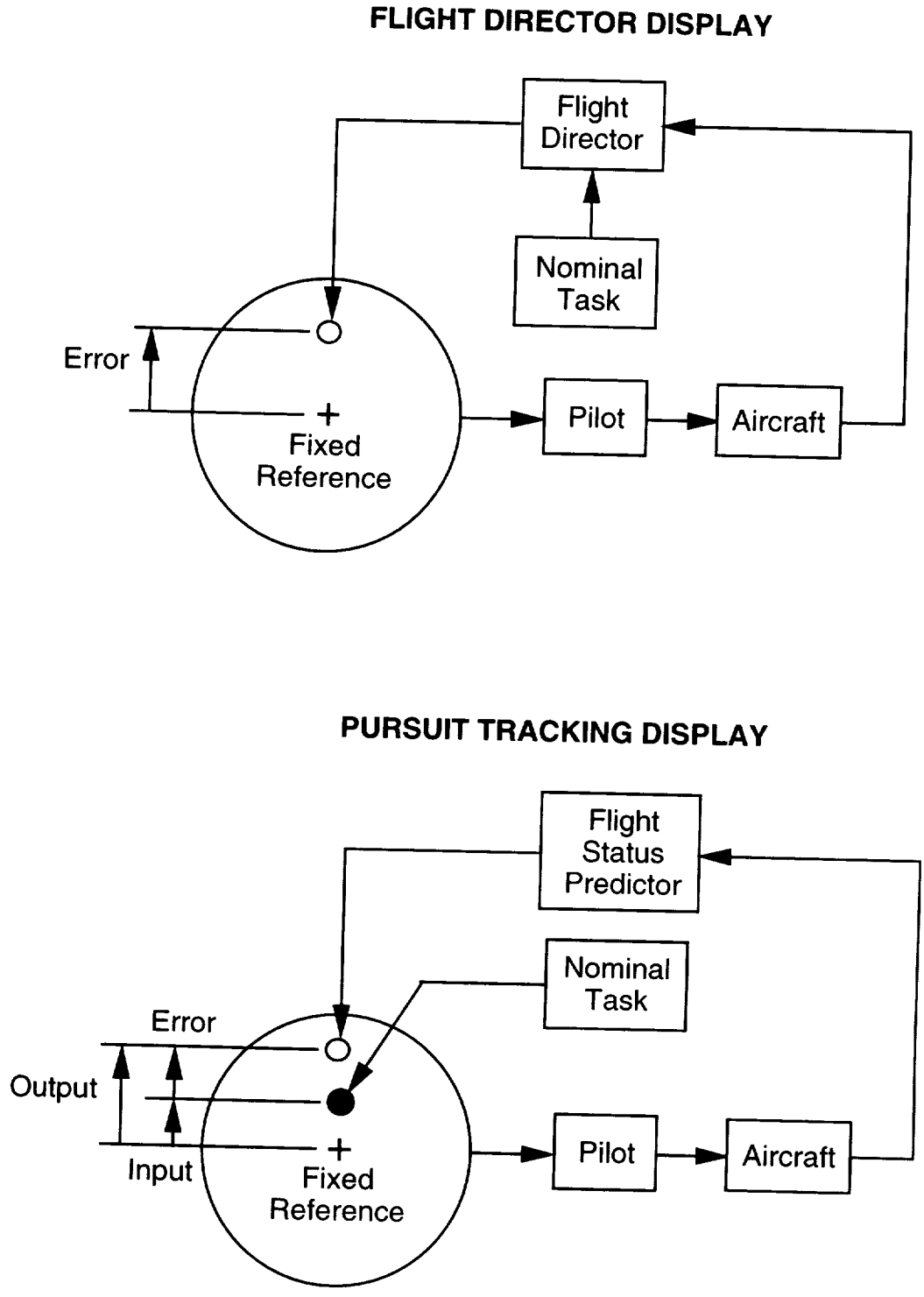

Figure 109. Comparison of flight director and pursuit-tracking display concepts.

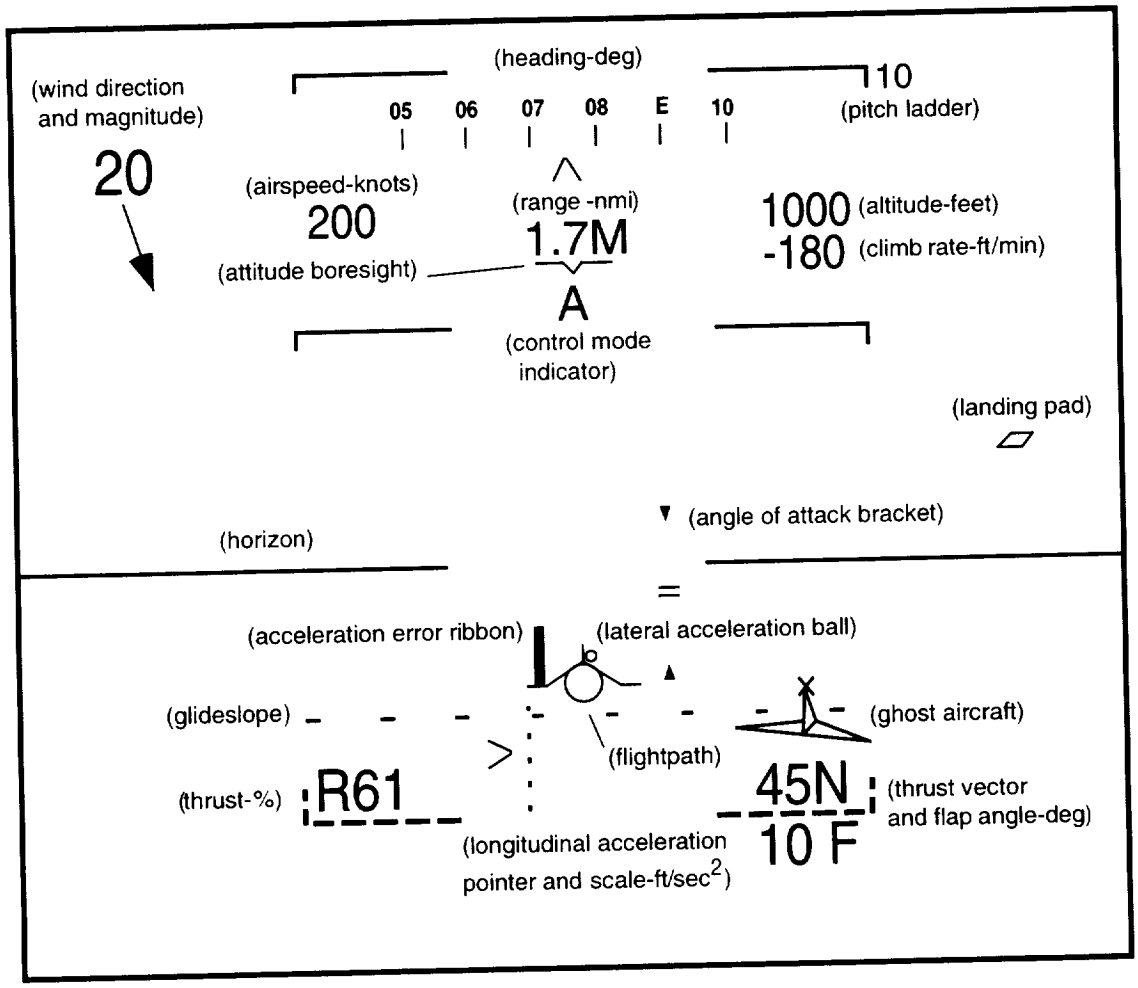

Figure 110. Pursuit tracking display for transition from cruise to hover flight.

An example of a pursuit-tracking display format applied to V/STOL aircraft is shown in figure 110. This format is presented on a head-up display placed in front of the pilot's eyes through which the external scene can also be observed. The circular symbol with gull-shaped wings represents the aircraft's flightpath in the vertical and horizontal planes. Thus this display element shows where the aircraft is going and can be used to guide the aircraft in reference to points in space or on the ground in the external scene. The flightpath symbol is read in reference to the pitch ladder, a vertical scale shown in degrees above and below the horizon. The aircraft's boresight, the vee-shaped symbol, is the reference for attitude and heading and is aligned with the aircraft's longitudinal axis or waterline. It gives an indication of where the aircraft is pointing. In this example, the aircraft's nose is raised above the horizon by 6.5 deg and the aircraft is on a 75 deg heading aligned with the flightpath. To complete the aircraft's state information, airspeed and altitude are presented to the left and right of the boresight symbol, respectively, and for this V/STOL aircraft, engine rpm and thrust-vector angle appear, respectively, at the bottom left and right. Thus this display format includes the intended and actual flightpath, body attitudes, altitude, airspeed, heading, and engine status information, all within a compact visual scan by the pilot.

The pursuit-tracking task is presented by the delta wing aircraft symbol. This aircraft appears in perspective as it would in the external scene following the prescribed flight profile. It is referenced to the center of the display, and the pilot can observe both the vertical and horizontal motion of the path of the leader aircraft through space. The pilot's task is to fly in formation behind the leader to follow the desired flightpath. The pilot can observe whether the leader is climbing, descending, turning left or right, and can see the "own" aircraft position with respect to the leader. Further, the anticipation provided by the view of the leader helps the pilot correct for displacement from the path. In the example, the leader is on a 3 deg glideslope and appears to the right and below the aircraft's flightpath symbol. This shows that the pilot's aircraft is displaced slightly to the left and above the leader's path. To make a correction back to the desired path, the pilot must fly the flightpath symbol toward the leader until the leader moves back into the center of the display and onto the 3 deg path. This is the same task the pilot would be expected to perform flying visually in formation with the other aircraft and represents the pursuit-tracking aspect of the display.

An explanation of the means by which both the leader aircraft and flightpath symbols are driven, as well as a full description of the display design principles, is provided by references 39 and 40. Those references describe the display concept as it was developed at Ames Research Center and flown on the V/STOL Systems Research Aircraft, a modified YAV-8B Harrier, and on the Quiet Short Haul Research Aircraft, a powered-lift STOL transport. The diagram in figure 111 graphically presents the basis for the leader aircraft drive logic. It shows a plan view of the "own" aircraft in relation to the leader aircraft, with the latter flying on the desired flightpath. The own aircraft is following at a distance behind the leader and is displaced to the right of the desired path. The distance in trail is related to the time in trail by the ground speed along track. The angle between the current heading of the own aircraft and the intercept course to the leader is the angle the flightpath must be turned through to pursue the leader and to eventually close on the leader's flightpath. The leader aircraft symbol is driven by the intercept angle for the own aircraft with respect to the leader's position on the desired path. Specifically, the leader aircraft

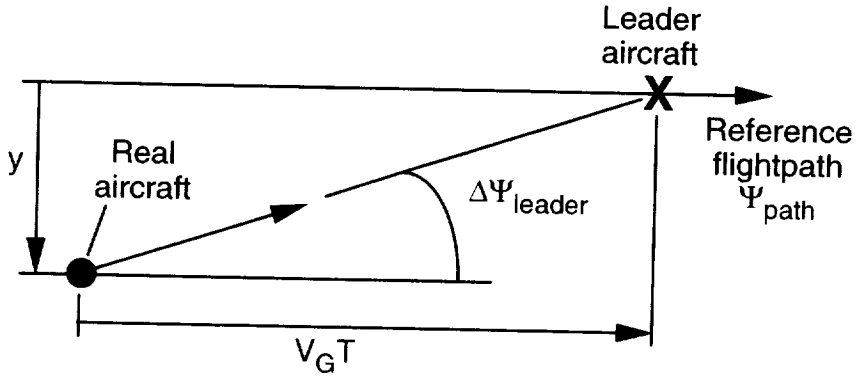

Figure 111. Drive-law concept for the pursuit-tracking display leader aircraft symbol.

symbol is moved relative to the center of the display through the intercept angle. The display shows angular rather than linear displacement, because the visual perception is an angular reference. The drive equation for the symbol for the horizontal path is

$$\Delta\Psi_{leader} = \Psi_{path} - \tan^{-1}\left(\frac{y}{V_G T}\right)$$

The angular displacement is the difference between the intended path angle and the intercept angle defined by the path displacement y and the distance in trail $V_G T$. Dynamically, the convergence to the desired path, when the pilot holds the flightpath symbol on the leader symbol, is represented by rewriting the above equation as

$$T\dot{y} + y = 0$$

where the rate of closure to the path $\dot{y}$ is the product of ground speed and the intercept angle. This is simply a first-order differential equation representing an exponential closure to the path with time constant T. The design variable for the leader aircraft is the time in-trail T and should be selected based on a compromise between the quickness of the closure to the path and the activity level of the display. The same display concept applies for vertical path control. Typically, time in-trail values of 10 sec for vertical path control and 20 sec for lateral path control are appropriate. When flying close to the leader, small displacements create large intercept angles that make the display sensitive and cause the pilot to tighten up control unnecessarily. The increase in level of precision achieved would not be commensurate with the increased control effort expended. Conversely, if the leader is too far ahead, the path tracking may be too loose, though easy for the pilot to perform. The shorter time in-trail for the vertical tracking task compared to the lateral is a consequence of the higher bandwidth that can be achieved for flightpath compared with that for ground track control. The latter must be accomplished by first banking the aircraft; the roll and heading dynamics introduce enough delay in the control loop to lower the ultimate control bandwidth for the lateral path.

With modern inertial instrumentation, flightpath angle can be sensed precisely in the vertical and horizontal planes. However, objectionable lags may be present in the aircraft's dynamics that could compromise flightpath-control bandwidth. Thus, it may be necessary to dynamically condition the flightpath measurement before presenting that information to the pilot. An illustration of this conditioning is shown in figure 112 as an example of vertical-path control.

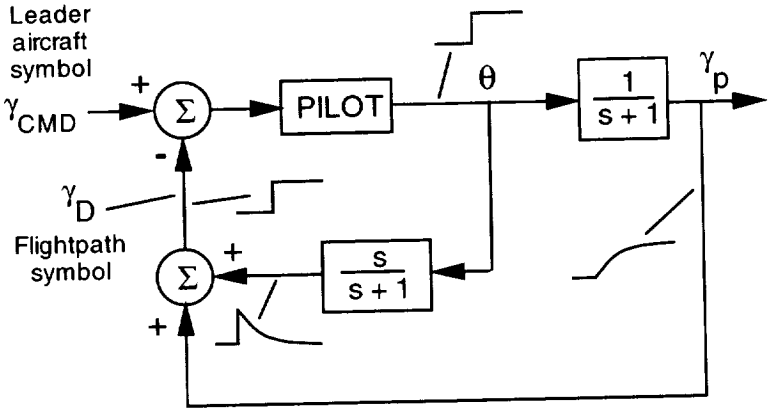

Figure 112. Dynamic conditioning for the flightpath symbol.

The input to the control loop is the desired flightpath, whereas the response of the aircraft to the pilot's control is typically that of a first-order lag with a time constant $1/T_{\theta_2}$. If that lagged response is presented to the pilot as the path error, the overall loop bandwidth will be compromised. However, if the flightpath measurement is complemented by adding to it the output of a washout filter driven by the pilot's control input, the resulting feedback of flightpath compared to the commanded path will be quickened substantially. If the washout time constant is identical to that of the aircraft's lag, the flightpath symbol will appear to follow the pilot's control input immediately. The washout feedback will respond instantly to the pilot and will decay at the same rate as the actual flightpath responds. However, the actual flightpath still lags the command and the tracking performance is determined by this lagged response. Tracking errors can be reduced by further conditioning the symbol to command the pilot to overdrive the pitch control in order to quicken the actual flightpath response. However, this will require the pilot to make more continuous control inputs, and workload will increase correspondingly. The dynamic compensation noted in figure 112 for the flightpath symbol has proved to be acceptable to pilots. Compared with the drive laws for a flight director, these display equations are quite simple. That fact, along with the ease with which the display can be flown and the readily assimilated situation information, makes this a compelling choice for display design.

To complete the discussion of the display symbology, the ribbon that grows out of the wing of the flightpath symbol indicates error in following a commanded airspeed or longitudinal deceleration profile that is typical for operation of a V/STOL aircraft in transition from conventional flight to hover. The command indicates to the pilot how rapidly to decelerate to arrive at the intended hover position based on the aircraft's current position and ground speed. Finally, the ball on top of the flightpath symbol serves the same purpose as the sideslip or lateral acceleration ball that normally is shown either by itself as an instrument, on a turn and bank instrument, or on the attitude director indicator. For the rest of the information on the display, pitch and roll attitude are derived from the aircraft's inertial measurement unit, altitude from barometric or radar measurements, and airspeed from pressure sensors processed through air-data calculations. Propulsion system performance, such as engine rpm representing thrust magnitude, and the resultant thrust-vector angle are based on propulsion system sensors. Depending on the complexity of the propulsion system, such as the number of thrust-producing components, these measurements could be directly extracted from electromechanical sensors or could be derived from the propulsion system control processor that derives the resultant thrust deflection.

Displays can also be provided for precision control in the hover. These may be useful under VMC for precision landing tasks and would be demanded for IMC. A representative display format is shown in figure 113. It is used for precision hovering over a landing pad and presents a mix of information in the conventional vertical format overlaid by a horizontal or plan view presentation. Since flightpath angles become exceedingly large at low speed and in hover, translational velocities in both the horizontal and vertical planes are shown. The vertical presentation contains information about pitch, roll, and yaw attitudes, ground speed, altitude, vertical velocity, and engine states. In the horizontal or plan view, the landing pad is displayed with respect to the aircraft reference symbol. The aircraft symbol represents the locations of the nose and main landing gear in scale with the pad. To provide the pursuit tracking aspect of the display, longitudinal and lateral inertial velocities are shown by the velocity vector in the horizontal plane. The pilot's commanded velocities are

shown by the predictor ball for the horizontal plane and by the diamond symbol for the vertical axis. To position the aircraft over the landing pad, the pilot uses the controls to move the velocity predictor toward the pad and then to follow the pad as it approaches and converges on the aircraft reference symbol. The actual velocities converge to their predicted values based on the dynamics of the control augmentation system and the display dynamics designed into the predictor ball. When the actual velocity vector is maintained on the pad symbol, the aircraft will exponentially converge to hover over the pad. For height control, the pilot holds the vertical velocity diamond on the zero reference to maintain a desired hover altitude and sets a desired vertical velocity for descent when performing the landing. The translational velocities are sensed by the inertial measurement unit and presented directly on the display. The deck bar symbol presents the vertical position situation in relation to the pad and is driven by radar altitude. All other information is derived from the sensors noted above.

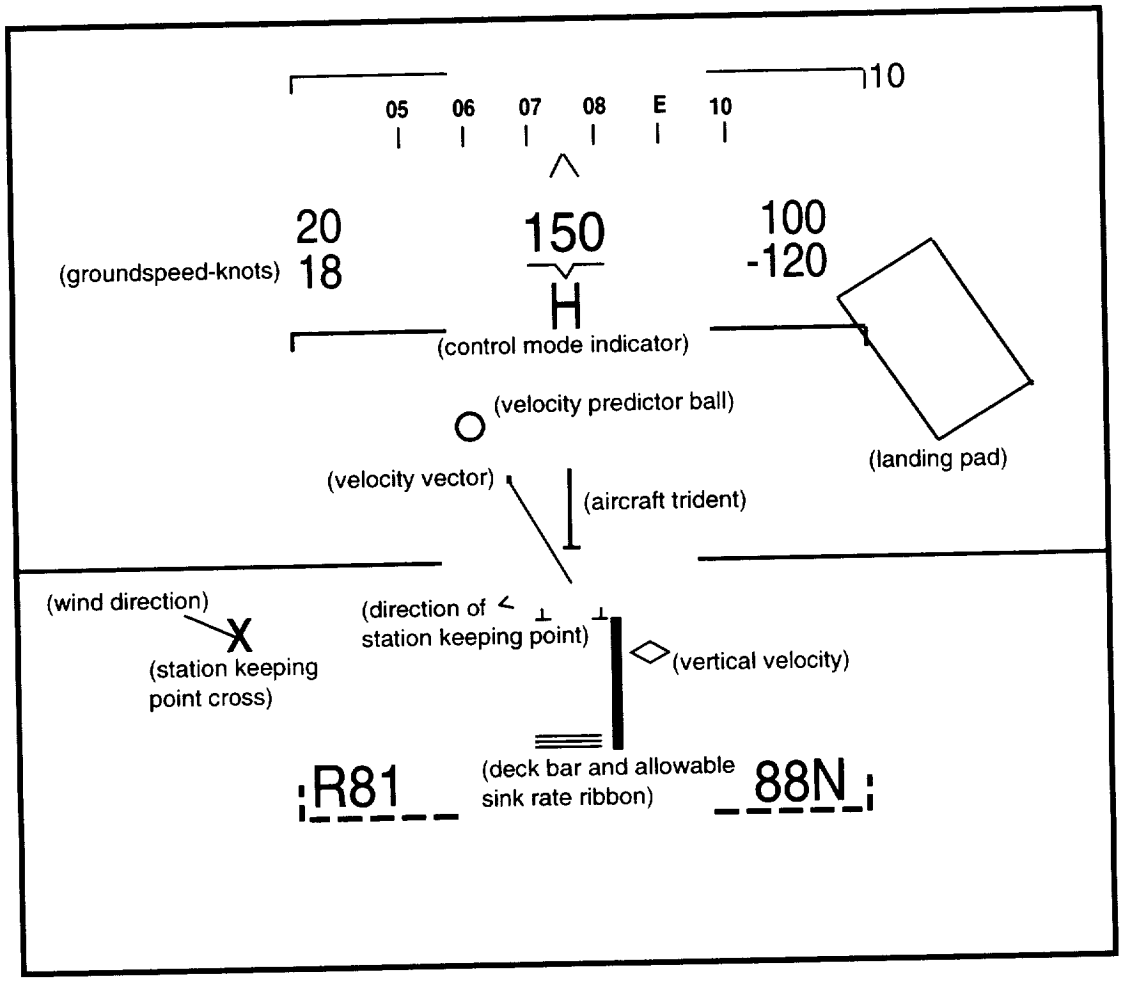

Figure 113. Pursuit tracking display for precision hover.

CONCLUDING REMARKS

This text was prepared to describe the contributions of a V/STOL aircraft's configuration to its dynamics, control, and flying qualities during hover and forward flight. The dynamic response characteristics of the V/STOL aircraft in these flight regimes were described in detail, along with requirements for achieving the desired flying qualities for representative V/STOL tasks. As evidenced from the behavior of the basic V/STOL aircraft, it is necessary to augment the response to the pilot's controls in order to achieve flying qualities that are acceptable for demanding V/STOL operations. Design approaches for this augmentation include both advanced stabilization and command augmentation systems and integrated guidance and control displays, where both are described in terms of basic system concepts and design criteria. The ability to produce these control and display systems rests with advances in high-performance digital computation, inertial and air-data sensing, and electronic display presentation, as well as with powerful and lightweight propulsion system effectors; these latter will generate the forces and moments required for control of the aircraft in hover and during semi-jet-borne flight. Applications of these principles are anticipated in the coming generation of V/STOL aircraft that will be developed for military and commercial use.

APPENDIX

AIRCRAFT STABILITY DERIVATIVES

Stability derivatives for example V/STOL aircraft and helicopters are presented in this appendix. The V/STOL examples are the McDonnell-Douglas YAV-8B Harrier, Bell XV-15 Tilt Rotor, Bell X-22A, Ling Temco Vought XC-142, and a conceptual design of a modern STOVL fighter, the General Dynamics E-7A Augmentor Ejector. The examples include stability and control derivatives for hover and forward flight conditions. The helicopters are the Bell UH-1H, Boeing-Vertol BO-105C, Boeing-Vertol CH-47A, and Sikorsky UH-60. This selection of aircraft is intended to provide wide ranging characteristics of vehicles in hover through transition to conventional flight. The characteristics of these aircraft reflect the contrast between a high-wing-loading configuration like the Harrier versus a helicopter like the UH-60 in hover and transition.

YAV-8B Harrier V/STOL Aircraft

The YAV-8B Prototype Demonstration Aircraft, shown in hover in figure 114, is a single-seat, high-performance, transonic, light attack V/STOL aircraft developed for the U. S. Marines by McDonnell Douglas. Its design represents a significant modification of the original Harrier

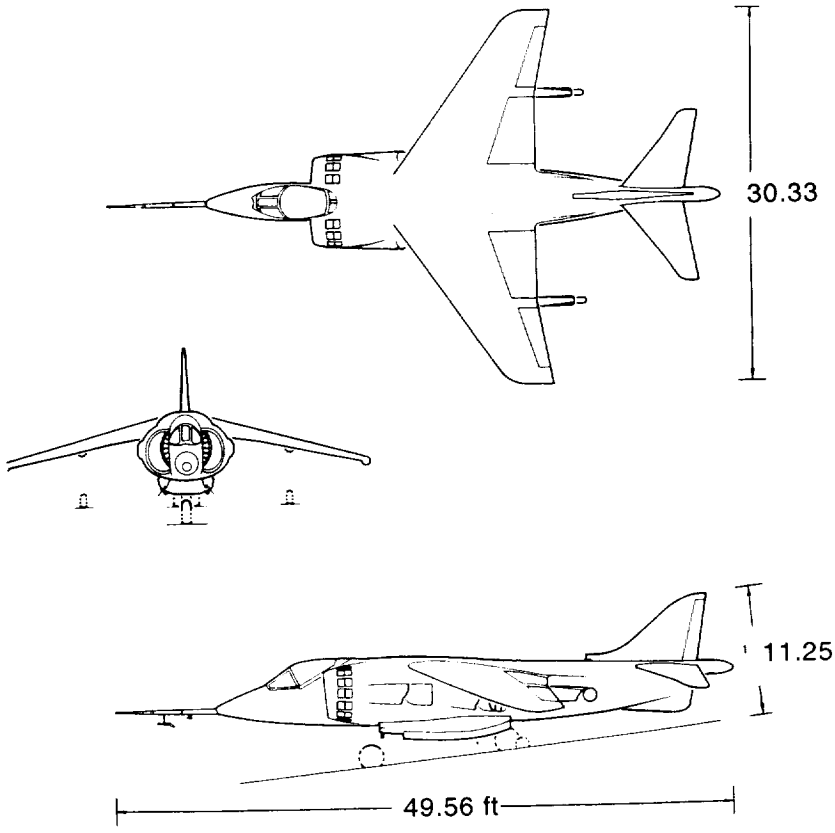

Figure 114. YAV-8B Harrier.

design developed in the United Kingdom by Hawker Aircraft. The aircraft is characterized by a shoulder-mounted, supercritical, swept wing and swept stabilator, both with marked anhedral. It has a single vertical fin and rudder, under-fuselage lift-improvement devices, and a large engine inlet with a double row of inlet doors. The aircraft is powered by a single Rolls-Royce Pegasus turbofan engine that provides lift thrust for takeoff and landing, cruise thrust for conventional wing-borne flight, deflected thrust for V/STOL, and in-flight maneuvering, and compressor bleed air for the aircraft's reaction control system. Four exhaust nozzles, two on either side of the fuselage, direct the engine thrust from fully aft to 98.5 deg below the thrust line, which is inclined 1.5 deg above the fuselage reference line.

The flight control system consists of conventional aerodynamic surfaces that are hydraulically powered, except for the rudder, which is completely mechanical, and reaction-control jets at the extremities which are pressurized by compressor bleed air when the exhaust nozzles are lowered. The reaction controls are mechanically linked to the respective aerodynamic control surfaces. Aircraft attitude is controlled by the reaction-control jets in hovering flight and by conventional aerodynamic surfaces in wing-borne flight. Both systems contribute to control during transition between wing-borne and propulsion-borne flight. Longitudinal control is accomplished through downward-blowing front and rear fuselage reaction-control jets and an all-moving stabilator. Lateral control is provided through wing-tip-mounted reaction jets, which thrust up and down, and by outboard ailerons. Directional control comes from a sideways-blowing reaction jet located in the aft fuselage extension and by the rudder.

The stability derivatives listed in table 8 were extracted from the nonlinear simulation model of the YAV-8B aircraft documented in reference 41.

XV-15 Tilt Rotor Research Aircraft

The XV-15 Tilt Rotor aircraft is a two-place, twin-engine light transport aircraft, shown in figure 115, that was developed by Bell Helicopter. It features two wingtip mounted proprotors and twin vertical tails. The proprotors can be rotated from 0 to 95 deg with respect to the wing. The propulsion system consists of twin Lycoming T-53-L-13B engines driving the proprotors through interconnected shafts and transmissions. The proprotors may be rotated from the horizontal to the vertical continuously during the transition from aircraft to helicopter flight.

The basic flight control system consists of the elevator, ailerons and twin rudders for aerodynamic controls. In hover, pitch control is provided by longitudinal cyclic, lateral control by differential thrust between the two proprotors, and directional control by differential cyclic between the two rotors.

The stability derivatives shown in table 8 were extracted from the nonlinear simulation model in reference 42.

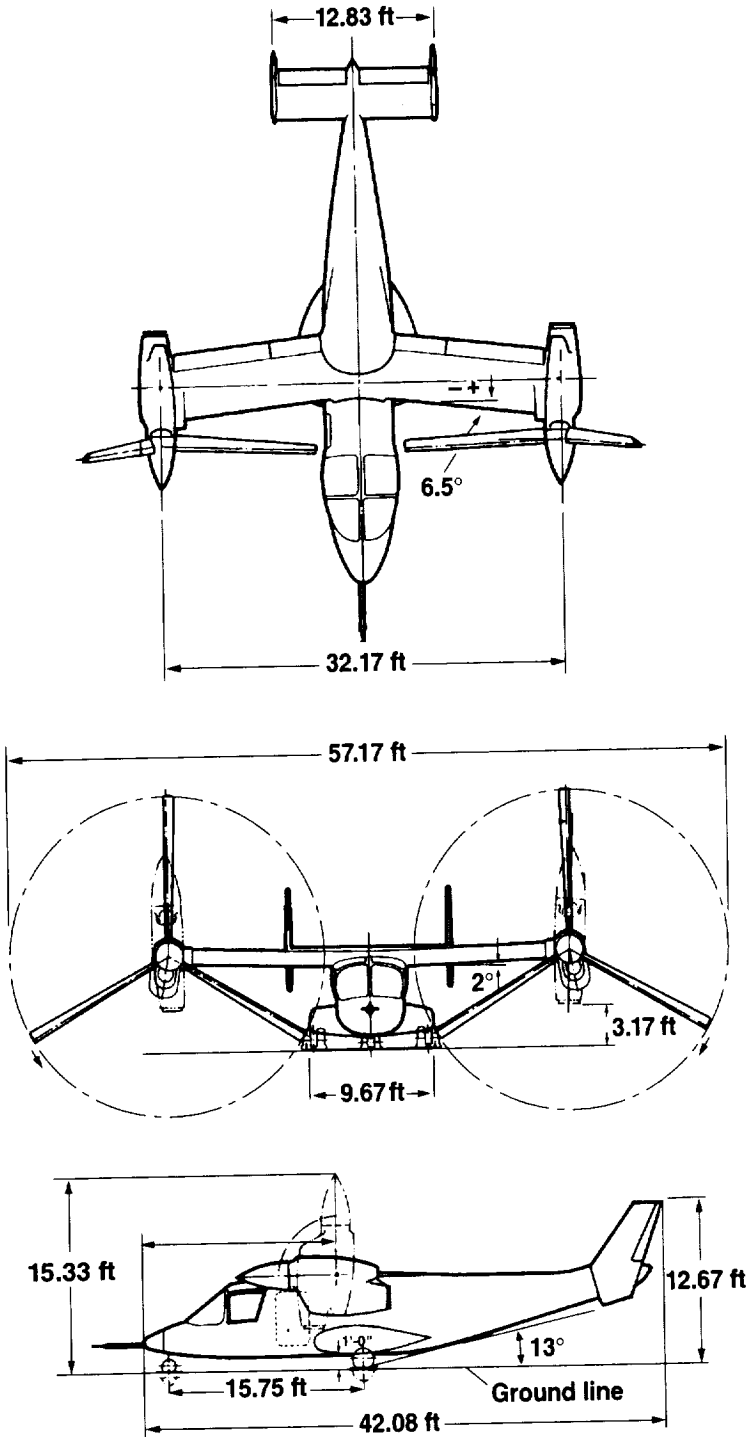

Figure 115. XV-15 Tilt Rotor research aircraft.

TABLE 8. STABILITY DERIVATIVES FOR THE YAV-8B AND XV-15

	YAV-8B (ref. 41)			XV-15 (ref. 42)		
Flight condition						
Speed, knots	0	100	200	0	110	150
Altitude, ft	100	100	100	200	200	200
Weight, lb	16280	16280	16280	13000	13000	13000
c.g., in.	343.6	343.6	343.6			
I_{xx}, slug-ft^2	6547	6547	6547	48668	48053	46823
I_{yy}, slug-ft^2	30927	30927	30927	17907	17570	16895
I_{zz}, slug-ft^2	34685	34685	34685	60254	60532	61087
I_{xz}, slug-ft^2	1382	1382	1382	1234	1181	1076
δ_N, deg	90	60	0	90	60	0
Derivatives						
X_u, sec^{-1}	–0.023	–0.09	–0.04	–0.025	–0.12	–0.081
X_w, sec^{-1}	0.0004	0.012	0.046	0.0033	0.15	0.12
X_q, ft/sec/rad	0.022	–0.1	–0.03	1.81	–0.23	0.5
X_{δ_S}, ft/sec^2/%	0	0	0	/in. 1.32	0.1	–0.02
X_{δ_T}, ft/sec^2/%	–0.0002	0.35	0.68	/in. 0.1	2.03	1.54
X_{δ_N}, ft/sec^2/deg	–0.54	–0.3	0	——	——	——
Z_u, sec^{-1}	–0.0077	–0.19	–0.14	0.0075	–0.096	–0.23
Z_w, sec^{-1}	–0.031	–0.34	–0.66	–0.22	–0.65	–0.82
Z_q, ft/sec/rad	0.24	–1.42	–3.1	–0.81	–2.88	–6.83
Z_{δ_S}, ft/sec^2/%	0.039	0.054	0.079	/in. –0.01	0.06	–1.3
Z_{δ_T}, ft/sec^2/%	–0.1	–0.69	–0.042	/in. –4.35	–3.81	0.25
Z_{δ_N}, ft/sec^2/deg	0.005	–0.12	0	——	——	——
M_u, rad/ft-sec	0.00027	–0.0022	0.0003	0.0021	0.012	0.0064
M_w, rad/ft-sec	0.0047	–0.0027	–0.014	–0.00012	–0.014	–0.014
$M_{\dot{w}}$, rad/ft	–0.0025	–0.0022	–0.0022	——	——	——
M_q, sec^{-1}	–0.047	–0.52	–1.0	–0.36	–0.99	–1.08
M_{δ_S}, rad/sec^2/%	0.026	0.023	0.024	/in. –0.24	–0.44	–0.68
M_{δ_T}, rad/sec^2/%	–0.0015	0.0055	0.0035	/in. 0.0028	–0.087	–0.093
M_{δ_N}, rad/sec^2/deg	–0.0015	0.0027	0	——	——	——
Y_v, sec^{-1}	–0.029	–0.164	–0.217	–0.0071	–0.13	–0.19
Y_p, ft/sec/rad	–0.023	–0.006	0.005	–1.75	0.19	–0.65
Y_r, ft/sec/rad	–0.25	–0.21	–0.17	–0.62	1.76	6.27
Y_{δ_P}, ft/sec^2/%	–0.012	–0.016	–0.03	/in. 0.23	–0.62	–0.95

TABLE 8. CONCLUDED

	YAV-8B			XV-15		
Derivatives						
L'_v, rad/ft-sec	–0.0021	–0.034	–0.01	–0.0078	–0.0025	–0.0075
L'_p, sec^{-1}	–0.019	–1.2	–2.4	–0.45	–1.39	–0.67
L'_r, sec^{-1}	–0.016	0.24	0.37	0.078	–0.24	–0.05
$L'_{\delta A}$, $rad/sec^2/\%$	0.034	0.033	0.068	/in. 0.26	0.38	0.22
$L'_{\delta P}$, $rad/sec^2/\%$	0	–0.0017	–0.0072	/in. 0.022	–0.067	–0.026
N'_v, rad/ft-sec	–0.0041	0.0075	0.021	0.0036	0.0051	0.0059
N'_p, sec^{-1}	–0.0036	–0.01	0.014	0.16	–0.32	–0.2
N'_r, sec^{-1}	–0.041	–0.21	–0.39	–0.021	–0.37	–0.97
$N'_{\delta A}$, $rad/sec^2/\%$	0	0	0.0042	/in. –0.015	0.11	0.07
$N'_{\delta P}$, $rad/sec^2/\%$	0.0039	0.0043	0.0069	/in. 0.108	0.091	0.14

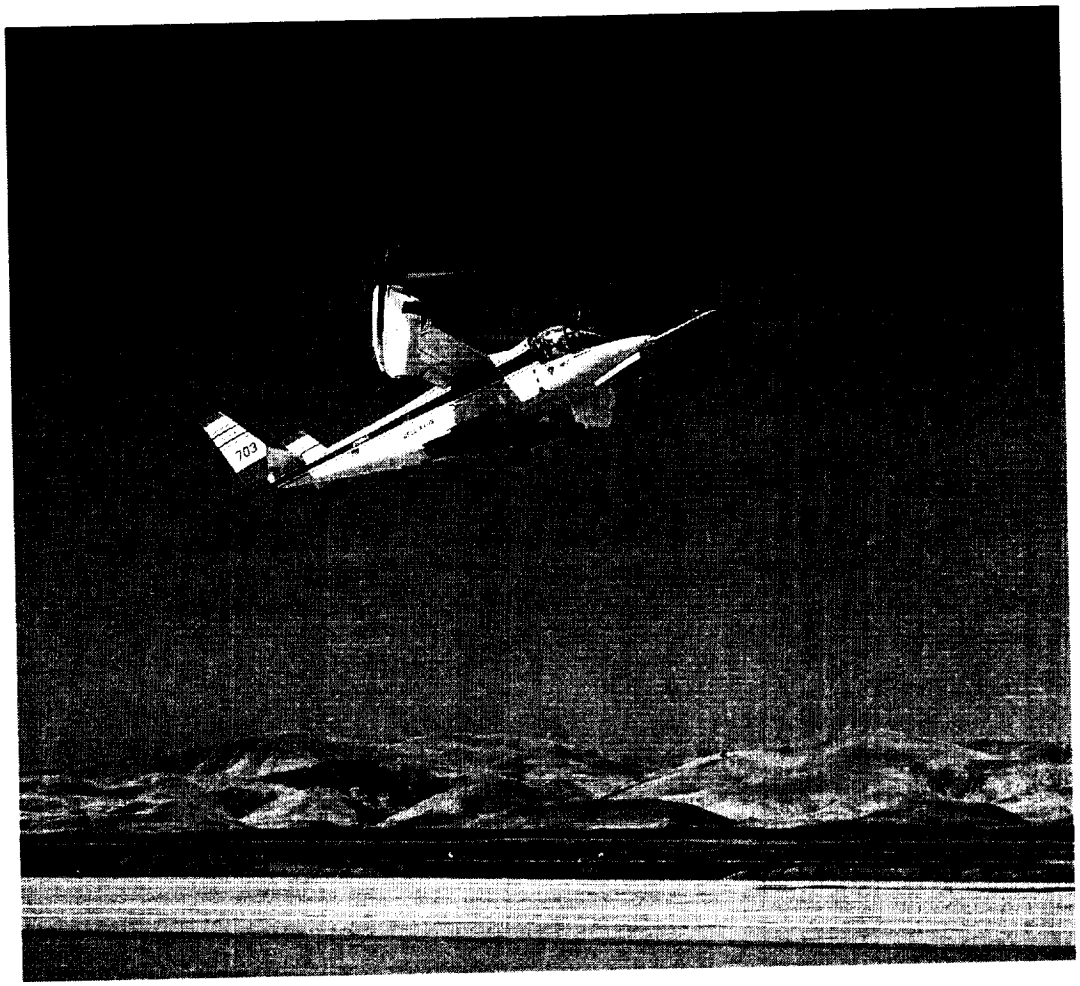

X-22A VTOL Research Aircraft

The X-22A is a two-place V/STOL research aircraft with quad-ducted tilting propellers (fig. 116). It was developed for the U. S. Navy by Bell Aerosystems as an assault transport under the Tri-Service V/STOL Test Program to demonstrate the tilt-duct propeller concept. It was modified to a variable stability VTOL research aircraft by Calspan Corporation. The aircraft is powered by four General Electric T-58-GE-8 turboshaft engines mounted at the root of the aft horizontal surface. The four ducted propellers are driven through interconnected shafts and gear boxes. Duct angle ranges from 0 to 90 deg with respect to the horizontal.

Flight control is provided through thrust modulation and deflection for the four propellers. In hover, pitch and roll control is accomplished by differential thrust control, which is achieved by changing blade pitch of the fore-aft and left-right propeller combinations. Yaw control is achieved using differential aileron deflection to deflect the propeller thrust in left-right ducts. In conventional flight, elevons are used for pitch and roll control. Yaw control is produced through differential left-right thrust control. At intermediate configurations during transition between hover and conventional flight, the differential-thrust and thrust-deflection controls are mixed based on duct tilt angle.

The stability derivatives shown in table 9 are based on flight data presented in references 43 and 44.

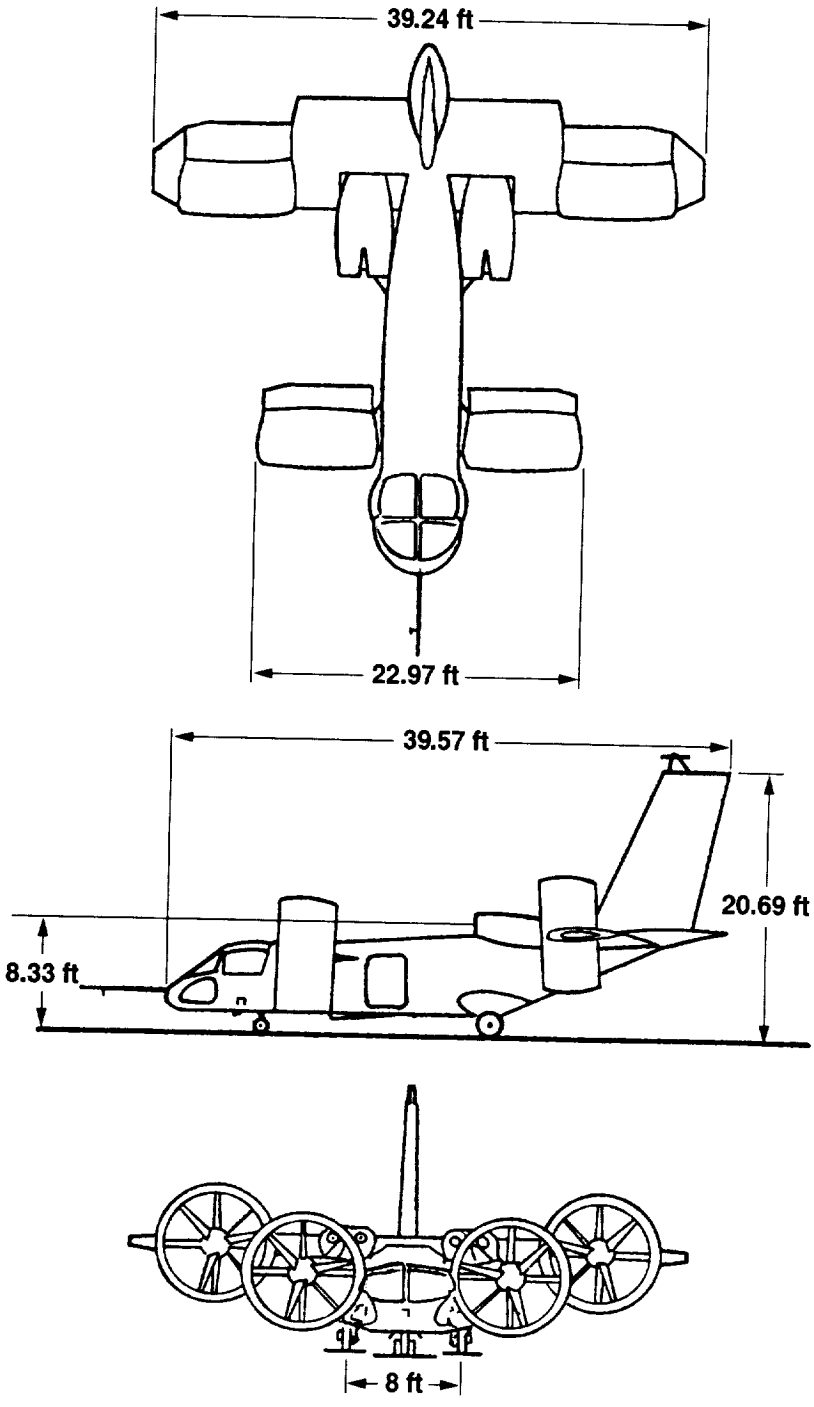

Figure 116. X-22A VTOL research aircraft.

XC-142 Tilt Wing Tactical Transport

The XC-142 is a four-propeller V/STOL transport (fig. 117) developed for the U. S. Air Force under the Tri-Service V/STOL Test Program by Ling-Temco-Vought. It is a tilt wing, deflected slipstream aircraft with wing tilt ranging from 0 to 100 deg with respect to the fuselage. It is powered by four General Electric T64-GE-1 turboshaft engines that drive the four propellers through interconnected shafts. A tail propeller is also driven for hover pitch control.

Flight control in hover is achieved by using the tail propeller for pitch, differential pitch of the wing-mounted propellers for roll, and differential aileron deflection for yaw control. In conventional flight, pitch control is provided by an all-moving horizontal stabilizer, roll control by the ailerons, and yaw control through the rudder. These controls are mixed appropriately between hover and forward flight based on wing incidence.

The stability derivatives shown in table 9 are from the examples of aircraft characteristics in reference 15.

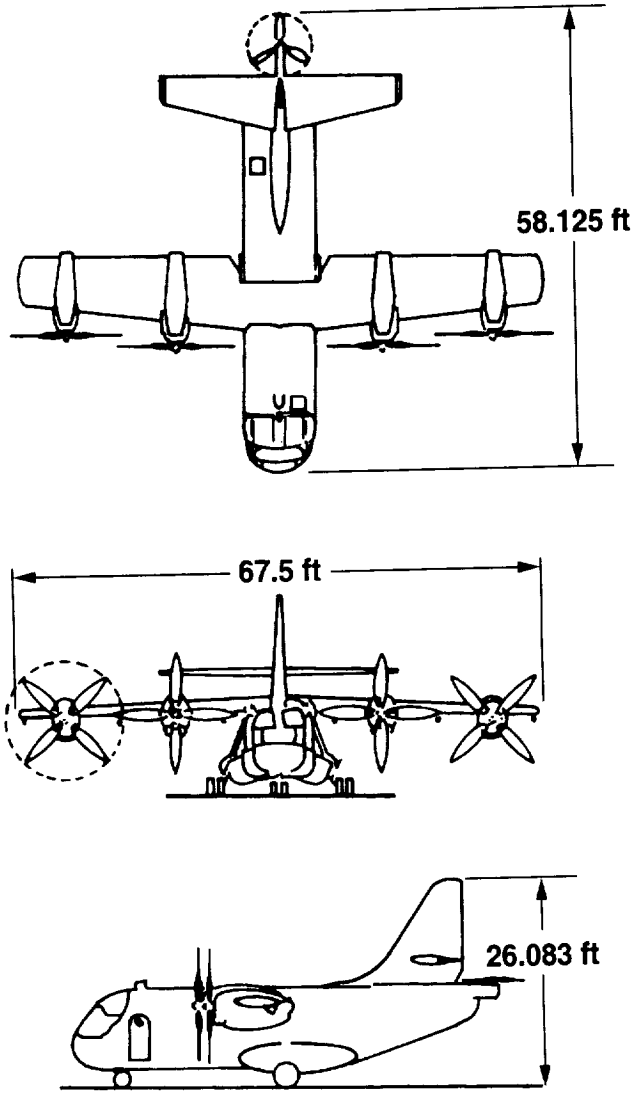

Figure 117. XC-142 tactical VTOL transport.

TABLE 9. STABILITY DERIVATIVES FOR THE X-22A AND XC-142

	X-22A (refs. 43, 44)			XC-142 (ref. 15)		
Flight condition						
Speed, knots	0	65	100	0	60	120
Altitude, ft	100	100	100	100	100	100
Weight, lb	15287	15287	15287	37474	37474	37474
δ_N, i_w, deg	90	65	15	90	14.5	1.25
Derivatives						
X_u, sec^{-1}	–0.16	–0.18	–0.19	–0.21	–0.2	–0.22
X_w, sec^{-1}	0	–0.03	0.087	0	0.035	0.06
X_q, ft/sec/rad	–3.52	0	0	–3.52	0	0
X_{δ_S}, $ft/sec^2/in.$	0	–0.356	0.147	0	0.124	0.12
X_{δ_T}, $ft/sec^2/deg$	0	0.52	1.12	/rad 0	73.	130.
Z_u, sec^{-1}	0	–0.2	–0.26	0	–0.278	–0.15
Z_w, sec^{-1}	–0.12	–0.55	–0.65	–0.065	–0.59	–0.85
Z_q, ft/sec/rad	0	0	0	——	——	——
Z_{δ_S}, $ft/sec^2/in.$	–0.16	0	0.61	2.58	3.12	4.58
Z_{δ_T}, $ft/sec^2/deg$	–1.5	–1.0	–0.36	/rad –119.	–130.	–97.
M_u, rad/ft-sec	0.023	–0.01	–0.0066	0.0073	0.0045	0.01
M_w, rad/ft-sec	0.000875	–0.0177	–0.0049	0.0003	–0.0002	–0.0095
M_q, sec^{-1}	0.2	–0.09	–0.5	–0.085	–0.486	–0.89
$M_{\dot{w}}$, rad/ft	——	——	——	–0.0013	–0.0013	–0.0013
M_{δ_S}, $rad/sec^2/in.$	0.479	0.33	0.3	0.77	0.87	1.2
M_{δ_T}, $rad/sec^2/deg$	0	0.021	0.037	/rad 0.26	–3.71	–5.1
Y_v, sec^{-1}	–0.175	–0.267	–0.3	–0.015	–0.095	–0.18
Y_p, ft/sec-rad	3.67	0.573	0.347	——	——	——
Y_r, ft/sec-rad	–1.68	–0.108	–1.49	——	——	——
Y_{δ_P}, $ft/sec^2/in.$	——	——	——	0	0.25	0.94
L'_v, rad/ft-sec	–0.038	–0.037	–0.0386	–0.0006	–0.0072	–0.0096
L'_p, sec^{-1}	–0.15	–0.75	–1.05	–0.24	–0.54	–0.86
L'_r, sec^{-1}	0	1.24	1.85	–0.034	0.38	0.56
L'_{δ_A}, $rad/sec^2/in.$	0.588	0.382	0.398	–0.29	–0.17	–0.19
L'_{δ_P}, $rad/sec^2/in.$	0.095	–0.15	–0.102	0.062	–0.087	0.091
N'_v, rad/ft-sec	0.0011	0.001	–0.00118	–0.00039	0.0022	0.0029
N'_p, sec^{-1}	0	–0.11	–0.178	–0.0062	–0.14	–0.12
N'_r, sec^{-1}	–0.17	–0.21	–0.1	–0.21	–0.33	–0.57
N'_{δ_A}, $rad/sec^2/in.$	0.043	0.052	0.068	–0.0075	–0.013	–0.027
N'_{δ_P}, $rad/sec^2/in.$	0.23	0.15	0.058	–0.21	–0.15	–0.13

E-7A Augmentor Ejector STOVL Fighter Concept

The E-7A is a single-place, single-engine STOVL fighter/attack aircraft (fig. 118) conceptual design developed by General Dynamics. The aircraft is a tailless delta configuration characterized by a 60 deg leading-edge sweep. A thrust-augmenting ejector arranged chordwise is located forward in the wing root. The propulsion system concept uses a turbofan engine in a separate flow arrangement; the fan air is collected and either ducted forward to the primary ejector nozzles or aft to a rearward-pointing exhaust nozzle. Core flow is directed to an augmented deflector exhaust nozzle that can be deflected up to 110 deg below the horizontal. In conventional flight, all the fan air and core flow are directed straight aft through the respective nozzles. In hover, the entire fan flow goes to the ejector nozzles and the core flow is deflected vertically through the rear nozzle. During transition from conventional to hover flight, the core flow is partially deflected and the fan flow is apportioned between the ejector and rear nozzle as required to provide acceleration or deceleration and longitudinal balance.

The basic flight-control system consists of elevons and a rudder for aerodynamic effectors during forward flight and reaction-control-system nozzles located in the nose, wingtips, and tail, powered by engine compressor bleed air for effectors during hover and transition flight. Pitch control is achieved by a combination of symmetric elevon deflection and down-blowing reaction controls in the nose and wingtips. Roll control is produced by differential actuation of the elevons and by the wingtip reaction controls. Coordinated application of the nose and wingtip reaction controls eliminates pitching moments when roll control is demanded. Yaw control is derived from the combination of rudder and tail reaction control.

Longitudinal stability derivatives (table 10) documented in references 45 and 46 were obtained from a nonlinear simulation model of the aircraft.

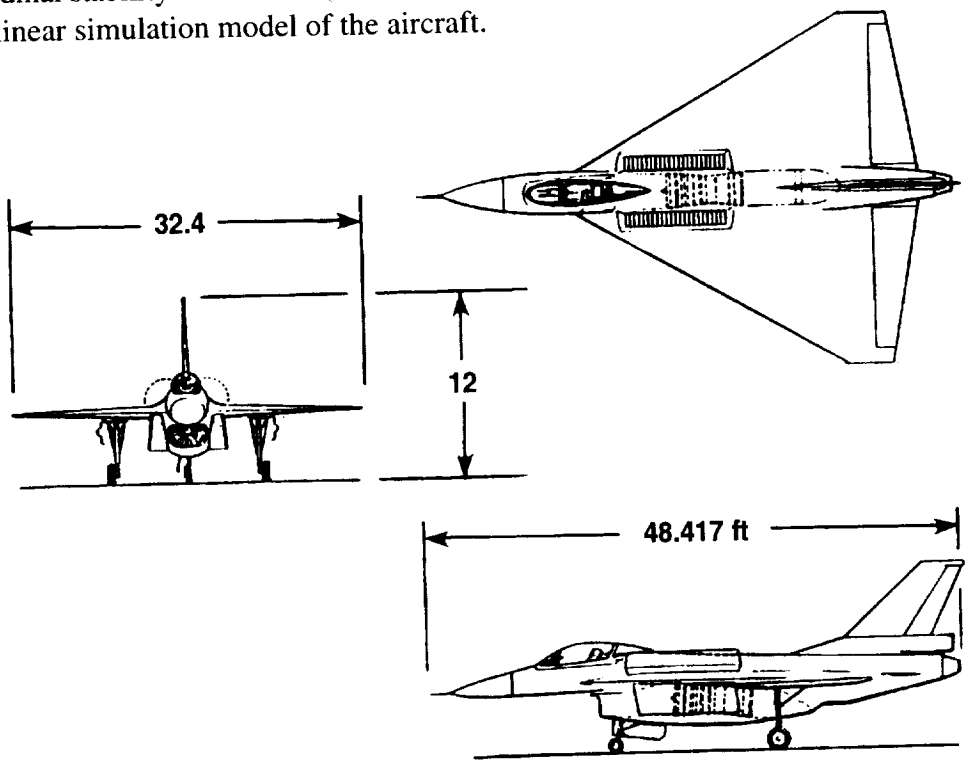

Figure 118. E-7A Augmentor Ejector conceptual STOVL fighter.

TABLE 10. STABILITY DERIVATIVES FOR THE E-7A

	E-7A (refs. 45, 46)		
Flight condition			
Speed, knots	0	100	200
Altitude, ft	200	200	200
Weight, lb	13800	13800	13800
δ_N, deg	90	60	0
Derivatives			
X_u, sec^{-1}	–0.0091	–0.051	–0.027
X_w, sec^{-1}	0	0.038	0.034
X_q, ft/sec/rad	0	0.9	1.44
X_{δ_S}, $ft/sec^2/deg$	0	0.04	–0.67
X_{δ_T}, $ft/sec^2/deg$	0.02	0.21	0.54
X_{δ_N}, $ft/sec^2/deg$	–0.34	–0.34	–0.1
Z_u, sec^{-1}	0	–0.064	–0.028
Z_w, sec^{-1}	–0.044	–0.7	–1.31
Z_q, ft/sec/rad	0	–5.62	–11.24
Z_{δ_S}, $ft/sec^2/deg$	–0.084	0.85	3.23
Z_{δ_T}, $ft/sec^2/deg$	–0.59	–0.4	0.014
Z_{δ_N}, $ft/sec^2/deg$	0.0024	–0.47	–0.15
M_u, rad/ft-sec	0.0006	–0.00013	0.00027
M_w, rad/ft-sec	0	–0.014	–0.03
M_q, sec^{-1}	–0.024	–0.63	–1.22
$M_{\dot{w}}$, rad/ft	0	–0.0014	–0.0014
M_{δ_S}, $rad/sec^2/deg$	0.026	0.12	0.43
M_{δ_T}, $rad/sec^2/deg$	–0.014	–0.0025	0.016
M_{δ_N}, $rad/sec^2/deg$	–0.015	0.02	0.04

UH-1H Utility Helicopter

The UH-1H is a single-engine utility helicopter manufactured for the U. S. Army by Bell Helicopter (fig. 119). It uses a two-bladed teetering main rotor powered by a Lycoming T53-L-13 turboshaft engine. Pitch control is achieved through longitudinal cyclic pitch of the rotor; lateral control is produced by lateral cyclic pitch; and yaw control comes from the tail rotor.

The stability derivatives shown in table 11 are based on a nonlinear simulation model and are listed in reference 47.

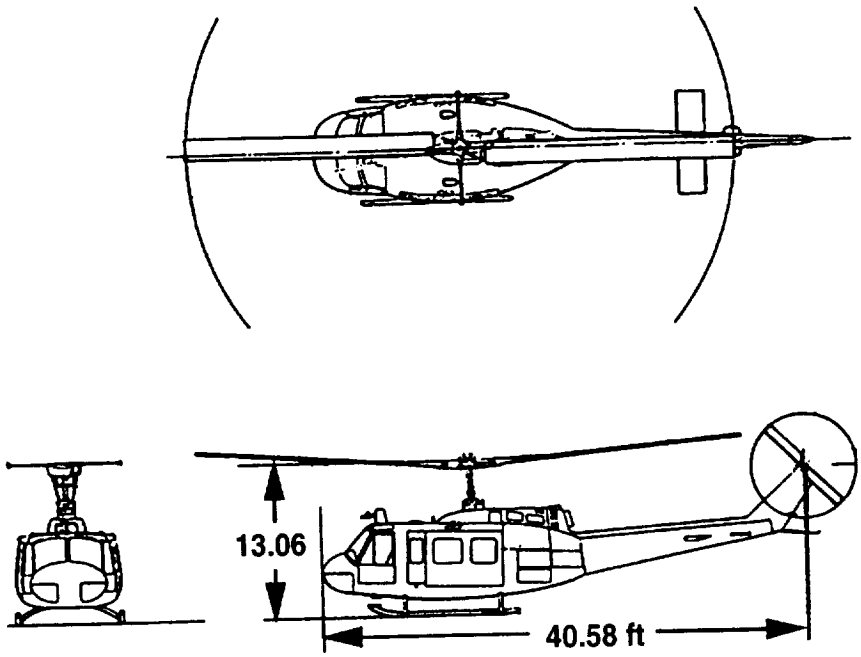

Figure 119. UH-1H utility helicopter.

BO-105C Utility Helicopter

The BO-105C is a twin-engine utility helicopter manufactured by Messerschmitt-Bölkow-Blohm (fig. 120). It uses a four-blade hingeless main rotor powered by two Allison 250-C-18 turboshaft engines. Pitch and roll control are achieved, respectively, by longitudinal and lateral cyclic pitch. Yaw control is provided by the tail rotor.

A nonlinear simulation model was used to produce the stability derivatives (table 11) that are listed in reference 47.

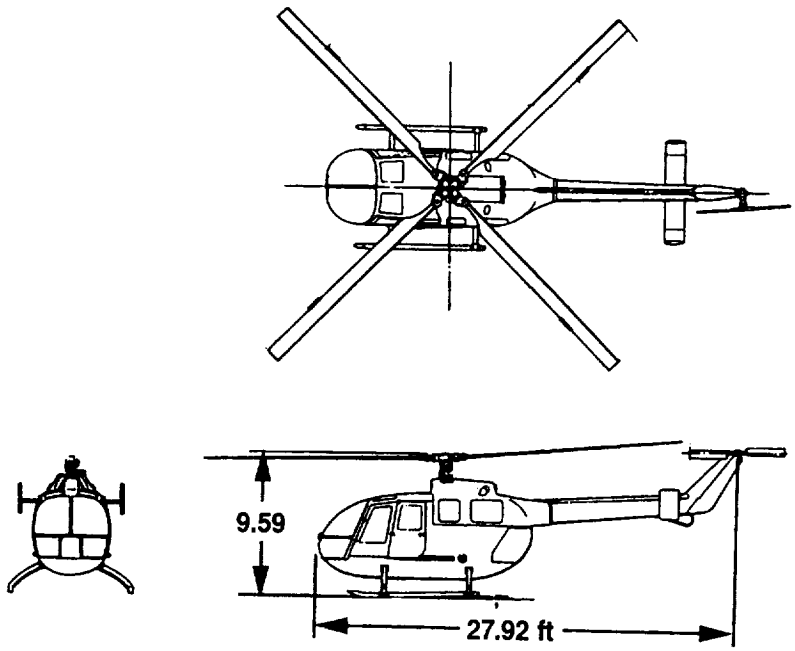

Figure 120. BO-105C utility helicopter.

TABLE 11. STABILITY DERIVATIVES FOR THE UH-1H AND BO-105C

	UH-1H (Ref. 47)		BO-105C (ref. 47)	
Flight condition				
Speed, knots	0	120	0	120
Altitude, ft	S.L.	S.L.	S.L.	S.L.
Weight, lb	8000	8000	4620	4620
C.G. (Fuselage Station), in.	137	137	98.4	98.4
Derivatives				
X_u, sec^{-1}	–0.0034	–0.056	–0.017	–0.065
X_w, sec^{-1}	0.025	0.105	0.012	0.021
X_q, ft/sec/rad	0.58	1.72	1.61	1.66
X_p, ft/sec/rad	–1.39	–0.84	–0.73	–0.69
$X_{\delta C}$, $ft/sec^2/in.$	0.68	1.34	0.45	–0.26
$X_{\delta B}$, $ft/sec^2/in.$	1.04	0.38	0.79	0.81
Z_u, sec^{-1}	–0.099	0.12	0.01	0.021
Z_w, sec^{-1}	–0.38	–1.03	–0.33	–1.0
Z_q, ft/sec/rad	0.29	–4.01	0.33	–0.52
Z_p, ft/sec/rad	–0.4	–3.62	0.15	–2.72
Z_r, ft/sec/rad	2.21	2.37	1.83	1.97
$Z_{\delta C}$, $ft/sec^2/in.$	–9.8	–13.6	–9.88	–15.0
$Z_{\delta B}$, $ft/sec^2/in.$	0.32	6.17	0.04	4.14

TABLE 11. CONCLUDED

	UH-1H		BO-105C	
Derivatives				
M_u, rad/ft-sec	0.0019	0.006	0.02	0.022
M_w, rad/ft-sec	–0.0038	–0.009	–0.0027	0.038
M_q, sec^{-1}	–0.19	–0.78	–3.4	–3.66
M_p, sec^{-1}	0.23	0.16	–0.84	–1.1
M_{δ_C}, $rad/sec^2/in.$	–0.0033	–0.048	–0.081	1.26
M_{δ_B}, $rad/sec^2/in.$	–0.17	–0.17	–0.97	–1.18
M_{δ_A}, $rad/sec^2/in.$	0	0	0.16	0.13
M_{δ_P}, $rad/sec^2/in.$	0.02	0.03	0.06	0.13
Y_q, ft/sec/rad	–1.34	–1.22	–0.48	–0.63
Y_v, sec^{-1}	–0.045	–0.21	–0.032	–0.15
Y_p, ft/sec/rad	–0.88	–1.74	–1.74	–1.74
Y_r, ft/sec/rad	0.88	2.25	0.21	0.8
Y_{δ_A}, $ft/sec^2/in.$	0.88	0.92	0.8	0.88
Y_{δ_P}, $ft/sec^2/in.$	1.63	2.72	–1.64	–2.01
L'_q, sec^{-1}	–0.88	–0.8	2.3	2.49
L'_v, rad/ft-sec	–0.013	–0.019	–0.063	–0.091
L'_p, sec^{-1}	–0.57	–1.0	–9.24	–8.75
L'_r, sec^{-1}	0.14	0.45	–0.22	0.12
L'_{δ_A}, $rad/sec^2/in.$	0.56	0.59	2.64	2.69
L'_{δ_P}, $rad/sec^2/in.$	0.42	0.71	–1.01	–1.26
N'_q, sec^{-1}	–0.06	–0.35	–0.12	0.32
N'_v, rad/ft-sec	0.021	0.042	0.01	0.029
N'_p, sec^{-1}	–0.32	–0.18	–0.076	–0.007
N'_r, sec^{-1}	–0.71	–1.89	–0.33	–0.87
N'_{δ_C}, $rad/sec^2/in.$	0.44	0.28	0.57	0.56
N'_{δ_A}, $rad/sec^2/in.$	0.083	0.088	0.034	0.003
N'_{δ_P}, $rad/sec^2/in.$	–1.2	–1.99	1.39	1.72

CH-47B Transport Helicopter

The CH-47B is a twin-engine transport helicopter manufactured by Boeing for the U. S. Army (fig. 121). It employs twin three-bladed tandem rotors powered by two Lycoming T-55-L-7C turboshaft engines. Pitch control is produced through differential collective pitch; roll control is achieved with lateral cyclic pitch; and yaw control is based on differential lateral cyclic pitch.

Stability derivatives (table 12) were provided in reference 48.

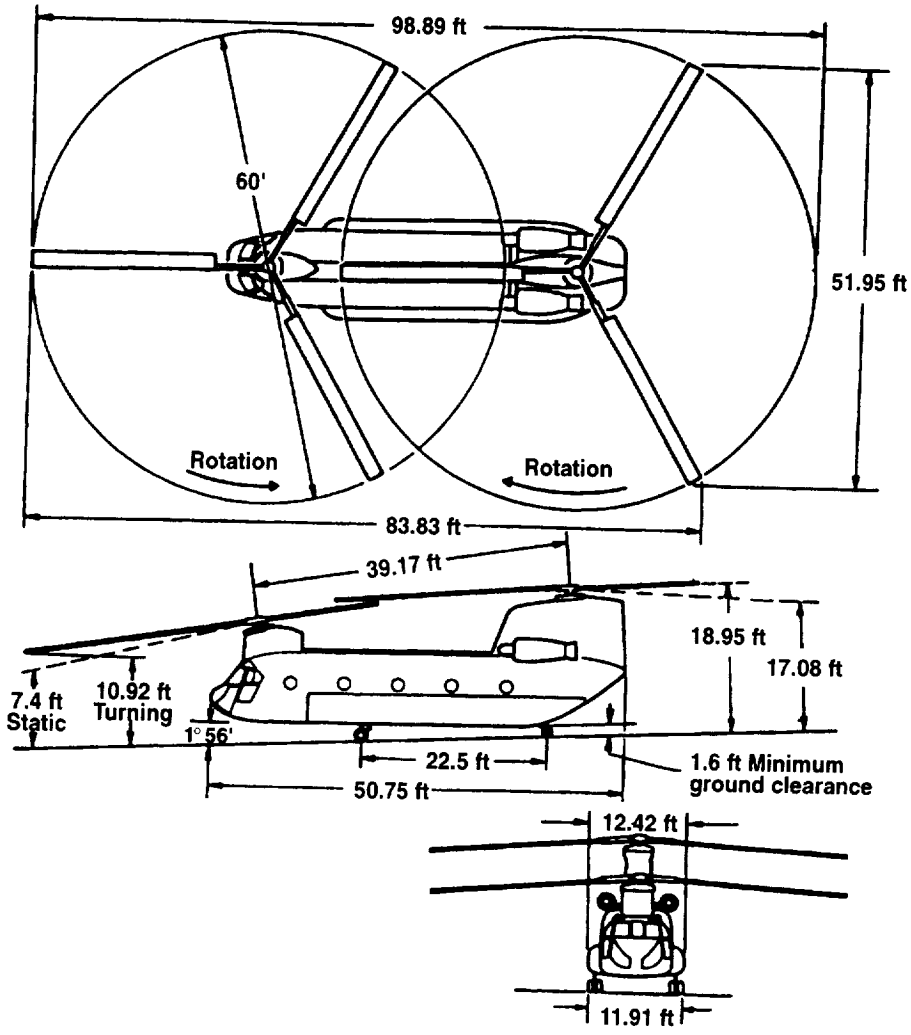

Figure 121. CH-47B transport helicopter.

UH-60 Utility Helicopter

The UH-60 is a twin-engine utility helicopter manufactured for the U. S. Army by Sikorsky (fig. 122). It consists of a four-blade articulated main rotor powered by twin General Electric T700-GE-700 turboshaft engines. Pitch and roll control are produced, respectively, by longitudinal and lateral cyclic pitch. Yaw control is derived from the canted tail rotor; the horizontal stabilizer is programmed for pitch trim in forward flight.

Stability derivatives (table 12) were extracted from a nonlinear simulation model described in reference 49.

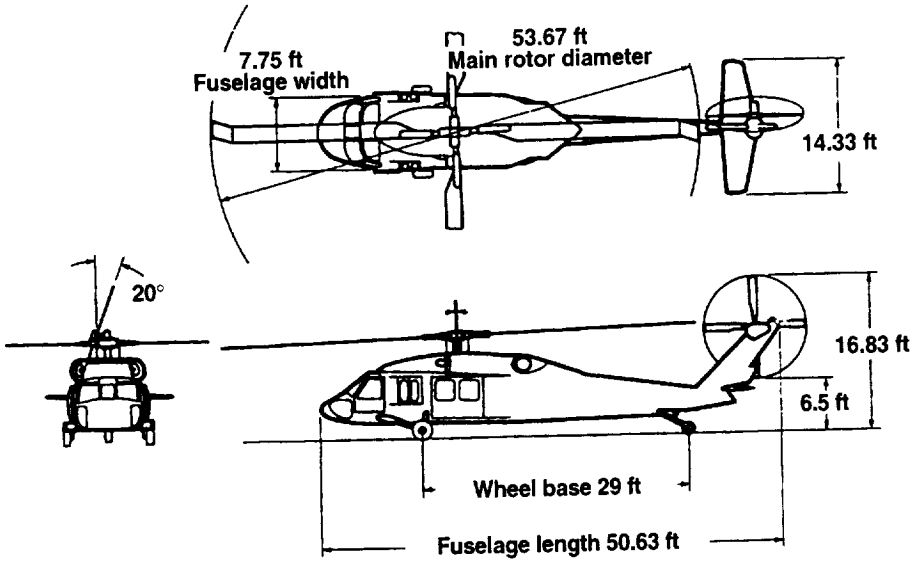

Figure 122. UH-60 utility helicopter.

TABLE 12. STABILITY DERIVATIVES FOR THE CH-47B AND UH-60

	CH-47B (Ref. 48)		UH-60 (ref. 49)	
Flight condition				
Speed, knots	0	60	0	140
Altitude, ft	S.L.	S.L.	S.L.	S.L.
Weight, lb	33000	33000	16400	16400
C.G. (Fuselage Station), in.	338	338	360.4	360.4
Derivatives				
X_u, sec^{-1}	–0.021	–0.02	–0.024	–0.041
X_w, sec^{-1}	0.033	0.038	0.025	0.08
X_q, ft/sec/rad	2.59	2.36	2.81	1.63
X_p, ft/sec/rad	0.021	0.0038	–0.26	–0.38
X_{δ_C}, $ft/sec^2/in.$	0.94	0.43	0.97	0.61
X_{δ_B}, $ft/sec^2/in.$	0.114	0.13	–1.66	–0.71
Z_u, sec^{-1}	0.025	–0.066	0.022	0.00034
Z_w, sec^{-1}	–0.3	–0.55	–0.29	–0.87
Z_q, ft/sec/rad	0.44	–1.18	0.36	6.64
Z_p, ft/sec/rad	0.042	0.21	–0.01	3.94
Z_r, ft/sec/rad	0.36	0.29	–0.21	–0.36
Z_{δ_C}, $ft/sec^2/in.$	–8.06	–9.36	–7.92	–10.76
Z_{δ_B}, $ft/sec^2/in.$	0.3	0.47	–0.14	–9.12
M_u, rad/ft-sec	0.0093	–0.0042	0.0036	0.0056
M_w, rad/ft-sec	0.0023	0.018	0.002	0.0089
M_q, sec^{-1}	–1.23	–1.68	–0.82	–2.0
M_p, sec^{-1}	0.043	0.023	0.31	0.007
M_{δ_C}, $rad/sec^2/in.$	0.019	0.15	–0.0056	0.1
M_{δ_B}, $rad/sec^2/in.$	0.33	0.39	0.33	0.52
M_{δ_A}, $rad/sec^2/in.$	0	0	–0.0036	0.065
M_{δ_P}, $rad/sec^2/in.$	0	0.0001	0.015	–0.17
Y_q, ft/sec/rad	0.0041	0.0034	–0.36	1.0
Y_v, sec^{-1}	–0.14	–0.074	–0.047	–0.18
Y_p, ft/sec/rad	–1.49	–2.04	–1.72	–2.23
Y_r, ft/sec/rad	–0.16	——	0.64	2.05
Y_{δ_A}, $ft/sec^2/in.$	1.16	1.12	0.94	0.97
Y_{δ_P}, $ft/sec^2/in.$	–0.054	–0.053	–1.49	–2.18

TABLE 12. CONCLUDED

	CH-47B		UH-60	
Derivatives				
L'_q, sec^{-1}	0.038	–0.031	–2.27	–1.27
L'_v, rad/ft-sec	–0.0065	–0.0057	–0.041	–0.039
L'_p, sec^{-1}	–0.72	–0.85	–3.55	–3.63
L'_r, sec^{-1}	–0.071	–0.085	0.075	0.78
L'_{δ_A}, rad/sec^2/in.	0.43	0.42	1.33	1.33
L'_{δ_P}, rad/sec^2/in.	–0.061	–0.059	–0.84	–1.3
N'_q, sec^{-1}	–0.16	–0.082	–0.34	–0.53
N'_v, rad/ft-sec	–0.0011	–0.00053	0.0097	0.02
N'_p, sec^{-1}	–0.054	–0.082	–0.1	–0.18
N'_r, sec^{-1}	–0.047	–0.046	–0.33	–1.0
N'_{δ_C}, rad/sec^2/in.	–0.0004	0.005	0.063	–0.089
N'_{δ_A}, rad/sec^2/in.	0.042	0.041	0.027	0.023
N'_{δ_P}, rad/sec^2/in.	0.2	0.19	0.6	0.93

REFERENCES

1. Bryan, G. H.: Stability in Aviation. Macmillan, London, 1911.

2. Gilruth, Robert: Requirements for Satisfactory Flying Qualities of Airplanes. NACA Rept. 755, 1943.

3. Anon.: Military Specification-Flying Qualities of Piloted Airplanes. MIL-F- 8785 (ASG), Sept. 1954.

4. Anon.: Military Specification-Flying Qualities of Piloted Airplanes. MIL-F- 8785B (ASG), Aug. 1969.

5. Anon.: Military Standard-Flying Qualities of Piloted Vehicles. MIL-STD-1797, March 1987.

6. Anon.: Military Specification-Helicopter Flying and Ground Handling Qualities. MIL-H 8501, Nov 1952.

7. Anon.: Military Specification-Helicopter Flying and Ground Handling Qualities. MIL-H-8501 A, Sept. 1961.

8. Botrel, A.: Recommendations for V/STOL Handling Qualities. AGARD Report 408, Oct. 1962.

9. Anon.: V/STOL Handling: 1. Criteria and discussion. AGARD Report 577, 1970.

10. Chalk, C. R.; Key, D. L.; Kroll, J., Jr.; Wasserman, R.; and Radford, R. C.: Background Information and User Guide for MIL-F-83300, - Military Specification-Flying Qualities of Piloted VSTOL Aircraft. AFFDL-TR-70-88, Nov. 1971.

11. Innis, R. C.; Holzhauser, C. A.; and Quigley, H. C.: Airworthiness Considerations for STOL Aircraft. NASA TN D-5594, 1970.

12. McRuer, D. T.; Graham, D.; and Krendel, E. S.: Manual Control of Single Loop Systems. Franklin Institute Journal, vol. 283, no. 1, Jan. 1967.

13. Hess, R. A.: Structural Model of the Adaptive Human Pilot. J. Guidance and Control, vol. 3, no. 5, Sept.-Oct. 1980, pp. 416-423.

14. Cooper, G. E. and Harper, R. P., Jr.: The Use of Pilot Rating in the Evaluation of Aircraft Handling Qualities. NASA TN D-5153, 1969.

15. McRuer, D. T.; Ashkenas, I. L.; and Graham, D.: Aircraft Dynamics and Automatic Control. Princeton University Press, Princeton, New Jersey, 1973.

16. Seckel, E.: Stability and Control of Airplanes and Helicopters. Academic Press, New York, 1964.

17. Etkin, B.: Dynamics of Flight—Stability and Control. John Wiley, New York, 1982.

18. Perkins, C. D. and Hage, R. E.: Airplane Performance Stability and Control. John Wiley, New York, 1949.

19. Roskam, J.: Airplane Flight Dynamics and Automatic Flight Controls. Roskam Aviation and Engineering Corp., Lawrence, Kansas, 1979.

20. Kuhn, R. E.: An Engineering Method for Estimating Induced Lift on V/STOL Aircraft Hovering In and Out of Ground Effect. Naval Air Development Center Report, NADC-80246-60, Jan. 1981.

21. Kuhn, R. E.: An Engineering Method for Estimating the Lateral/Directional Characteristics of V/STOL Aircraft in Transition. Naval Air Development Center Report, NADC-81031-60, Feb. 1981.

22. Margason, R.: Propulsion-Induced Effects Caused by Out-of-Ground Effects. NASA TM-100032, 1987.

23. Hoh, R. H. and Ashkenas, I. L.: Development of V/STOL Flying Qualities for Low Speed and Hover. Naval Air Development Center Report, NADC-77052-30, Dec. 1979.

24. Franklin, J. A.: Criteria for Design of Integrated Flight/Propulsion Control Systems for STOVL Fighter Aircraft. NASA TP-3356, 1993.

25. Franklin, J. A.; Stortz, M. W.; Borchers, P. F.; and Moralez, Ernesto III: Flight Evaluation of Advanced Controls and Displays for Transition and Landing on the NASA V/STOL Systems Research Aircraft. NASA TP-3607, 1996.

26. Franklin, J. A. and Stortz, M. W.: Moving Base Simulation Evaluation of Translational Rate Command Systems for STOVL Aircraft in Hover. NASA TM-110399, 1996.

27. Ashkenas, I. L. and Craig, S. J.: Multiloop Piloting Aspects of Longitudinal Approach Path Control. International Council of the Aeronautical Sciences ICAS Paper No. 72-46, Sept. 1972.

28. Neumark, S.: Problems of Longitudinal Stability Below Minimum Drag Speed, and Theory of Stability Under Constraint. Aeronautical Research Council of Great Britain R and M No. 2983, July 1953.

29. Scott, B. C.; Hynes, C. S.; Martin, P. W.; and Bryder, R. B.: Progress Toward Development of Civil Airworthiness Criteria for Powered-Lift Aircraft. NASA TM X-73124, 1976 (also FAA-RD-76-100).

30. Franklin, J. A.; Innis, R. C.; Hardy, G. H.; and Stephenson, J. D.: Design Criteria for Flightpath and Airspeed Control for the Approach and Landing of STOL Aircraft. NASA TP-1911, 1982.

31. Franklin, J. A.: Experience with Integrated Flight/Propulsion Controls from Simulation of STOVL Fighter Concepts. AIAA Paper 93-4874, International Powered-Lift Conference, Dec. 1993.

32. Hoh, R. H. and Ashkenas, I. L.: Handling Quality Criterion for Heading Control. Journal of Aircraft, vol. 14, no. 2, Feb. 1977.

33. Anon.: Aeronautical Design Standard—Handling Qualities Requirements for Military Rotorcraft. U.S. Army Report ADS 33D, July 1994.

34. Lebacqz, J. V.; Merrick, V. K.; and Franklin, J. A.: Control and Display Requirements for Decelerating Approach and Landing of Fixed- and Rotary-Wing V/STOL Aircraft. American Helicopter Society Paper 86-42-70-100, 1986.

35. Franklin, J. A.: Revised Simulation Model of the Control System, Displays, and Propulsion System for an ASTOVL Lift Fan Aircraft. NASA TM-112208, Oct. 1997.

36. Anon.: Displays for Approach and Landing of V/STOL Aircraft. AGARD Advisory Report 51, Nov. 1972.

37. Weir, D. H.; Klein, R. H.; and McRuer, D. T.: Principles for the Design of Advanced Flight Director Systems Based on the Theory of Manual Control Displays. NASA CR-1748, 1971.

38. Bray, R. S.: A Head-Up Display Format for Application to Transport Aircraft Approach and Landing. NASA TM-81199, 1980.

39. Merrick, V. K.; Farris, G. G.; and Vanags, A. A.: A Head-Up Display for Application to V/STOL Aircraft Approach and Landing. NASA TM-102216, 1990.

40. Hynes, C. S.; Franklin, J. A.; Hardy, G. H.; Martin, J. L.; and Innis, R. C.: Flight Evaluation of Pursuit Displays for Precision Approach of Powered-Lift Aircraft. J. Guidance, Control, and Dynamics, vol. 12, no. 4, July-August 1989.

41. Anon: YAV-8B Simulation and Modeling. Vol. 1: Aircraft Description and Program Summary. NASA CR-170397, 1983.

42. Harendra, P. B.; Joglekar, M. M.; Gaffey, T. M.; and Marr, R. L.: A Mathematical Model for Real-Time Flight Simulation of the Bell Model 301 Tilt Rotor Research Aircraft. NASA CR-114614, 1973.

43. Lebacqz, J. V. and Aiken, E. A.: A Flight Investigation of Control, Display, and Guidance Requirements for Decelerating Descending VTOL Instrument Transitions Using the X-22A Variable Stability Aircraft. Calspan Report AK-5336-F-1, Vol. II: Background Information and Supporting Data, Sept. 1975.

44. Radford, R. C.; Andrisani II, D.; and Beilman, J. L.: An Experimental Investigation of VTOL Flying Qualities Requirements for Shipboard Landings. Naval Air Development Center Report NADC-77318-60, Aug. 1981.

45 Engelland, S. A.: Evaluation of the Longitudinal Stability and Control Characteristics of the E-7A STOVL Aircraft in Hover. Master's thesis, University of Kansas, Mar. 1989.

46. Borchers, P. F.: A Comparison between Classical and Optimal Longitudinal Controllers for E-7A Aircraft in Transition. Master's thesis, University of Kansas, April 1991.

47. Heffley, R. K.; Jewell, W. F.; Lehman, J. M.; and Van Winkle, R. A.: A Compilation and Analysis of Helicopter Handling Qualities Data. NASA CR-3144, 1979.

48. Ostroff, A. J.; Downing, D. R.; and Rood, W. J.: A Technique Using a Nonlinear Helicopter Model for Determining Trims and Derivatives. NASA TN D-8159, 1976.

49. Hilbert, K. B.: A Mathematical Model of the UH-60 Helicopter. NASA TM-85890, 1984.

REPORT DOCUMENTATION PAGE

Form Approved
OMB No. 0704-0188

1. AGENCY USE ONLY *(Leave blank)*	2. REPORT DATE	3. REPORT TYPE AND DATES COVERED
	October 2000	Technical Publication

4. TITLE AND SUBTITLE
V/STOL Dynamics, Control, and Flying Qualities

5. FUNDING NUMBERS
706-25-11

6. AUTHOR(S)
James A. Franklin

7. PERFORMING ORGANIZATION NAME(S) AND ADDRESS(ES)
Ames Research Center
Moffett Field, CA 94035-1000

8. PERFORMING ORGANIZATION REPORT NUMBER
A-0003625

9. SPONSORING/MONITORING AGENCY NAME(S) AND ADDRESS(ES)
National Aeronautics and Space Administration
Washington, DC 20546-0001

10. SPONSORING/MONITORING AGENCY REPORT NUMBER
NASA/TP–2000-209591

11. SUPPLEMENTARY NOTES
Point of Contact: James A. Franklin, Ames Research Center, MS 210-5, Moffett Field, CA 94035-1000
(650) 604-6004

12a. DISTRIBUTION/AVAILABILITY STATEMENT
Unclassified — Unlimited
Subject Category 08 Distribution: Standard
Availability: NASA CASI (301) 621-0390

12b. DISTRIBUTION CODE

13. ABSTRACT *(Maximum 200 words)*

This publication presents material that constituted the lectures presented by the author as part of Course AA 234, Dynamics, Control, and Flying Qualities of V/STOL Aircraft that was taught in the Department of Aeronautics and Astronautics at Stanford University. It covers representative operations of vertical and short takeoff and landing (V/STOL) aircraft, a discussion of the pilot's strategy in controlling these aircraft, the equations of motion pertinent to V/STOL tasks, and their application in the analysis of longitudinal and lateral-directional control in hover and forward flight. Following that development, which applies to the characteristics of the basic airframe and propulsion system, the text concludes with a discussion of the contributions of control augmentation in specific flight tasks and of the integration of modern electronic displays with these controls.

14. SUBJECT TERMS
V/STOL, Flying qualities, Flight Control

15. NUMBER OF PAGES
193

16. PRICE CODE
A09

17. SECURITY CLASSIFICATION OF REPORT	18. SECURITY CLASSIFICATION OF THIS PAGE	19. SECURITY CLASSIFICATION OF ABSTRACT	20. LIMITATION OF ABSTRACT
Unclassified	Unclassified	Unclassified	